STUDY OF CRUSTAL AND UPPER MANTLE STRUCTURE ALONG SELECTED PATHS IN IRAN USING SURFACE WAVE DISPERSION

A THESIS

submitted in fulfilment of the
requirements for the award of the degree
of
DOCTOR OF PHILOSOPHY

By

NASROLLAH KAMALIAN

Professor and Head
Department of Earth Sciences
University of Roorkee
ROORKEE

DEPARTMENT OF EARTH SCIENCES
UNIVERSITY OF ROORKEE
ROORKEE-247 667 (INDIA)

MAY, 1994

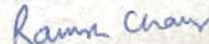Gratis

CANDIDATE'S DECLARATION

I hereby certify that the work which is being presented in the thesis entitled "STUDY OF CRUSTAL AND UPPER MANTLE STRUCTURE ALONG SELECTED PATHS IN IRAN USING SURFACE WAVE DISPERSION" in fulfillment of the requirements for the award of the Degree of Doctor of Philosophy, and submitted in the Department of Earth Sciences, University of Roorkee, is an authentic record of my own work carried out during the period from August 1990, to May 1994, under the supervision of Professor Ramesh Chander.

The matter presented in this thesis has not been submitted by me for the award of any other degree of this or any other University.

(NASROLLAH KAMALIAN)

This is to certify that the above statement made by the candidate is correct to the best of my knowledge.
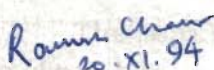
Date: 20 May 1994

(Dr. Ramesh Chander)
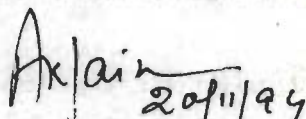
Professor
Department of Earth sciences
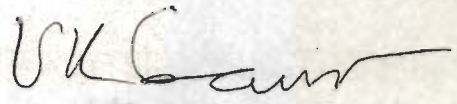University of Roorkee
Roorkee, 247 667

The Ph.D. Viva-Voce examination of Mr. Nasrollah Kamalian, Research Scholar, has been held on 20 Nov 1994

Signature of
Supervisor

Signature of
H.O.D.

Signature of
External Examiner

I

APOLOGY

Every possible care has been taken to remove typographical and other errors of English. However I am aware of the possibility that still some errors may have escaped my notice. This holds especially for the fact that the singulars and plurals are indicated differently in Persian and English.

ABSTRACT

Seismological studies in Iran have been motivated by the need to reduce earthquake hazards. A significant event in this regard was the setting up of three WWSSN stations at Tabriz, Shiraz, and Mashhad. We investigate in this study the dispersion characteristics of Rayleigh waves in the Zagros, Central Iran, and Alborz regions by computing phase speeds using seismograms for the three pairs of stations, namely Tabriz-Shiraz, Shiraz-Mashhad, and Mashhad-Tabriz respectively. Starting from an initial list of 3500 earthquakes data for 9, 8, and 11, earthquakes were found usable for Zagros, Central Iran, and Alborz region respectively.

Fundamental mode Rayleigh waves on all the seismograms were digitized. Calibration pulses on the respective seismograms were also digitized for correction of instrumental phase shifts.

Dziewonski and Hales's (1972) cross-correlogram variant of Aki's two station method was used to compute phase speed from these digitized signals. The algorithm was tested extensively through a set of 16 carefully designed experiments on synthetic data. A new method was proposed and tested to take instrumental phase shift into account.

The phase speed dispersion curves obtained using extended Rayleigh wave trains in the group speed range of 4.0 to 2.9 km/s were not smooth in spite of all the precautions probably because

of noise on seismograms. Smoother phase speed dispersion curves were obtained, through trial and error, using Rayleigh wave train segments corresponding to narrower ranges of group speeds. The latter data were interpreted for crust and upper mantle structures.

It is estimated that the maximum error in a phase speed value for a given period in any particular case was less than ±0.12 km/s.

The inversion of phase speed results for crust and upper mantle structure was carried out using the singular value decomposition (SVD) variant of the generalized inverse method. A computer program was written for the purpose independently and tested thoroughly.

Rayleigh wave phase speed data for the fundamental mode in the period range of about 20 to 70 seconds were considered for inversion for the Zagros, Central Iran, and Alborz regions. Limited data in the period range of 70 to 230 seconds were provided by the inversely dispersed waves for the Alborz region.

Layered models consisting of 1, 2, and 18 layers for the crust and a uniform half space corresponding to upper mantle were considered with Rayleigh wave data in the 20 to 70 seconds period range. Five and six layered models, with 2 to 3 layers representing the crust, were considered for the inversely dispersed Rayleigh waves. Shear wave speeds and layer thicknesses were determined in all cases through inversion keeping

compressional wave speeds and densities of layers constant as initially prescribed. The number of converged model considered for each region was in the range of 60 to 70.

The inverted models based on 20 to 70 seconds period Rayleigh waves showed that the crustal thicknesses varied in Zagros, Central Iran, and Alborz regions though shear wave speeds in different layers were broadly similar in the three regions. Crustal thicknesses of 45 km, 39 km, and 35 km were obtained for Zagros, Central Iran and Alborz regions respectively. A low shear wave speed zone in upper mantle of Alborz region is inferred from inversely dispersed Rayleigh waves. The non-uniqueness of the interpretation is acknowledged.

Comparison of our results with those by a few other worker using much less data indicate broad similarities and some differences.

Inferences regarding crustal thicknesses in Zagros and Alborz regions are supported by limited gravity data and seismological studies using Iranian earthquake data.

The 45 km thick crust for Zagros region is consistent with crustal thickening under lateral compression due to northeastward subduction of the Arabian plate beneath Iran.

ACKNOWLEDGEMENT

LIST OF FIGURES

XVII

XXII

LIST OF TABLES

XXVIII

CONTENTS

XXIX

CHAPTER-1
INTRODUCTION AND REVIEWS

1.1 GENERAL

Out of the intellectual activities of men in different parts
of the world over many centuries, gradually science has emerged as
a tool for systematic study of nature. It has benefited mankind in
innumerable ways, although some of the fruits of this progress
have been misused for harm. Here we wish to delve on the positive
aspects of science. Science has its own powerful method in which
observations are held supreme and hypotheses are proposed to
explain them. If the hypotheses do not stand up to the scrutiny of
further observations then they are discarded ruthlessly and
efforts are made to seek better explanations. In science there is
no seniority, only rational examination of hypotheses on the anvil
of observations. We like to think that the present thesis is an
effort in the cause of science.

Although physics and chemistry today have the dominant place
in the realm of science, earth sciences probably have a longer
history. The inputs from earth sciences to the progress of science
as a whole are also profound. For example, in the last twenty five
years or so earth sciences have made a fundamental contribution
even to the way in which scientists interpret their observations
quantitatively. We are referring here to the formalism of Backus
and Gilbert (1967) for geophysical inverse problems.

The contributions of earth sciences to the well being of society are numerous also. From the systematic exploration of natural resources to systematic investigations of natural disasters covers a wide spectrum. No country in the world today can progress without a strong program in earth sciences . In Iran (Fig. 1.1) the study of earth sciences in the modern sense has a relatively recent history. But it's importance today is well recognized and broad features of geology and geophysics of Iran have emerged especially through exploration for oil. Important results have also emerged through general geophysical and geological studies in which the applicability of the plate tectonics hypothesis to the Iranian region has been examined critically.

In this thesis the aim is to aid the progress of earth sciences in Iran. The method we have chosen is to interpret seismic surface waves recorded at three WWSSN stations, namely, Tabriz, Shiraz, and Mashhad situated in a triangle spanning northwestern half of Iran broadly (Fig. 1.1). We investigate the phase speed dispersion of Rayleigh waves recorded at pairs of these stations and thus construct models of crust and upper mantle along the different side of this triangle. The idea was to make use of the observation available already and seek information about the Iranian crust from another angle. The literature survey using the library resources available to us indicates that although a few similar studies have been undertaken earlier for the Iranian region, the amount of Rayleigh wave data analyzed in this study is the maximum so far.
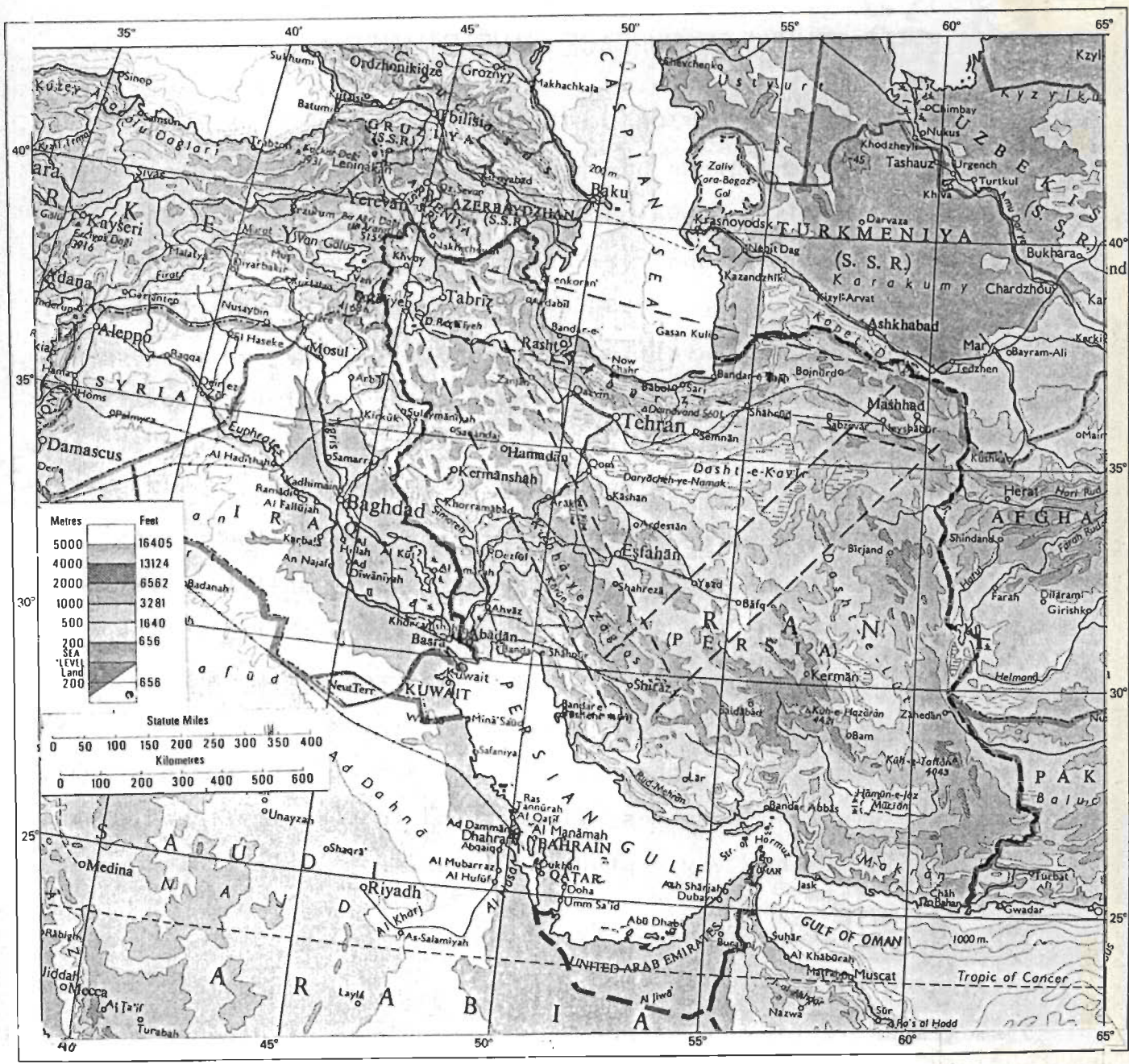
FIG. 1.1 THE GEOGRAPHIC LOCATION OF IRAN. THE LOCATIONS OF THREE
WWSSN STATIONS WHOWS DATA WERE INVESTIGATED ARE SHOWN ALSO.
THE DASHED LINES INDICATE THE SWATHS OF COUNTRY OVER WHICH
RAYLEIGH WAVE PROPAGATION OCCURED. THESE ARE IDENTIFY AS
ZAGROS, CENTRAL IRAN, AND ALBORZ REGIONS.

3

1.2 A BRIEF REVIEW OF SURFACE WAVE STUDIES

1.2.1 REVIEW OF OBSERVATIONAL STUDIES

Theoretical progress has preceded observations several times in the study of seismic waves. Thus, the theory of elastic body waves of the compressional (P) and shear (S) types was given by Poisson in 1825. Around 1885 Rayleigh proposed the theory of elastic solid waves travelling unattenuated along the surface of an elastic half space. The credit for first identifying compressional, shear, and surface waves on the seismograms of the great Indian earthquake of 1897 goes to Oldham (1899). Thereafter the use of surface waves for study of structure of the earth was hindered because neither seismographs with suitable response curves for recording these waves nor computational facilities for calculating dispersion curves for multilayered earth models were available. Still Carder, Rohrbach, Gutenburg, Richter, and Sezawa (see Ewing et al. 1957, page 196), were the early workers who, during the nineteen thirties, first tried to identify continental and oceanic paths by studying surface wave dispersion.

Observational studies of surface waves were greatly facilitated by the invention of the Press-Ewing long period seismographs in late nineteen forties. These instruments were deployed around the world during the International Geophysical Year (IGY) ca 1958. This led to availability of high quality surface wave data from virtually all parts of the globe, and made possible investigation of crustal and upper mental structures over many geographic areas. The present thesis is a part of these studies although slightly belated.

Beginning in 1969 Pomeroy et al., a further development in instrumental seismology occurred with the advent of wide band long period seismographs with which longer period surface waves and normal mode vibrations of the earth could be recorded. Initially slowly but in recent years much more rapidly such broad band instruments with digital recording have been deployed and observational studies about surface wave are seeing a minor revival (e.g. Braile 1991).

In the mean time, computers facilitated evaluation of Fourier Transforms of long surface wave trains after digitization. The Cooley-Tukey (1965) type Fast Fourier Transform (FFT) algorithms also became available as aids to surface wave studies.

1.2.2 REVIEW OF THEORETICAL STUDIES

On the theoretical side, after the initial work of Rayleigh, Lamb (1904) showed how a transient line load on the surface of an elastic half space gives rise to transient surface particle displacements with the same phase relationship between vertical and horizontal component as the surface waves of Rayleigh. However, these surface waves were not dispersive. In 1911, Love gave the theory of dispersed surface waves traveling in an elastic layer resting on an elastic half space. Around 1924 Stoneley (Ewing et al., 1957, Chap. 9) investigated the theory of interface waves along the boundary between two solid media. At about the same time, Sezawa (see Ewing et al. 1957, Chap. 4) contributed to the theory of Rayleigh waves in layered elastic media. Progress in the use of these theories for analyses of surface waves dispersion observations was restrained because of lack of facilities for

lengthy numerical calculations. This difficulty was removed with the availability of first generation computers in the nineteen fifties. However, in the mean time, two notable theoretical developments occurred. Firstly Pekeris 1948 computed the synthetic seismogram due to an explosive source in an elastic liquid layer over an elastic liquid half space. These computations explained certain observations of dispersed acoustic waves from the oceans made by Ewing and his group during the second world war with great fidelity (see Ewing et al. 1957 Chap. 4). Secondly Haskell (1953) gave a matrix formulation for computing surface wave dispersion curves for multilayered elastic half space models. Dorman et al. (1960) implemented and used Haskell's theory for computing dispersion curves for a variety of models to explain observations of mantle Rayleigh and Love waves. Since then there has been a flood of surface wave investigations. During the nineteen sixties the problem of numerical instability faced in computations using Haskell's theory was solved by Dunkin (1965), Schwab and Knopoff (1972), and others. The nineteen seventies saw progress in dealing with propagation of dispersive surface waves in laterally varying layered media.

The period of late nineteen fifties and early nineteen sixties saw major theoretical and observational investigations in which the connection between surface travelling waves and normal mode oscillations (free oscillation) of the earth as a whole was made transparent (e.g. Ben-Menahem, 1964).

A fundamental difficulty in using surface wave dispersion observation for investigation of crust and upper mantle structure

is the nonuniquness of interpretation. Backus and Gilbert (1967) made this difficulty into a virtue by suggesting that automated inversion of geophysical observations using programing methods was possible only because of the nonuniquness.

1.2.3 SURFACE WAVE STUDIES IN IRAN

The limited library resources available to us reveal that some Rayleigh wave phase and group speed data for the Iranian region have been examined by Bird ((1978), McCowan (1978), and Asudeh (1982). Propagation of Lg phase was considered by Kadinsky-Cade et al. (1981). The results are discussed later in this chapter (Section 1.4.6) along with the review of other geophysical studies.

1.3 A BRIEF REVIEW OF THE GEOLOGY OF IRAN

1.3.1 INTRODUCTION

The geological study of Iran was started about a century ago, when foreign experts were searching for oil (Darvichzade 1992). The first geological map of Iran on the scale of 1:2,500,000 was published by the National Iranian Oil Company (NIOC) in 1957. In the following three decades, valuable work has been done by many different organizations, of which NIOC and Geological survey of Iran (GSI) need special mention.

The Iranian region forms a part of the Alpine-Himalayan system of mountain ranges. Traditionally Iran has been divided into three main path, namely, two great mountain ranges, the Alborz ranges on the north and Zagros-Makran ranges on the

7
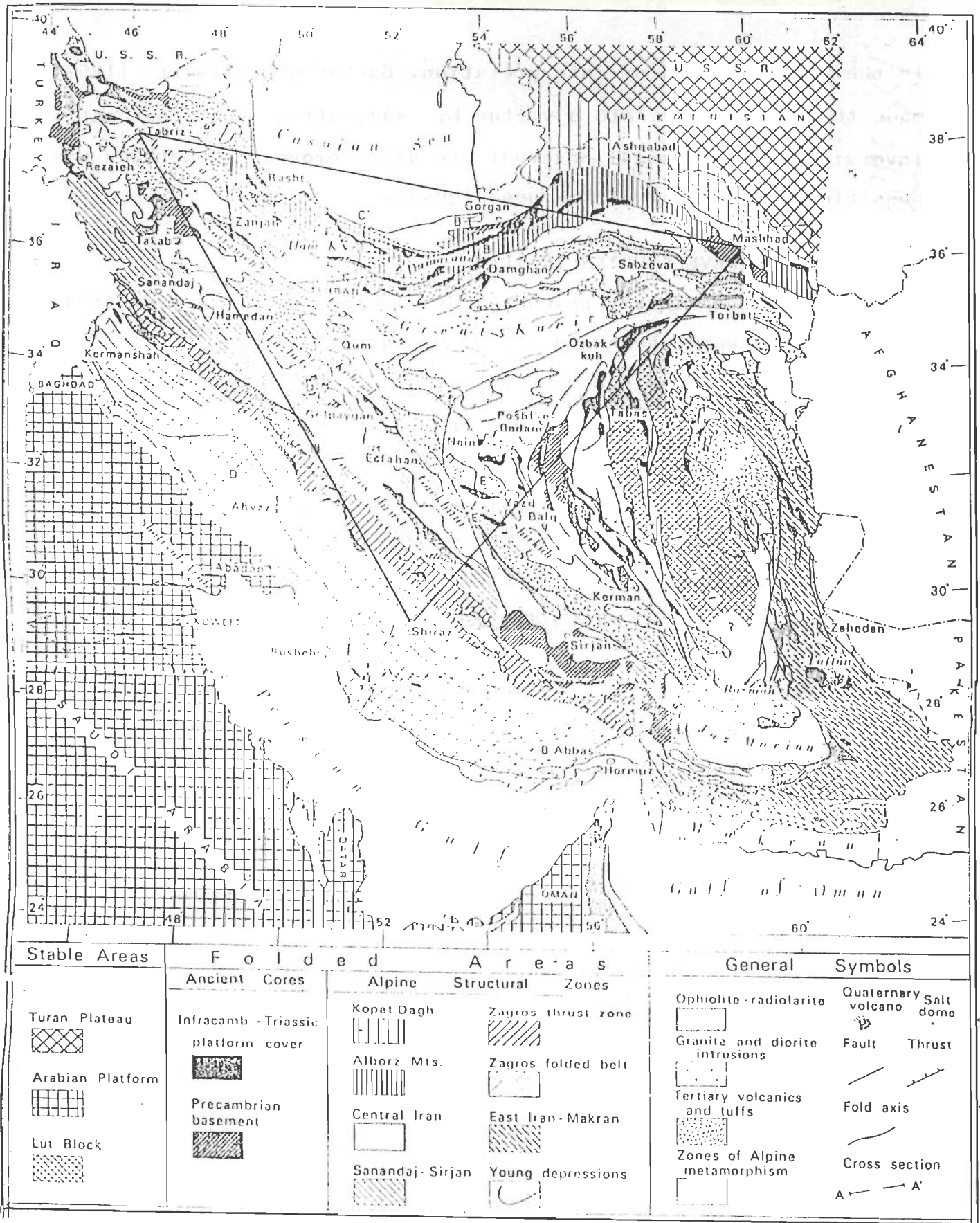
FIG. 1.2 THE GEOLOGIC-CUM-TECTONIC MAP OF IRAN (According to Stocklin 1968). THE TRIANGLE FORMED BY THE STATIONS IS ALSO SHOWN.
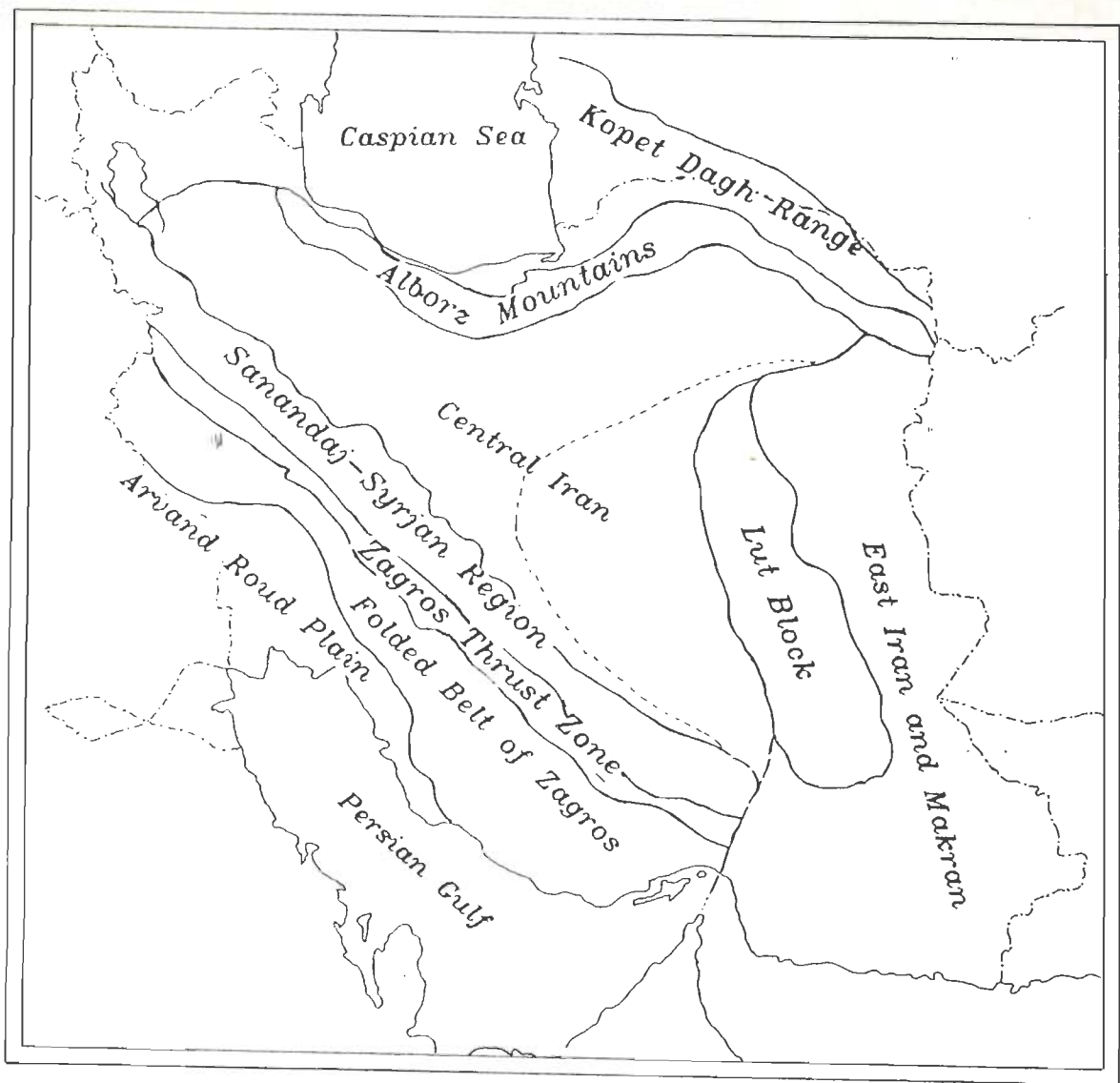
FIG. 1.3 THE NINE GEOLOGICAL PROVINCES OF IRAN DISCUSSED BY STOCKLIN (1968).

9

southwest and south, and the geologically complex central region of Iran in the middle (Fig. 1.2). It so happens that the Tabriz to Shiraz and Mashhad to Tabriz paths of surface waves investigated here lie broadly along the Zagros and Alborz mountains ranges respectively. The Shiraz to Mashhad path lies mainly in the Central Iran (Fig. 1.2).

Stocklin (1968) recognized nine structural zones in Iran (Fig. 1.3). Each zone has a different structural history and tectonic style. The following summary of the geology of Iran is based on the work of Stocklin (1968).

1.3.1.1 PLACE NAMES

Recently many Iranian names have been revised. In the following paragraphs we use the current Iranian names, but to link the present work with previous reports in the literature we provide in parenthesis the names used by Stocklin (1968) also.

1.3.2 PLAINS OF ARVAND ROUD (SHAT-AL-ARAB)

The extreme southwestern administrative province of Khozestan in Iran (Figs. 1.2 and 1.3) are called the plains of Arvand Roud. These plains are geologically part of the Mesopotamian plains. Structurally this is a part of the Arabian platform. Young alluvial deposits on the surface hide geologic deposits of Paleozoic to Tertiary ages. The latter deposits are mainly shallow marine to lagoonal in nature (Stocklin 1968).

1.3.3 FOLDED BELT OF ZAGROS

In this region (Figs. 1.2 and 1.3) a conformable sequence of

10

deposits from Infracambrian to Neogene age was deposited in the Zagros trough, or Zagros geosyncline, over the subsiding Precambrian shield of Arabia. This entire sedimentary sequence was folded in Pliocene-Pleistocene time during the latest phase of the Alpine orogeny. Thick Infracambrian salt deposits form a notable part of the Zagros belt. According to Stocklin (1968), the folding in this belt is characterized by long parallel, asymmetric anticlines and synclines created by tangential stress from the northeast. In anticipation of subsequent work by McKenzie (1972), Stocklin (1968) recognized the possibility that the result would be the same if the Arabian peninsula moved northeastward and underthrusted. Within the sedimentary record of the Zagros there is evidence of gentle epeirogenic movements prior to folding.

1.3.4 ZAGROS THRUST ZONE

The Zagros folded belt passes northeastward continuously in to a narrow zone of thrusting bounded on the northeast by the Main Zagros Thrust (MZT) line (Figs 1.2 and 1.3). In this zone, older Paleozoic and Mesozoic rocks were thrust southwestward in several schuppenlike slices on younger Mesozoic and Tertiary rocks of the folded belt. The thrust zone represents the deepest part of the Zagros geosyncline in Mesozoic and early Tertiary times. The MZT has a remarkably straight alignment. It is a deep reverse fault splitting a once continuous platform into Arabian and Iranian segments. According to Nowroozi (1976) a right-lateral strike-slip component is discernible along the MZT .

1.3.5 SANANDAJ-SYRJAN REGION

This mountainous region lies immediately northeast of the MZT

11

(Figs. 1.2 and 1.3). The sedimentary regime and the structural framework of these mountains are those of Central Iran. But the existence of a consistent Zagros trend and nearly total lack of Tertiary volcanism helps to distinguish them from Central Iran. However a typical Central Iranian fault pattern with south-north, northeast, and west-east directions intersects the dominant northwestward Zagros trend (Stocklin 1968).

1.3.6 CENTRAL IRAN

Stocklin (1968) uses this term in a restricted sense. This structural zone (Figs. 1.2 and 1.3) consists of a roughly triangular area bounded by the Lut Block on the east, the Alborz mountains on the north and Sanandaj-Syrjan ranges on the southwest. The Central Iranian structural zone is separated from the Sanandaj-Syrjan ranges by a continuous zone of depressions including the Lake Oromieh (Rezaeieh), Gavkhuni and Jazmorian depressions. Central Iran was a platform during Paleozoic time and became a mobile orogenic zone in Mesozoic and Tertiary times. During the Mesozoic times pronounced unconformities, granite intrusions and incipient metamorphism occurred. At the same time the region was broken into numerous irregularly shaped fault blocks, some of which acted as subsiding grabens and others as horsts. The Alpine orogenic movements were also quite strong and are seen in the complex fault, fold and thrust structures in the ranges of central Iran. In the eastern part Stocklin (1968) noted a subzone bounded on the east by the Lut block and on the northwest and south by a conspicuous, bow-shaped westward-convex fault line. Within this region there is a series of subparallel faults with convexity decreasing eastward. These faults were

12

created in Late Triassic. The faults separate grabens with great thicknesses of Jurassic sediments from horsts where corresponding sediments are thin.

1.3.7 ALBORZ MOUNTAINS

The Alborz is a well defined mountain range at least in the central and eastern parts while the northwestern part is contiguous with the Zagros (Figs 1.2 and 1.3). This range has steep south thrusting on the south and steep north thrusting on the north. But normal faulting and folding have been equally important. The folding intensity decreases toward the Caspian Sea depression. According to Stocklin (1968) a nascent Alborz range existed in Paleocene time. Eastward, the Alborz range appears to be linked with the northern Hindukush and through this with the Pamir.

1.3.8 KOPET DAGH RANGE

The Kopet Dagh range lies in the border region between Iran and Turkmenistan (Figs. 1.2 and 1.3). This range consist of a Mesozoic-Tertiary sedimentary rock sequence deposited in a subsiding trough. The mountains arose in the latest Alpine orogenic movement. Stocklin (1968) recognized many similarities between Kopet Dagh and Zagros mountains.

1.3.9 LUT BLOCK

According to Stocklin (1968) to the Lut block is an irregularly outlined, essentially north-south-trending rigid mass smoothly surrounded by the ranges of Central and East Iran (Figs. 1.2 and 1.3). The block forced the north-south trend on the

13

bordering ranges. The block is divided in the north by the Nayband fault and Shotori range. This division occurred in Late Triassic time. Otherwise the Lut block has been remarkably stable through geologic time.

1.3.10 EAST IRAN AND MAKRAN RANGES

East of the Lut block there are the thick sedimentary sequences of Cretaceous to Eocene rocks and volcanic material which are folded intensely. These mountains lie outside the Iranian region. Extensive upper Cretaceous and Eocene rocks occur also in the west-east-trending Makran ranges which lie in the southeast corner of Iran (Figs. 1.2 and 1.3). These mountains appear to be a continuation of the Zagros.

1.4 SOME GEOPHYSICAL STUDIES IN IRAN

Several geophysical investigations have been carried out in Iran over the years . Here we summarize the results of gravity and seismological investigations specifically because the results are available in the public domain. Moreover the results from these investigations have a bearing upon the present work.

1.4.1 GRAVITY STUDIES

Dehghani and Makris (1983) have prepared summary maps of gravity investigations in Iran. Fig.1.4a is a contour map of Bouguer gravity anomalies. The maximum negative Bouguer anomaly of about 230 mgal occurs along the surface trace of MZT. Over much of Iran the Bouguer anomaly is of the order of -100 mgal. The Bouguer anomaly has small positive values along the northern boundary of Iran. The Zagros, Makran, and Alborz orogenic trends are very

14
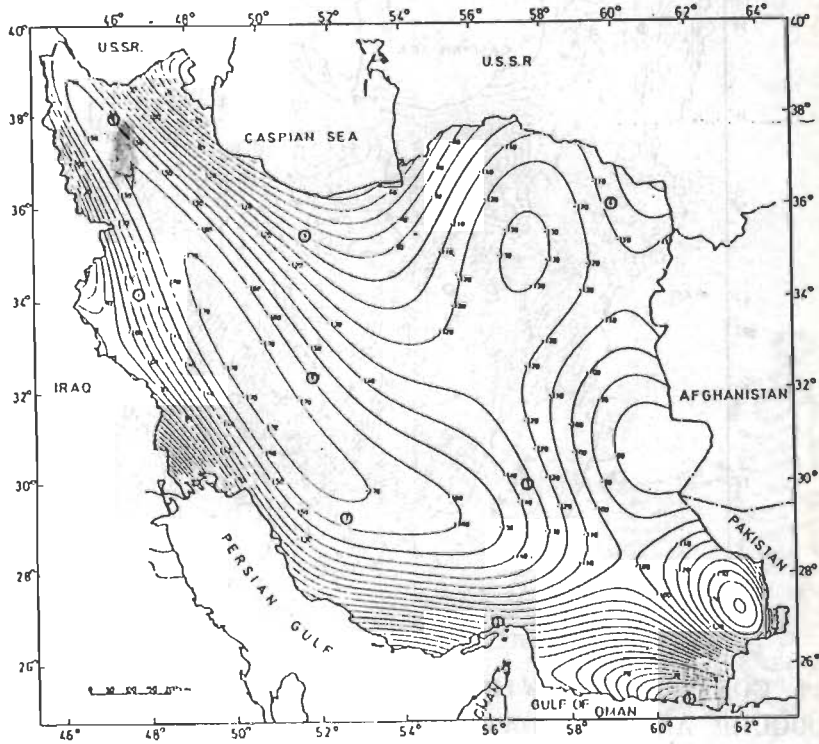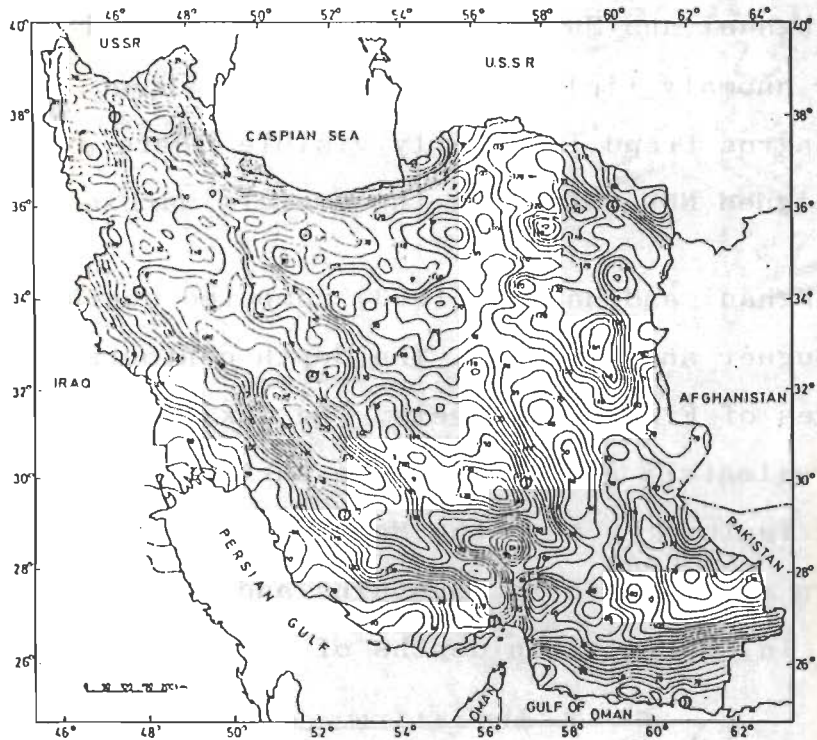
FIG. 1.4 BOUGUER GRAVITY ANOMALY (part a) AND REGIONAL BOUGUER ANOMALY (part b) MAPS OF IRAN (After Dehghani and Makris, 1983).

15

clearly brought out by the contours of Bouguer anomaly.

Dehghani and Makris (1983) also prepared a map of regional Bouguer anomaly field over Iran. It is shown in Fig. 1.4b. The broad Zagros trend is clearly visible There are three prominent lows aligned NNW-SSE along the eastern margin of Iran.

Dehghani and Makris (1983) computed depth of Moho (Fig. 1.5) from Bouguer anomaly data. The depth contours reflect the Bouguer anomalies of Fig. 1.4 closely. The maximum estimated depth of Moho is approximately 55 km under the surface trace of MZT. The other notable feature is that the Moho becomes rapidly shallow under the northern side of Alborz mountains and southern side of the Makran ranges. In Central Iran depths of the order of 35 km are reported.
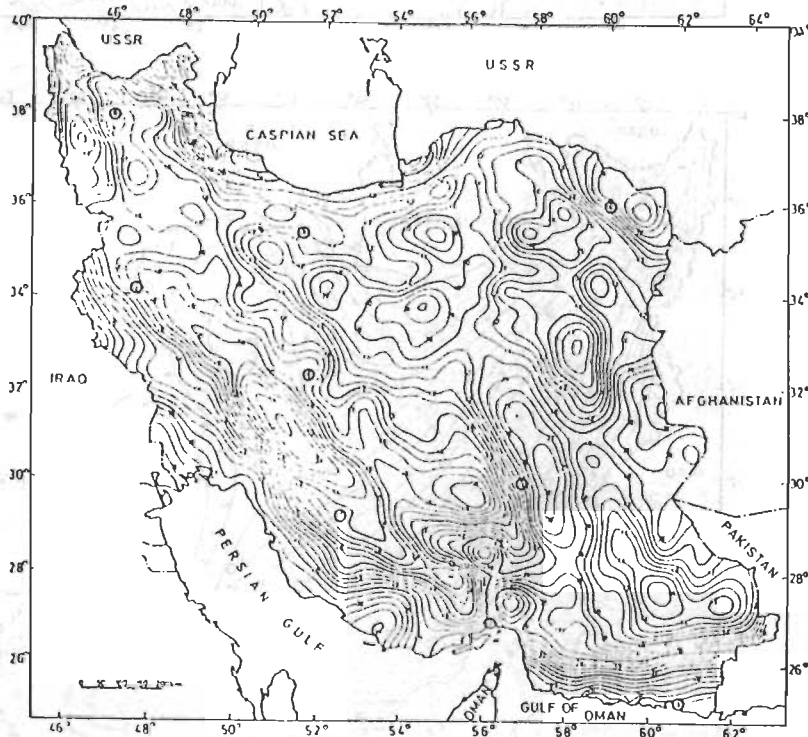
FIG. 1.5 CONTOURS SHOWING DEPTHS OF MOHO, COMPUTED ON THE BASIS OF BOUGUER ANOMALY DATA (After Dehghani and Makris 1983).

Tabriz   Shiraz

0
10
20
30
40
50
60

Mashhad   Shiraz

0
10
20
30
40
50
80

Tabriz   Mashhad

0
10
20
30
40
50
60

?
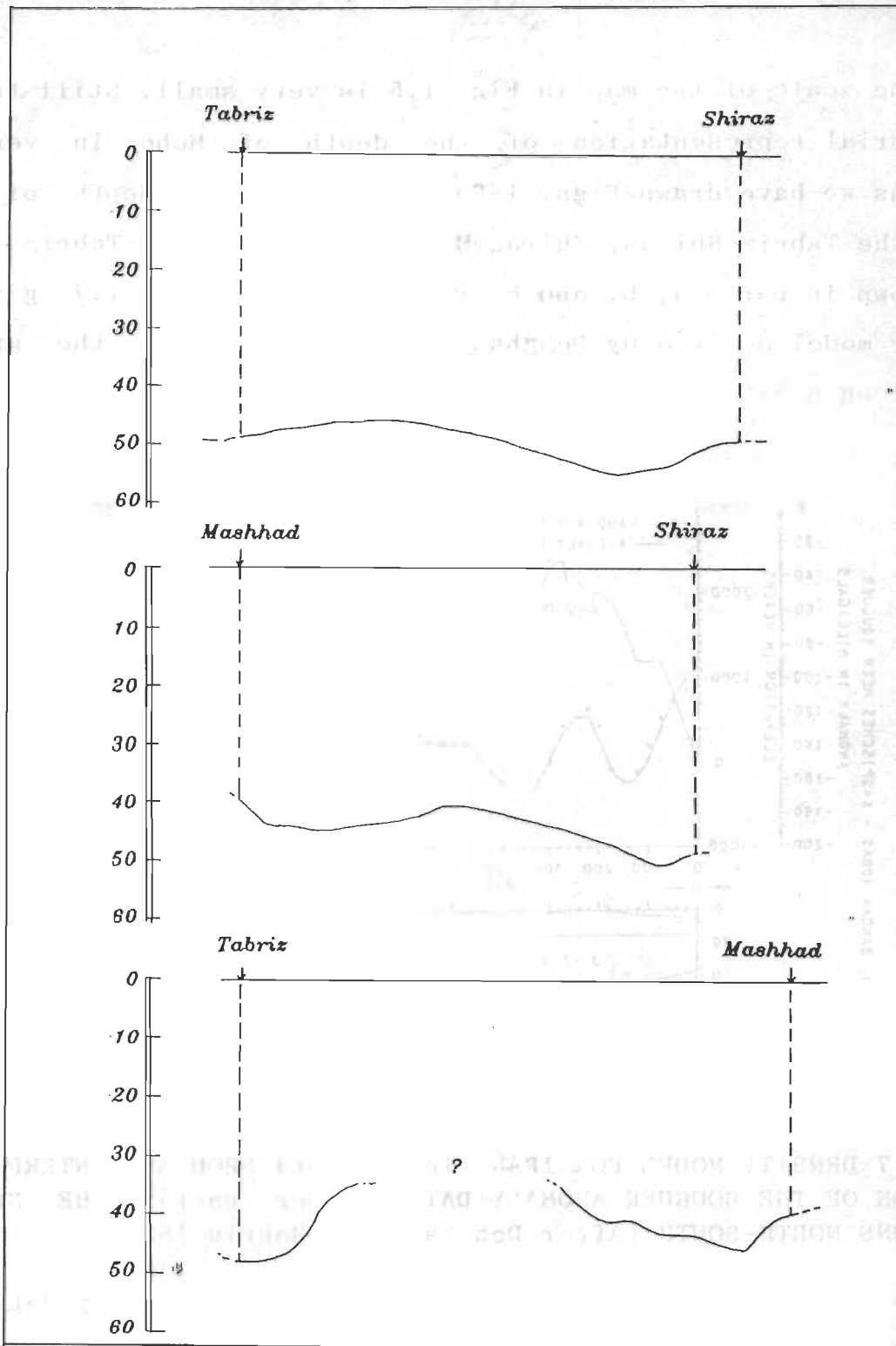
FIG. 1.6 DEPTHS OF MOHO ALONG TABRIZ-SHIRAZ, SHIRAZ-MASHHAD, AND MASHHAD-TABRIZ LINES DRAWN FROM Fig. 1.5.

The scale of the map in Fig. 1.5 is very small. Still to have a pictorial representation of the depth of Moho in vertical sections we have drawn Figs. 1.6a, b, and c. The depth of Moho along the Tabriz-Shiraz, Shiraz-Mashhad, and Mashhad-Tabriz lines are shown in parts a, b, and c respectively. Fig. 1.7 gives a density model derived by Dehghani and Makris. from the gravity data along a N-S section through Iran.
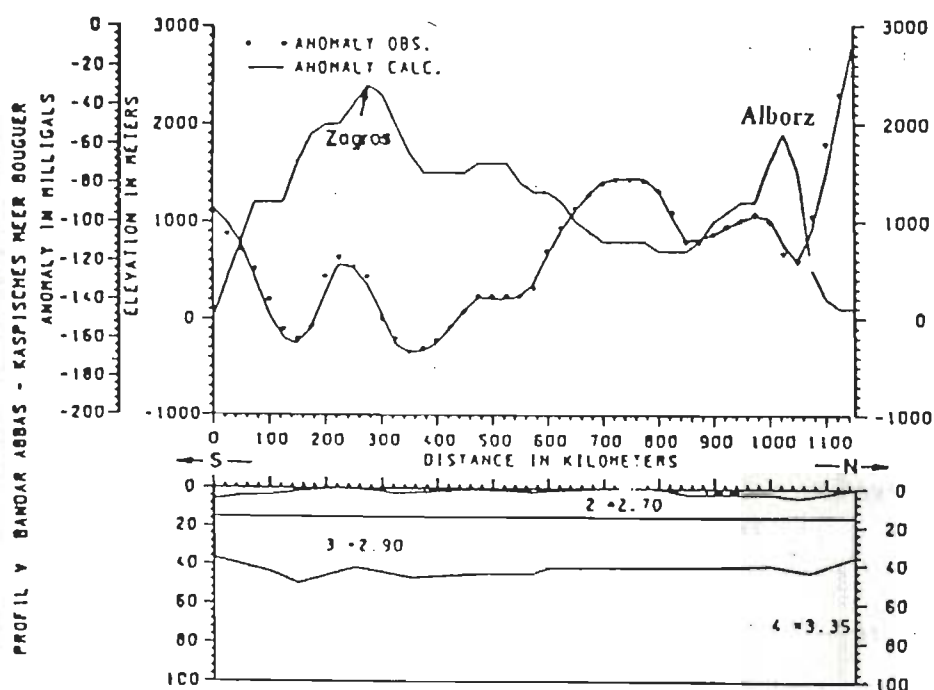
FIG. 1.7 DENSITY MODEL FOR IRAN (lower part) FROM AN INTERPRETAT-ION OF THE BOUGUER ANOMALY DATA (upper part). THE SECTION RUNS NORTH-SOUTH (After Dehghani and Makris 1983).

Snyder and Barazangi (1986) interpreted the gravity data for the Zagros mountain belt region to determine the deep crustal structure and flexure of the Arabian plate beneath the Zagros (Fig. 1.8). They estimated that the Moho dips about 1° to the

northeast beneath the Zagros folded belt and about 5° under the MZT. They estimated the depth of Moho to be 40 km under the Persian Gulf and about 65 km beneath the MZT. They suggested that a combination of isostatic, elastic flexure, horizontal compression forces acting on the edge of the Arabian craton and the transitional lithosphere of Central Iran appears to best model the crust of the Zagros region (sic).
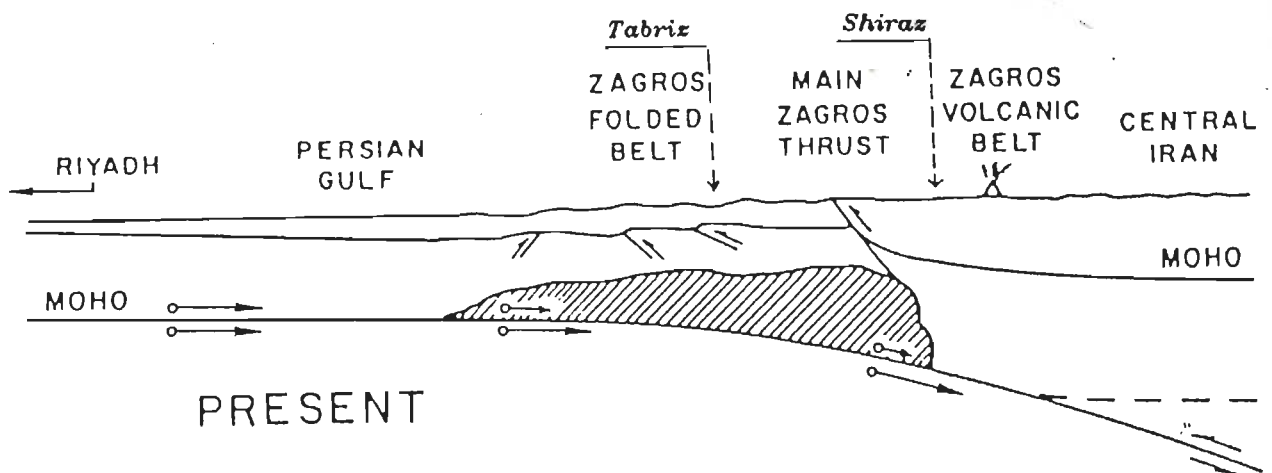
FIG. 1.8 A SCHEMATIC VERTICAL SECTION NORMAL TO THE TREND OF ZAGROS MOUNTAINS (After Snyder and Barazangi 1986)

1.4.2 SEISMOLOGICAL INVESTIGATIONS OF IRAN

Iran is a seismicaly active region (Fig.1.9). No part of Iran appears to be entirely free of earthquakes. As a result, several seismological studies have been carried out for the region. We

IRAN Earthquakes Distribution

(1900-1988)
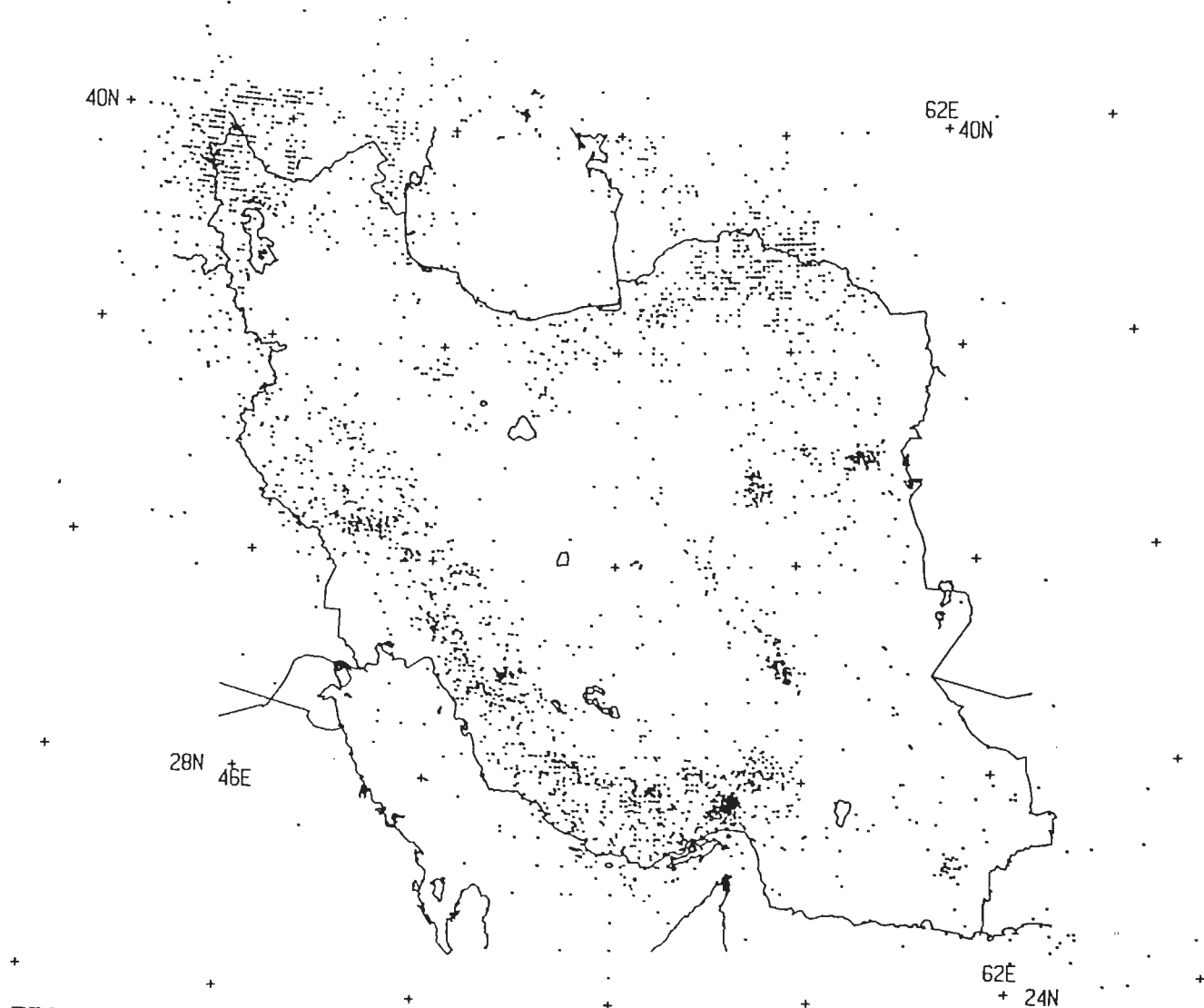
FIG. 1.9 EPICENTRAL MAP OF IRAN FOR THE PERIOD 1900-1988, THE
COORDINATES ARE TAKEN FROM A VARIETY OF SOURCES SUCH AS
USCGS, USGS, ISS, BCIS, MOS,... etc. (After Kamalian and
Mehrabian 1990).

shall discuss them in the following order:

    -Seismicity and seismotectonics

    -Crustal studies:

        . Near earthquake body waves

        . Attenuation of seismic waves

        . Surface waves

1.4.2.1 SEISMICITY AND SEISMOTECTONICS OF IRAN

Although Iran has an ancient civilization and the scourge of earthquakes has been felt for millennia, yet the first seismograph station appears to have been set up as late as 1959 (Moazami-Goudarzi 1972). Subsequently seismograph stations of WWSSN configuration were setup at Mashhad, Shiraz and Tabriz. Still later ILPA (Iranian Long Period Array) with telemetry system and seven stations was set up. Also since ca 1970 short term observation with portable seismographs have been initiated. As a result whereas before 1965 only earthquakes of magnitude (mb) grater than 4.5 could be located from teleseismic observations, the situation has improved somewhat in recent years. In addition an SRO instrument has been oprating since 1975.

Moazami-Goudarzi (1972) gave a list of 101 destructive earthquakes between 634 A.D. and 1898 A.D.. Ambraseys and Melville (1982) examined the historical records of Iran to prepare a list of damaging earthquakes. They expand the list by adding 6 earthquakes prior to 634 A.D.. The earthquake cited is of 3rd Millennium B.C..

1.4.2.2 EPICENTERS

Seismicity and seismotectonics studies of Iran have been carried out by Nowroozi (1976), Berberian (1976) and Kamalian and Mehrabian (1990). Most of these studies used epicentral and magnitude data for earthquakes since ca 1900 A.D. . The map shown in Fig. 1.9 is after Kamalian and Mehrabian (1990) and covers the period 1900-1988. Also Table 1.1 gives a list of the relatively more destructive (in terms of loss of lives) earthquakes of the past ninety years. During this time alone, casualties number about 130,000. Fortunately, the population density in most of the seismically active zones is relatively low, otherwise the casualties would have been many times more. This is borne out by the large number of casualties in the case of the Buyin Zahra earthquake of 1962 and Rudbar earthquake of 1990, which occurred in the moderately density populated regions. Fig. 1.10 shows the epicenters of these destructive earthquakes.

Nowroozi (1976), and Berberian(1976) have tried to correlate earthquake epicenters with specific tectonic features and faults in Iran. However because of lack of sufficient precision in estimating the epicentral coordinates the attempts were not very successful. Still we note that Nowroozi (1976) has divided Iran in 23 seismotectonics provinces Fig. 1.11. Broadly, the Zagros mountains the Alborz mountains are seismicaly most active in Iran. In addition several important earthquakes have occurred in and around the Lut block.

1.4.2.3 FOCAL DEPTH

Estimation of focal depths of Iranian earthquakes has posed a

TABLE 1.1 SOME STRONG AND DESTRUCTIVE EARTHQUAKES OF IRAN (1900 - 1990)

No	Date	Orig. Time	coordinate N	E	mb	No. of casualties	Location
1	1909 01 23	02 48 18	33.	50.	7.4	5000	Silakhor (Dorud)
2	1923 05 01	15 37 22	38.	56.8	7.0	3257	N Shirvan
3	1923 05 25	22 21 25	35.3	59.2	5.5	2219	Torbat Heydariyeh
4	1930 05 06	22 34 27	37.	44.	7.2	2514	Salmas
5	1953 02 12	08 15 31	35.8	55.	7.	930	Torud (E Semnan)
6	1957 07 02	00 42 22	36.21	52.72	6.5	970	Sangechal (S Babol)
7	1957 12 13	01 45 05	34.4	47.67	6.5	1130	Farsinaj (N Sahneh)
8	1960 04 24	12 14 27	27.7	54.43	5.5	1500	Lar
9	1962 09 01	19 20 40	35.58	49.88	7.2	12225	Buyin Zahra
10	1968 08 31	10 47 37	34.	59.	7.3	7000	Dasht-e-Bayaz
11	1972 04 10	02 06 53	28.4	52.8	6.1	5000	Qir Karzin
12	1976 11 24	12 22 19	39.12	44.03	6.1	400	Maku
13	1978 09 16	15 35 57	33.386	57.434	6.5	15000	Tabas
14	1981 07 28	17 22 25	30.013	57.794	5.7?	??	Golbaf
15	1990 07 20	21 00 10	36.957	49.409	7.3	40000	Rudbar

IRAN Earthquakes Distribution (Mb>6.0)

(1900-1990)

Caspian Sea

Persian Gulf
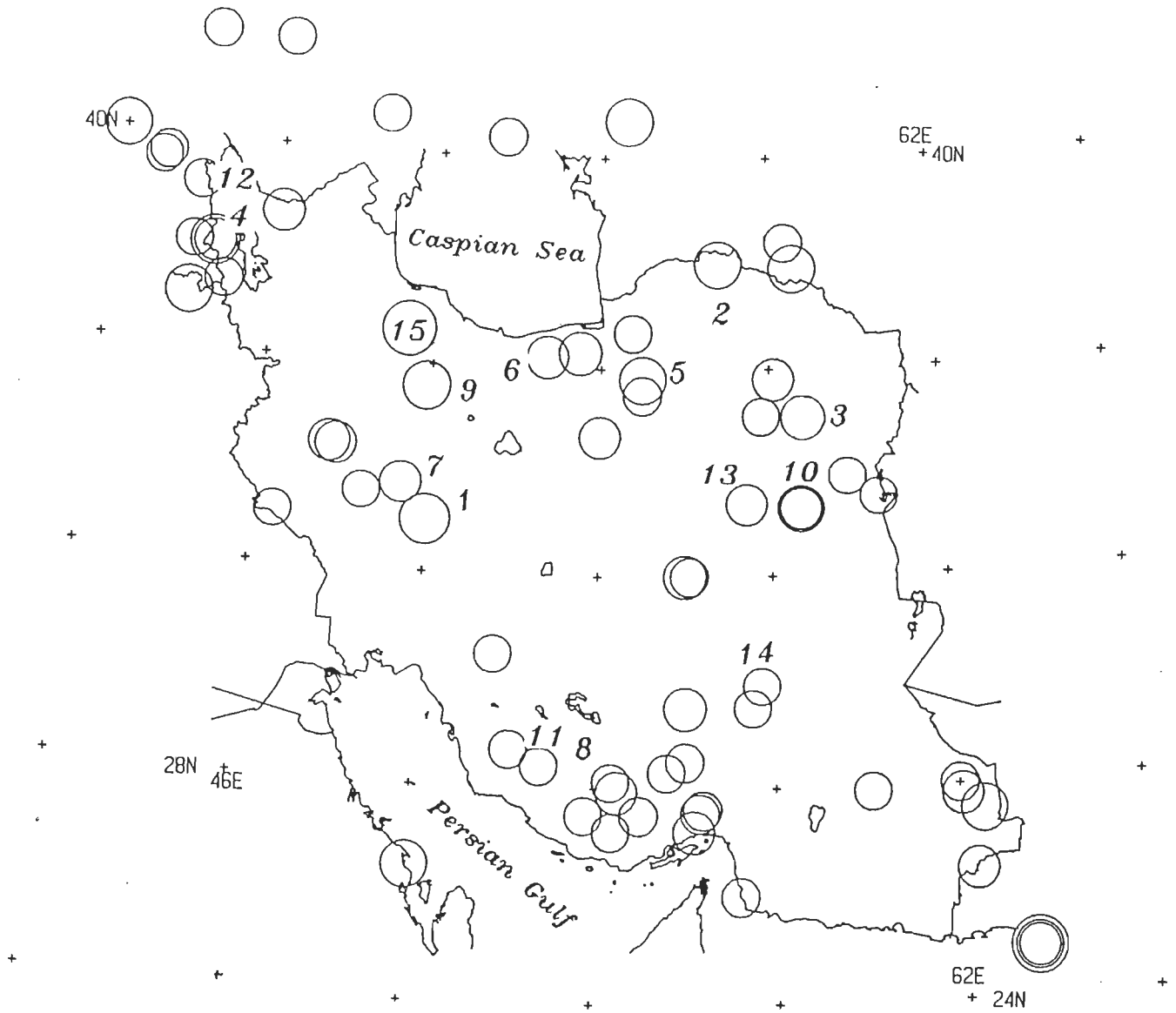
FIG. 1.10 EPICENTERS OF EARTHQUAKES LISTED IN TABLE 1.1 ARE SHOWN WITH THE HELP OF NUMBERS GIVEN IN THE FIRST COLUMN OF THE TABLE. THE FIGURE ALSO CONTAINS EPICENTERS OF EARTHQUAKES WITH MAGNITUDE mb>6 DURING THE PERIOD 1900-1990.

24
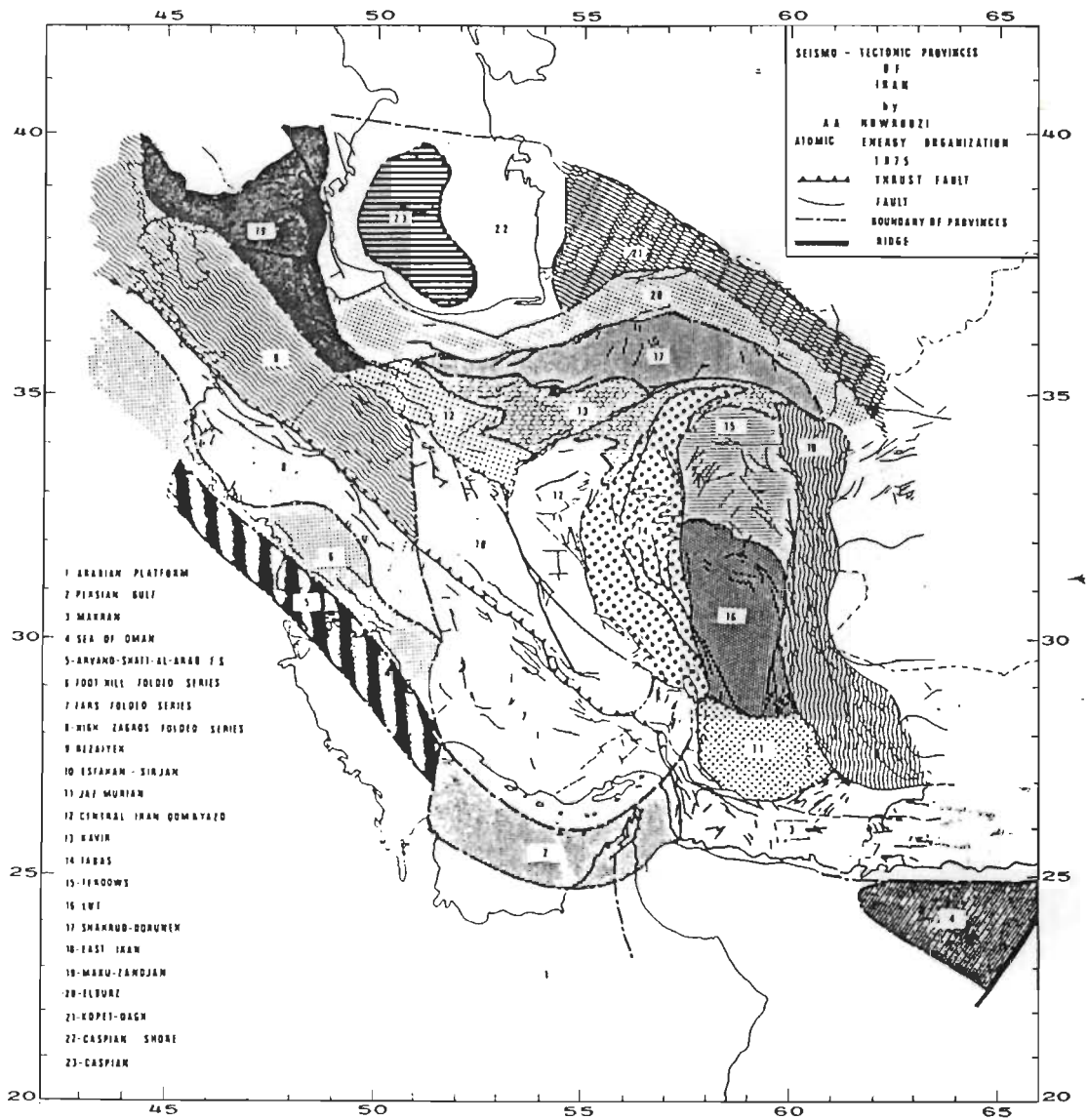
FIG. 1.11 SEISMOTECTONIC PROVINCES OF IRAN ACCORDING TO Nowroozi 1976.

Tabriz

Caspian Sea

Mashhad

Tehran

60〉Dep.〉70   km
70〉Dep.〉100   km
Dep.〉100   km

Shiraz

Persian Gulf

Oman Sea
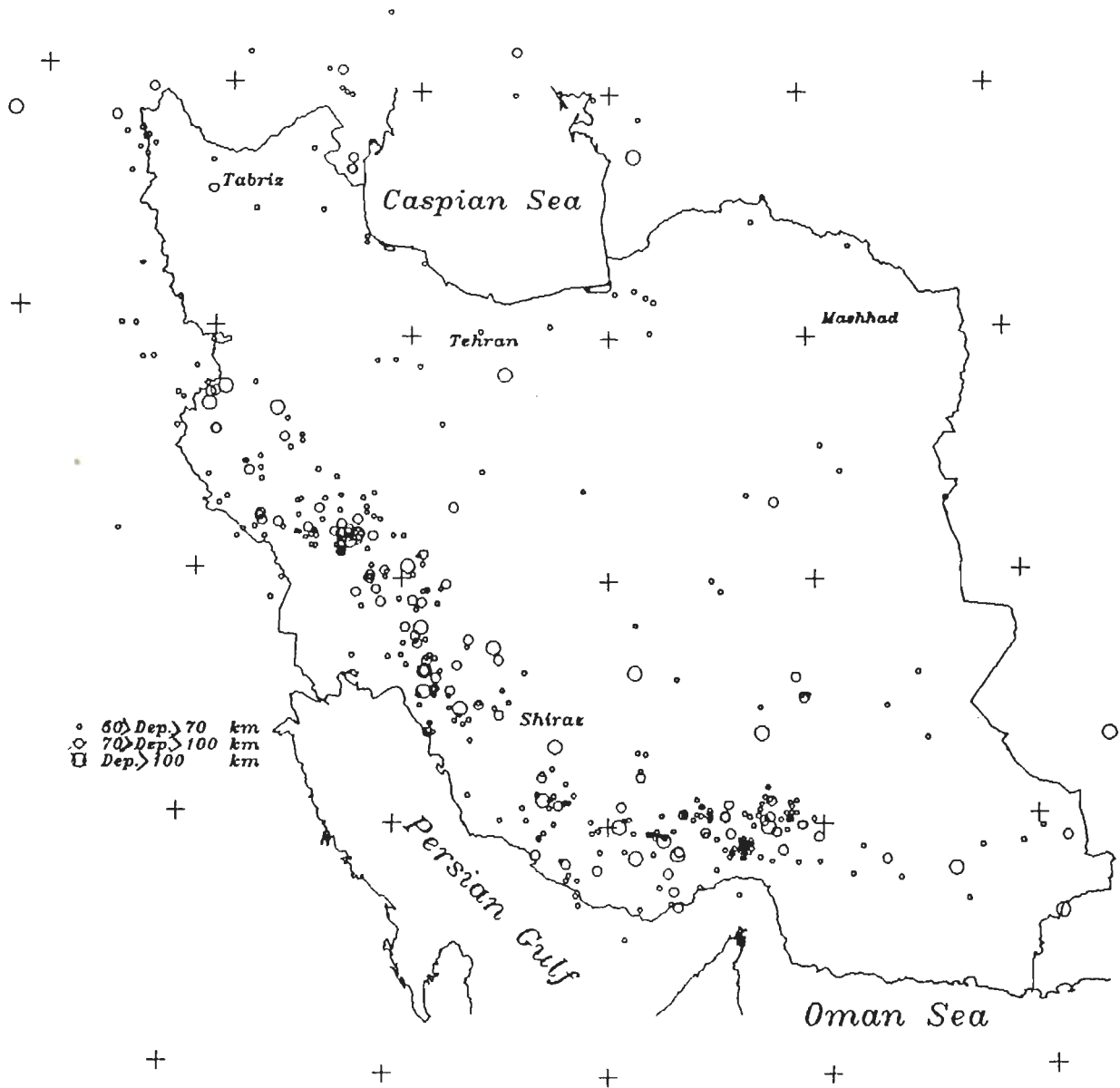
FIG. 1.12 EPICENTRAL OF EARTHQUAKES WITH ESTIMATED FOCAL DEPTH
GREATER THAN 50 KM. THE SOURCES OF DATA ARE THE SAME AS FIG. 1.9

problem due to paucity of near stations. However the situation has improved somewhat in the past twenty five years. Among the reported estimates of focal depths, the range is between 10 and 279 km. The vast majority of earthquakes with focal depths greater than 50 km have been observed along the Zagros and Makran Ranges, with only a handful of such earthquakes scattered over the rest of Iran Fig. 1.12.

1.4.3 FAULT PLANE SOLUTIONS

The number of fault plain solutions available for Iranian earthquakes is still relatively limited. An important early compilation was by Nowroozi (1971) (Fig. 1.13). For earthquakes of the Zagros mountains, the solutions are similar and the compressional axes are approximately perpendicular to the trend of the Zagros. Nowroozi (1971) reports an average trend of N42° for the compressional axes which is only 3° from perpendicular to the N315° strike of the Zagros thrust. In Central Iran and the Alborz region the compressional axes are again approximately perpendicular to the general trends of the structures. This is in agreement with the NE movement of the Arabian plate and absorption of the movement in the the compressional features north of the Zagros thrust. The compressional axes for the earthquakes in the Caucasus and Kopet Dagh structure are also nearly perpendicular to the general trend of the geological structures.

Dewey and Grantz (1973) reported the U.S. Geological Survey determination of the fault plain solution for the Qir earthquake (No. 11 in Fig. 1.10) of April 10, 1972, which occurred in the Zagros folded belt. The WNW striking nodal plain with reverse

motion was picked as the fault plain. Its strike is parallel to the local trend of the folds and thrust faults of the Zagros folded belt.
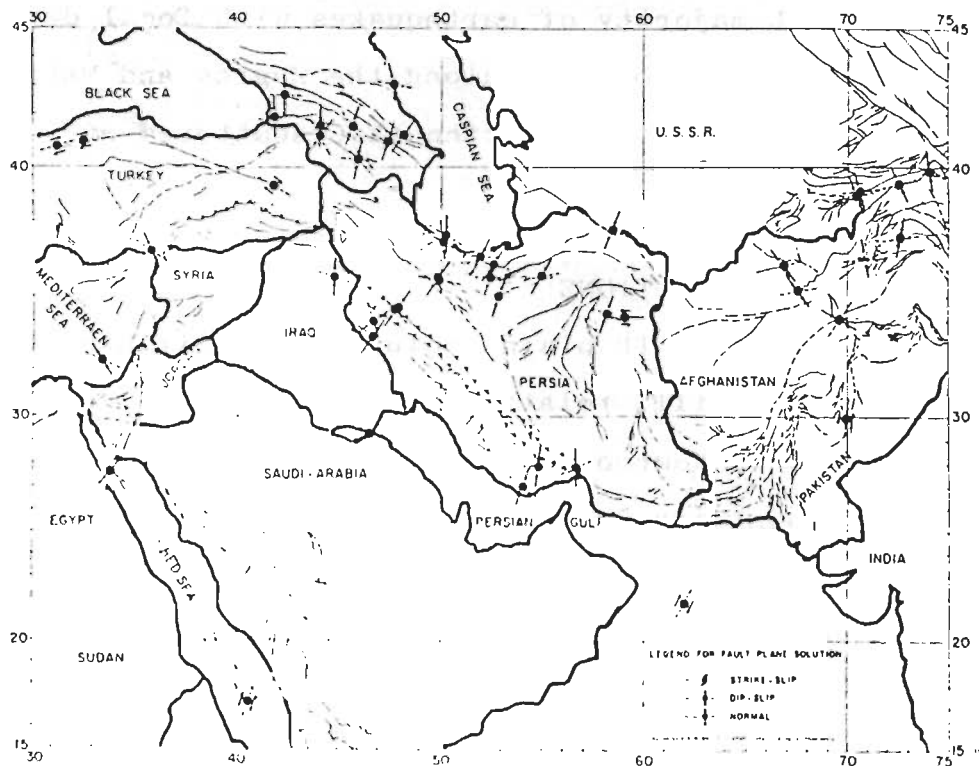
FIG. 1.13 SELECTED FAULT PLANE SOLUTION IN IRAN. THE ARROWS SHOW (i) THE DIRECTION OF MOTION FOR STRIKE-SLIP FAULT, (ii) THE DIRECTION OF COMPRESSIONAL AXIS FOR THE NORMAL FAULT. (After Nowroozi 1971)

For the Rudbar earthquake (No. 15 in Fig. 1.10) of June 20, 1990, U.S. geological survey has given a strike slip fault plain solution. The reported azimuth of $N63^\circ$ for the compressional axes is in general agreement with the compressional axes shown by Nowroozi (1971) for the earlier earthquakes of region (Fig. 1.13). Fig. 1.14 is a display of aftershock epicenters. Choice of the nodal plain with a strike of $N288^\circ$ as the fault plain is preferable.

28

City

Station

Aftershock

Main shock

Anzali

Rasht

Masuleh

Zanjan

Manjil

Loshan
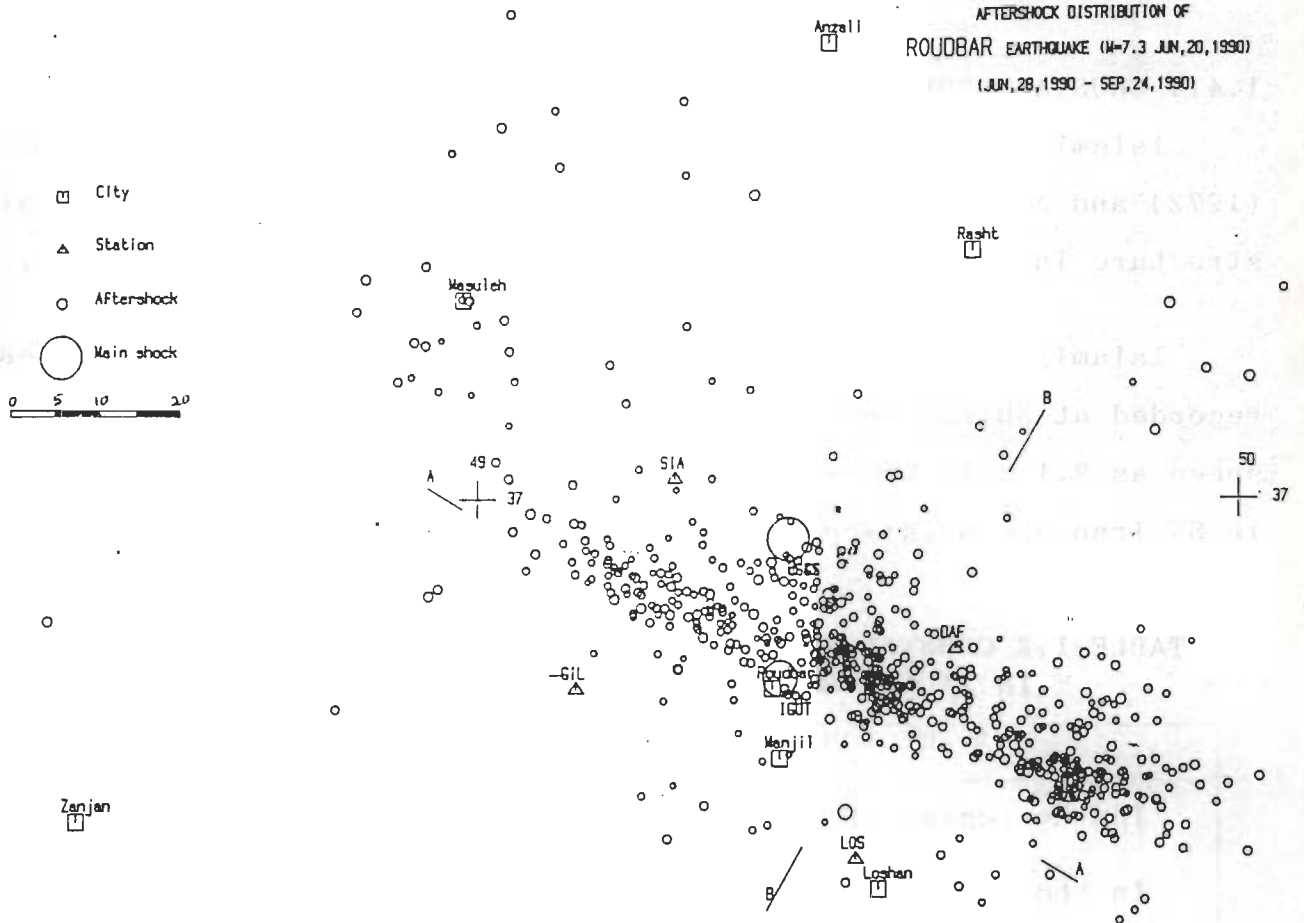
FIG. 1.14 EPICENTRAL DATA FOR THE ROUDBAR EARTHQUAKE OF 1990.
THREE STATION DATA WERE USED IN MOST CASES. EPICENTRAL
LOCATIONS OBTAINED BY USING HYPO-71. FOR ABOUT %25 OF
EARTHQUAKES DATA FROM ADDITIONAL STATIONS COULD BE USED
(After Kamalian and Mozzafari 1990).

29

Recently Baker et al. (1993) have investigated fault plain solution of earthquakes on the Kazerun line in the Zagros mountains and have documented evidence for strike slip faulting within this fold-and-thrust belt.

1.4.4 CRUSTAL STRUCTURE

Islami (1972 and 1974), Moazami-Goudarzi and Sadeghzadeh (1972) and Anzabi (1981) have attempted to determine the crustal structure in different parts of Iran using local earthquake data.

Islami (1972) investigated seismograms of 59 earthquakes recorded at Shiraz and Kermanshah. He estimated subMoho P wave speed as 8.1 ±.11 km/sec. His estimates of the thickness of crust in SW Iran are as given in Table 1.2.

TABLE 1.2 CRUSTAL THICKNESSES NEAR SHIRAZ AND KERMANSHAH IN ZAGROS MOUNTAINS (After Islami, 1972).

REGION	Thickness
In the region S to SE of Shiraz	42 ±4 km
In the region N to NW of Shiraz	57 ±3 km
In the region S and SE of Kermanshah	57 ±6 km
In the region around Shiraz	48 ±4 km
In the region around Kermanshah	48 ±6 km

Moazami-Goudarzi and Sadeghzadeh (1972) interpreted data for 284 near earthquakes recorded at Shiraz to estimate P wave speeds in a two layered crust resting on the upper mantle. The model is

summarized in Table 1.3. The total crustal thickness estimated was
45 km.

TABLE 1.3 CRUSTAL MODEL NEAR SHIRAZ
(After Moazami – Goudarzi 1972)

Layer	Thickness(km)	P speed (km/sec)
I	15	6.
II	30	7.
III	Moho	Not given

Islami (1974) calculated the thickness of the crust around
Shiraz by using 32 earthquakes recorded at Shiraz.   The estimated
thickness is 42±7 km using all the data and 44±5 km using 21
selected earthquakes.

Hedayati et al., (1976) used data from a micro-earthquake
investigation of Tehran region to propose a model with three
layers over a half space for the crust and upper mantle. They
estimated a total crustal thickness of about 31 km Table 1.4. This
region is in north central   Iran (Fig. 1.1).

TABLE 1.4 CRUSTAL MODEL FOR TEHRAN REGION
(After Hedayati 1976)

Layer No.	Thickness (km)	α (km/s)	β (km/s)
1	2	3.45	2.0
2	16	5.85	3.4
3	13	6.70	3.9
Mantle	—	Not given	

31

Maleki 1980 used the HYPO-71 computer program to analyze data for 300 local earthquakes recorded by the ILPA . He constructed a model with two layers upon a half space that gave the smallest root mean square error. He concluded that the depth of Moho in Iran is greater than 35 km and it is between 40 to 50 km in Zagros region.

Anzabi (1981) estimated the thickness of Moho and the subMóho P wave speed using P_n data recorded at Tehran and Tabriz for earthquakes occurring in eastern Iran and Turkey. The results are summarized in Table 1.5.

TABLE 1.5 CRUSTAL THICKNESS IN NORTHERN IRAN
(After Anzabi 1981)

Earthquake epicenter	Station	P wave speed (km/s)	Thickness (km)
E. Iran	Tabriz	8.1	56
E. Iran	Tehran	8.0	47
E. Turkey	Tabriz	7.9	46
E. Turkey	Tehran	8.1	56

Chen et al. (1980) examined propagation of upper mantle P (i.e. Pn phase) in the Iranian region using data from Tabriz, Shiraz, and Mashhad stations. They hypothesized that the Moho dips under Iran at about 1° due SSE. They estimated that the crustal thickness increases from 34 km in the north to 49 km in the south. The P wave speed in uppermost mantle was estimated to be 8.0 ± 0.1 km/s.

Kadinsky-Cade et al. (1981) examined propagation of Pn, Sn
and Lg phases under the Iranian plateau. Fig. 1.15 is extracted
from their Fig. 24. In this figure values of 8.0 km/s and above
refer to Pn speeds, 4.4 to 4.7 km/s to Sn speeds, and 3.1 to 3.5
km/s for Lg speeds. They observed that Sn phase does not propagate
efficiently under the Alborz mountains and northeastern Iran.
However this phase propagates under the Caspian Sea as well as in
the rest of the Iranian region.
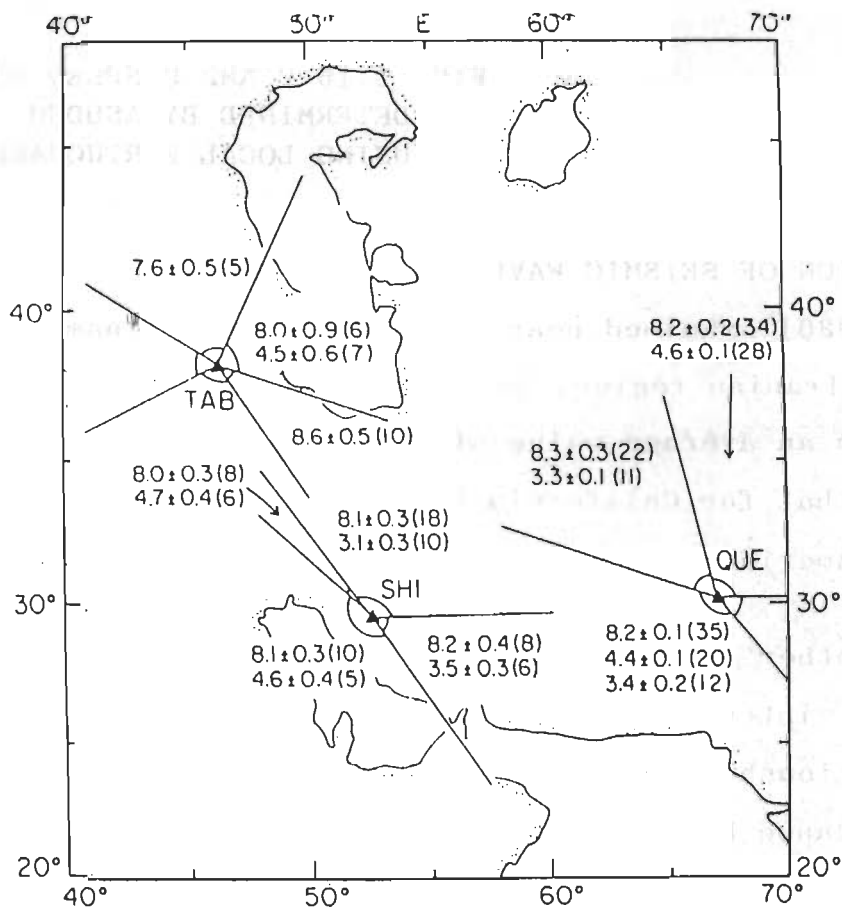
FIG 1.15 EXTRACT OF RESULTS FROM KADINSKY-CADE et al. (1981)
REGARD Pn, Sn, AND Lg PHASE IN AND AROUND IRAN (SEE TEXT)

Asudeh (1982) examined near earthquake data recorded at Mashhad and Shiraz from the aftershock sequence of the Tabas earthquake of October 1978. Fig. 1.16 is a display of the inferred P and S speeds. The surprising result is the value of 7.7 km/s for the upper mantle P speed.

VELOCITY, KM/S
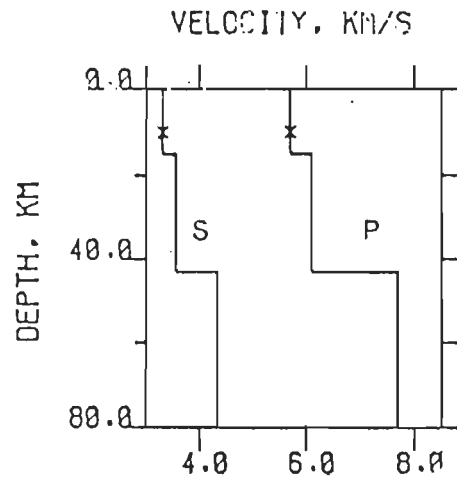
FIG. 1.16 P AND S SPEED PROFILES
DETERMINED BY ASUDEH (1982)
USING LOCAL EARTHQUAKES DATA

1.4.5 ATTENUATION OF SEISMIC WAVES

Nuttli (1980) examined near earthquakes phases namely P_n, P_g, S_n, and L_g for Iranian region. He estimated that the anelastic attenuation has an average value of 0.0045 km^{-1}. He regarded it to be similar to that for California but much greater than that for eastern North America.

On the other hand Chandra et al., (1979) estimated attenuation of intensities in Iran. They gave the following empirical relationship for average attenuation of intensity with epicentral distance R in km .

$$I(R) = I_o + 6.453 - 0.00121R - 4.960 \log(R+20) \qquad R < 120 \text{ km}$$

1.4.6 CRUSTAL STRUCTURE FROM SURFACE WAVES IN IRAN

In order to test his ideas about lithosphere deformation along the Zagros mountain belt, Bird (1978) considered Rayleigh wave dispersion for local earthquakes. Using the Multiple Filter Technique. He computed group speeds and then fitted the model of Table 1.6 and Fig. 1.17 to these data. In this way a crustal thickness of 45.6 km along the Zagros was estimated.
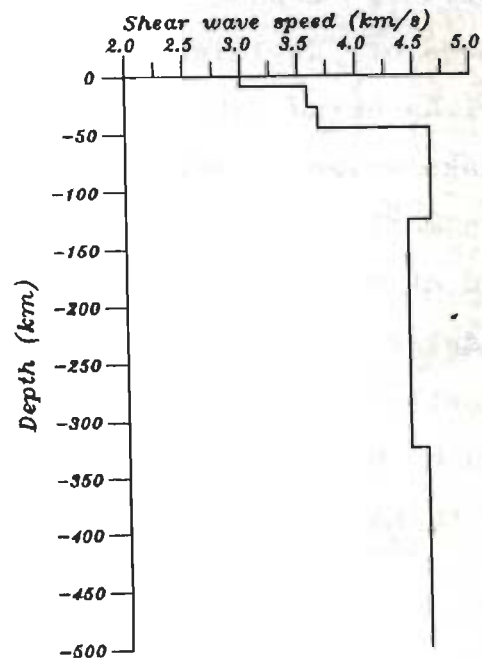
FIG 1.17 SHEAR WAVE PROFILE IN THE CRUST AND UPPER MANTLE UNDER ZAGROS (AFTER BIRD 1978)

TABLE 1.6 CRUSTAL AND UPPER MANTLE MODEL FOR ZAGROS USING RAYLEIGH WAVE GROUP SPEEDS (After Bird 1978)

Depth range (km)	Vp (km/s)	Vs (km/s)	Density (g/cm^3)
0. – 9.0	5.2	3.00	2.6
9.0 – 27.3	6.2	3.58	2.7
27.3 – 45.6	6.4	3.67	2.87
45.6 – 125.0	8.17	4.65	3.4
125.0 – 325.0	8.17	4.45	3.4
325.0 – ∞	8.80	4.60	3.65

McCowan (1978) examined
propagation of fundamental and
first mode of Rayleigh waves
across Iran using data for an
earthquake which occurred in
southern most Zagros and was
recorded at Mashhad. Fig. 1.18
is a display of crustal and
upper mantle P and S speeds
obtained by him. The estimated
crustal thickness is 55 km.

The surface wave
analysis by Asudeh (1982)
comes closest to the analysis
undertaken by us. He examined
Rayleigh wave phase speeds
along the Zagros and Central
Iran paths using two station
technique and data from
Tabriz, Shiraz, and Mashhad
stations. However the number
of earthquakes considered were
only 4 and 2 for these paths

FIG. 1.18 CRUSTAL AND UPPER MANT-
LE MODEL FOR IRAN BY Mc-COWAN
(1978) USING RAYLEIGH WAVE
GROUP SPEEDS.

respectively. In addition he examined Rayleigh wave data for two
earthquakes recorded at Mashhad (SRO) and ILPA. Fig. 1.19 is a
display of the shear wave speed profiles obtained by Asudeh (1982)
for these regions. Crustal thicknesses of 46, 43, and 45 km in the
Zagros, Central Iran and Alborz regions were estimated.
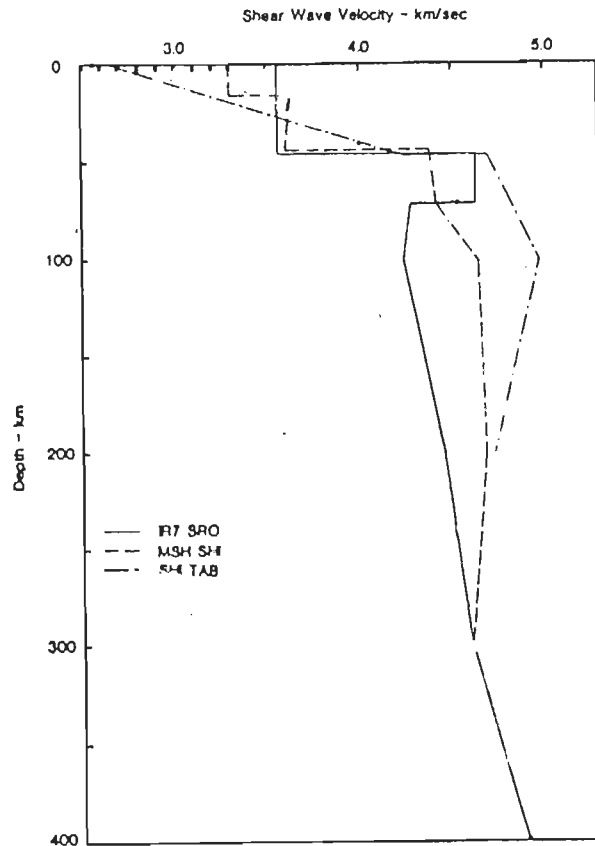
FIG. 1.19 SHEAR WAVE SPEED PROFILE DETERMINED BY ASUDEH (1982) USING RAYLEIGH WAVE PHASE SPEEDS.

1.5 ABOUT OF THE THESIS

The following chapters provide a description of our investigations of Rayleigh wave dispersion across Iran. Chapters 2 and 3 summarize the theoretical formulations, algorithms and computer programs and their tests. The next three chapters are devoted to discussions of data collection, Rayleigh wave phase speed results and inversion of these results. Chapter 7 includes a critical discussion of the various aspects of the work described in Chapters 2 to 6. This is followed by a chapter on conclusions. Suggestion for future work and four appendices are also included.

37

CHAPTER-2
THEORETICAL FRAMEWORK

2.1 GENERAL

In this thesis the determination of the phase speeds of Rayleigh waves recorded at Mashhad, Tabriz, and Shiraz follows the standard two station procedure. Also for the interpretation of observed dispersion curves in terms of crust and upper mantle structure we use the well known generalized inverse solution (e.g., Yuan and Nazarian, 1993) using the approach of Singular Value Decomposition (SVD) of a rectangular matrix . The matrix method of Schwab and Knopoff (1972) is used to compute phase speed curves for assumed crustal and upper mantle structures. Hence no claim is made here regarding originality in these matters. However every computer program used in this thesis was written by us and tested thoroughly. The only exception to this statement is the subroutine for evaluation of layer matrices which was adopted directly from Schwab and Knopoff (1972). But a review of all these methods is included here for the sake of completeness as well as with the hope that other Iranian workers who will read this thesis may get necessary direction for further background reading. The fast Fourier transform (FFT) program is also used in the present thesis and compilation of relevant formula in this connection are given in Appendix A.

2.2 PHASE SPEED AND GROUP SPEED

Following Dziewonski and Hales (1972), assume that an earthquake has generated single mode surface waves, for example, the fundamental Rayleigh mode, and that these waves have been recorded at a seismograph station at an epicentral distance r and azimuth β from the source. The Fourier transform of the recorded signal $f(t)$ { $f(t)=0$, $t\leq 0$}, is

$$F(\omega)=\int_{0}^{\infty} f(t).e^{-i\omega t} dt=A(r,\beta,\omega).e^{i\phi(r,\beta,\omega)} . \qquad ...(2.1)$$

Here ω is the angular frequency. The amplitude function $A(r,\beta,\omega)$ depends, in general, on the earthquake source mechanism, source depth, orientation of fault, elastic and dissipative parameters of the medium, and amplitude response of the seismograph system at the recording station. Measurements of the amplitude function are of primary importance in earthquake mechanism studies and determination of **Q** (attenuation information). The phase $\phi(r,\beta,\omega)$ is the sum of three terms

$$\phi(r,\beta,\omega)=-k(\omega).r+\phi_{o}(\beta,\omega) +\phi_{i}(\omega) \qquad ...(2.2)$$

where $k(\omega)$ is the wave number ($k(\omega)=2\pi/\lambda$, $\lambda(\omega)$ is the wavelength), $\phi_{o}(\beta,\omega)$ is the source phase shift, and $\phi_{i}(\omega)$ is the instrument phase shift.

For the purpose of defining the basic parameters, phase and group speeds, describing a dispersive wave train, let us neglect for the time being, the phase shift ϕ_{o}, and ϕ_{i}. The inverse Fourier transform of eq. (2.1) is

$$f(t) = \frac{1}{2\pi} \int_0^\infty A(r,\beta,\omega) . e^{i(\omega t - kr)} \, d\omega \qquad . \qquad \ldots(2.3)$$

The speed of propagation of monochromatic wave of frequency ω_0 can be found from the condition that

$$\omega_0 . t - k(\omega_0) . r = \text{constant} \qquad \ldots(2.4)$$

for all r, provided that k is not a function of r. Thus, differentiating (2.4) with respect to r we have

$$\omega_0 \frac{dt}{dr} - k(\omega_0) = 0$$

and the phase speed $c(\omega_0)$ is

$$c(\omega_0) = \frac{dr}{dt} = \frac{\omega_0}{k(\omega_0)} \qquad . \qquad \ldots(2.5)$$

The signal is dispersed if $c(\omega)$ is not a constant.

Group speed corresponds to the speed of propagation of the maximum energy. Let us evaluate Eq. (2.3) in the vicinity of frequency ω_0

$$f(t)_{\omega_0} = \int_{\omega_0 - \varepsilon}^{\omega_0 + \varepsilon} A(r,\beta,\omega) . e^{i(\omega t - kr)} \, d\omega. \qquad \ldots(2.6)$$

The function $f(t)_{\omega_0}$ will assume its maximum value when all the waves within the frequency band ($\omega_0 - \varepsilon$, $\omega_0 + \varepsilon$) are in phase, or

$$\frac{d}{d\omega} \left(\omega t - kr \right)_{\omega = \omega_o} = 0 \qquad \qquad \ldots(2.7)$$

The group speed $u(\omega_o)$ will be found from the relation

$$t_{\omega_o} = \left(\frac{dk(\omega)}{d\omega} \right)_{\omega_o} \cdot r$$

Therefore

$$u(\omega_o) = \frac{r}{t_{\omega_o}} = \left(\frac{d\omega}{dk(\omega)} \right)_{\omega = \omega_o} \qquad \ldots(2.8)$$

Group speed can be found from phase speed as

$$u(\omega) = c(\omega) + k(\omega) \cdot \frac{dc(\omega)}{dk(\omega)} \qquad \qquad \ldots(2.9)$$

2.3 DETERMINATION OF PHASE SPEED BY AKI'S TWO STATION METHOD USING THE CONVOLUTION APPROACH

For the retrieval of phase speed information from seismograms we have chosen to rely exclusively on Aki's two station method because in principle, it eliminates the need for complete knowledge of the seismic source. The two stations involved should lie, as nearly as possible, on the same great circle through the epicenter. Let us assume that we have digitized seismograms from two such stations. They contain a single mode surface wave train. Let t_1 and t_2 be the times of starting of digitization at first and second stations respectively from the epicenter. By application of the Fourier transform we can extract the phase information and construct a phase delay curve $\phi(\omega)$. Since the Fourier transform yields phase information only for an angle

42

interval $(0, 2\pi)$ it is necessary to assure continuity of the function $\phi(\omega)$ by addition or subtraction of $2N\pi$ where N is an appropriate integer number of circles. It follows from (2.6), without neglecting any phase shift term, that

$$\omega t_1 - k(\omega).r_1 = \phi_1(r_1,\beta_1,\omega) + \phi_0(\beta_1,\omega) + \phi_{i1}(\omega) + 2\pi n_1 = \phi_1 + 2\pi N_1$$

$$\omega t_2 - k(\omega).r_2 = \phi_2(r_2,\beta_2,\omega) + \phi_0(\beta_2,\omega) + \phi_{i2}(\omega) + 2\pi n_2 = \phi_2 + 2\pi N_2$$

By subtraction of say the first equation from the second and rearrangement, we have

$$c(\omega) = \frac{\omega}{k(\omega)} = \frac{r_2 - r_1}{(t_2 - t_1) - ((\phi_2 - \phi_1) + 2\pi N)/\omega} \qquad \ldots(2.10)$$

where $\phi_2 - \phi_1$
$$= \phi_2(r_2,\beta_2,\omega) - \phi_1(r_1,\beta_1,\omega) + \phi_{i2}(\omega) - \phi_{i1}(\omega) + \phi_0(\beta_2,\omega) - \phi_0(\beta_1,\omega) + 2\pi N$$
$$\ldots(2.11)$$

and $N = N_2 - N_1$. The formula may be rewritten in terms of period T as follow

$$c(T) = \frac{r_2 - r_1}{(t_2 - t_1) - T.((\phi_2 - \phi_1)/2\pi + N)} \qquad \ldots(2.12)$$

In Eqs. 2.10 and 2.11 the term $(\phi_0(\beta_1,\omega) - \phi_0(\beta_2,\omega)) \cong 0$ because of the location of stations and the epicenter on the same great circle approximately. The term $(\phi_{i2}(\omega) - \phi_{i1}(\omega))$ may be neglected if the two stations use the same instruments with the same impulse responses or have identical calibration curves.

The term $\phi_2(\omega)-\phi_1(\omega)$ can be computed by taking separate Fourier transforms of the wave trains recorded at two stations . Alternatively we may take first the cross correlation of the two signals and then compute the phase of this function using the FFT. According to Dziewonski and Hales (1972), the latter procedure is to be preferred in view of instabilities in the former method in the presence of noise. We have adopted the convolution approach consistently.

2.4 SCHWAB AND KNOPOFF'S ALGORITHM FOR COMPUTATION OF PHASE SPEEDS FOR A LAYERED MEDIUM

All geophysical data interpretation problems are inverse problems in which, we have to construct models of the earth from the observations. Mathematical solution of such a problem can be achieved only if the complementary forward problem has been solved. In the latter problem we acquire the capability of computing theoretically the phase speed when the model of the earth is adequately specified. For the interpretation of Rayleigh wave phase speed data Haskell (1953) provided a matrix solution to the complementary forward problem, namely, given a layered model of crust and upper mantle structure, to compute the Rayleigh wave phase speeds at different periods. Knopoff (1964) has given an equivalent alternative matrix formation which is superior in terms of speed of computation. It also has an inbuilt feature to control loss of precision during computations. In this section we outline the basic result of this formulation.

Knopoff (1964) has shown that the Rayleigh wave function $F_R(\omega,c)$ of Haskell (1953) (see Appendix B Eq. B.7) has the

11

following equivalent form.

$$F_R(\omega,c) = T^{(0)} \overset{-(1)}{F} \overset{(2)}{F} \overset{-(3)}{F} \cdots \begin{cases} \overset{(n-2)}{F} \overset{-(n-1)}{F} \overset{(n)}{T} & \text{if n is even} \\ \overset{-(n-2)}{F} \overset{(n-1)}{F} \overset{-(n)}{T} & \text{if n is odd} \end{cases}$$

$$\ldots(2.13)$$

$n-1$ being the number of layers in the model and nth medium being the half space Fig. 2.1. According to Schwab and Knopoff (1972),

$$T^{(0)} = [\ -\gamma_1(\gamma_1-1),0,(\gamma_1-1)^2,\gamma_1^2,q/c^2\rho_1,\gamma_1(\gamma_1-1)\ ] \quad ;$$
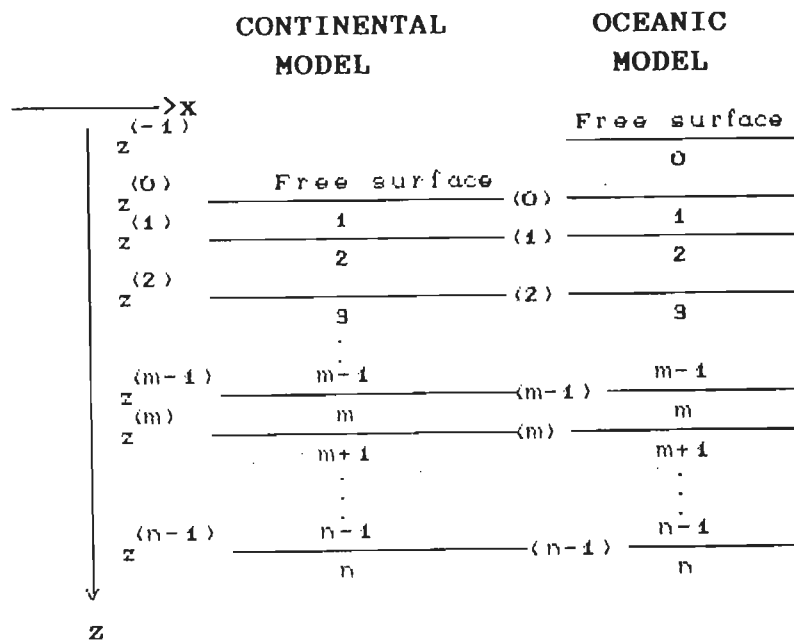
Fig. 2.1 COORDINATE SYSTEM AND GEOMETRY FOR THE PROBLEM OF RAYLEIGH WAVES IN FLAT LAYERED CONTINENTAL AND OCEANIC STRUCTURES. (After Schwab 1970)

$$F^{(m)} = \begin{bmatrix} F^{(m)}_{1212} & F^{(m)}_{1213} & F^{(m)}_{1214} & F^{(m)}_{1223} & F^{(m)}_{1224} & F^{(m)}_{1234} \\[4pt] F^{(m)}_{1312} & F^{(m)}_{1313} & F^{(m)}_{1314} & F^{(m)}_{1323} & F^{(m)}_{1324} & F^{(m)}_{1334} \\[4pt] F^{(m)}_{1412} & F^{(m)}_{1413} & F^{(m)}_{1414} & F^{(m)}_{1423} & F^{(m)}_{1424} & F^{(m)}_{1434} \\[4pt] F^{(m)}_{2312} & F^{(m)}_{2313} & F^{(m)}_{2314} & F^{(m)}_{2323} & F^{(m)}_{2324} & F^{(m)}_{2334} \\[4pt] F^{(m)}_{2412} & F^{(m)}_{2413} & F^{(m)}_{2414} & F^{(m)}_{2423} & F^{(m)}_{2424} & F^{(m)}_{2434} \\[4pt] F^{(m)}_{3412} & F^{(m)}_{3413} & F^{(m)}_{3414} & F^{(m)}_{3423} & F^{(m)}_{3424} & F^{(m)}_{3434} \end{bmatrix} ;$$

$$\bar{F}^{(m)} = \begin{bmatrix} F^{(m)}_{3434} & -F^{(m)}_{3424} & F^{(m)}_{3423} & F^{(m)}_{3414} & -F^{(m)}_{3413} & F^{(m)}_{3412} \\[4pt] -F^{(m)}_{2434} & F^{(m)}_{2424} & -F^{(m)}_{2423} & -F^{(m)}_{2414} & F^{(m)}_{2413} & -F^{(m)}_{2412} \\[4pt] F^{(m)}_{2334} & -F^{(m)}_{2324} & F^{(m)}_{2323} & F^{(m)}_{2314} & -F^{(m)}_{2313} & F^{(m)}_{2312} \\[4pt] F^{(m)}_{1434} & -F^{(m)}_{1424} & F^{(m)}_{1423} & F^{(m)}_{1414} & -F^{(m)}_{1413} & F^{(m)}_{1412} \\[4pt] -F^{(m)}_{1334} & F^{(m)}_{1324} & -F^{(m)}_{1323} & -F^{(m)}_{1314} & F^{(m)}_{1313} & -F^{(m)}_{1312} \\[4pt] F^{(m)}_{1234} & -F^{(m)}_{1224} & F^{(m)}_{1223} & F^{(m)}_{1214} & -F^{(m)}_{1213} & F^{(m)}_{1212} \end{bmatrix} ;$$

$$T^{(n)}_{solid} = \begin{bmatrix} 0 \\ -r_{\alpha n} \\ r_{\alpha n} r_{\beta n} \\ 1 \\ -r_{\beta m} \\ 0 \end{bmatrix} .\varepsilon , \qquad \bar{T}^{(n)}_{solid} = \begin{bmatrix} 0 \\ -r_{\beta n} \\ 1 \\ r_{\alpha n} r_{\beta n} \\ r_{\alpha m} \\ 0 \end{bmatrix} .\varepsilon . \qquad \ldots(2.14)$$

q is zero for a continental model, and is given by $i\rho_0 c^2 \tan(p_0/r_{\alpha 0})$ for an oceanic model; the elements $F^{(m)}_{ijkl}$ are obtained from Table 2.1.

46

TABLE 2.1 EXPRESSIONS FOR THE QUANTITIES $F_{ijkl}^{(m)}$

ij \ kl	12	13	14	23	24	34
12	$-\varepsilon_8^{(m)}$	0	$\varepsilon_{13}^{(m)}$	$\varepsilon_6^{(m)}$	0	$\varepsilon_{10}^{(m)}$
13	$-i(\varepsilon_{11}\zeta_9 + \varepsilon_7\zeta_{10})$	$\varepsilon_{15}\zeta_{14}$	$i(\varepsilon_{14}\zeta_9 + \varepsilon_{12}\zeta_{10})$	$i(\varepsilon_9\zeta_9 + \varepsilon_5\zeta_{10})$	$-\varepsilon_{15}\zeta_7$	$i(\varepsilon_{11}\zeta_9 + \varepsilon_7\zeta_{10})$
14	$\varepsilon_{11}\zeta_7 - \varepsilon_7\zeta_{12}$	$i(\varepsilon_{15}\zeta_{10})$	$-\varepsilon_{14}\zeta_7 + \varepsilon_{12}\zeta_{12}$	$-\varepsilon_9\zeta_7 + \varepsilon_5\zeta_{12}$	$i(\varepsilon_{15}\zeta_8)$	$-\varepsilon_{11}\zeta_7 + \varepsilon_7\zeta_{12}$
23	$-\varepsilon_{11}\zeta_{15} + \varepsilon_7\zeta_7$	$i(\varepsilon_{15}\zeta_9)$	$\varepsilon_{14}\zeta_{15} - \varepsilon_{12}\zeta_7$	$\varepsilon_9\zeta_{15} - \varepsilon_5\zeta_7$	$i(\varepsilon_{15}\zeta_{11})$	$\varepsilon_{11}\zeta_{15} - \varepsilon_7\zeta_7$
24	$-i(\varepsilon_{11}\zeta_{11} + \varepsilon_7\zeta_8)$	$-\varepsilon_{15}\zeta_7$	$i(\varepsilon_{14}\zeta_{11} + \varepsilon_{12}\zeta_8)$	$i(\varepsilon_9\zeta_{11} + \varepsilon_5\zeta_8)$	$\varepsilon_{15}\zeta_{13}$	$i(\varepsilon_{11}\zeta_{11} + \varepsilon_7\zeta_8)$
34	ε_{10}	0	$-\varepsilon_{13}$	$-\varepsilon_6$	0	$-\varepsilon_8$

$$\varepsilon_0^{(m)} = \rho_{m+1}/\rho_m \qquad \varepsilon_8^{(m)} = \varepsilon_1^{(m)}\varepsilon_4^{(m)} \qquad \zeta_1^{(m)} = \cos P_m \qquad \zeta_9^{(m)} = \zeta_1^{(m)}\zeta_6^{(m)}$$
$$\varepsilon_1 = \gamma_m - \varepsilon_0\gamma_{m+1} \qquad \varepsilon_9 = \varepsilon_2^2 \qquad \zeta_2 = \cos Q_m \qquad \zeta_{10} = \zeta_2\zeta_3$$
$$\varepsilon_2 = \varepsilon_1 - 1 \qquad \varepsilon_{10} = \varepsilon_2\varepsilon_3 \qquad \zeta_3 = r_{\alpha m}\sin P_m \qquad \zeta_{11} = \zeta_2\zeta_4$$
$$\varepsilon_3 = \varepsilon_1 + \varepsilon_0 \qquad \varepsilon_{11} = \varepsilon_2\varepsilon_4 \qquad \zeta_4 = \sin P_m/r_{\alpha m} \qquad \zeta_{12} = \zeta_3\zeta_5$$
$$\varepsilon_4 = \varepsilon_2 + \varepsilon_0 \qquad \varepsilon_{12} = \varepsilon_3^2 \qquad \zeta_5 = r_{\beta m}\sin Q_m \qquad \zeta_{13} = \zeta_4\zeta_5$$
$$\varepsilon_5 = \varepsilon_1^2 \qquad \varepsilon_{13} = \varepsilon_3\varepsilon_4 \qquad \zeta_6 = \sin Q_m/r_{\beta m} \qquad \zeta_{14} = \zeta_3\zeta_6$$
$$\varepsilon_6 = \varepsilon_1\varepsilon_2 \qquad \varepsilon_{14} = \varepsilon_4^2 \qquad \zeta_7 = \zeta_1\zeta_2 \qquad \zeta_{15} = \zeta_4\zeta_6$$
$$\varepsilon_7 = \varepsilon_1\varepsilon_3 \qquad \varepsilon_{15} = -\varepsilon_0 \qquad \zeta_8 = \zeta_1\zeta_5$$
$$\varepsilon_{16} = \varepsilon_8 + \varepsilon_{10}$$

The symbols used in this formulation are the same as in the Haskell formulation (Appendix B). The only additions are as follows. In the mth layer

$$P_m = (\omega/c)r_{\alpha m}d_m$$
$$Q_m = (\omega/c)r_{\beta m}d_m \ .$$

$r_{\alpha m}$ and $r_{\beta m}$ take the following form when $m=n$.

$$r_{\alpha m} = -i(1-c^2/\alpha_m^2)^{1/2}$$

$$r_{\beta m} = -i(1-c^2/\beta_m^2)^{1/2}$$

The quantity $\varepsilon = (-1)^{n-1}\rho_1^2 c^2/(\gamma_n r_{\alpha n} r_{\beta n}\rho_n^2\alpha_n^2)$ is included in (2.14) in

47

order that $F_R(\omega,c)$ may have the same numerical value as the dispersion function of the original Haskell formulation.

2.5 FINDING ROOTS OF RAYLEIGH WAVE FUNCTION

In our computer program the Newton Raphson method (Pennington 1965) is used nominally to find the zero's of the Eq. (2.13). Occasionally the method fails to find the desired root because one is trapped into an endless loop of repetitive trial solutions in a part of the c axes where the function $F_R(\omega,c)$ for a given ω has no zero crossing (Fig. 2.2). If the number of iterations exceeds a pre-set limit then the program gets out of the loop and proceeds to a sequential evaluation of the function $F_R(\omega,c)$ for different values of c in steps of Δc until a zero crossing is encountered. The program now steps back in c and proceeds with a reduced step in Δc until the zero crossing is found again. The procedure is repeated until the step size Δc is sufficiently small and thus the root of $F_R(\omega,c)$ is found. A flowchart of the root finding program is given in Fig. 2.3.
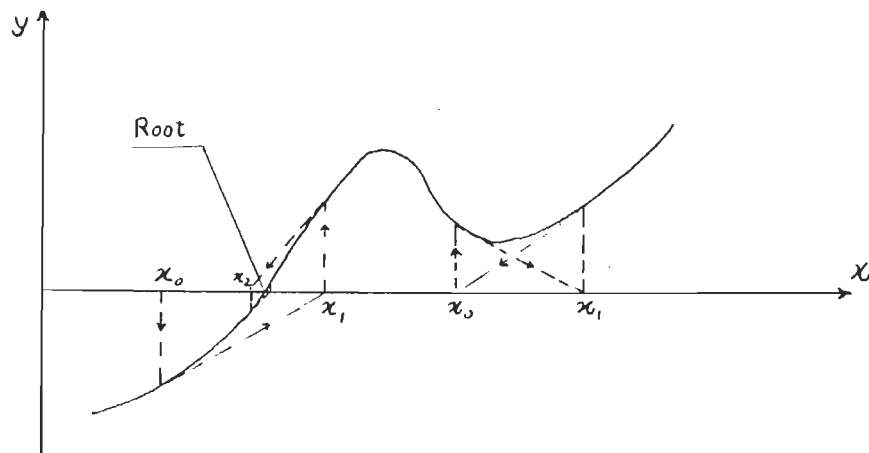
FIG. 2.2 THE LEFT PART OF THE FIGURE ILLUSTRATES THE NEWTON-RAPHSON METHOD OF FINDING THE ROOT OF AN NON-LINEAR EQUATION. IN THE RIGH PART OF THE FIGURE WE SHOW HOW METHOD MAY FAIL TO FIND A ROOT.
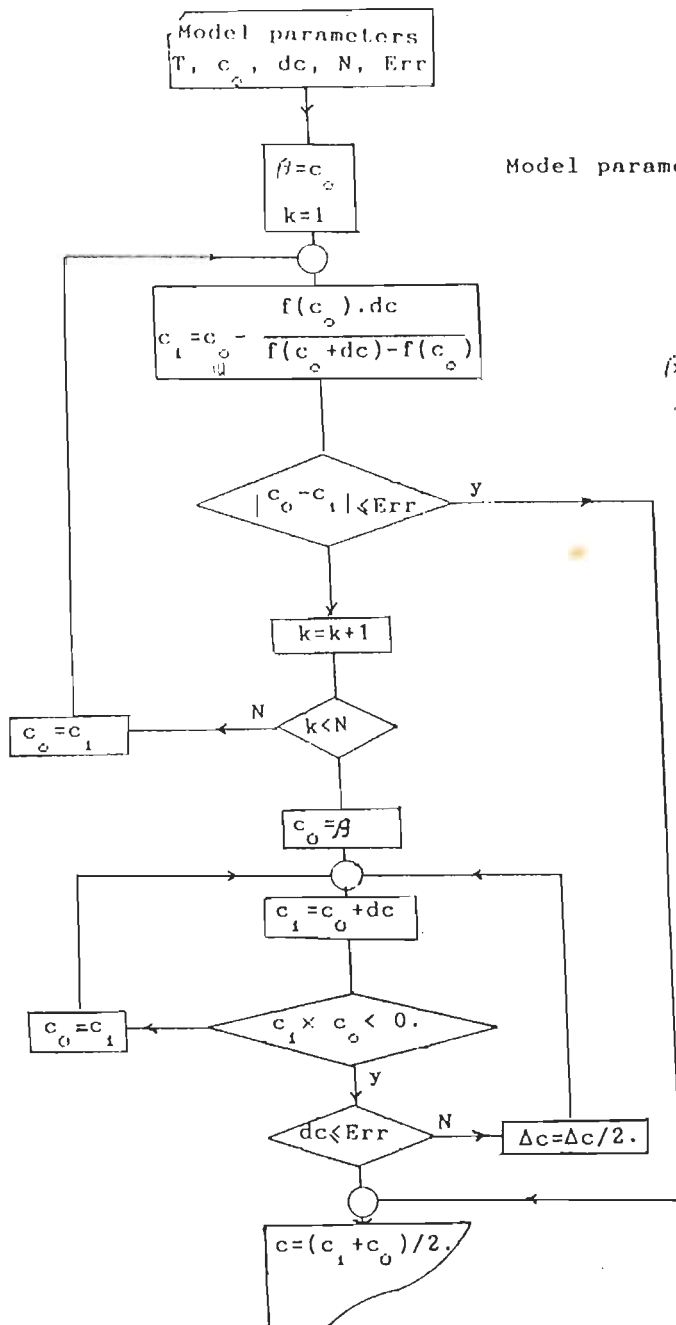
FIG. 2.3 FLOWCHART FOR FINDING THE ROOT OF Eq. 2.13. THE PROCEDURE ALLOWS DETERMINATION OF c FOR ONE VALUE OF PERIOD. IT IS TO BE REPEATED FOR DIFFERENT PERIODS.

2.6 THE INVERSION ALGORITHM

The problem of obtaining parameters of a layered earth model from observations of Rayleigh wave phase speeds at different period is nonlinear. We adopted an iterative linearized procedure. In this we have to solve the following system of N linear equations for K parameters increments Δp_j, j=1,... K.

$$\sum_{j=1}^{K} (\delta c_i^{th} / \delta p_j) \Delta p_j = c_i^{obs} - c_i^{th} \quad , \quad i=1,... N . \qquad ...(2\text{-}15)$$

Here the parameters of an M-layered model that may be considered are compressional wave speeds, α_m, shear wave speeds, β_m, densities ρ_m, (m=1,...M) and thicknesses h_m (m=1,....M-1) of the layers. Thus the K may be any number between 1 and 4M-1 depending upon the number of quantities about the layered model we wish to estimate by keeping the remaining 4m-1-K parameters fixed. c_i^{obs} i=1,... N are the observed values of Rayleigh wave phase speed at N different periods. c_i^{th} i=1,... N are the corresponding theoretical values for a layered earth model for which the p_j^o j=1,... K are initial estimates parameters. $\delta c_i^{th} / \delta p_j^o$ represents partial derivative of ith phase speed value with jth layer parameter. Finally Δp_j j=1,...K are the increments in parameter values which when added to the starting estimates p_j^o j=1,... K will improve estimate of layer parameters. In matrix from

$$G\Delta p = \Delta c \qquad . \qquad ...(2.16)$$

Here

$$\Delta c = (\Delta c_1, \Delta c_2 ......\Delta c_N)^T, \quad \text{and} \quad \Delta c_i = c_i^{obs} - c_i^{th}, \quad i=1,... N.$$

$\Delta p = (\Delta p_1, \ldots, \Delta p_k)^T$ is defined as a correction or modification vector that is added to original parameter vector p^o to determine the vector of unknowns p^i for the next iteration in the vector.

G is $N \times K$ matrix of partial derivatives whose elements are $G_{ij} = \delta c_i^{th} / \delta p_j^o$. Vector p^i is considered to be the solution to the unknowns when it yields a vector Δc in (2.16) that is sufficiently small. In practice, it is assumed that N (number of dispersion data points) is greater than K (number of unknown parameter in p^o). Thus the problem defined by (2.16) is over determined.

In general ,(2.16) cannot be solved exactly by computing the conventional matrix inverse G^{-1} of matrix G . Matrix G^{-1} exists only if G is square and nonsingular. An approach to solve (2.16) is to construct its normal or Gauss-Newton equation. This results in the classical least-squares solution

$$\Delta p = (\ G^T\ G\ )^{-1}\ G^T\ \Delta c \qquad . \qquad \qquad \ldots (2.17)$$

and leads to minimization of $(\Delta c - G\ \Delta p)^T (\Delta c - G\ \Delta p)$ with respect to Δp. This solution is called the optimization solution by Yuan and Nazarian, (1993).

The computation of matrix $G^T G$ may involve numerical inaccuracy, which can be troublesome when the number of dispersion data or number of layers are large. To avoid this drawback, the singular value decomposition of the matrix G (Golub and Reinsch 1970) has been utilized to develop the generalized inverse solution of (2.16).

The singular value decomposition of matrix G comprises a product of three matrices

$$G = U \ S \ V^T \qquad \qquad \ldots(2.18)$$

where U is an N×K matrix whose columns are eigenvectors, u_j (j=1,... ,K), of length n associated with the columns (observations) of G, V is a K×K matrix whose columns are eigenvectors, v_j (j=1,.....,K), of length K associated with the rows (parameters) of G, and S=K×K diagonal matrix with diagonal entries, S_{ii} (i=1,...,K), which are the nonnegative square roots of the eigenvalues of symmetric matrix $G^T G$, and are known as the singular values of G.

By substituting (2.18) into (2.17), and utilizing the orthonormal property of U and V [i.e., $U^T U = V^T V = I$ (unit matrix)], it is easy to show that

$$\Delta p = V \ S^{-1} \ U^T \ \Delta c \qquad \qquad \ldots(2.19)$$

This expression gives the generalized inverse solution of (2.16).

Adding Δp to p^o yields an updated parameter vector from which a new set of phase speeds (c^{th}) and a new set of partial derivatives can be calculated. This procedure is repeated until Δc_i's [elements of vector Δc described in (2.16)] are sufficiently small. At this time, the parameter vector that satisfies the given data is obtained.

The convergence of successive iterations is monitored by the following root-mean-square (RMS) error criterion:

$$\text{RMS error} = \left[\frac{1}{N} \sum_{i=1}^{N} \Delta c_i \right]^{1/2} \qquad \ldots (2.20)$$

The iteration procedure is terminated when RMS error reaches an acceptably small value or when all elements of vector Δc are within the standard error bounds of each experimental datum or some other pre-specified limit.

Small eigenvalues of the $G^T G$ matrix introduce instability in the inversion process. Therefore it is desirable to sort the eigenvalues in decreasing order and disregard those which are smaller than a pre-assigned cut-off value. The corresponding eigenvectors of the V matrix are discarded also.

Theoretically there is no limit on the number (K) of parameters and number (N) of observed data. A limit is posed only by the capacity and speed of the computer that we use for solving our inverse problem.

2.6.1 SENSITIVITY OF PARAMETERS IN THE INVERSE PROBLEM

The N×K matrix G in eq.(2.16) can give us some information about of the behavior of parameters, because the ijth element of this matrix is a partial derivative $\delta c_i / \delta p_j$ In common with the general experience so far in the inversion of Rayleigh wave phase speeds (e.g. Yuan and Nazarian, 1993),we will show in chapter 3 that the shear speeds β_m's are the most important parameters during inversion. After that the h_m's are important too, but the α_m's and the ρ_m's of layers are not as important. Further,the α_m's and ρ_m's are controllable with Poisson's ratio and Nafe Drake

53

curve (Sheriff 19??) respectively.

2.7 FLOWCHART FOR THE INVERSE PROBLEM

There are five main parts of the inversion program written by us. These parts are now descried briefly (Fig. 2.4).

Part I The observed data and the initial model parameters are read . The tolerance levels for convergences in various iteration loops are set. The program ensures that the number of observations are more than the number of parameters to be inverted for. Otherwise an error massage is written and the program stops.

Part II The initial model is tested for goodness of fit between the observed and computed Rayleigh wave phase speeds at various ω's. The control is transferred to this part from part V also, and the current parameter model brought out during the various iterations are also tested in this way.

Part III Termination or continuation of iterations is decided in this part. If the RMS value of the difference between observed and calculated phase speeds is less than a pre-set level then program terminates. Alternatively when more than two iterations have gone then RMS errors of the previous two iterations are compared and if the differences is less than a pre-set limit then also the program stops. Lastly, if the number of iterations exceeds the pr-set limit the program can stop. In each of three options for termination the parameter values of last model are printed.

54

Step I

Parameters of initial model
N, P^0, Mit, Err1, Err2, Err3

Phase speed observations
$(c_{obs}, T)_i$ i=1,... M

No. of   iteration
Mi=1

M >N   y   stop

1

- -

Step II

Call Rayleigh function
⇓
$(c_{th}, T)_i$ i=1,..., M

Generation of matrix Δc
$\Delta c_i = c_{obs} - c_{th}$

RMS1= 100

$$RMS2 = \left(\left(\sum_{i=1}^{M} \Delta c_i \right)^2 / M \right)^{1/2}$$

2

55

②

$$\text{RMS2} < \text{Err1} \quad \xrightarrow{y} \quad \boxed{\text{Print final Model}}$$

$$|\text{RMS2}-\text{RMS1}| < \text{ERR3} \quad \xrightarrow{y}$$

$$\text{Mi}=\text{Mit} \quad \xrightarrow{y}$$

Step IV

$$
\boxed{
\begin{array}{c}
\text{Generation of matrix G} \\
G_{i,j} = \delta c_i^{th}/\delta P^0 \quad
\begin{array}{l}
i=1,\ldots M \\
j=1,\ldots N
\end{array}
\end{array}
}
$$

$$\boxed{A = G^T . G}$$

$$
\boxed{
\begin{array}{l}
\text{Calculation of eigenvalues} \\
\text{and eigenvectors} \\
\text{(using Jacobi method)} \\
\lambda_i \qquad i=1,\ldots N \\
V_{i,j} \qquad j=1,\ldots M
\end{array}
}
$$

$$
\boxed{
\begin{array}{l}
\text{Sorting of } \lambda \quad \text{and} \quad \text{rejection} \\
\text{of} \quad \text{small} \quad \lambda s \quad \text{and} \quad \text{their} \\
\text{eigenvectors} \\
\qquad N \longrightarrow K
\end{array}
}
$$

③

③

Generation of matrix S and V

$$S_{i,j} = \frac{0 \quad (i \neq j)}{\lambda_i \quad (i = j)} \quad i \ \& \ j = 1, \ldots K$$

$$V_{i,j} \quad \begin{array}{l} i=1, \ldots N \\ j=1, \ldots K \end{array}$$

$$U = G . V . S^{-1}$$

$$G^{-1} = V . S^{-1} . U^{T}$$

$$\Delta P = G^{-1} . \Delta C$$

$$P^{O} = P^{O} + \Delta C$$

Step V

Control of elements
of matrix P^{O}
with Poisson's ratio

RMS1=RMS2
Mi=Mi+1

①

FIG. 2.4 FLOWCHART FOR INVERSION OF RAYLEIGH WAVE PHASE SPEED CURVE FOR PARAMETERS OF MULTI-LAYERED EARTH MODEL. RELEVANT PARAMETERS ARE DEFINED IN THE TEXT.

Part IV Elements of matrix G of partial derivatives are computed. Matrix $G^T G$ is computed. Eigenvalues of this matrix are computed. The corresponding eigenvectors are computed by Jacobi's rotations algorithm (Kohn 1987). The $N \times N$ matrix V of eigenvectors is formed. The eigenvalues are ranked according to their magnitudes and eigenvalues smaller than a pre-set limit are discarded. At this point if one or more eigenvalues have been discarded then in the V matrix the corresponding eigenvectors columns are also deleted. Matrix U is formed. The inverse of matrix G is computed from the matrix product $VS^{-1}U^T$. The change in model parameters are computed from $G^{-1} \Delta c$ and a new model $p^U = p^U + \Delta p$ is defined.

Part V The Poission's ratio of each layers is computed from the P and S wave speeds and if it is outside a pre-set range then the P waves speeds are adjusted. The flow of the program is shifted to part II.

2.8   A NEW METHOD FOR ELIMINATION OF THE INSTRUMENT RESPONSE FOR TWO STATION METHOD

2.8.1 INTRODUCTION

The two station method has been a common procedure for finding the phase speed of surface waves for many years. It requires the calculation of the phase delay $\{\phi_2(\omega) - \phi_1(\omega)\}$ experienced by surface waves of angular frequency ω between the two stations.

If similar instruments, are used at both stations, then the

phase shifts due to instruments can be ignored. But if the seismographs used at the two stations are different, or if, with passage of time, the instrumental parameters change at the two stations then the phase shift introduced by each instrument has to be estimated as accurately as possible.

Here we present a slightly novel solution to the problem. It depends upon the availability of calibration pulses on the seismograms of both stations.

2.8.2 THE PROPOSED METHOD

Our suggestion is to convolve in the time domain the digitized seismogram of surface waves at the first station with the digitized calibration pulse of the second station. At the same time the digitized surface waves signal from the second station is convolved with the digitized calibration pulse for the first station. If now Fourier transforms of the two convolved sequences are computed, then the frequencywise differences in the phases of the two convolutions should provide the $\phi_2(\omega) - \phi_1(\omega)$ in which the instrumental correction has been taken care off.

The idea may be explained mathematically in the following way. Let $s_1(t)$ and $s_2(t)$ be the time series representing the surface waves recorded at station one and two. Let $h_1(t)$ and $h_2(t)$ be, in a similar way, the time series representing the instrumental impulse responses at the two stations. Let $k_1(t)$ and $k_2(t)$ be the time series representing the calibration pulses due to step function input at the two stations. Finally let $g_1(t)$ and $g_2(t)$ be the ground motion time series for surface waves at the two stations. Then the following convolutional relations hold.

59

$$s_1(t)=g_1(t)*h_1(t)$$
$$s_2(t)=g_2(t)*h_2(t)$$
$$k_1(t)=A.H(t)*h_1(t)$$
$$k_2(t)=B.H(t)*h_2(t)$$

Here $H(t)$ represent Heaviside step function which is zero for $t<0$ and one for $t \geq 0$.

In the existing method phase difference $\phi_2(\omega)-\phi_1(\omega)$ is supposed to represent the difference in phase of the Fourier transform of $g_1(t)$ and $g_2(t)$ at angular frequency ω. Our suggestion is to define two time series $f_1(t)$ and $f_2(t)$ such that,

$$f_1(t)=s_1(t)*k_2(t)=\{g_1(t)*h_1(t)\}*B.H(t)*h_2(t)$$
$$f_2(t)=s_2(t)*k_1(t)=\{g_2(t)*h_2(t)\}*A.H(t)*h_1(t)$$

Therefore if $\phi_{1f}(\omega)$ and $\phi_{2f}(w)$ are the Fourier transform phases of $f_1(t)$ and $f_2(t)$ at the angular frequency ω then $\phi_{f2}(\omega)-\phi_{f1}(w)$ .should equal the desired $\phi_2(\omega)-\phi_1(w)$ of the conventional method. For computational efficiency, a cross-correlation of $f_1(t)$ and $f_2(t)$ may be taken followed by a use of FFT to determine $\phi_{f2}(\omega)-\phi_{f1}(w)$ which is equal to $\phi_2(\omega)-\phi_1(w)$. We note in passing that the Fourier phase of the impulse response and step function response of a linear system are equal.

The following flowchart shows the method graphically.
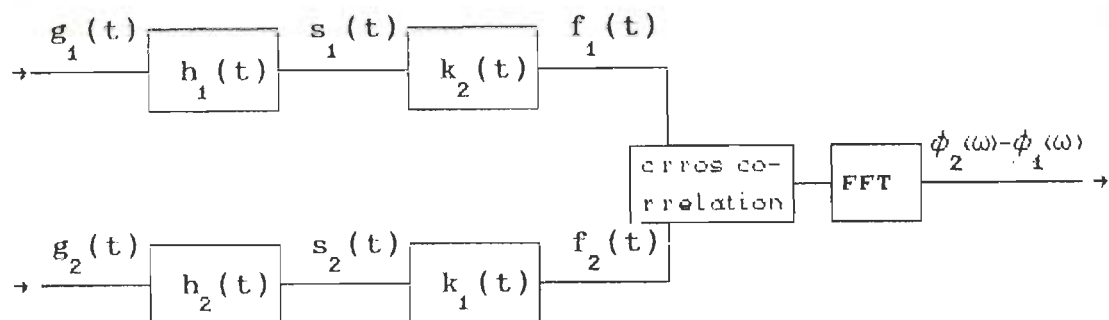
FIG. 2.5 FLOWCHART OF PROPOSED METHOD FOR CORRECTION OF
INSTRUMENTAL PHASE SHIFT

This method has been tested on synthetic signals and the
results are discussed in the next chapter.

CHAPTER-3
TESTING OF COMPUTER PROGRAMS

3.1 INTRODUCTION

Two major and many minor computer programs were developed by us during the course of the present research. In this chapter we present evidence and results of tests to show that these program are working as desired.

3.2 A TEST OF AKI'S FORMULA, EQ. 2.12 : 16 EXPERIMENTS

Since Aki's formula is central to the determination of phase speed curves for inversion in terms of crust and upper mantle structure, we carried out a synthetic exercise to gain a appreciation of this formula. For this purpose we assumed a phase speed dispersion relation as

$$c(k) = 4 - 3\tan^{-1}(k) \qquad \qquad ...(3.1)$$

with k as wavenumber. The group speed dispersion curve was determined through

$$u(k) = c + k \cdot \frac{dc}{dk} = c - \frac{3k}{1+k^2} \qquad \qquad ...(3.2)$$

Graphs for c(T) and u(T) are plotted in Fig. 3.1.

Then the following asymptotic formula (Bullen 1963 Pg. 61)
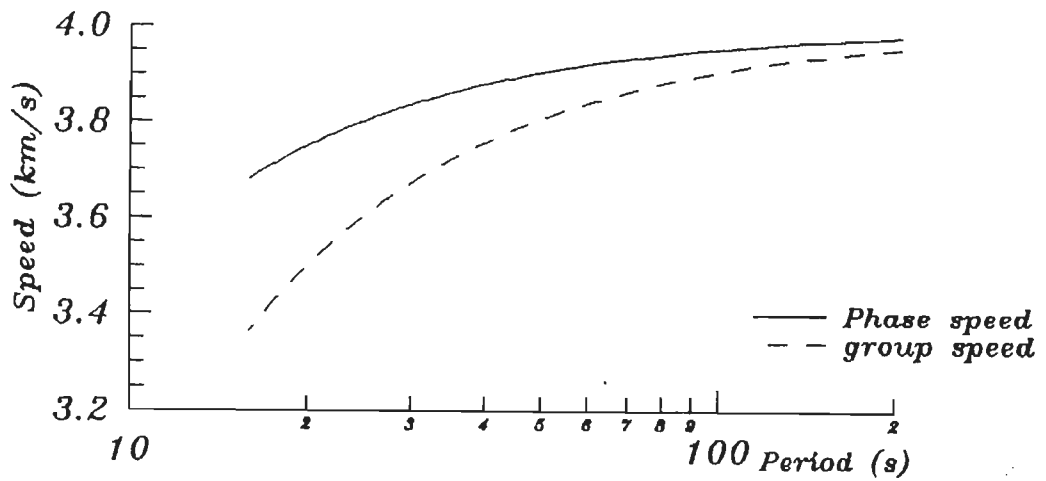
FIG. 3.1 PHASE AND GROUP SPEED CURVES FOR THE FORMULA OF Eq. 3.1
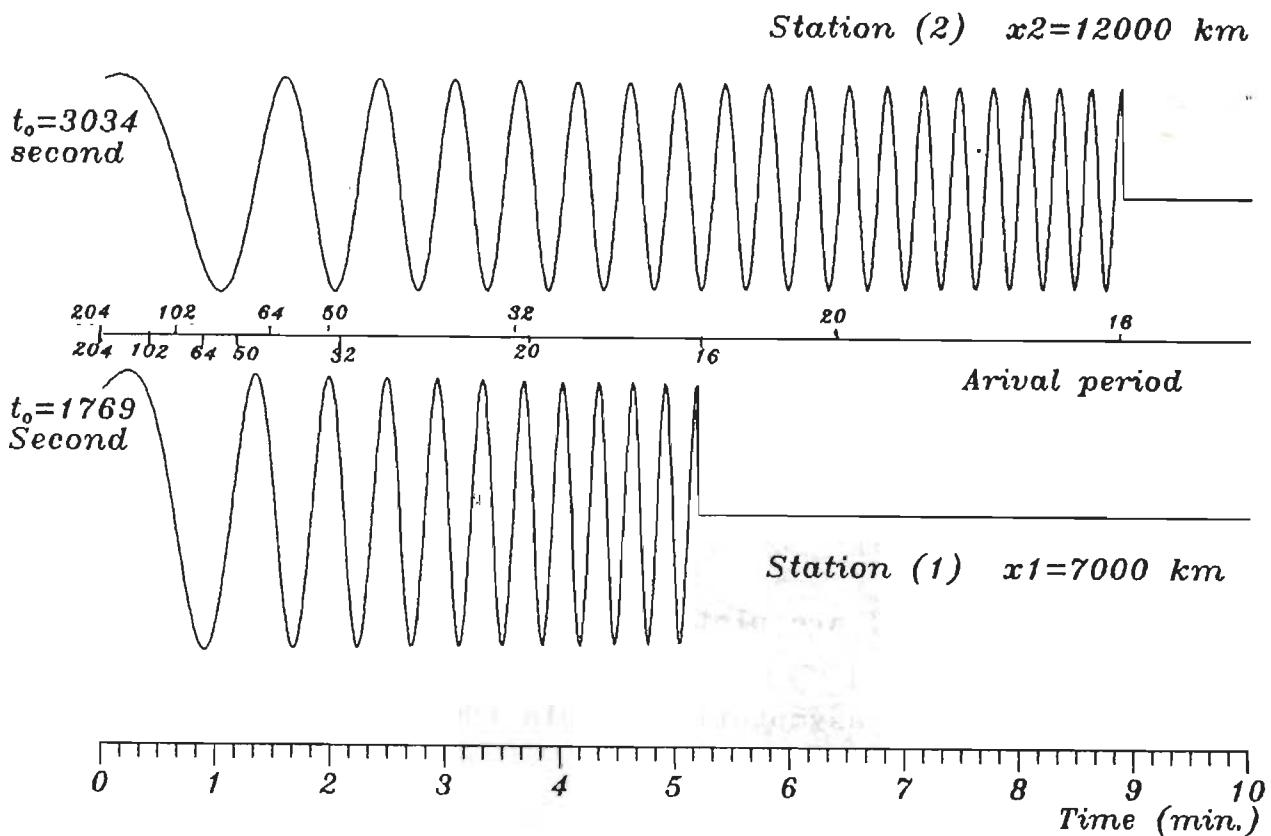
FIG. 3.2 SYNTHETIC SEISMOGRAMS AT EPICENTRAL DISTANCES OF 7000
AND 12000 KM USING THE DISPERSION CURVES OF Fig. 3.1

was used for computing synthetic seismograms. For a given epicentral distance x and time t, the ground displacement $y(x,t)$ is given by

$$y(x,t) \cong \frac{\Phi(k)}{(\pi/2|\frac{du}{dk}|.t)^{1/2}} \cos(kx - \omega t + \pi/4). \qquad \ldots(3.3)$$

Here $\Phi(k)$ is amplitude of wave group with wavenumber k. The original formula (Bullen 1963) comes with a choice of $\pm\frac{\pi}{4}$ depending upon the nature of inversion, whether direct or inverse. The $+\frac{\pi}{4}$ is appropriate in our case. Fig. 3.2 shows the synthetic seismograms at two epicentral distances of 7000 and 12000 km. Instrumental effects are not introduced to keep the test as stringent as possible by keeping out all considerations other than the dispersion and Fourier transform operation. We now applied Aki's two station method to determine the phase speed dispersion curve. Fig. 3.3 (see Experiment 16 below) is a comparison of the computed phase speed dispersion curve with the original analytical formula of Eq. 3.1. The agreement is reassuring. While Aki's two station formula is thus tested there were a number of questions which we had to answer to arrive at this figure. We shall pose and discuss these questions now.
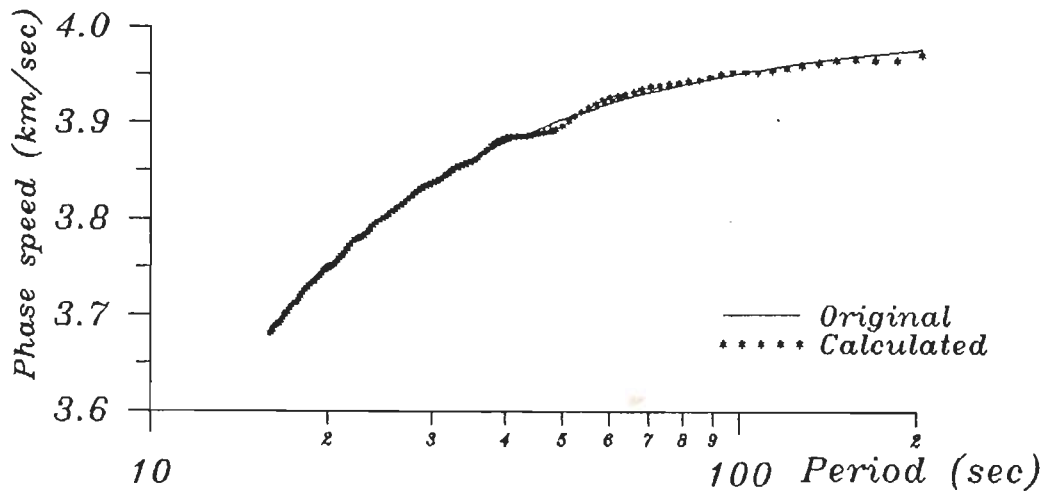
FIG 3.3 COMPARISON OF THE ORIGINAL PHASE SPEED CURVE OF FIG. 3.1 AND THE RESULTS OBTAINED BY APPLYING AKI'S TWO STATION PROCEDURE ON SYNTHETIC SEISMOGRAMS OF FIG 3.2. THE N OF EQ. 2.12 IS THE SAME AT ALL PERIODS. IN OTHER WORD THE COMPUTED $\phi_2 - \phi_1$ WAS WITHIN ONE CYCLE OF 2π.

3.2.1 16 EXPERIMENTS

We had to see for ourselves why FFT is actually superior to DFT. Also since the two seismograms were of unequal duration, we had to learn whether we should use all or parts of the two seismograms. We had to learn also whether the digitization interval should be the same or different for the two seismograms. With the above two synthetic seismograms we performed 16 experiments, divided into four groups of four experiments each. We display the results of the tests in Figs 3.4 to 3.19 and Tables 3.1 to 3.4.

66

Before describing the experiments we make a few general remarks which should make the discussion of the experimental results more specific and precise. Since we are dealing with synthetic seismograms we are assured that all waves and wave groups may be assumed to have travelled the same great circle path between the epicenter and the point of observation. At a given time t on the synthetic seismogram a wave group of group speed $u=x/t$ should arrive. From the group speed dispersion curve the period of waves in this group can be ascertained. If the initiation of digitization at both stations starts at times appropriate for arrival of wave groups of group speed u_i, then the wave group of same period was arriving at both stations at the times corresponding to initiation of digitization. Similarly, let u_t be the group speed appropriate for the time of termination of digitization. We shall add subscript 1 or 2 to u_i and u_t to indicate whether it refers to the first station or the second station. Thus u_{i1} to u_{t1} is the group speed range involved in the digitized portion of first station seismogram. Similarly u_{i2} and u_{t2} have the meaning for the second station.

"period range of overlap" In the following paragraphs we shall use this phrase a number of times. Let T_{i1} and T_{t1} be the periods of wave groups corresponding to u_{i1} and u_{t1} respectively. Similarly let T_{i2} and T_{t2} have the same meaning relative to u_{i2} and u_{t2}. Then the period range which is common to the ranges T_{i1} to T_{t1} and T_{i2} and T_{t2} is called the period range of overlap. In other words the period range of overlap is the period range for which wave groups are present in the digitized portions of

67

seismograms for both stations.

In each figure displaying results of Experiments 1 to 12 three curves are shown , namely (i) the original phase speed dispersion curve of Eq. 3.1 (solid line), (ii) the computed phase speed dispersion curve in which the integer N of Aki's formula (Eq. 2.12) was the same for all periods (dashed line between astrices) and (iii) the computed phase speed dispersion curve for which different N's were used at different periods after unwrapping of the phase (solid line between circles). The need to adjust N becomes apparent when the phase speed are computed at different periods, compared with each other and the values found to be too irregular. This has to be done sometimes when the cross correlogram technique is used for phase speed determination. For figures displaying results of Experiments 13 to 16, only curves corresponding to (i) and (ii) above are included. At the bottom of each of these figures the period ranges of wave groups in the two digitized seismograms used in that experiment. are indicated.

I GROUP OF EXPERIMENTS

In this group of experiments the number of digitized points on the seismograms of station 1 and 2 was the same, namely either 100, 200, 300, or 550. Also the initiation and termination of digitization was controlled by the arrival times of wave groups of specified upper and lower group speeds. In other words $u_{i1}=u_{i2}$ and $u_{t1}=u_{t2}$. Details are given in Table 3.1. Consequently the duration of the seismogram digitized at each station and in each experiment was different. The digitization rate for each seismogram was

different also. DFT had to be used out of necessity because the number of digitized points in all four experiments were not in integral powers of 2.

The results of these four experiments are shown in Fig. 3.4 to Fig. 3.7. In each figure there is at least some range of periods for which the agreement between the original known phase speed dispersion curve and the computed dispersion curve after phase unwrapping and using same N (curve with dashed between astrices) is reasonable. The agreement in each case is best over the period range of overlap and it improves as the number of digitized points considered increases.

TABLE 3.1 NECESSARY INFORMATION ABOUT FIRST GROUP OF EXPERIMENTS

experiment No.	Station No.	$u_i(T)$	$u_t(T)$	Seismogram duration (s)	sampling rate (s)	No. of digitized points
1	I	u(204)	u(64)	49	0.49	100
1	II	"	"	83	0.83	"
2	I	u(102)	u(32)	104	0.52	200
2	II	"	"	177	0.89	"
3	I	u(204)	u(32)	126	0.42	300
3	II	"	"	214	0.71	"
4	I	u(204)	u(16)	311	0.57	550
4	II	"		532	0.97	"
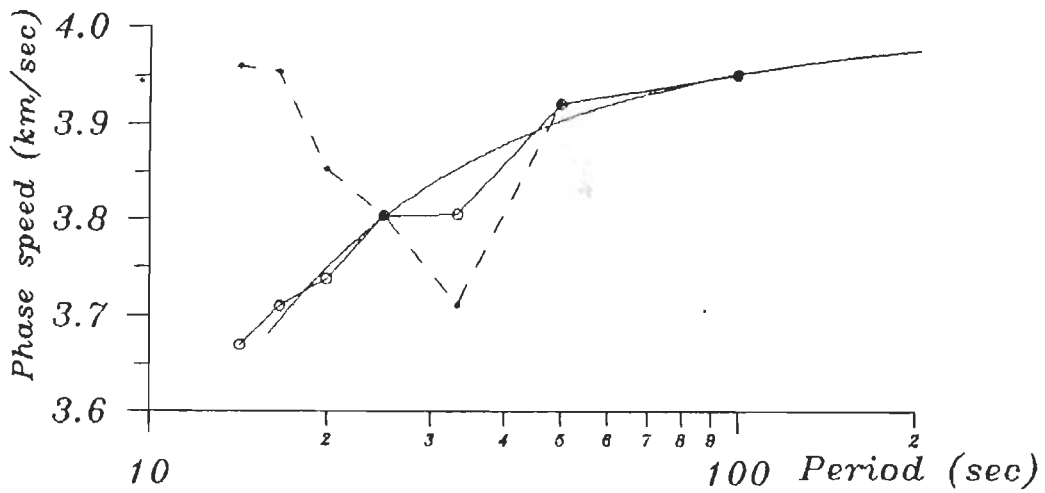
FIG. 3.4 COMPARISON OF COMPUTED AND ORIGINAL PHASE SPEED CURVES FOR EXPERIMENT 1. DFT USED IN THE ANALYSIS (See text for further explanations of different curves).
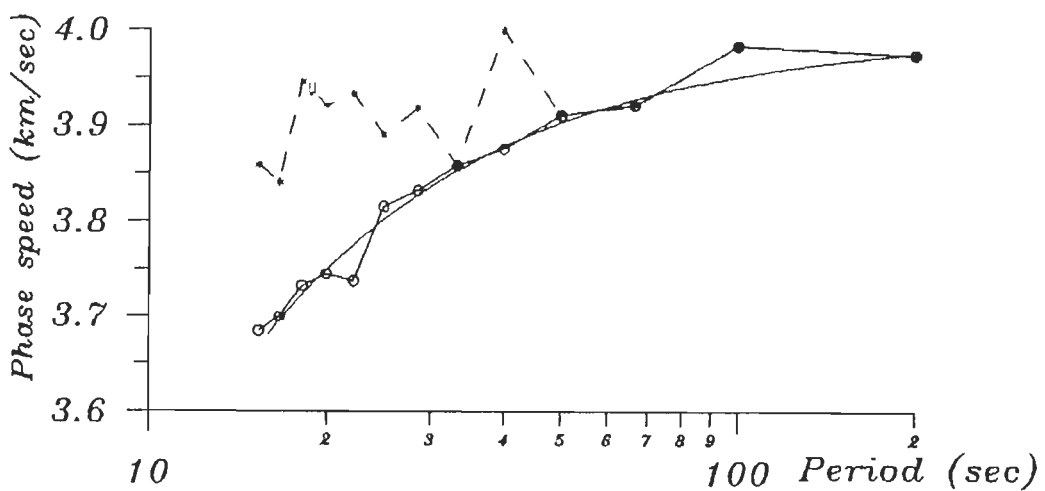
FIG. 3.5 COMPARISON OF COMPUTED AND ORIGINAL PHASE SPEED CURVES FOR EXPERIMENTS 2.
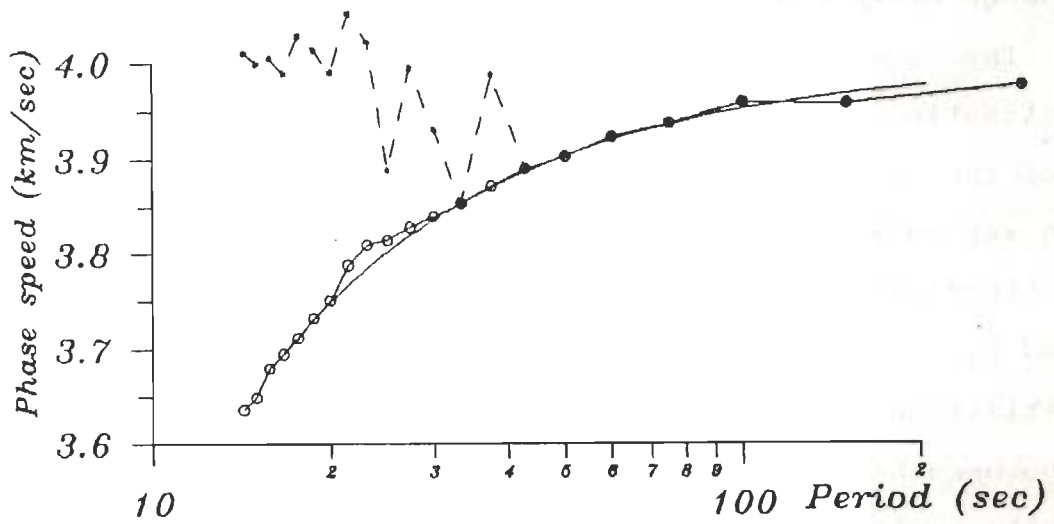
FIG. 3.6 COMPARISON OF COMPUTED AND ORIGINAL PHASE SPEED CURVES FOR EXPERIMENTS 3.
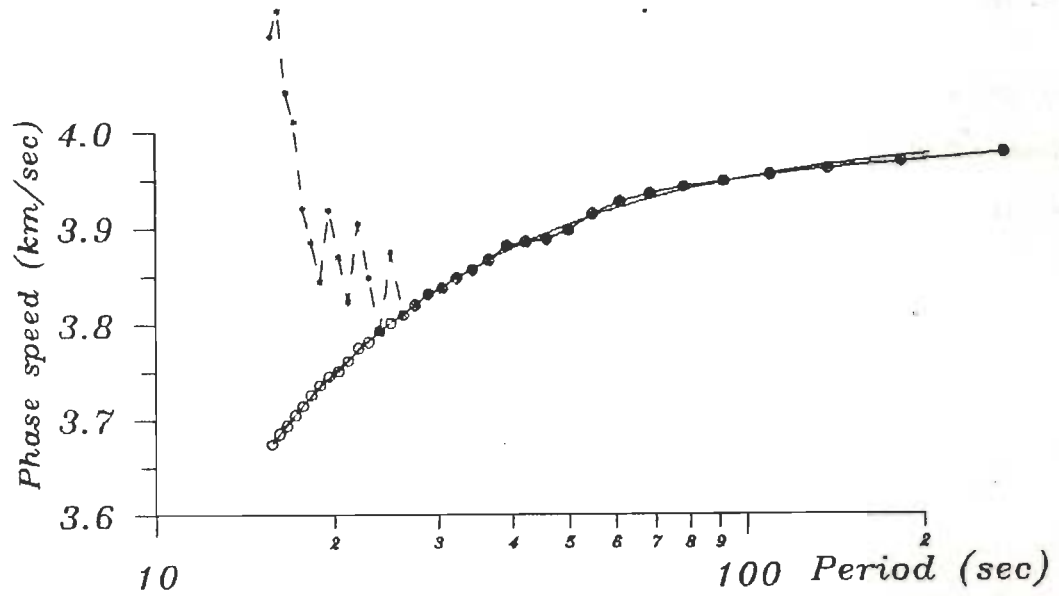
FIG. 3.7 COMPARISON OF COMPUTED AND ORIGINAL PHASE SPEED CURVES FOR EXPERIMENTS 4.

II GROUP OF EXPERIMENTS

The common feature of these experiments is that the digitization rate is the same at both stations. In Experiments 5 and 6 the initiation and termination of digitization was in the same way as in Experiments 1 to 4 . As a result the number of digitized points was different for the two stations. In Experiment 7 and 8, $u_{t1} = u_{t2}$, but the number of digitized points and the digitization rates being equal at both stations, $u_{t1} < u_{t2}$. DFT had to be used necessarily. Details are shown in Table 3.2. The DFT results could not be used directly in Experiments 5 and 6 because the periods or frequencies for which the DFT program gave amplitude and phases were different at two stations. Necessary interpolation was carried out using a fourth order spline.

The results are shown in Figs 3.8 to 3.11. Experiments 5 and 6 give totally unacceptable results. On the other hand the results in Experiments 7 and 8 are very good for the period range of overlap.

The main lesson we learn from these four experiments is that number of digitized points and digitization rates should be the same at both stations.
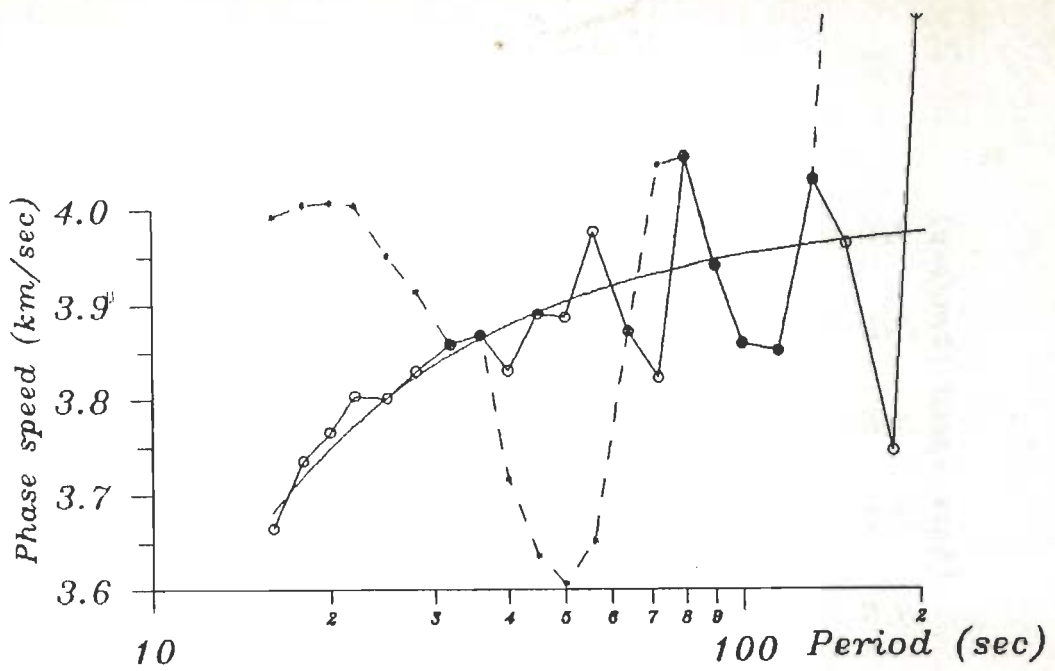
FIG. 3.8 COMPARISON OF COMPUTED AND ORIGINAL PHASE SPEED CURVES FOR EXPERIMENTS 5.
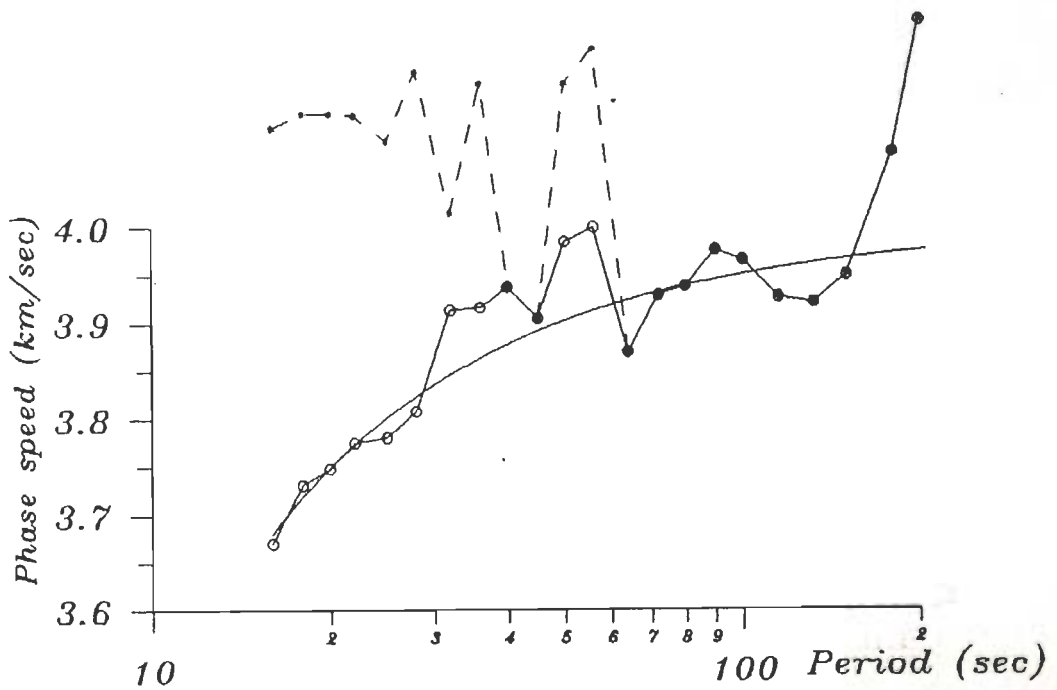
FIG. 3.9 COMPARISON OF COMPUTED AND ORIGINAL PHASE SPEED CURVES FOR EXPERIMENTS 6.
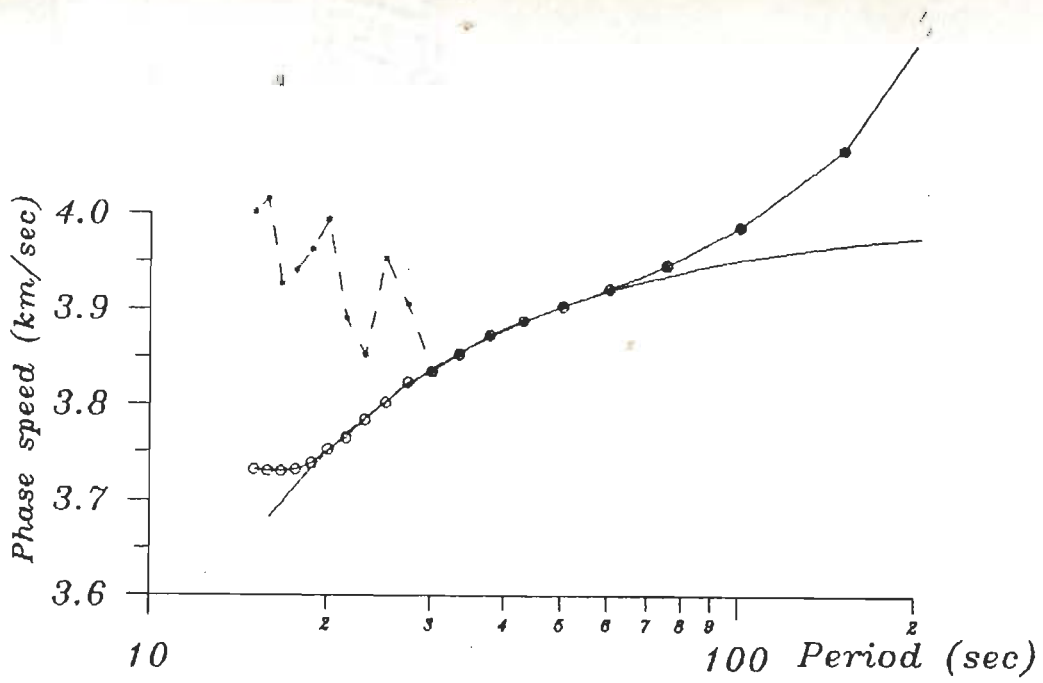
FIG. 3.10 COMPARISON OF COMPUTED AND ORIGINAL PHASE SPEED CURVES FOR EXPERIMENTS 7.
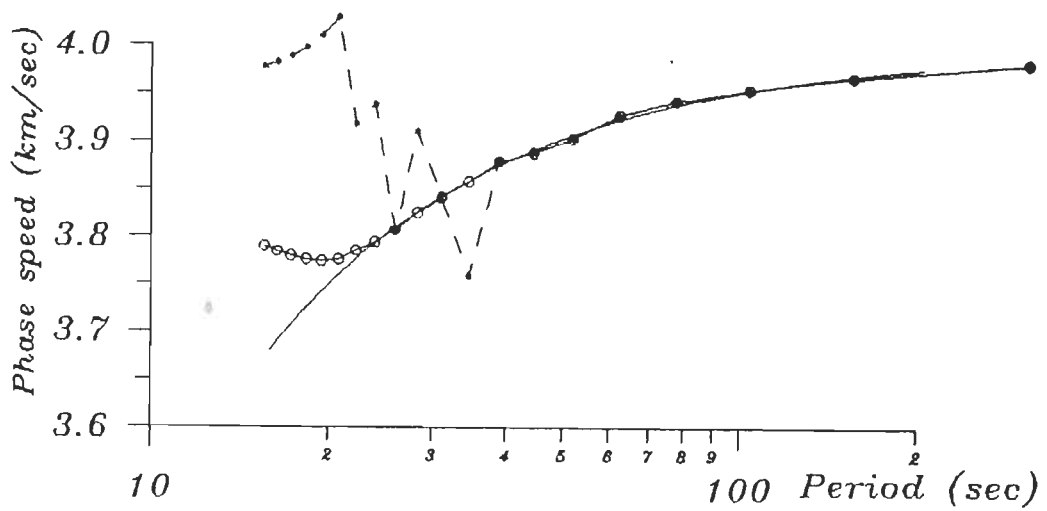
FIG. 3.11 COMPARISON OF COMPUTED AND ORIGINAL PHASE SPEED CURVES FOR EXPERIMENTS 8.

TABLE 3.2 NECESSARY INFORMATION ABOUT SECOND GROUP OF EXPERIMENTS

experiment No.	Station No.	$u_i(T)$	$u_l(T)$	Seismogram duration (s)	sampling rate (s)	No. of digi-tized points
5	I	u(64)	u(16)	264	1	264
5	II	"	"	450	"	450
6	I	u(204)	u(16)	312	"	312
6	II	"	"	532	"	532
7	I	u(64)	u(16)	302	"	302
7	II	"	u(24)	"	"	"
8	I	u(204)	u(16)	312	"	312
8	II	"	u(32)	"	"	"

III GROUP EXPERIMENTS

In this group of experiments the number of digitized point was 2^{10} or (1024) at both stations. Thus FFT could be used. For experiments 9 and 10 $u_{i1}=u_{i2}$ and $u_{l1}<u_{l2}$. As a result the durations and rates of digitizations were different at both stations. For experiments 11 and 12 $u_{i1}=u_{i2}$ but the duration and rate of digitization being the same at both stations $u_{l1}<u_{l2}$. Details are shown in Table 3.3. Needless to say, the number of digitized points is the same for both stations in each of these two experiments.

As seen from Figs. 3.12 and 3.13 Experiments 9 and 10 do not give good results. On the other hand Figs. 3.14 and 3.15 show that
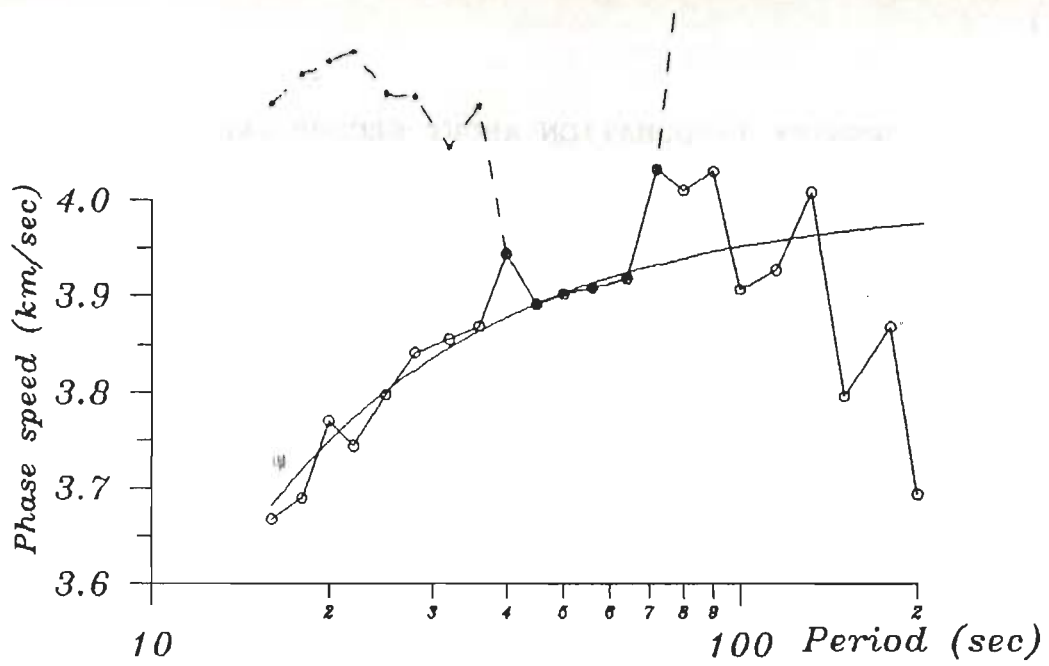
FIG. 3.12 COMPARISON OF COMPUTED AND ORIGINAL PHASE SPEED CURVES FOR EXPERIMENTS 9.
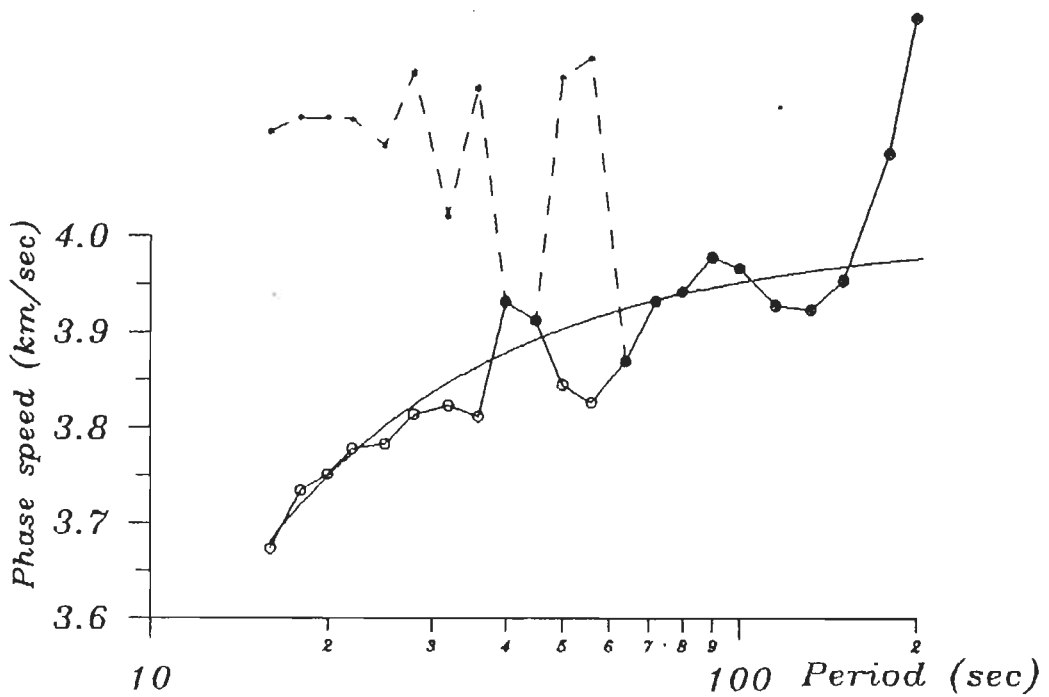
FIG. 3.13 COMPARISON OF COMPUTED AND ORIGINAL PHASE SPEED CURVES FOR EXPERIMENTS 10.
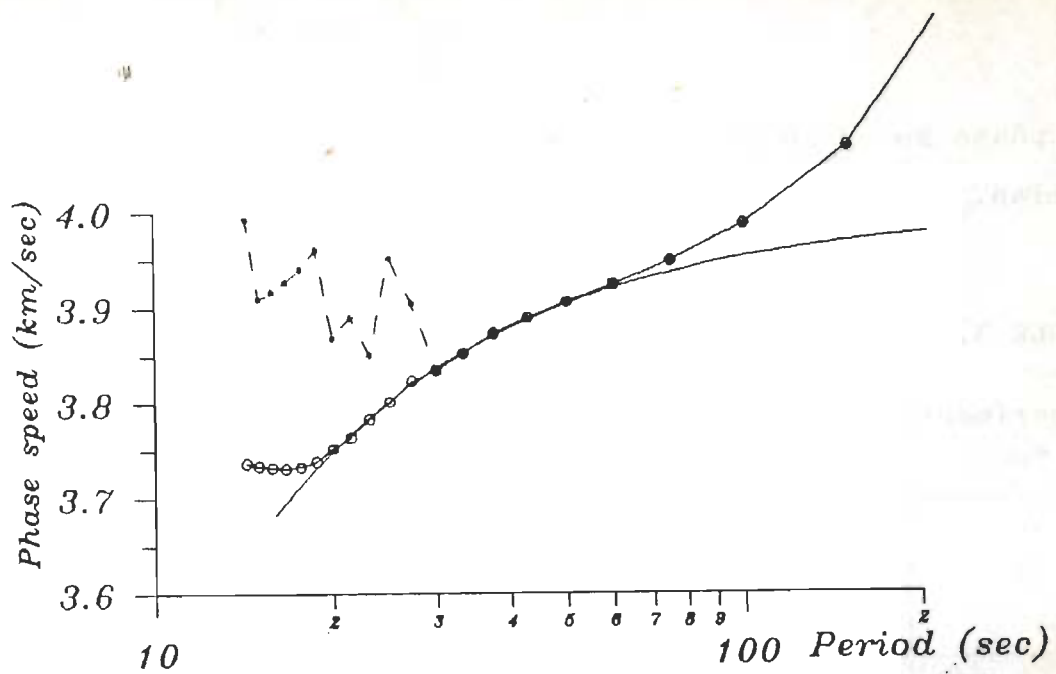
FIG. 3.14 COMPARISON OF COMPUTED AND ORIGINAL PHASE SPEED CURVES
FOR EXPERIMENTS 11.
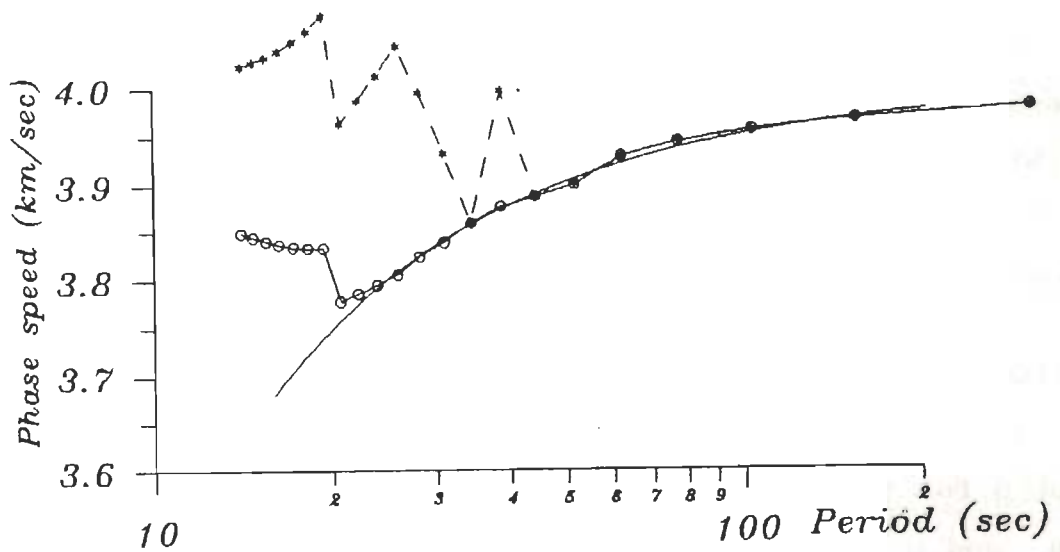
FIG. 3.15 COMPARISON OF COMPUTED AND ORIGINAL PHASE SPEED CURVES
FOR EXPERIMENTS 12.

77

the phase speed results are very good in the period range of overlap.

TABLE 3.3 NECESSARY INFORMATION ABOUT THIRD GROUP OF EXPERIMENTS

experiment No.	Station No.	$u_1(T)$	$u_2(T)$	Seismogram duration (s)	sampling rate (s)	No. of digitized points
9	I	u(64)	u(16)	262	0.26	1024
	II	"	"	449	0.44	"
10	I	u(204)	"	310	0.30	"
	II	"	"	531	0.52	"
11	I	u(64)	"	300	0.29	"
	II	"	u(24)	"	"	"
12	I	u(204)	u(16)	310	0.30	"
	II	"	u(24)	"	"	"

Thus the lesson of the previous group (II groups) of experiments is reinforced. In addition even though the number of digitized points was very large, the use of FFT enabled us to get the results in less time than the use of DFT in the previous experiments.

IV GROUP EXPERIMENTS

For Experiments 13 to 16 the same rate of digitization was adopted for the both stations. However for Experiments 13 and 14 $u_{i1}=u_{i2}$ and $u_{i1} \neq u_{i2}$ because the number of digitized points was

the same at the both stations. Before taking FFT the time series were padded at the end with zeros to bring the total number of point to 2^{10} (Table 3.4). For Experiment 15 and 16 $u_{i1}=u_{i2}$ and $u_{t1}=u_{t2}$ As a result, since the digitization rate is the same also at both stations, therefore the number of samples were different at two stations. Thus different number of zeros were padded at the end of the time series to bring the number of digitized points to 2^{10} in each case.

TABLE 3.4 NECESSARY INFORMATION ABOUT FOURTH GROUP OF EXPERIMENTS

experiment No.	Station No.	u_i (T)	u_t (T)	Seismogram duration (s)	sampling rate (s)	NO. of zeros padded *
13	I	u(64)	u(16)	301	1	723
	II	"	u(20)	"	"	"
14	I	u(204)	u(16)	311	"	713
	II	"	u(25)	"	"	"
15	I	u(64)	u(16)	263	"	761
	II	"	"	450	"	574
16	I	u(204)	"	311	"	713
	II	"	"	532	"	492

* The number of points in the sequence is 2^{10} (1024) after the padding.

The common theme of the results shown in Figs. 3.16 to 3.19 are that good phase speed results are obtained over the period range of overlap. Also the digitization rates should be the same

79
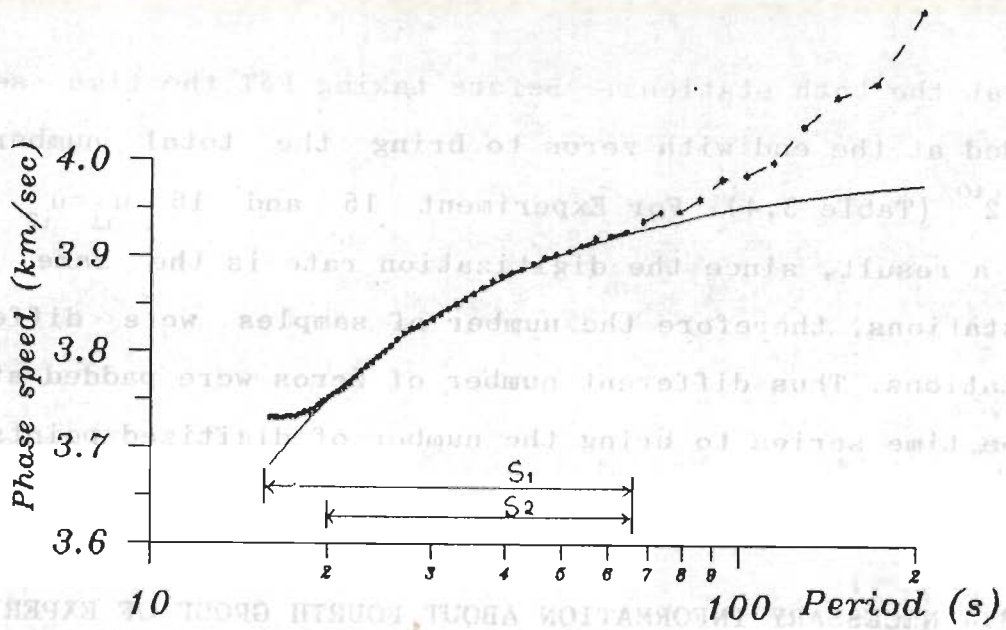
FIG. 3.16 COMPARISON OF COMPUTED AND ORIGINAL PHASE SPEED CURVES
FOR EXPERIMENTS 13.
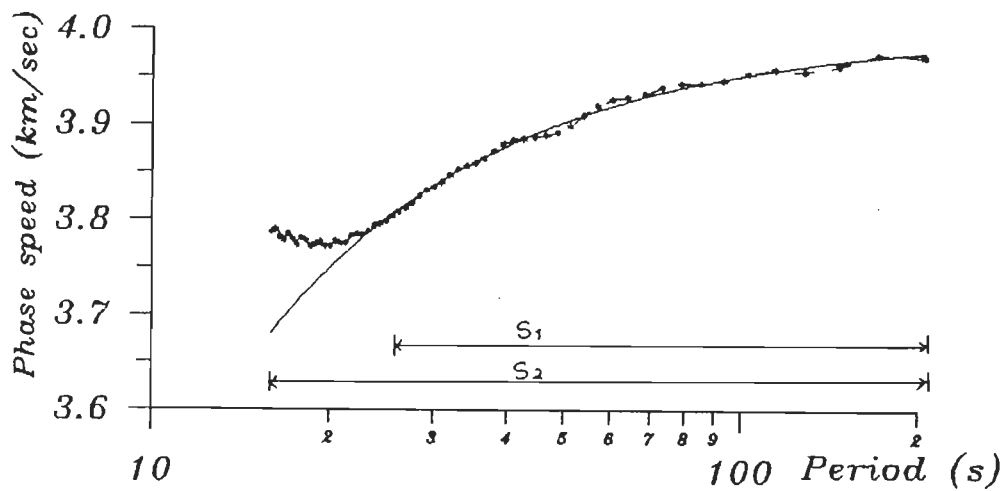
FIG. 3.17 COMPARISON OF COMPUTED AND ORIGINAL PHASE SPEED CURVES
FOR EXPERIMENTS 14.
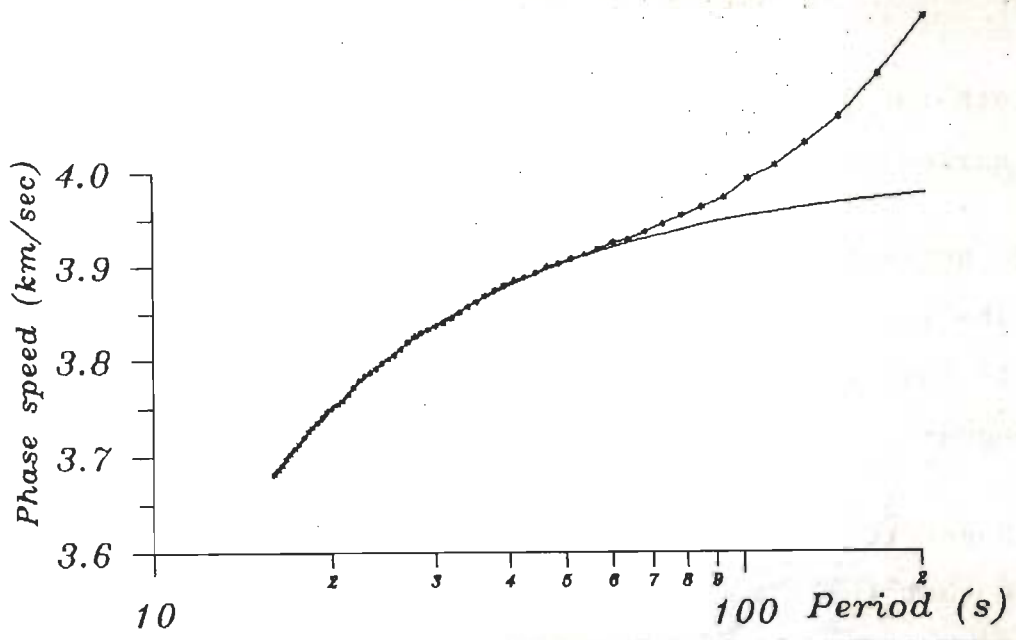
FIG. 3.18 COMPARISON OF COMPUTED AND ORIGINAL PHASE SPEED CURVES FOR EXPERIMENTS 15.
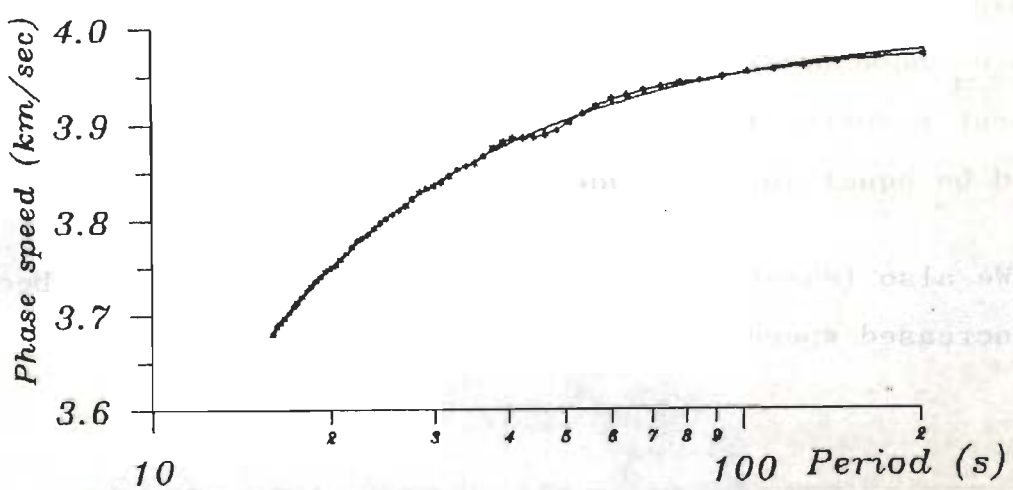
FIG. 3.19 COMPARISON OF COMPUTED AND ORIGINAL PHASE SPEED CURVES FOR EXPERIMENTS 16.

81

for both the stations and the total number of points in the padded
time series should be the same.

3.2.2 RULES LEARNT FROM THE 16 EXPERIMENTS

The following rules may be given.

1- Same rate of digitization must be used for both the
seismograms.

2-Before using the DFT or FFT programs it is necessary to
ensure that the time series obtained from digitization of two
seismograms have the same number of terms. This may require
suitable padding by zeros at the end of one or both the digitized
series.

3- In these experiments, as the total number of points in
each of the two time series increased, the agreement between the
computed and original known dispersion curves increased.

4- The phase speed results are most reliable for the period
range of overlap, i.e. period range for which wave groups exist in
the digitized parts of both the seismograms. Thus in principle
while u_{i1} need not equal u_{i2} and u_{i1} and need not equal u_{i2}, but
for best results, the two u_i's should be equal and the two u_i's
should be equal in magnitude.

We also learnt that FFT may be preferred over DFT because of
the increased speed of computation.

3.3 CHECKING THE PROGRAM FOR COMPUTATION OF RAYLEIGH WAVE PHASE SPEED DISPERSION FOR A GIVEN HORIZONTALLY LAYERED MODEL

Our primary interest in this thesis is to interpret the observed phase speed dispersion curve for Rayleigh wave in terms of layered models of the earth in the Iranian region. To solve this inverse problem we need to be able to solve the corresponding direct problem, namely, to compute the Rayleigh wave phase speed dispersion curves for specified horizontally layered models. In the preceding chapter we have summarized the computational algorithm of Schwab and Knopoff (1972). In order to be sure that this algorithm and the corresponding computer program are working satisfactorily we searched the literature for an article in which the layered model and corresponding Rayleigh wave phase speed dispersion data are displayed in tabular rather than graphical form. The article by Dorman et al., (1960) was the only one we could find in our library.

The results of the comparison are displayed in Table 3.5 to 3.8 for four different layered models. The model is given in the left part of each table and the phase speed results in the right part. Tables 3.5 and 3.6 refer to different thicknesses of Jeffreys-Bullen P and S speeds and density profiles of the earth while Tables 3.7 and 3.8 refer to models 8026 and 8096 considered by Dorman et al., (1960). Column 4 in lower part of each of these tables gives the differences between our and Dorman et al.'s computed phase speeds at different periods.

It is acknowledged that Dorman et al.'s (1960) calculations

TABLE 3.5 MODEL AND PHASE SPEED RESULTS FOR JEFFRYS-BULLEN EARTH MODEL. TOTAL THICKNESSES OF LAYERS IS 1200 km.

Layer No.	Thick. (km)	Vp (km/s)	Vs (km/s)	Density g/cm³
1	15.0	5.57	3.36	2.65
2	18.0	6.50	3.74	2.87
3	17.0	7.775	4.36	3.33
4	25.0	7.83	4.39	3.35
5	35.0	7.92	4.44	3.37
6	40.0	8.04	4.49	3.41
7	50.0	8.19	4.56	3.45
8	50.0	8.35	4.64	3.49
9	50.0	8.50	4.72	3.53
10	50.0	8.67	4.80	3.57
11	63.0	8.86	4.90	3.615
12	37.0	9.14	5.04	3.70
13	100.0	9.65	5.31	3.89
14	100.0	10.25	5.66	4.125
15	100.0	10.68	5.93	4.32
16	100.0	11.00	6.13	4.49
17	150.0	11.28	6.29	4.62
18	200.0	11.57	6.44	4.739
19	∞	11.99	6.62	4.915

Period (s)	Phase speed (km/s) Kamalian	Dorman	Difference K - D
66.036	4.002	4.002	1.6E-6
68.350	4.011	4.011	2.7E-4
70.853	4.02	4.02	2.7E-6
93.528	4.10	4.10	2.0E-7
96.300	4.11	4.11	3.4E-4
99.252	4.12	4.12	2.3E-6

TABLE 3.6 MODEL AND PHASE RESULTS FOR JEFFRYS-BULLEN EARTH MODEL.
TOTAL THICKNESSES OF LAYERS IS 650 km.

Layer No.	Thick. (km)	Vp (km/s)	Vs (km/s)	Density g/cm^3
1	15.0	5.57	3.36	2.65
2	18.0	6.50	3.74	2.87
3	17.0	7.775	4.36	3.33
4	25.0	7.83	4.39	3.35
5	35.0	7.92	4.44	3.37
6	40.0	8.04	4.49	3.41
7	50.0	8.19	4.56	3.45
8	50.0	8.35	4.64	3.49
9	50.0	8.50	4.72	3.53
10	50.0	8.67	4.80	3.57
11	63.0	8.86	4.90	3.615
12	37.0	9.14	5.04	3.70
13	100.0	9.65	5.31	3.89
14	100.0	10.25	5.66	4.125

Period (s)	Phase speed (km/s)		Difference K - D
	Kamalian	Dorman	
43.898	3.90004	3.90004	1.5E-6
45.57	3.90995	3.91004	8.9E-5
47.384	3.92004	3.92004	4.2E-6

TABLE 3.7 MODEL AND PHASE RESULTS FOR CASE-8026 EARTH MODEL. TOTAL THICKNESSES OF LAYERS IS 550 km.

Layer No.	Thick. (km)	Vp (km/s)	Vs (km/s)	Density g/cm^3	Period (s)	Phase speed (km/s) Kamalian	Dorman	Difference K - D
1	19.0	6.15	3.55	2.817	44.515	3.99127	4.00157	1.0E-2
2	19.0	6.58	3.80	2.922	46.345	3.99874	4.00887	1.0E-2
3	37.0	8.14	4.70	3.300	48.341	4.00611	4.01606	1.0E-2
4	35.0	7.92	4.44	3.37	50.526	4.01348	4.02323	9.8E-3
5	40.0	8.04	4.49	3.41	52.925	4.02096	4.03051	9.5E-3
6	50.0	8.19	4.56	3.45	58.501	4.03688	4.04595	9.1E-3
7	50.0	8.35	4.64	3.49	55.571	4.02871	4.03802	9.3E-3
8	50.0	8.50	4.72	3.53	61.762	4.04568	4.05450	8.8E-3
9	50.0	8.67	4.80	3.57	65.411	4.05536	4.06390	8.5E-3
10	63.0	8.89	4.90	3.615	69.519	4.06622	4.07448	8.3E-3
11	37.0	9.14	5.04	3.70	74.178	4.07864	4.08658	7.9E-3
12	100.0	9.65	5.31	3.89	76.748	4.08559	4.09336	7.8E-3
13	——	10.25	5.66	4.125	79.501	4.09312	4.10072	7.6E-3
					82.235	4.10070	4.10877	8.1E-3

86

TABLE 3.8 MODEL AND PHASE RESULTS FOR CASE-8096 EARTH MODEL. TOTAL
     THICKNESSES OF LAYERS IS 220 km.

Layer No.	Thick. (km)	Vp (km/s)	Vs (km/s)	Density g/cm³	Period (s)	Phase speed (km/s) Kamalian	Dorman	Difference K − D
1	5.0	1.52	0.000	1.0300	13.102	2.97	2.97	2.2E-5
2	1.0	2.10	1.0000	2.1000	18.131	3.90	3.90	2.1E-5
3	5.0	6.41	3.7000	2.8400	19.002	3.923	3.920	3.2E-3
4	49.0	7.82	4.6125	3.3400	19.873	3.94	3.94	4.6E-6
5	100.0	8.17	4.3000	3.4425	21.243	3.958	3.955	3.2E-3
6	60.0	7.94	4.6375	3.3800	22.614	3.97	3.97	2.6E-6
7	—	8.49	4.7660	3.5265	24.375	3.9795	3.9775	1.9E-3
					26.137	3.985	3.985	3.0E-7
					27.942	3.9882	3.9875	7.1E-4
					29.747	3.99	3.99	2.0E-7
					43.513	3.995	3.995	1.0E-7
					45.980	3.9972	3.9975	3.3E-4
					48.447	4.00	4.00	6.0E-7
					51.556	4.004	4.005	5.0E-4
					54.665	4.01	4.01	8.0E-7

were carried out on a IBM 650 early generation computer. The maximum floating point number that could be handled by that computer must have restricted the accuracy of results. But such a problem is much less severe for our computer. In fact the feature of Schwab and Knopoff algorithm to control overflow (Appendix C) during these computations was never used by us.

We suspect that the overflow problem must have been severe for computations by Dorman et al. in case of their model 8026 because the agreement between our and their results in this case is only of the order of 1×10^{-2}. For other models the agreement is better, being as good as 1×10^{-7} at some periods.

Fig. 3.20 is a graphical comparison of Rayleigh wave phase speed values reported by Bullen and Bolt (1985) and those from our computer program. Similarly Fig. 3.21 is a comparison of Rayleigh wave group speed dispersion values computed by Chen and Molnar (1975) and our program for a simple two layered model of crust in Tibet. Tables 3.9 and 3.10 shows the layer parameters of those models.

We conclude from these comparisons that our computer program for computation of Rayleigh wave phase speed dispersion is working reasonably. We thus proceeded to use it as a subroutine in our inversion program which is tested next.
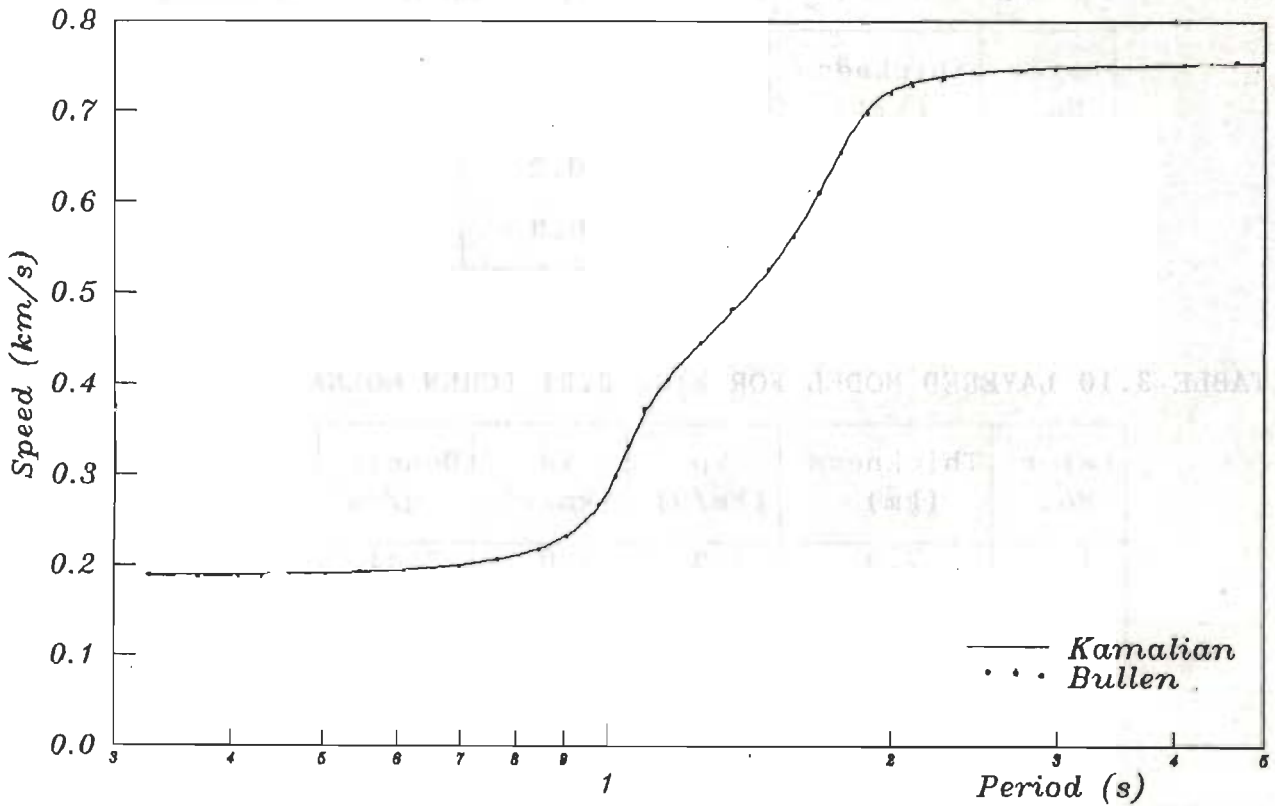
FIG. 3.20 COMPARISON OF PHASE SPEED VALUES GIVEN BY BULLEN AND BOLT AND THOSE COMPUTED BY OUR PROGRAM FOR THE SAME MODEL (See Table 3.9)
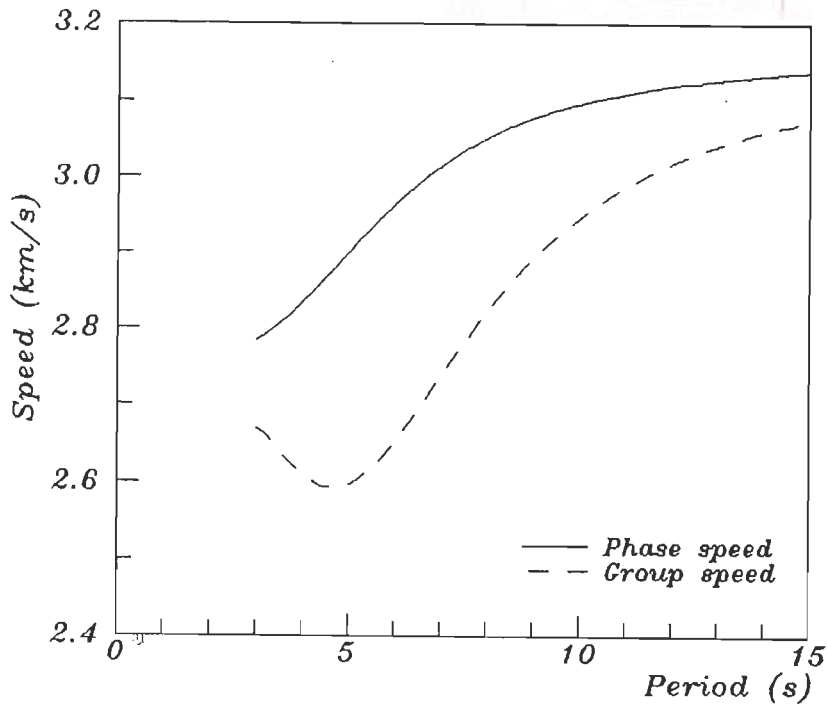
FIG. 3.21 COMPARISON OF PHASE SPEED VALUES GIVEN BY CHEN AND MOLNAR 1975 AND THOSE COMPUTED BY OUR PROGRAM FOR THE SAME MODEL (See Table 3.10)

89

TABLE 3.9 LAYERED MODEL FOR FIG. 3.20 (BULLEN AND BOLT 1984).

Layer No.	Thickness (km)	Vp (km/s)	Vs (km/s)	Density g/cm^3
1	0.1	0.57	0.2	1.7
2	—	2.6	0.8	2.2

TABLE 3.10 LAYERED MODEL FOR FIG. 3.21 (CHEN MOLNAR 1975).

Layer No.	Thickness (km)	Vp (km/s)	Vs (km/s)	Density g/cm^3
1	7.0	5.9	3.0	2.41
2	—	6.05	3.5	2.67

3.4 TESTING OF THE PROGRAM FOR INVERSION OF RAYLEIGH WAVE PHASE SPEEDS IN TERMS OF A HORIZONTAL LAYERED MODEL OF THE EARTH

As noted in Chapter 2, we adopted the theory of Yuan and Nazarian (1993) for the proposed inversion and wrote our own algorithm and computer program to implement it. Since inversion of observed Rayleigh wave phase speed dispersion curve using this program is a necessary operation for all our data, it is important to test this program rigorously. For the purpose, we created elaborate synthetic exercises with error free and error prone data. The layered model comprising of three layers resting on a half space shown in Table 3.11 and Fig. 3.22 was assumed. The phase and group speed dispersion curves for the fundamental model Rayleigh waves were computed and are displayed in Fig. 3.23. The

speed (km/s) & density (g/cm³)
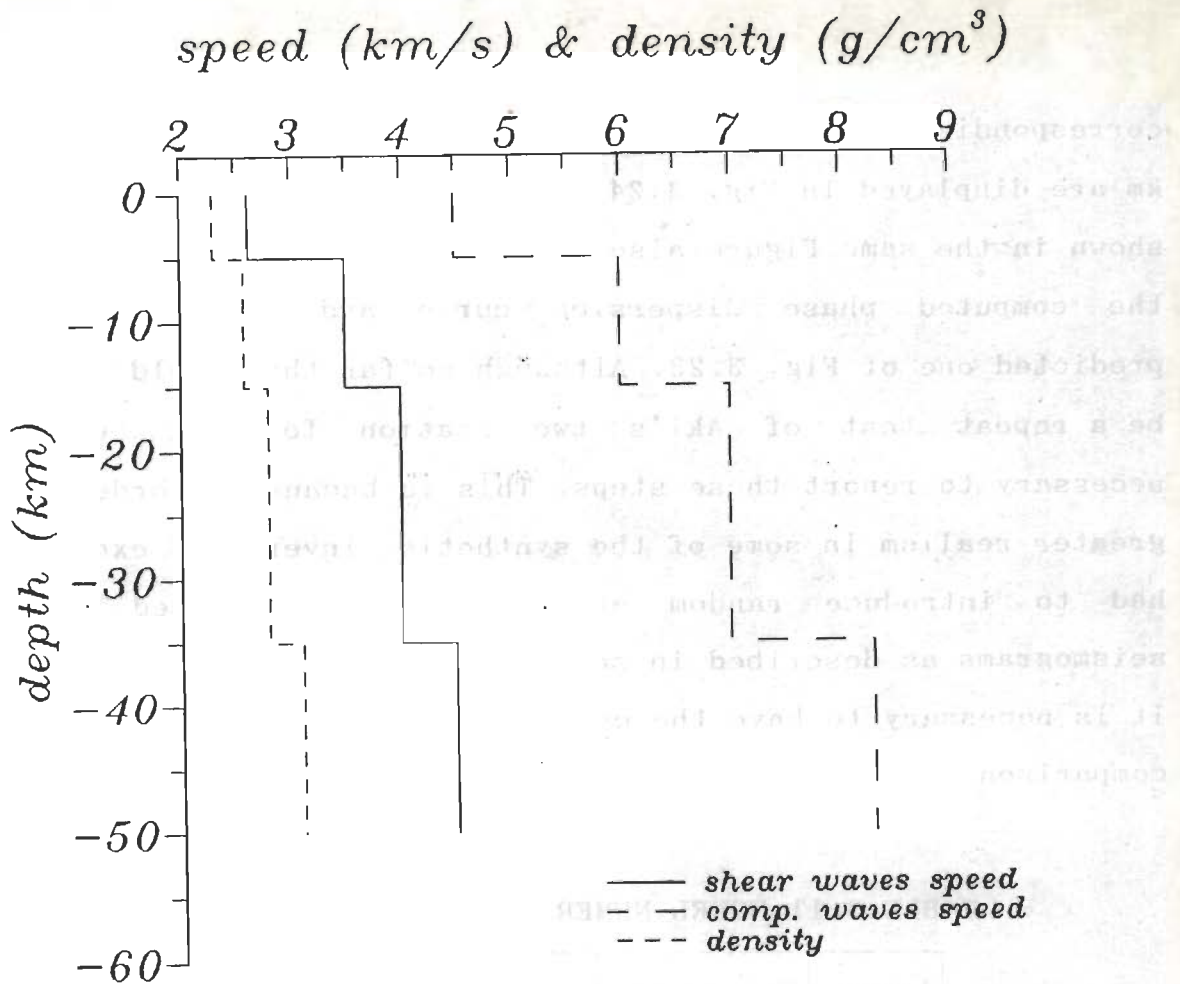
FIG. 3.22 GRAPHICAL DISPLAY OF LAYERED MODEL USED TO TEST THE INVERSION PROGRAM
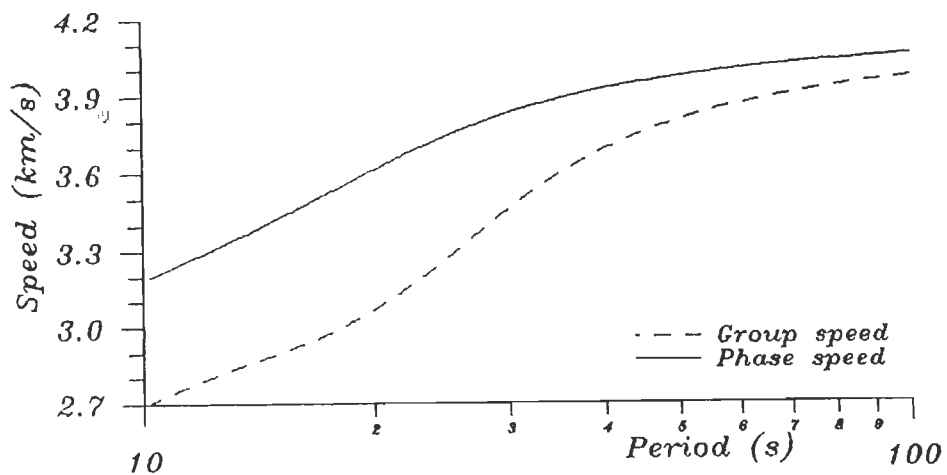
FIG. 3.23 THEORETICAL PHASE AND GROUP SPEEDS CURVES FOR MODEL OF FIG. 3.22.

91

corresponding synthetic seismograms for distances of 4000 and 5500 km are displayed in Fig. 3.24. The cross correlogram of the two is shown in the same Figure also. Fig. 3.25 is a display comparing the computed phase dispersion curve and the theoretically predicted one of Fig. 3.23. Although so far this would appear to be a repeat test of Aki's two station formula, but it was necessary to report these steps. This is because in order to bring greater realism in some of the synthetic inversion exercises we had to introduce random errors in the computed synthetic seismograms as described in some of the following subsections and it is necessary to have the case of error free data available for comparison.

TABLE 3.11 MODEL NUMERICAL DATA FOR FIG. 3.22.

Layer No.	Thickness (km)	Vp (km/s)	Vs (km/s)	Density g/cm^3
1	5.0	4.5	2.6	2.3
2	10.0	6.0	3.5	2.6
3	20.0	7.0	4.0	2.8
4	——	8.3	4.5	3.1

3.4.1 INVERSION FOR SHEAR WAVE SPEEDS ONLY

3.4.1.1 ERROR FREE SEISMOGRAMS

The Rayleigh wave phase speed dispersion curve so computed was then used as the input for the inversion program. In the first exercise we maintained the same number of layers as in the known

$t_o=1002$ s

$r1=4000$ km

$r2=5500$ km

$t_o=1377$ s

$t_o=375$ s

Cross-correlogram

0 1 2 3 4 5 6 7 8 9 10 11 12

Time (min)
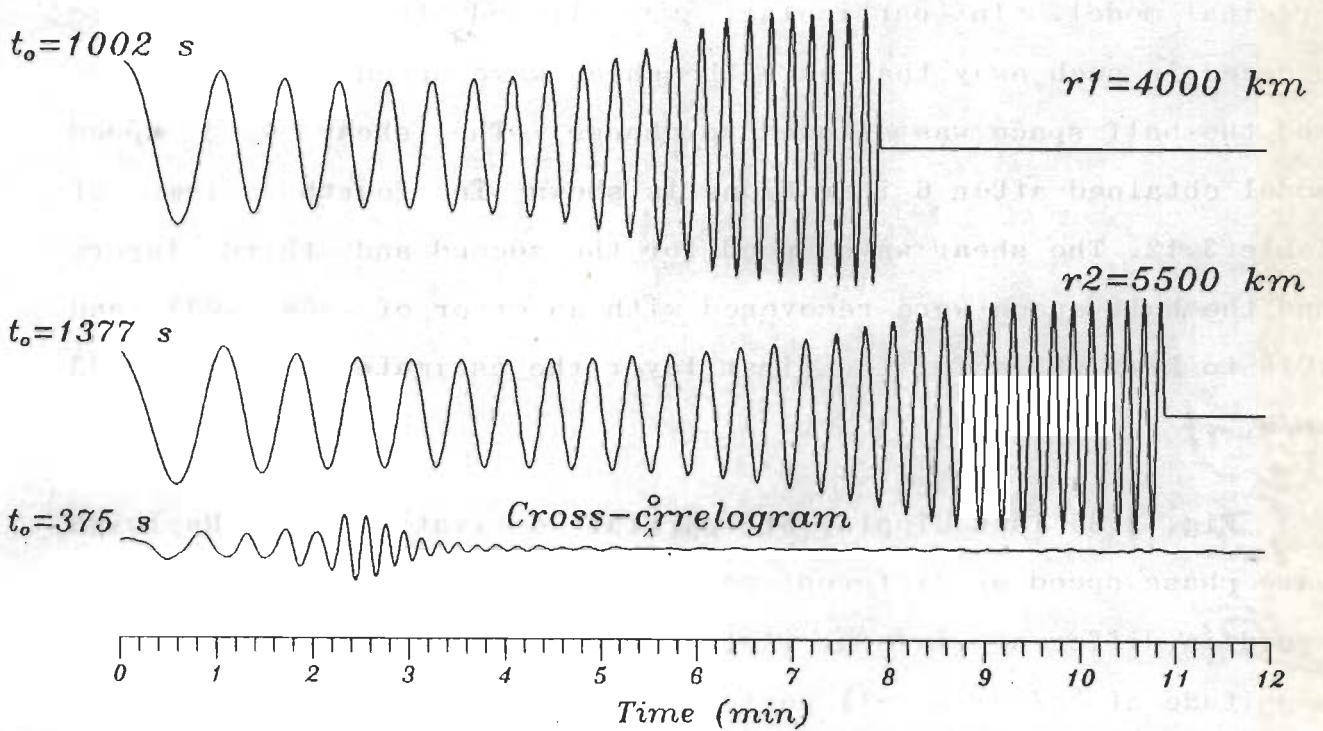
FIG. 3.24 SYNTHETIC SEISMOGRAMS AT DISTANCES OF 4000 AND 5500 km CORRESPONDING TO DISPERSION CURVE OF FIG. 3.23. tHE GROUP ARRIVAL TIME AT THE BEGINNING OF EACH SEISMOGRAM IS NOTED. THE BOTTOM TRACE IS THE CROSS CORRELOGRAM OF THE TWO SEISMOGRAMS FOR A TIME SHIFT OF 375 s.

4.2

3.9

3.6

3.3

3.0

2.7

Phase speed (km/s)

– – – *Model*

* * * * * *Result*

10

100

Period (s)
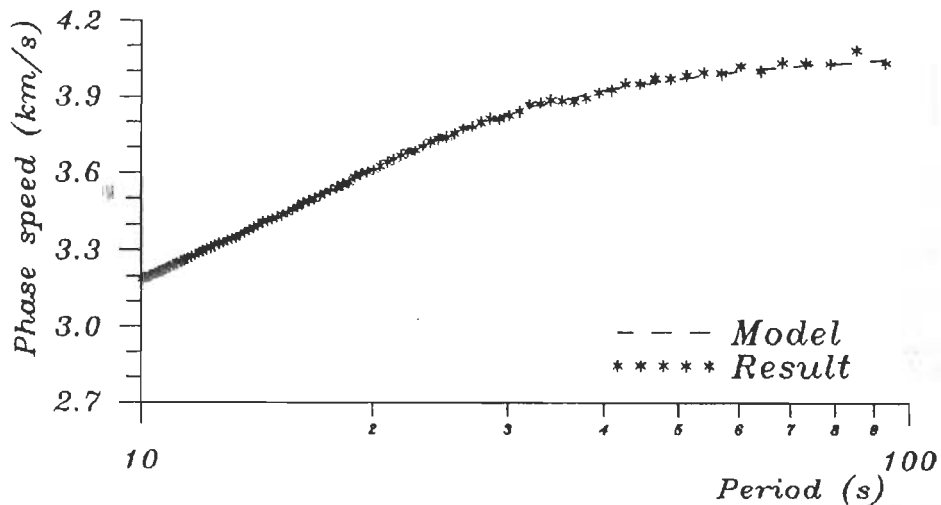
FIG. 3.25 COMPARISON OF PHASE SPEEDS COMPUTED FROM SEISMOGRAMS OF FIG. 3.24 AND THE KNOWN CURVE FROM FIG. 3.23.

93

original model. In particular, we allowed the iterations to proceed in such away that only the shear wave speed in the layers and the half space was allowed to change. The shear wave speed model obtained after 6 iterations is shown in fourth column of Table 3.12. The shear wave speed for the second and third layers and the half space were recovered with an error of .054, .037 and .016 to km/s while for the first layer the estimate was off by .33 km/s.

Fig. 3.26 is a display of partial derivatives of Rayleigh wave phase speed at different period with respect to shear wave speed in different layers ($\delta c(T)/\delta \beta_i$, i=1,2,3,4). The small magnitude of $\delta c/\delta \beta_1$ at all periods greater than about 1 second should account for the relatively large error in recovering the value of β_1 in this synthetic exercise.

TABLE 3.12 CHECKS ON THE INVERSION PROGRAM (See text). ONLY SHEAR WAVE SPEED INVERTED.

Layer No.	$\beta_{original}$	$\beta_{initial}$	β After inversion		
			Free	4% Noise	10% Noise
1	2.6	2.5	2.27	2.30	2.29
2	3.5	3.5	3.55	3.56	3.55
3	4.0	4.0	4.04	4.03	4.03
4	4.5	4.2	4.52	4.51	4.51
RMS error			0.0069	0.0064	0.0064
No. of iterations			6	4	5

β in km/s
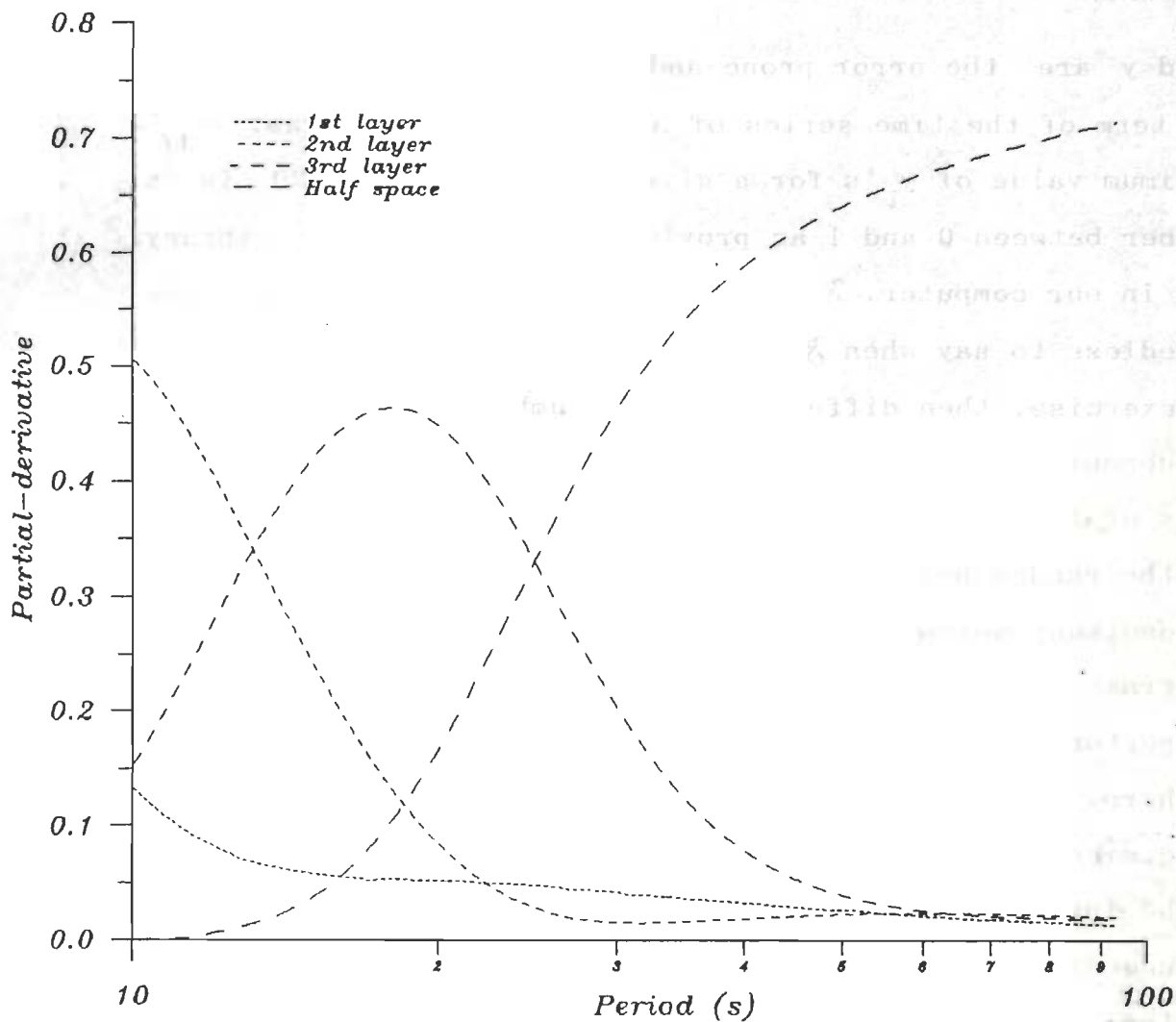
FIG. 3.26 PARTIAL DERIVATIVE OF PHASE SPEED WITH RESPECT TO SHEAR
WAVE SPEED FOR LAYERS 1 TO 4.

3.4.1.2 RANDOM NOISE ADDED TO SYNTHETIC SEISMOGRAMS

Next we introduced random noise of $\beta\%$ (say) to the synthetic seismograms using the following scheme.

$$y_i' = y_i + (y_{Max} . (RND-.5).2.\beta/100) \qquad \qquad ...(3.4)$$

Here y_i' and y_i are the error prone and exact values respectively of the ith term of the time series of a synthetic seismogram. y_{Max} is the maximum value of y_i's for a given time series. RND is a random number between 0 and 1 as provided by a standard library subroutine in our computer. β was 4 in one test and 10 in the second. Needless to say when $\beta\%$ random noise is introduced in a synthetic exercise, then different random numbers yielded by the computer subroutine are used in Eq. 3.4 to generate error prone seismograms of the first and the second stations. Fig. 3.27 indicates the random noise generated from the computer. Fig 3.28 displays resultant seismograms after adding 10% random noise to the seismograms of Fig. 3.24. Seismograms with 4% random noise were less perturbed than those shown in Fig. 3.28 and are not displayed here. Fig. 3.29 and 3.30 are displays of computed phase speed dispersion curves in the two cases. Column 5 and 6 of Table 3.12 are the inverted shear wave speeds in different layers. The recovered speeds are fairly comparable with those for the error free case (column 4 of Table 3.12).

3.4.2 INVERSION FOR SHEAR WAVE SPEEDS AND LAYER THICKNESSES SIMULTANEOUSLY

In these synthetic exercises the input data for the inversion program were the same as in the preceding section 3.4.1
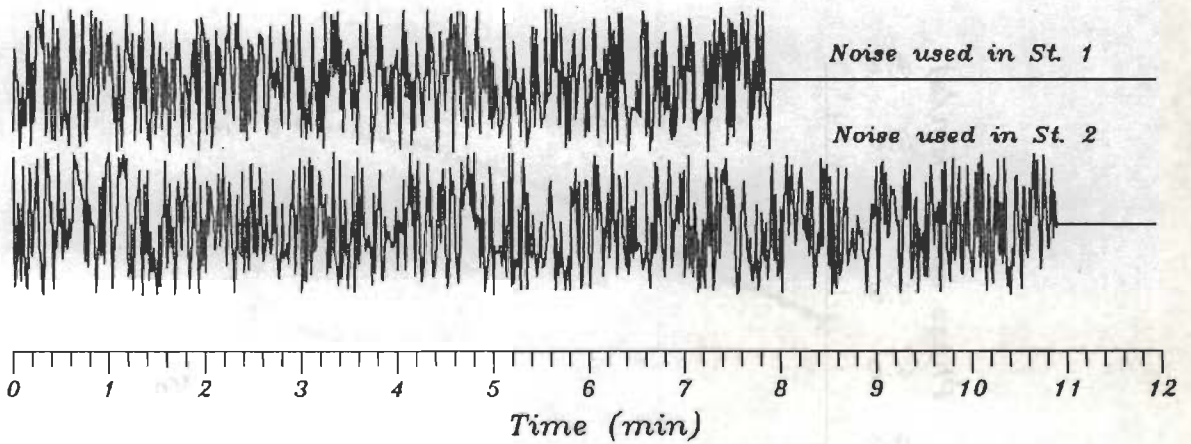
FIG. 3.27 RANDOM NOISE GENERATED BY THE COMPUTER FOR ADDITION TO SYNTHETIC SEISMOGRAMS OF STATIONS 1 AND 2 SHOWN IN Fig. 3.24
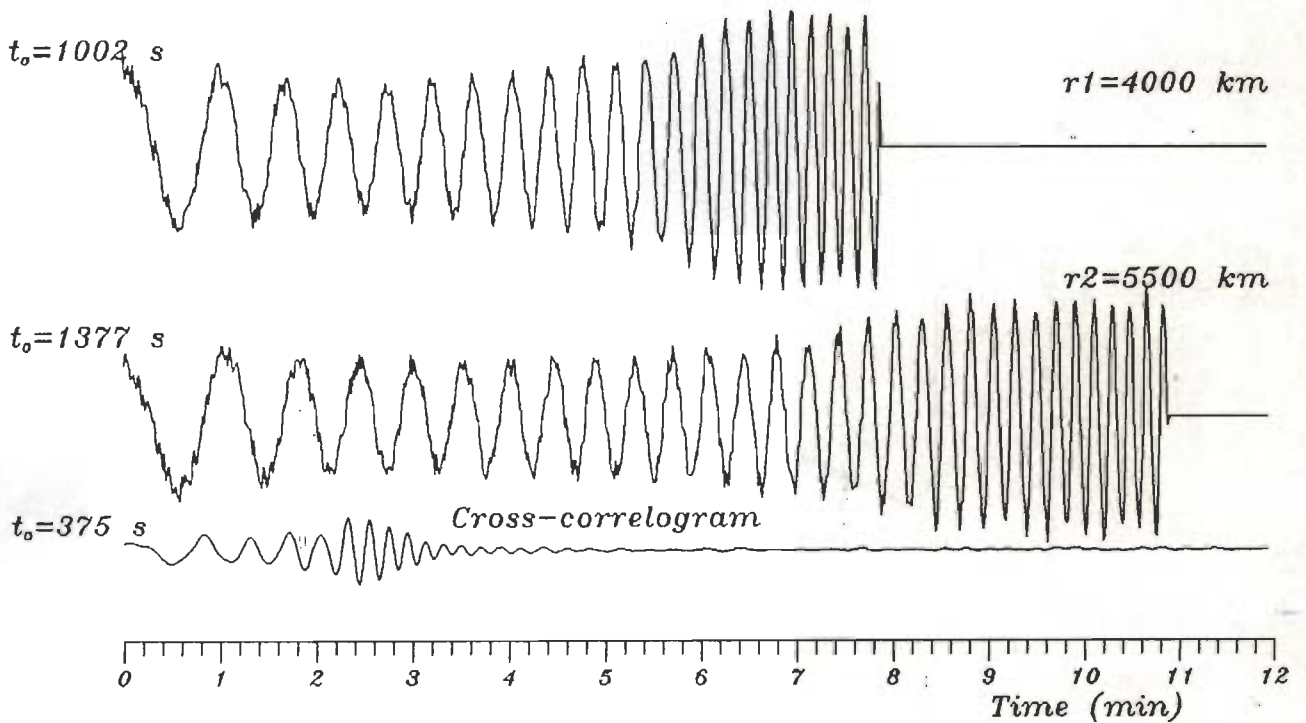
FIG. 3.28 THIS FIGURE IS SIMILAR TO Fig. 3.24. IT IS OBTAINED BY ADDING 10% OF RANDOM NOISE SERIES SHOWN IN Fig. 3.27 TO NOISE FREE SEISMOGRAMS OF Fig. 3.24.
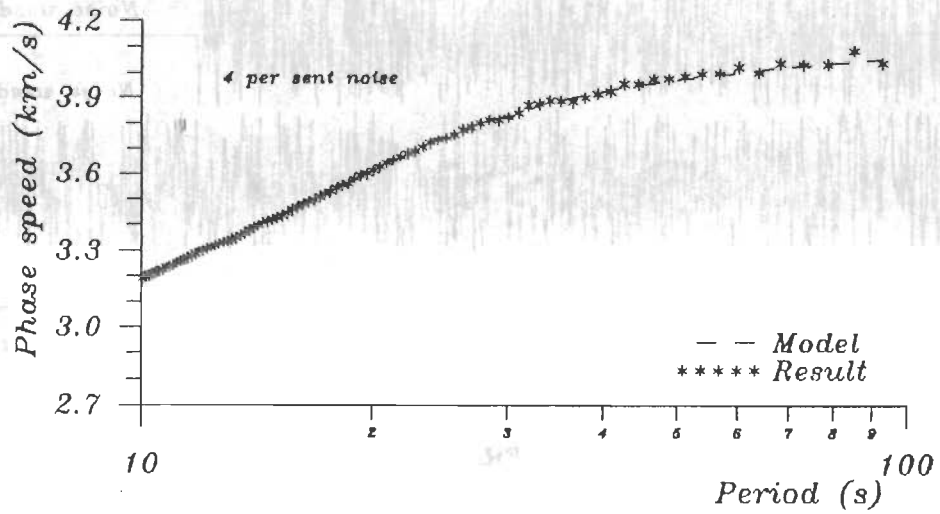
FIG. 3.29 SIMILAR TO Fig. 3.25, 4% RANDOM NOISE ADDED TO THE SYNTHETIC SEISMOGRAMS.
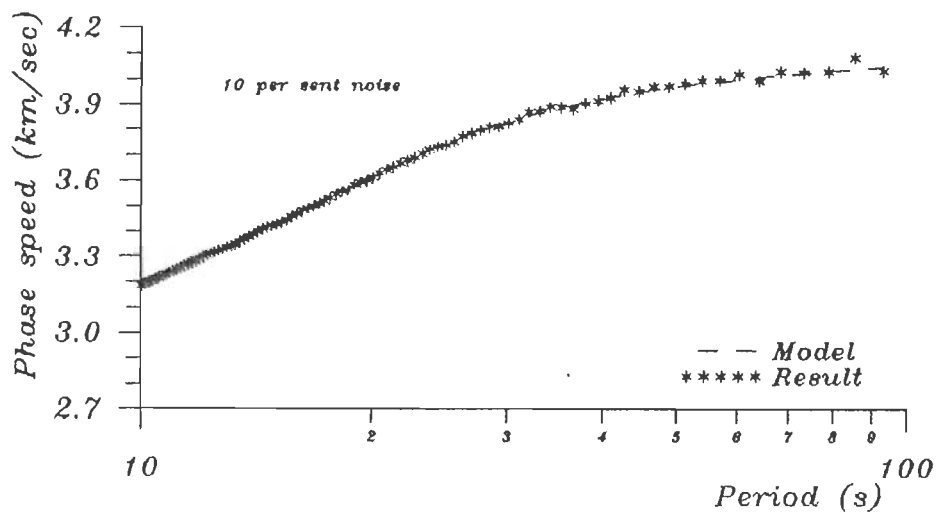
FIG. 3.30 SIMILAR TO Fig. 3.25, 10% RANDOM NOISE ADDED TO THE SYNTHETIC SEISMOGRAMS.

3.4.2.1 ERROR FREE SEISMOGRAMS

The results of the inversion are compared with the known exact values in Table 3.13. The recovered β_1 in this case is a slight improvement over that obtained in Section 3.4.1.1. On the other hand the recovered layer thicknesses h_1 and h_3 are in error by -0.15 and $+0.04$ km. However h_2 is in error by 1.56 km. Again the large error in h_2 has to be ascribed to small value of partial derivative $\delta c(T)/\delta h_2$.

3.4.2.2 4% RANDOM NOISE IN SYNTHETIC SEISMOGRAMS

The results of inversion are displayed in Table 3.13 (columns 8 and 9). The recovered values are only marginally different than those for the error free case.

3.4.2.3 10% RANDOM NOISE IN SYNTHETIC SEISMOGRAMS

The results are displayed in Table 3.13 (columns 10 and 11). Four out of seven parameter inverted are closer to the correct values than in case of 4% random noise!

TABLE 3.13 CHECKS ON THE INVERSION PROGRAM (See tesxt). ONLY SHEAR VAVE SPEED AND LAYER THICKNESSES ARE INVERTED.

Layer No.	Original		Initial		Inverted Results					
					Noise free		4% Noise		10% Noise	
	β	h	β	h	β	h	β	h	β	h
1	2.6	5.0	2.55	6.0	2.41	4.85	2.43	4.51	2.41	4.82
2	3.5	10.0	3.4	11.0	3.57	11.56	3.53	11.67	3.56	11.20
3	4.0	20.0	4.0	22.0	4.08	20.04	4.07	20.49	4.04	19.59
4	4.5	—	4.6	—	4.52	—	4.51	—	4.52	—
RMS error					0.0069		0.0064		0.0068	
No. of iterations					99		21		54	

β in km/s : h in km

3.4.2.4 CONCLUSION

In short, the inversion program does give inverted parameter values close to the known exact values. The discrepancies arise from numerical inaccuracies incurred at various stages of the synthetic exercise as well as from the nature of partial derivatives of phase speed with the layer parameters.

It is our opinion that inversion for shear wave speed and layer thicknesses should be carried out simultaneously.

It turns out that adding random noise to noise free data does not effect the results significantly. This is probably because the noise added is of a relatively higher frequency than the frequencies of interest in the inversion.

3.4.3 INVERSION FOR SHEAR WAVE SPEED IN A CRUSTAL MODEL WITH A LARGE NUMBER OF THIN LAYERS

The phase speed dispersion curve corresponding to 4% random noise in synthetic seismograms was used also to estimate shear wave speed for a crustal model with 7 layers of 5 km thickness each. Table 3.14 displays the results. The second and third layers of the original model were subdivided into 2 and 4 sublayers respectively in this inversion exercise. For the sake of specificness let us call the two sublayers of original layer 2 as 2a and 2b, similarly let the four sublayers of the third layer be called 3a, 3b, 3c, and 3d. As seen from Table 3.14 the inverted shear wave speeds in sublayers 2a and 2b are different but comparable to the original β_2. Similarly shear wave speed in sublayers 3a to 3d are different but comparable to β_3. All the departures are less than 0.19 km/s. Fig. 3.31 is a comparison of phase speed dispersion curves corresponding to shear wave speeds shown in last three columns of Table 3.14. Fig. 3.32 is a display of these shear wave speeds profiles.

In our opinion this strategy should be useful where the number of crustal layers in a region is unknown.
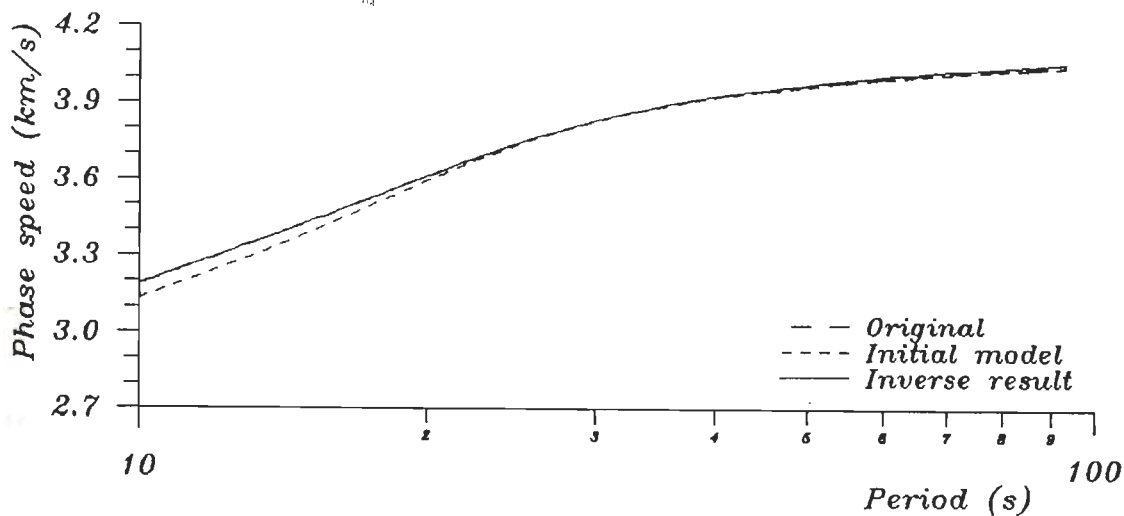
FIG. 3.31 COMPARISON OF PHASE SPEED DISPERSION CURVES CORRESPONDING TO SHEAR WAVE SPEEDS SHOWN IN LAST THREE COLUMNS OF TABLE 3.14.
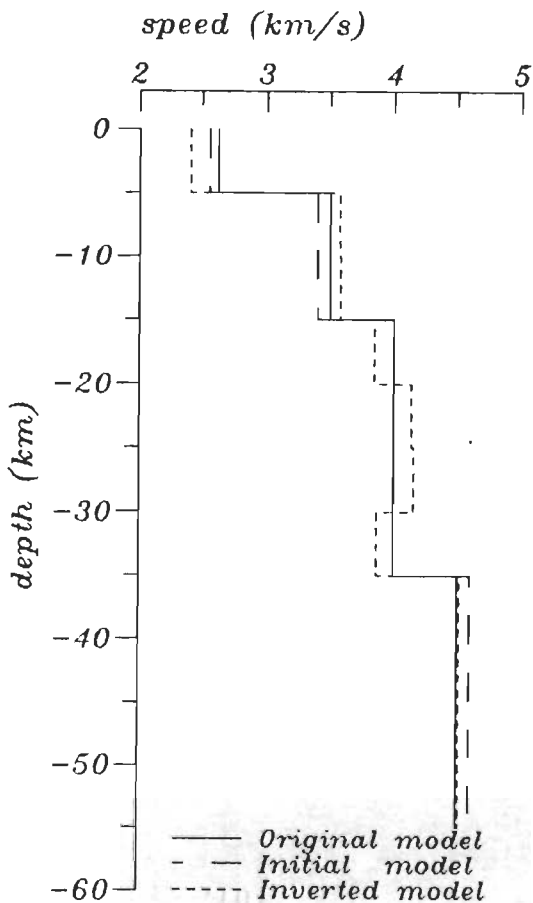
FIG. 3.32 DISPLAY OF SHEAR WAVE SPEEDS LISTED IN TABLE 3.14

TABLE 3.14 RESULTS OF INVERSION WITH SEVERAL THIN LAYERS.

Layer No.	Thickness (km)	α (km/s)	Density g/cm^3	β (km/s) Original	Initial	Result
1	5.0	4.5	2.3	2.6	2.55	2.405
2a	5.0	6.0	2.6	3.5	3.4	3.573
2b	5.0	6.0	2.6	3.5	3.4	3.577
3a	5.0	7.0	2.8	4.0	4.0	3.845
3b	5.0	7.0	2.8	4.0	4.0	4.138
3c	5.0	7.0	2.8	4.0	4.0	4.156
3d	5.0	7.0	2.8	4.0	4.0	3.867
4	—	8.3	3.1	4.5	4.6	4.515
				RMS error	0.03910	0.0071
				No. of Iterations	0	26

3.5 TEST FOR PROPOSED METHOD OF CORRECTING FOR INSTRUMENTAL RESPONSE

As indicated in chapter 2, we have proposed an alternative procedure for taking account of instrumental phase shifts before computing the phase speed dispersion curve using Aki's two station method. Here we provide graphical evidence that, under suitable conditions, the method works as desired.

Let two WWSSN vertical long period seismographs have similar calibration pulses initially. Let the responses of the two instruments change with passage of time through unnoted degradation of instrumental components. Then it is necessary to take into account the instrumental phase shifts carefully. For our synthetic exercise we used the theoretical formula of Mitchell and

Landisman (1969) to compute first the instrumental impulse responses and second through integration the step-function calibration pulses for the two instruments. The instrumental parameters assumed were $T_{1s}=13$, $T_{1g}=90$, $T_{2s}=15$, and $T_{2g}=100$ sec. Here T_s and T_g are the free period of seismometer and galvanometer respectively. The damping factor was assumed to be 1 for both seismographs and galvanometers of the two stations. The instrumental coupling factor was assumed to be unity for both instruments. The computed curves are displayed in Fig. 3.33a and b for Station 1 and 2 respectively.

The input ground motions of surface waves at the two stations were the same as used in the preceding 16 experiments (Fig. 3.2). Fig. 3.34 shows the seismograms corresponding to above impulse responses. Station 1 response is used on the ground motion at 7000 km and station 2 response on ground motion at 12000 km.

Fig. 3.35 shows the phase speed dispersion curve computed without applying the instrumental correction in the belief that the instrumental parameters are unchanged since installation. We find that while no serious error is committed at shorter period up to 30 seconds the situation gets increasingly bad at longer periods of the order of 200 seconds.

Phase speeds shown in Fig. 3.36 are obtained using the proposed method for instrumental phase correction. In particular the seismogram of Station 1 was convolved with the calibration pulse of station 2 (Fig. 3.33b). Similarly seismogram of Station 2 was convolved with the calibration pulse of station 1 . The
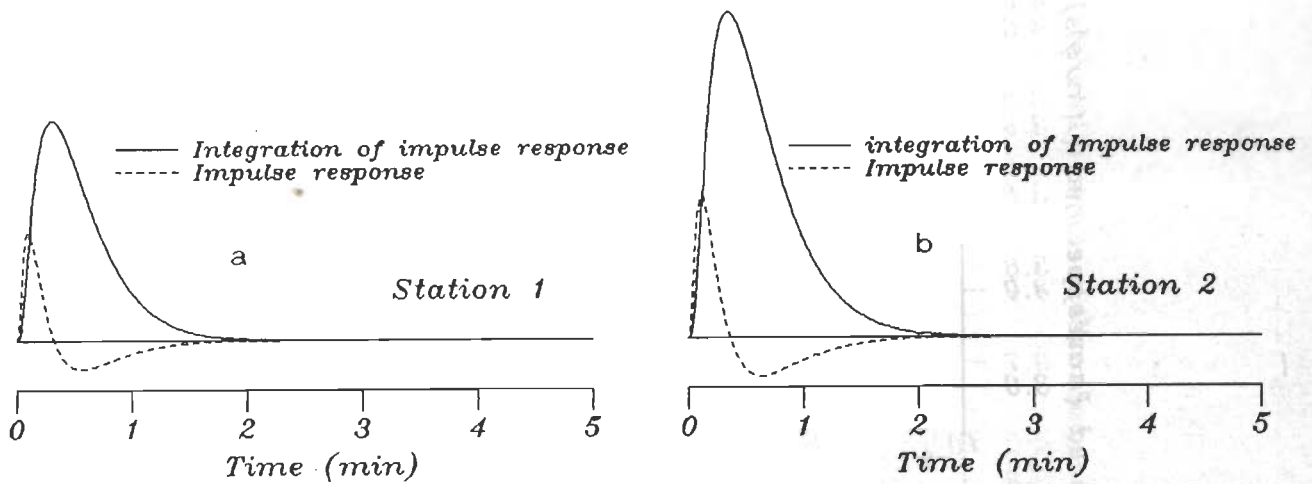
FIG. 3.33 IMPULSE RESPONSE AND STEP FUNCTION RESPONSE OF
SEISMOGRAPHS FOR STATIONS 1 AND 2 ASSUMING INSTRUMENTAL
PARAMETERS AS GIVEN IN TEXT.
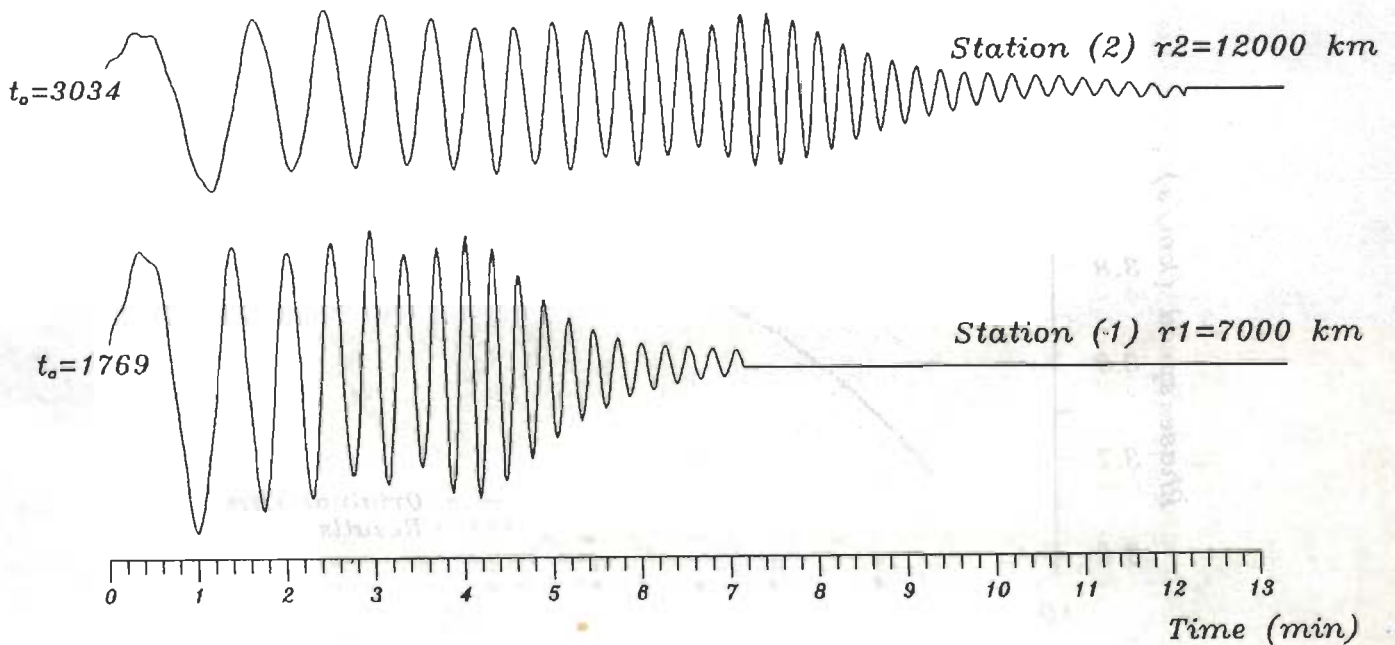
FIG. 3.34 SYNTHETIC SEISMOGRAMS OBTAINED BY CONVOLVING GROUND
MOTIONS SHOWN IN FIG. 3.2 AND IMPULSE RESPONSES SHOWN IN FIG.
3.33.
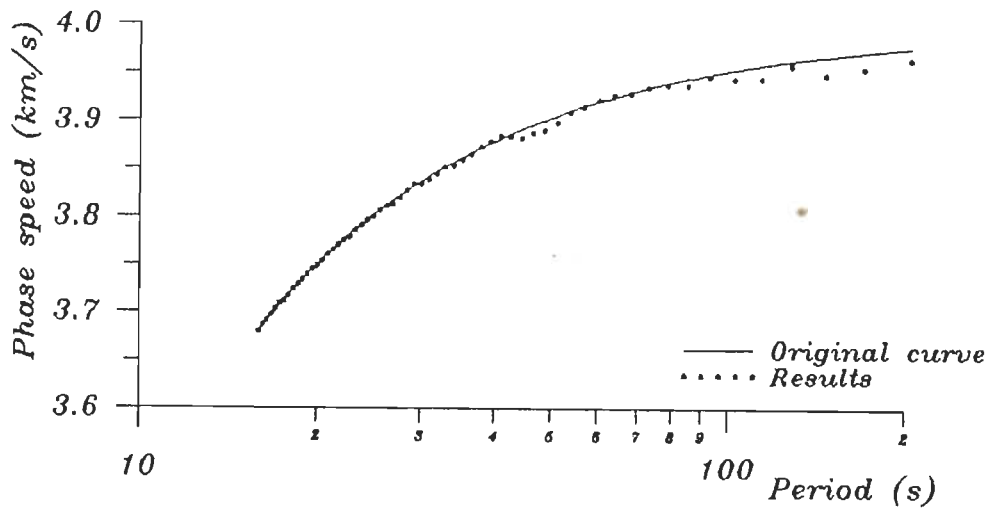
FIG. 3.35 PHASE SPEED RESULTS OBTAINED FROM SEISMOGRAMS OF Fig. 3.31 WITHOUT APPLYING INSTRUMENTAL CORRECTION.
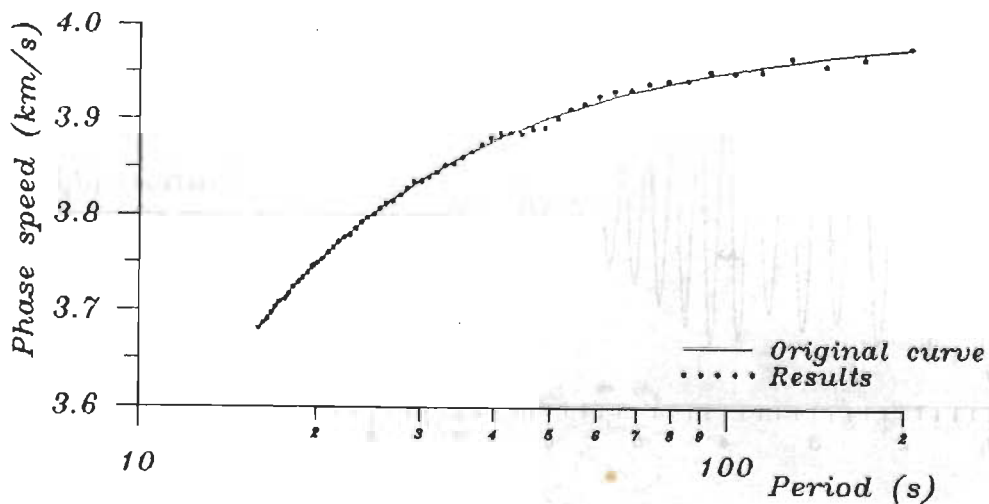
FIG. 3.36 SAME AS Fig. 3.32 BUT INSTRUMENTAL CORRECTION APPLIED USING THE PROPOSED METHOD.

106

improvement in results is small but still noticeable. Credence can be given to these small improvements because we are dealing with synthetic data here.

Thus we conclude that the proposed method of taking instrumental effects into account does work.

3.6 OTHER COMPUTER PROGRAMS

In order to carry out the complete analysis for this thesis we had to write the following computer programs also.

1. Program for computing synthetic impulse response and integration of impulse response, using formulas given by Mitchell and Landisman (1969) (used in section 3.5).

2. Program for calculation the distance and azimuth of epicenter of earthquake to seismogram stations and for selecting earthquakes from the USGS lists for analysis by the two station method (Appendix D).

3. Program for interpolation of data with 4th order splines.

4. Program for plotting of epicenter of earthquake on a map, Lambert projection (used in chapter 1 Fig. 1.12).

5. Program for cross-correlation of two time series.

6. A Gw-Basic program to display and store the digitized seismograms.

These programs were thoroughly tested also, but we omit a report on these tests because of their routine nature.

CHAPTER-4
DATA COLLECTION AND PRELIMINARY PROCESSING

4.1 INTRODUCTION

In this chapter we set out in detail all the steps taken by us to isolate 28 earthquakes occurring in different parts of the earth but yielding seismograms at Tabriz, Shiraz, and Mashhad that were suitable for further analysis.

4.2 PRELIMINARY STEPS

4.2.1 STATION DETAILS

A few data about the WWSSN stations at Tabriz, Shiraz and Mashhad are given in Table 4.1.

As seen from Fig. 1.1, the Tabriz-Shiraz line lies along the Zagros mountain chain and the Mashhad-Tabriz line along the Alborz mountain chain, Shiraz-Mashhad line cuts across several geological provinces of Iran in the central region. Together the three lines span northwest Iran in fairly comprehensive way.

By 1975 one or more components at each station were not recording regularly, therefore it was not worthwhile to consider surface wave data from these stations after the end of 1974.

TABLE 4.1 SOME DETAILS ABOUT THE WWSSN SEISMOGRAPH STATIONS
AT TABRIZ, SHIRAZ, AND MASHHAD*

Station	Latitude	longiyude	elevation (m)	T_a (s)	T_g (S)
Tabriz	38° 04' 03"	46° 19' 36"	1430	15	100
Mashhad	36° 18' 40"	59° 35' 16"	987	15	100
Shiraz	29° 38' 17.9"	52° 31' 11.8"	1959	15	100

* Reference: Report No. 49 Institute Geophysics University of Tehran 1970

4.2.2 SEARCH FOR GREAT CIRCLE PATHS

A primary requirement of the two station method for determination of phase speed is that the epicenter of the earthquake and the two stations should be located on the same great circle as nearly as possible . Also the surface waves should be well recorded at the both stations. Thus we had to deal with three great circles, namely, the great circles passing through Tabriz-Shiraz, Shiraz-Mashhad, and Mashhad-Tabriz. We had to pick out first earthquakes occurring along each of these three great circles during the period between 1967 to 1974 years.

The U.S. Geological Survey list of all the earthquakes for this time period was sifted for earthquakes of magnitude (mb) greater than or equal to 5.4. There were 3500 earthquakes in this sifted list. The list was fed into the computer and a simple search program was used to identify earthquakes whose epicenters would lie on one or the other of the above three great circles. In

110

order not to reject too many earthquakes in this way we permitted the angle $S_1 E S_2$ to have a value of up to $3°$. Here ES_1 and ES_2 are the great circles passing through the epicenter E and stations S_1 and S_2. The program identified 410, 250, and 1170 earthquakes for the Zagros (Tabriz-Shiraz), Central Iran (Shiraz-Mashhad) and Alborz (Mashhad-Tabriz) regions suitable for further scrutiny. It may be noted at this point that we have shifted the nomenclature and, for example, introduced the notion of Zagros region for the swath of country between Tabriz and Shiraz over which the Rayleigh waves investigated here propagated. This is because the stations and the epicenter do not lie on the same great circle. Compare Fig 1.1 and 4.1.

The three lists of epicenters obtained in this way were then used while examining the WWSSN long period seismograms recorded at Mashhad, Tabriz and Shiraz visually to see whether the Rayleigh waves were well recorded and could be used for phase speed determinations. Occasionally the earthquakes and seismograms which survived the above test had still to be discarded because the traces on the seismograms were crisscrossing each other or because some local earthquakes were also recorded at the time of the desired surface waves.

4.3 HYPOCENTERAL DATA FOR SELECTED EARTHQUAKES

Tables 4.2, 4.3, and 4.4 provide the necessary hypocenteral data about the earthquakes selected on the bases of good Rayleigh waves records at Tabriz, Shiraz, and Mashhad. The column with r_2-r_1 as the heading indicates the distance in km used in Eq. 2.12

TABLE 4.2 HYPOCENTERAL AND OTHER DATA FOR SELECTED EARTHQUAKES ALONG TABRIZ-SHIRAZ GREAT CIRCLE

No.	Date	Origin Time	Coordinates Latit. Longi.	Geographic location	Azimuth to Tabriz Shira	Ep. dist.(km) Tabriz Shiraz	r_2-r_1
1	1967 04 10	16 47 50	63.38°S 167.47°W	E Pasific Rise S Pasific Ocean	234.83° 236.21°	16413 15320	1093
2	1968 03 02	22 02 25	06.10°S 71.4°E	Chagos Archipe-lago	334.16° 334.10°	5554 4456	1098
3	1968 03 15	06 34 18	41.9°S 88.44°E	SE Mid Indian Ocean ridge	328.15° 328.72°	9860 8764	1096
4	1968 07 10	11 16 45	36.81°S 78.54°E	"	334.82° 336.19°	8959 7872	1087
5	1968 10 08	07 43 23	39.86°S 87.72°E	"	328.57° 329.03°	9637 8541	1098
6	1971 08 11	14 23 32	62.75°S 155.71°E	"	273.85° 273.39°	14667 13570	1097
7	1972 10 20	08 17 49	18.78°N 06.73°W	South Coast of Mexico	23.78° 22.88°	13087 14180	1093
8	1973 08 09	13 06 37	56.27°S 147.42°E	SE Mid Indian Ocean ridge	285.65° 283.81°	14083 13000	1083
9	1973 08 28	09 50 40	18.27°N 96.60°W	SE Mexico	31.24° 32.38°	12652 13744	1092

TABLE 4.3 HYPOCENTERAL AND OTHER DATA FOR SELECTED EARTHQUAKES
ALONG SHIRAZ-MASHHAD GREAT CIRCLE

No.	Date	Origin Time	Coordinates Latit.	Longit.	Geographic location	Azimuth to Shiraz	Mashhad	Ep. dist.(km) Shiraz	Mashhad	r_2-r_1
1	1967 06 12	23 22 46	47.4° N	154.3° E	Kuril Island	298.68°	299.24°	8438	7448	990
2	1968 07 28	21 12 38	55.43°N	166.58°E	Komandoriski Island region	305.82°	304.54°	8688	7705	983
3	1968 08 22	14 00 07	53.01°N	171.05°E	W Bering Sea	309.45°	308.25°	9077	8094	983
4	1970 06 14	00 00 11	51.95°S	73.85°W	S Chile	98.22°	96.97°	15007	15995	988
5	1970 07 18	01 48 39	51.4° N	178.5° W	Rat Island	317.44°	315.76°	9718	8744	974
6	1971 09 09	23 01 07	44.44°N	150.89°E	Kuril Island	297.20°	298.42°	8361	7378	983
7	1971 12 02	17 18 22	44.83°N	153.34°E	Kuril Island	298.62°	299.62°	8510	7524	986
8	1972 08 04	17 51 13	49.16°N	156.07°E	Onekaton Island E Kamchatka	299.48°	299.67°	8457	7465	992

TABLE 4.4 HYPOCENTERAL AND OTHER DATA FOR SELECTED EARTHQUAKES ALONG MASHHAD-TABRIZ GREAT CIRCLE

No	Date	Origin Time	Coordinates Latit. Longit.	Geographic location	Azimuth to Mashhad Tabriz	Ep. dist.(km) Mashhad Tabriz	r_2-r_1
1[*]	1970 01 08	17 12 39	34.74°S 178.57°E	North of New-Zealand	290.54° 289.38°	14586 15772	1186
2	1970 08 28	01 09 49	4.57°S 153.06°E	Solomon Island	306.09° 308.35°	10619 11783	1164
3[*#]	1970 10 31	17 53 09	4.93°S 145.47°E	E New-Guinea	306.51° 307.83°	9965 11146	1181
4	1970 11 08	14 58 54	9.13°N 126.33°E	SSE Philippines	305.81° 307.13°	7329 8511	1182
5	1970 11 08	22 35 47	3.44°S 135.63°E	N New-Guinea	307.62° 308.05	8994 10183	1189
6	1972 05 05	23 16 28	4.16°S 152.68°E	New-Guinea	306.13° 308.41	10558 11722	1164
7[#]	1972 05 28	01 40 42	6.00°S 151.12°E	"	306.07° 307.88	10539 11712	1173
8	1973 05 31	23 39 57	4.28°N 93.55°E	Bangladesh	300.48° 300.63	3502 4691	1189
9[#]	1973 12 29	00 19 31	5.12°S 166.90°E	S Solomon Island	303.50° 305.91	12532 13698	1166
10	1974 02 19	03 30 22	3.91°N 122.12°E	S Philippine	304.18° 305.88	6649 7829	1180
11	1974 03 06	19 29 08	6.6° S 128.98°E	New-Guinea	309.46° 308.63	8636 9822	1186

* (R2) type of Rayleigh wave recorsed and used.

Inversely dispersed mantle Rayleigh wave recorded and used.

for computing phase speed. This distance is obtained by taking the difference in epicentral distances to the first and second stations.

4.4 DIGITIZATION

The digitizer available to us had a flat tablet and a cross-wire cursor. The digitizer tablet had an area of 55×33 cm^2. The minimum step of distance between digitized points in the x or y direction was 0.1 mm, Among the various option for output of digitized data, we selected the one corresponding to 10 digitized x and y values per second. A short program in Gw-Basic was written to display on the computer screen the digitized seismogram graphically. This was to ensure at the first level whether the actual seismogram was being digitized properly. The digitized data were also saved on a floppy disk for subsequent analysis.

The digitized coordinates of the minute marks on the WWSSN long period seismograms were also saved in a separate file on the floppy for the relevant portion of a digitized seismogram. This helped to assign time values to the digitized seismogram amplitudes with considerable confidence. Next the hard copy plotter output of the digitized seismogram was obtained on the scale of the actual WWSSN seismogram. This plot was superimposed on the seismogram to make a second check of the accuracy of digitization. Finally a quartic spline was used to interpolate and obtain the seismogram digitized at regular intervals of time.

Sample results of digitization are not shown here because all

the digitized seismograms are displayed in figures of Chapter 5.

Usually the start and termination of digitization was controlled using pre-selected Rayleigh wave group speeds. Only vertical component seismograms were used in this analysis.

All calibration pulses which were clear and noise free and available on the selected seismograms were also digitized to take into account instrumental effects according to the scheme proposed by us and discussed in section of 2.8 and 3.5 above.

4.4.1 TABRIZ-SHIRAZ GREAT CIRCLE

Nine earthquakes (Fig. 4.1) produced good Rayleigh wave trains along this path which lies in the Zagros mountain chain. Two earthquakes occurred northwest of Iran and seven to the southeast. The surface waves in the latter cases traveled along paths through the Indian Ocean before entering the continental crust of Iran.

4.4.2 SHIRAZ-MASHHAD GREAT CIRCLE

Eight earthquakes (Fig. 4.2) gave useful records. Seven earthquakes occurred northeast of Iran and one to the southwest. In all cases surface waves traveled significant lengths of continental paths before reaching Iran.

4.4.3 MASHHAD-TABRIZ GREAT CIRCLE

In all 11 earthquakes could be identified with usable records of Rayleigh waves at this pair of stations. The relevant
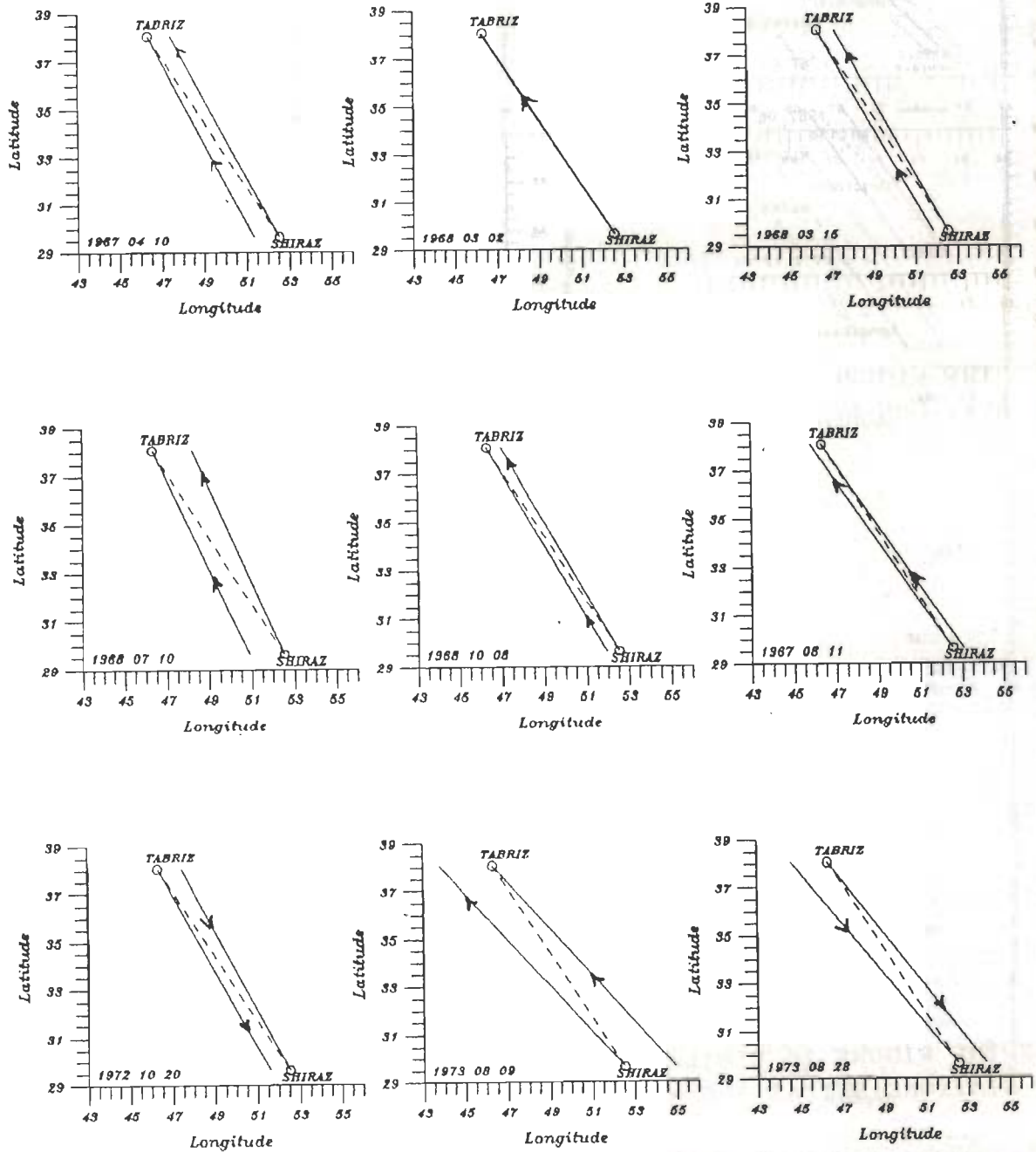
Fig. 4.1 SOLID LINES DISPLAY GREAT CIRCLES JOINING TABRIZ AND SHIRAZ TO THE EARTHQUAKE EPICENTERS SHOW IN TABLE 4.2. ONLY THE SEGMENTS OF THESE CIRCLES BETWEEN TABRIZ AND SHIRAZ ARE SHOWN. THE ARROWS SHOWN THE DIRECTION OF WAVE TRAVEL. THE DASHED LINE IS THE GREAT CIRCLE THROUGH TABRIZ AND SHIRAZ. INDIVIDUAL FIGURES ARE IDENTIFIED BY THE DATES OF THE EARTHQUAKES.
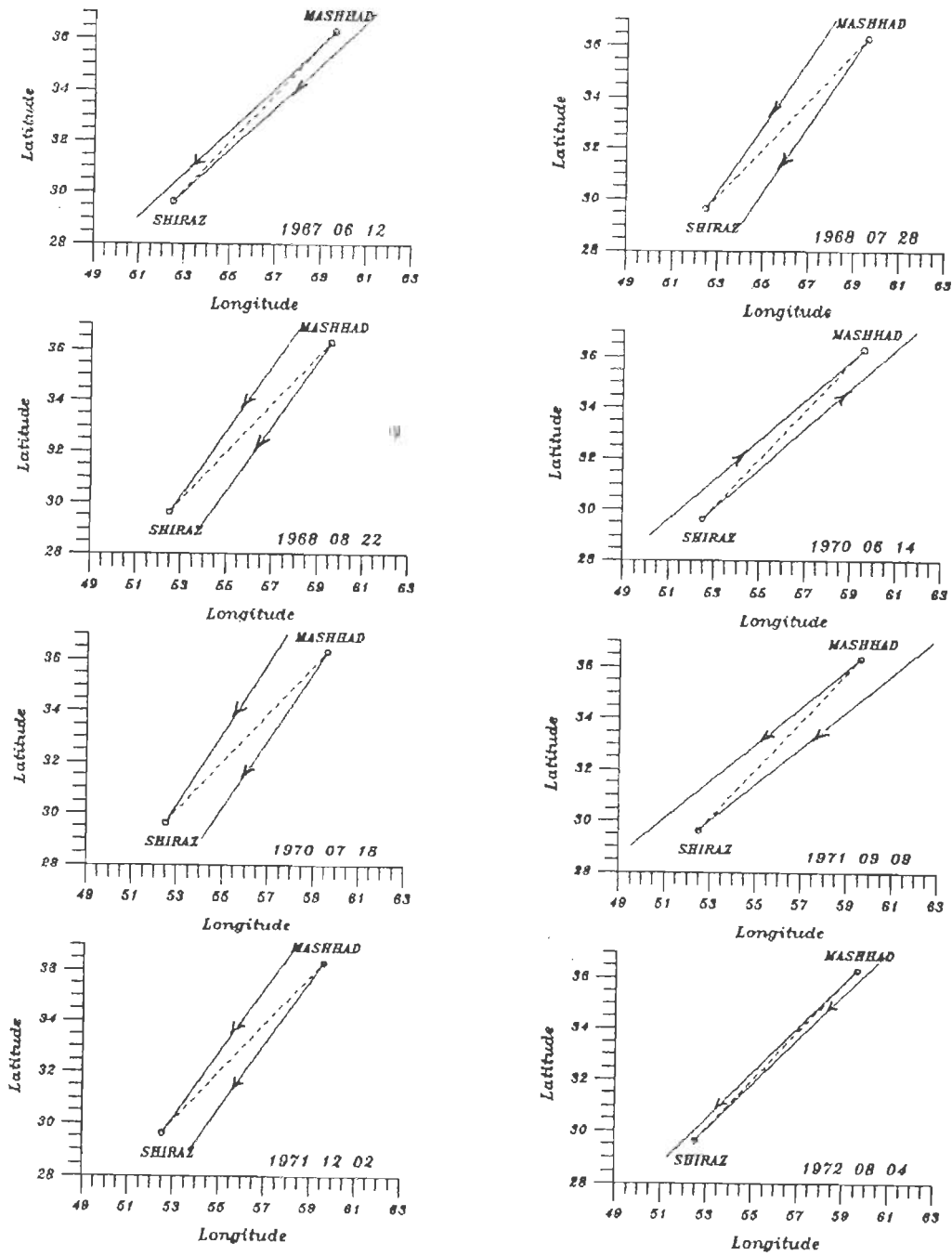
Fig. 4.2 THE FIGURE IS SIMILAR TO Fig. 4.1 EXCEPT THAT IT REFERS TO STATIONS SHIRAZ AND MASHHAD.

118
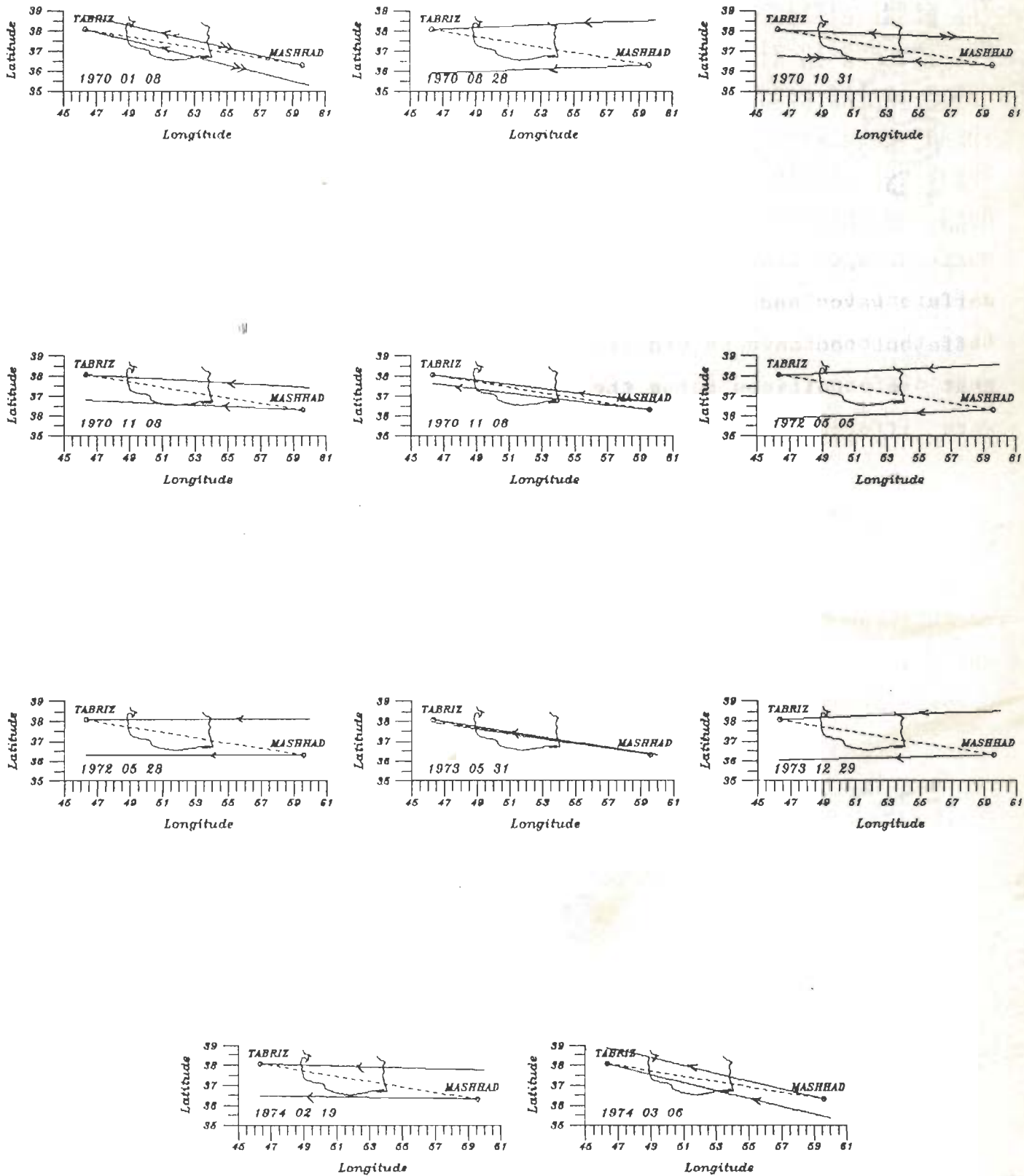
Fig. 4.3 THE FIGURE IS SIMILAR TO Fig. 4.1 EXCEPT THAT IT REFER TO
STATIONS MASHHAD AND TABRIZ. THE OUTLINE OF CASPIAN SEA IS
INCLUDED FOR REFERENCE. THE DOUBLE ARROWS IN TWO GRAPHS
INDICATE THE DIRECTION OF PROPAGATION OF R2 RAYLEIGH WAVES.

earthquakes occurred to the east and southeast of Iran (Fig. 4.3). The great circle between the epicenter and Tabriz crosses the Caspian Sea in all cases. This is a source of geology related noise in the present surface waves analysis. In 10 out of 11 cases the Mashhad-Tabriz great circle is at a considerable angle with the great circles between the epicenter and Mashhad on the one hand and epicenter and Tabriz on the other. In all these cases the surface waves had to travel large continental paths crossing different tectonic provinces. The possibility cannot be ruled out that the conditions along the great circles to Tabriz and Mashhad were different even for a given earthquake.

CHAPTER-5
RESULTS OF RAYLEIGH WAVE PHASE SPEED DETERMINATIONS
ALONG THREE REGIONS IN IRAN

5.1 INTRODUCTION

In this chapter we present the results of Rayleigh wave phase speed determination along the Zagros (Tabriz-Shiraz), Central Iran (Shiraz-Mashhad) and Alborz (Mashhad-Tabriz) regions of Iran. The selected seismograms were analyzed for the first time by us and the results are our original contributions to the accumulation of geophysical data for Iran.

5.2 ABOUT THE PRESENTATION OF RESULTS

In all we present here results for data from 28 earthquakes split into group of 9, 8 and 11 for the Zagros, Central Iran and Alborz regions respectively. We discuss in the following subsection the results of one of these 28 analyses in detail so as to indicate the main steps of computations and explain the method of presentation of the results for the remaining 27 cases.

5.2.1 CASE STUDY OF RAYLEIGH WAVE PHASE SPEED CURVE FOR TABRIZ-SHIRAZ PATH USING DATA FOR THE EARTHQUAKE OF AUGUST 11, 1971,

The results of the analysis are displayed on Fig. 5.1. This figure is in six parts as explained in the following paragraphs.

Date	Orig. Time	Epicenter	Location	mb	Depth
1971 08 11	14 23 31.6	62.75S 155.71E	SE Mid Indian Ocean ridge	5.4	33

Ep. distanc	
Tabriz	Shiraz
14667	13570

Azimuth to:	
Tabriz	Shiraz
273.85°	273.39°
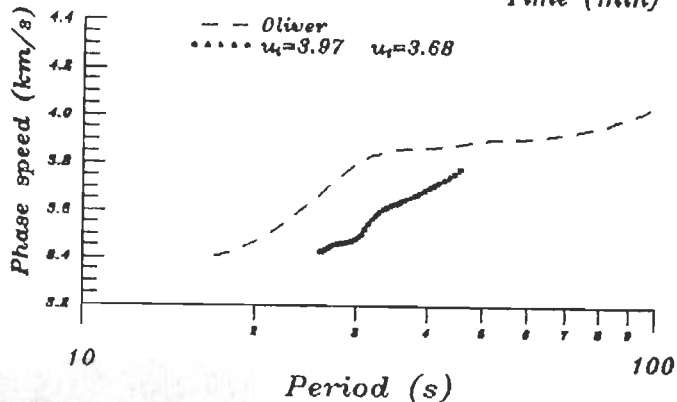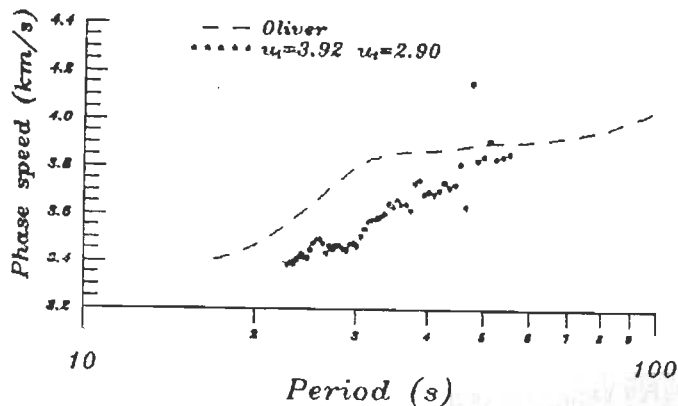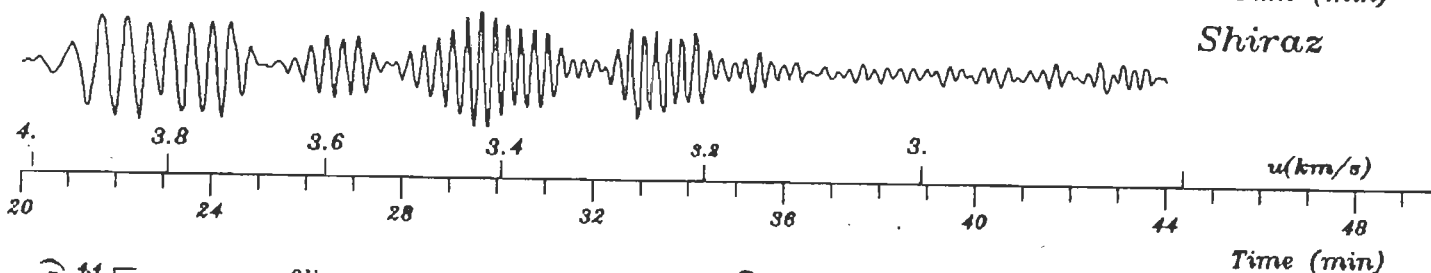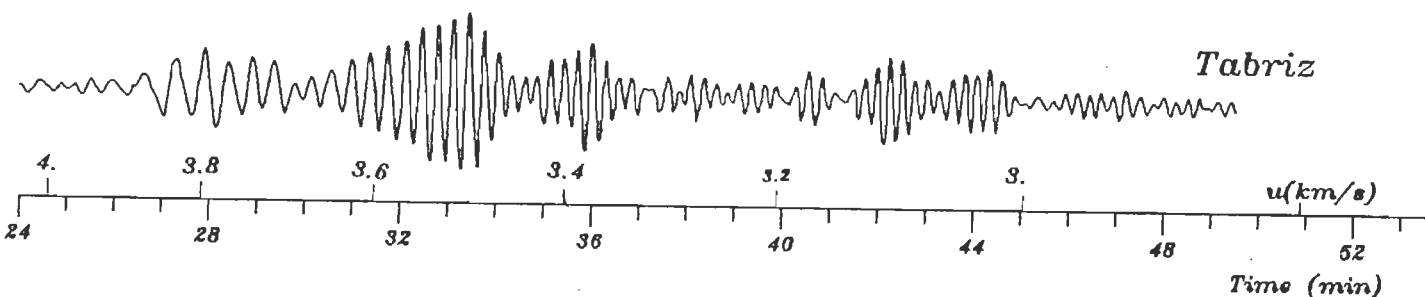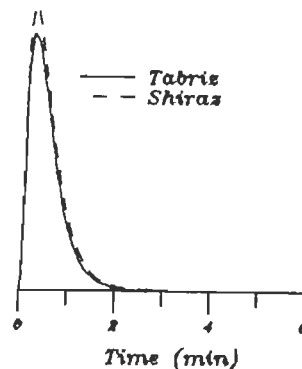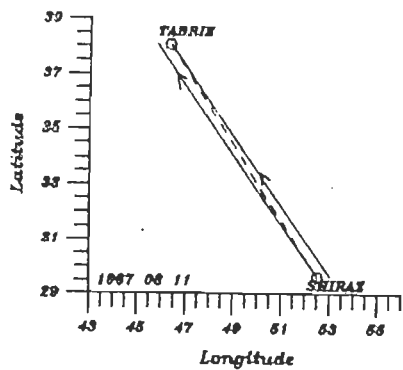
FIG. 5.1 DETAILS OF PHASE SPEED DETERMINATION USING SEISMOGRAMS RECORDED AT TABRIZ AND SHIRAZ FOR THE EARTHQUAKE OF 11, AUG. 1971. SEE SECTION 5.2.1 FOR DETAILS ABOUT VARIOUS PARTS OF THIS FIGURE. FIGS. 5.4 TO 5.12, 5.15 TO 5.22, AND 5.25 TO 5.37 ARE SIMILAR TO THIS FIGURE.

Numerical Data : The earthquake of August 11, 1971, had the epicenter at 62.75°S, 155.71°E, on the Mid SE Indian Ocean ridge south of Australia. The Rayleigh wave from the earthquake were recorded at Shiraz and Tabriz with epicentral distances of 13570 km and 14667 km respectively. The great circle azimuth to Shiraz and Tabriz were N273°.39 and N273°.84 respectively. The reported focal depth was 33 km and the body wave magnitude mb for this earthquake was 5.4 . This information is displayed at the top of Fig. 5.1.

Map : A small map indicating great circles passing through Shiraz and the epicenter and Tabriz and the epicenter is shown at the left in the second row of the figure.

Calibration pulses : The calibration pulses recorded on the seismograms were also digitized and are shown at the right in the second row of the figure.

Seismograms : The Rayleigh waves recorded on the vertical component WWSSN seismograms at Shiraz and Tabriz are shown in the middle of the figure. These seismograms are reproduced from the digitized data. For each of the seismograms, at the bottom, the running time (GMT) in minutes is indicated along with the estimated times of arrival of Rayleigh waves of different group speeds between 4.0 and 2.9 km/s. The vertical scales on the seismograms are normalized.

Dispersion curves : The graph at the bottom left is a display of calculated phase speeds when the digitized part of each

seismogram began and terminated at times corresponding to the arrival of Rayleigh waves with group speeds of 3.92 and 2.9 km/s. Thus in the notation of section 3.3.1 above, we had $u_{t1}=u_{t2}=3.92$ km/s and $u_{t1}=u_{t2}=2.9$ km/s. The digitization rate was 1 sample per second in both cases and the total number of digitized samples were 1217 and 1316 for Shiraz and Tabriz respectively. The number of digitized points was increased to 2048 (2^{11}) in each case by padding suitable number of zeros at the end. Instrumental correction has been considered duly. The range of periods displayed is governed broadly by the periods which can be actually seen on the seismograms. The world average Rayleigh wave phase speed curve of Oliver (1962) for continental paths is shown by the dashed curve for comparison.

The graph at bottom right is a display of results for a similar computation of phase speed except that $u_{t1}=u_{t2}=3.97$ km/s and $u_{t1}=u_{t2}=3.68$ km/s. In other words more restricted portions of the seismograms are considered in this computation. A comparison with the dispersion curve at bottom left of the figure indicates that the phase speed curve is much smoother in the present case. Referring to the seismograms in the middle part of the figure, a probable reason for this should be the fact that fundamental mode Rayleigh waves un-contaminated by other mods or multipath signal arrivals are being considered in the present more restricted case. Error analysis for phase speed estimates is discussed later in this chapter (Section 5.6).

Summary : Although the inversion and geological implications

of phase speed curves are discussed in detail in subsequent chapters, we note that the Rayleigh wave phase speeds estimated in this case for the fundamental mode in the period range of 26 to 45 seconds are distinctly lower than the world average curve given by Oliver (1962).

5.2.2 FURTHER COMMENTS ON BOTTOM RIGHT GRAPHS IN SUCH FIGURES

In some of the subsequent figures of the type just discussed, the graph at bottom right will contain more than one phase speed dispersion curve obtained by considering more than one segment of Rayleigh waves at each of the two stations (e.g. Fig. 5.11). Some trial and error was involved in selecting Rayleigh wave segments. Such factors as interference due to multipathing multiple modes on seismograms and possibility of interference from late arriving body phases through the core were taken into consideration. Such body phases may include for example (PKKP, PKKS, SKKS, PKPPKP, PPP, SKKKS, etc.). Both of these are sources of noise for us.

Some times comprises were necessary during these trial and error exercises. The aim was to consider segments of two seismogram defined by $u_{L1} = u_{L2}$ and $u_{L1} = u_{L2}$ (see 16 experiments of section 3.2.1). We also tried to ensure that a full and complete wave packet from each seismogram was considered. However this was not always possible and in some cases the wave packet at the first or second station was either incomplete are contained some part of the next wave packet. We attribute this difficulty to the presence of still unaccounted "noise" arising from such causes as heterogeneity in crust and upper mantle along the respective wave

paths. In other words we are dealing here with a trade off between the effects on the phase speed curve of (i) considering complete wave packets on the two seismograms which could mean that u_{t1} is not equal to u_{t2}, and (ii) sticking to the requirement that u_{t1} should be equal to u_{t2} as we learnt from the 16 experiments in section 3.2.1 . We realize that none of the options is entirely satisfactory. A choice has to be made. We choose the second option.

5.3 CUMULATIVE PHASE SPEED RESULTS FOR THE ZAGROS REGION

The data for Zagros path are obtained from analyses of seismograms recorded at Shiraz and Tabriz. In all there were 9 earthquakes (see Table 4.2 for hypocentral information) short listed by the computer program for selecting earthquakes with epicenters on or close to the great circle through the two recording stations. That list was further trimmed by the requirement that the Rayleigh wave trains should be well recorded at both the stations. Fig. 5.2 displays the results obtained for all 9 earthquakes together . The data presented in this figure come from bottom left parts of Figs. 5.4 to 5.12. The data show remarkably small scatter at all periods. The solid line curve of this figure is the average curve of Fig. 5.3. averages for available phase speed values. The dashed curve is the curve of Oliver (1962) mentioned above.

Fig. 5.3 summarizes the results shown in bottom right parts of Figs. 5.4 to 5.12. The scatter in results is greatly reduced in comporison to that in Fig. 5.2. The solid line curve of this

FIG. 5.2 A SUMMARY FIGURE IN WHICH PHASE SPEED DATA SHOWN AT BOTTOM RIGHT CORNER OF FIGS. 5.4 TO 5.12 IS COMPILED. SEE TEXT UNDER SECTION 5.3 FOR FURTHER DETAILS. AVERAGE CURVE HERE IS ACTUALLY THE AVERAGE CURVE OF FIG. 5.3.
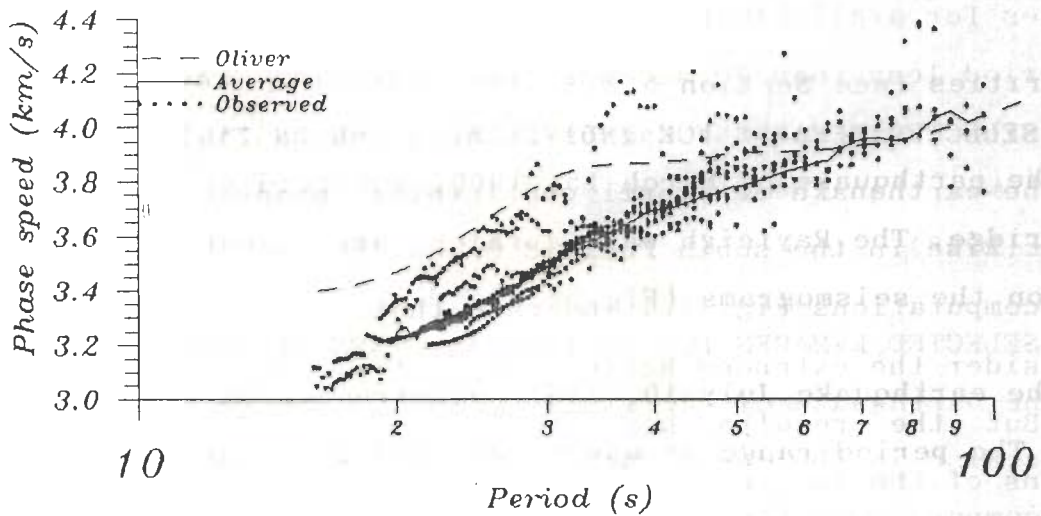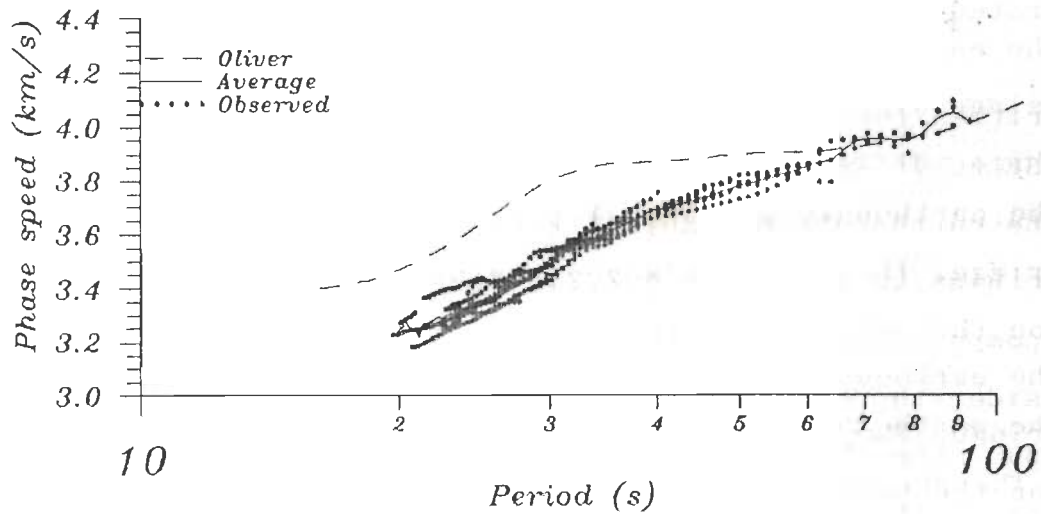

FIG. 5.3 A SUMMARY FIGURE IN WHICH PHASE SPEED DATA SHOWN AT BOTTOM RIGHT CORNER OF FIGS. 5.4 TO 5.12 IS COMPILED. SEE TEXT UNDER SECTION 5.3 FOR FURTHER DETAILS.

127

figure is obtained by joining points representing periodwise averages for available phase speed values. It can be said that for period less than 70 seconds the Rayleigh wave phase speed dispersion curve for the Zagros path is substantially (up to 0.2 km/s) lower than the average continental phase speed curve of Oliver (1962).

5.3.1 SELECTED REMARKS FOR INDIVIDUAL CASES OF ZAGROS REGION

The earthquake of April 10, 1967, occurred on the East Pacific Rise in the south Pacific Ocean. The results of the phase speed computations Fig. 5.4 indicate that there is a scatter when we consider the extended Rayleigh wave train (bottom left of Fig. 5.4). But the results are much smoother if more restricted portions of the two seismograms are used (bottom right of Fig. 5.4). (see Section 5.2.1 paragraph headed "Dispersion curves" and also Section 5.2.2).

The earthquake of March 2, 1968, occurred in the Chagos Archipelago of south central Indian Ocean. The phase speed results for three different segments of Rayleigh wave trains are illustrated in bottom right of Fig. 5.5 and they show considerable similarities (see Section 5.2.2).

The earthquake of March 15, 1968, occurred on SE Mid Indian Ocean ridge. The Rayleigh wave trains are exceptionally clear on the seismograms (Fig. 5.6).

The earthquake July 10, 1968, occurred in SE Mid Indian Ocean ridge. The period range of waves recorded is relatively narrow as

Date	Orig. Time	Epicenter	Location	mb	Depth
1967 04 10	16 47 50.	63.38S 167.47W	Ecast Paaific Rine in south Pacific	5.5	29

Ep. distanc		Azimuth to:	
Tabriz	Shiraz	Tabriz	Shiraz
16413	15320	234.83°	236.21°
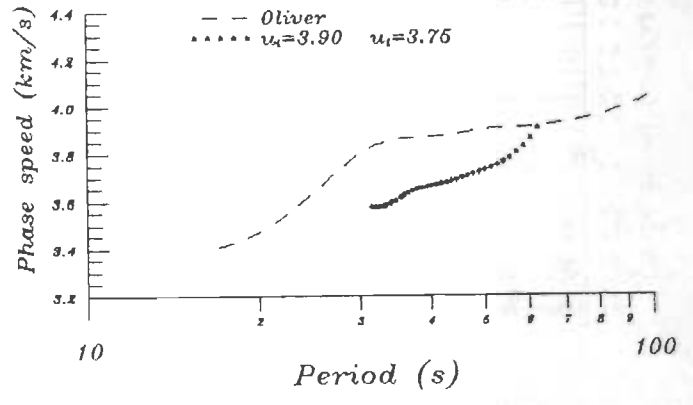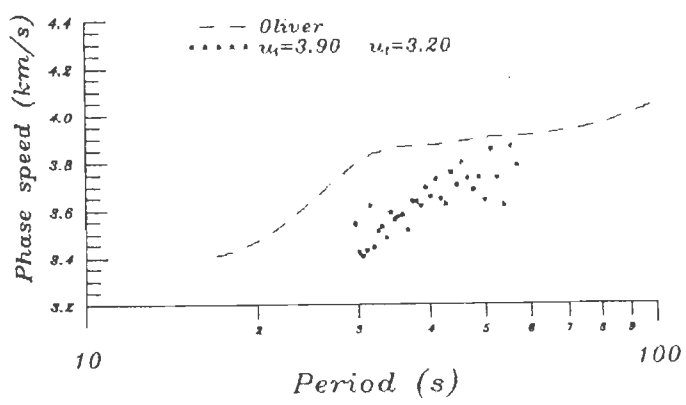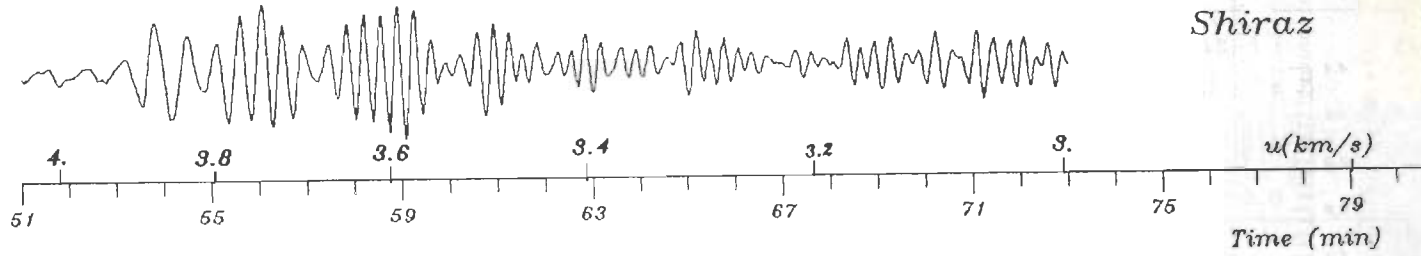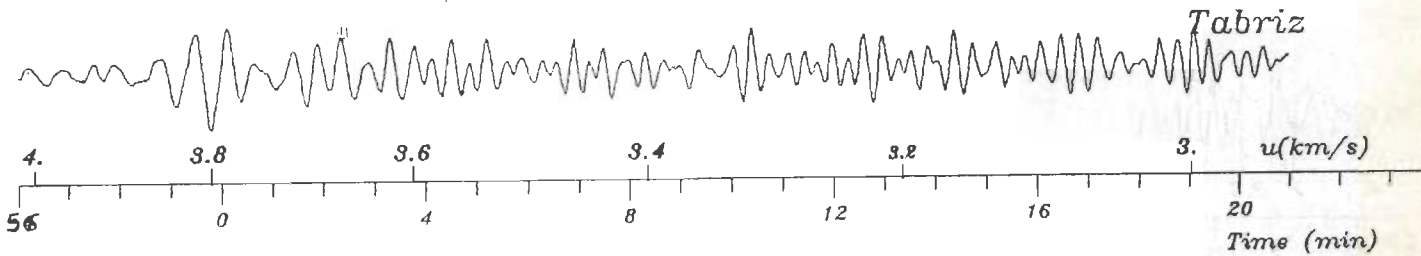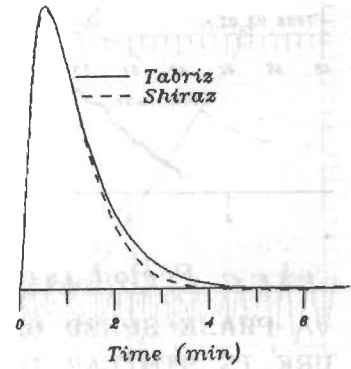
FIG. 5.4 A PHASE SPEED DETERMINATION FOR THE ZAGROS REGION. THIS FIGURE IS SIMILAR TO FIG 5.1 IN THE METHOD OF PRESENTATION OF DATA.

129

Date	Orig. Time	Epicenter	Location	mb	Depth
1968 03 02	22 02 24.8	6.1 S 71.4 E	Chagos Archipelago S Central Indian Ocean	5.6	33

Ep. distanc	
Tabriz	Shiraz
5554	4456

Azimuth to:	
Tabriz	Shiraz
334.16°	334.10°

Tabriz
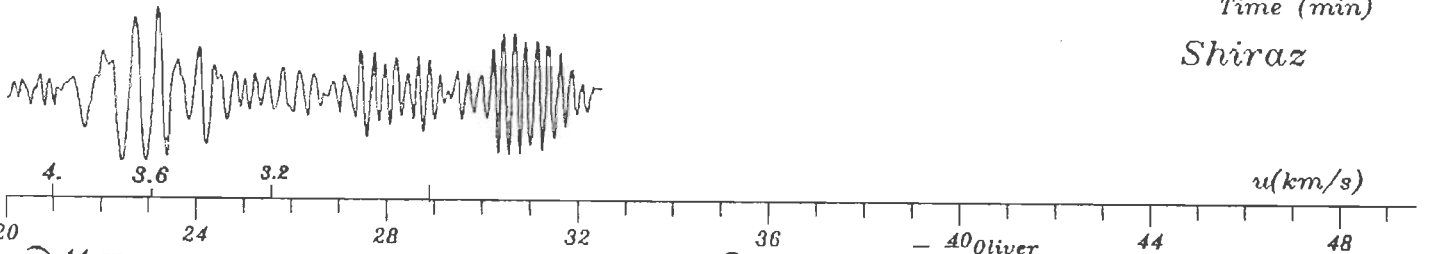
Shiraz
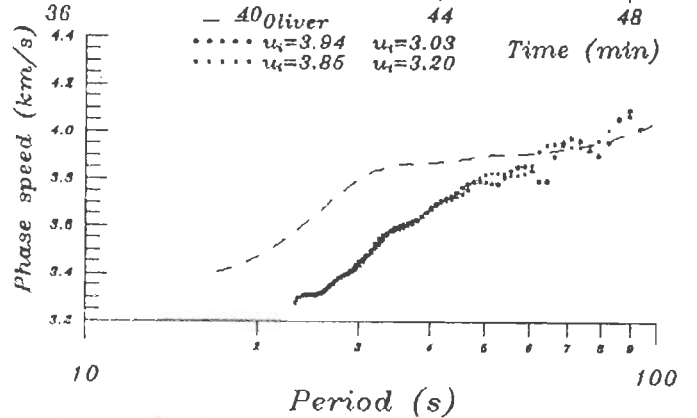
FIG. 5.5 A PHASE SPEED DETERMINATION FOR THE ZAGROS REGION. THIS FIGURE IS SIMILAR TO FIG 5.1 IN THE METHOD OF PRESENTATION OF DATA.

Hypocentral Data

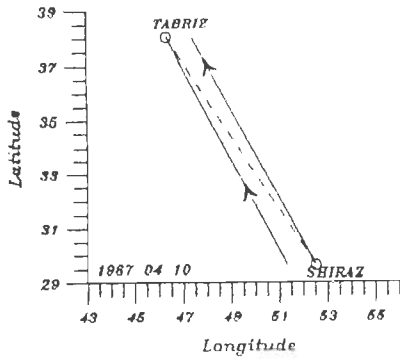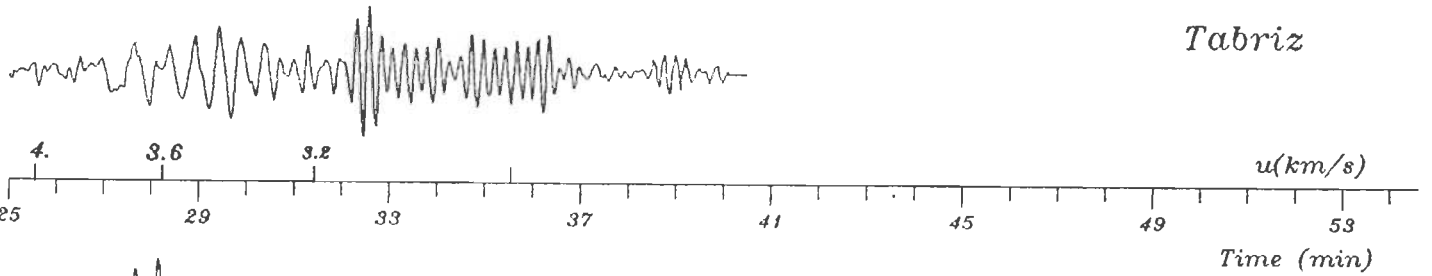| Date	Orig. Time	Epicenter	Location	mb	Depth
1968 03 15	06 34 18 ?	41.9 S 88.4 E	SE Mid Indian Ocean ridge	5.4	

Ep. distanc	
Tabriz	Shiraz
9860	8764

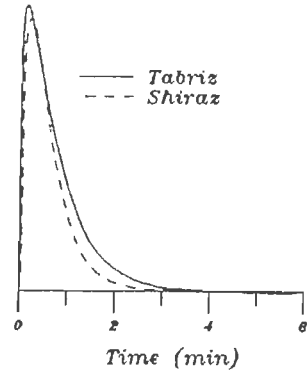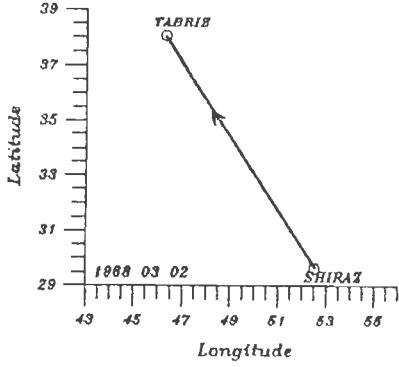| Azimuth to:	
Tabriz	Shiraz
328.15°	328.72°

Tabriz

Shiraz
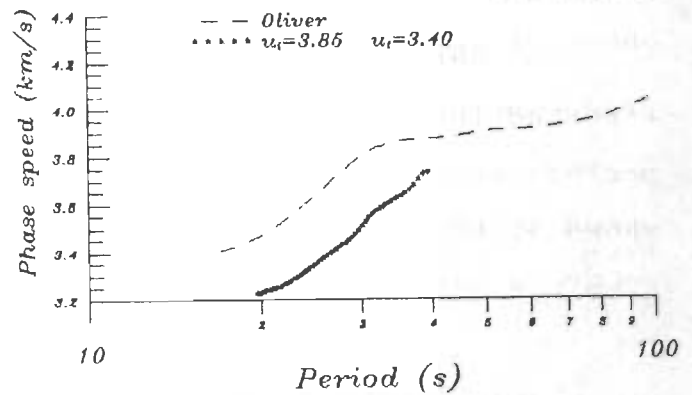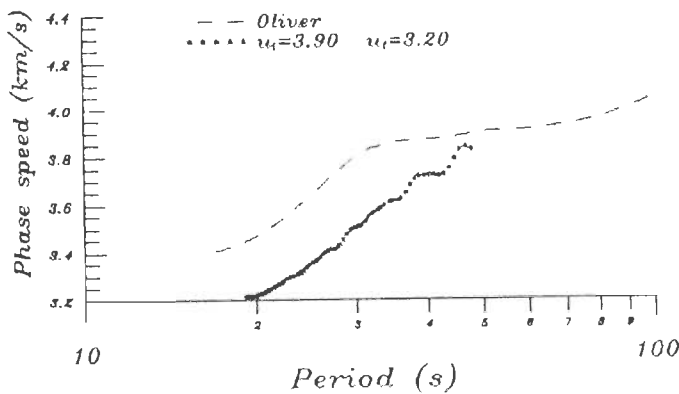
FIG. 5.6 A PHASE SPEED DETERMINATION THE FOR ZAGROS REGION. THIS FIGURE IS SIMILAR TO FIG 5.1 IN THE METHOD OF PRESENTATION OF DATA.

131

seen from the phase speed results in Fig. 5.7.

The earthquake of October 8, 1968, occurred in SE Mid Indian Ocean ridge. Again the Rayleigh wave trains are clear and noise free. The results are shown at the bottom of Fig. 5.8.

The earthquake of August 11, 1971, occurred in SE Mid Indian Ocean ridge, south of Australia. The Rayleigh wave trains show a beat pattern. The phase speed curve is considerably smoother when we consider the first segment of the Rayleigh wave train which arrives at group speeds higher than 3.68 km/s(Fig. 5.9).

The earthquake of October 20, 1972 is different than the preceding earthquakes in that it occurred near the southern Coast of Mexico. The waves arrived in Iran from the NW. The mixed oceanic and continental path produced a complicated pattern in the recorded Rayleigh waves (Fig. 5.10). The results obtained by considering three different segments of the Rayleigh wave trains are displayed at the bottom right of Fig. 5.10.

The earthquake of August 9, 1973, occurred in SE Mid Indian Ocean ridge south of Australia. The results are shown at the bottom of Fig. 5.11.

The earthquake of August 28, 1973, occurred in SE Mexico. The reported focal depth is 84 km. Rayleigh waves of relatively long periods are well recorded. The phase speed dispersion curves are shown at the bottom of Fig. 5.12.

Hypocentral Data

Date	Orig. Time	Epicenter	Location	mb	Depth
1968 07 10	11 16 44.6	36.81S 78.54E	SE Mid Indian Ocean ridge	5.7	33

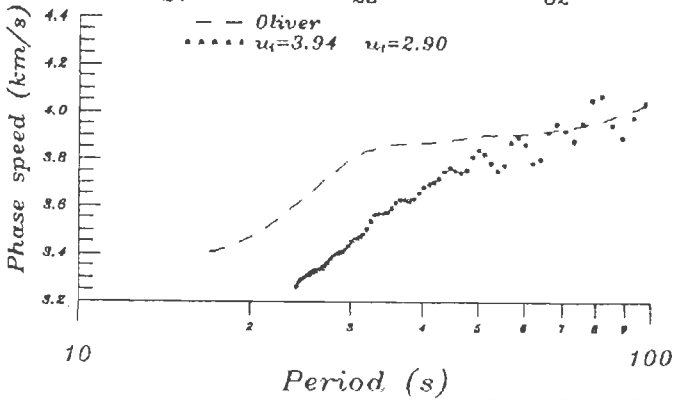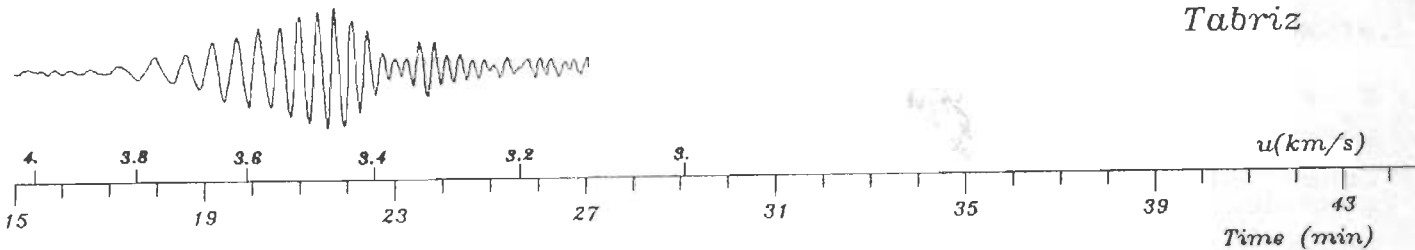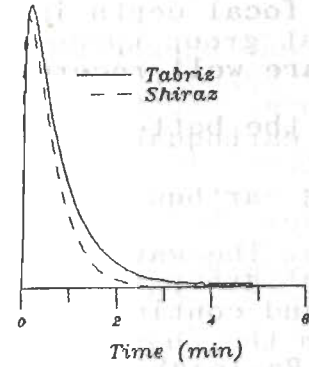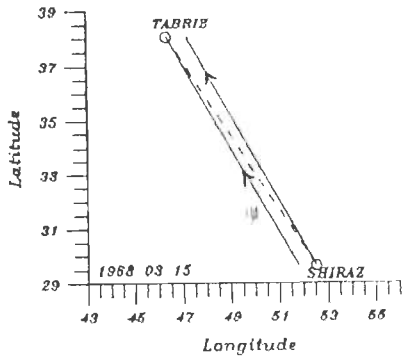| Ep. distanc		Azimuth to:	
Tabriz	Shiraz	Tabriz	Shiraz
8959	7872	334.82°	336.19°

Tabriz

Shiraz
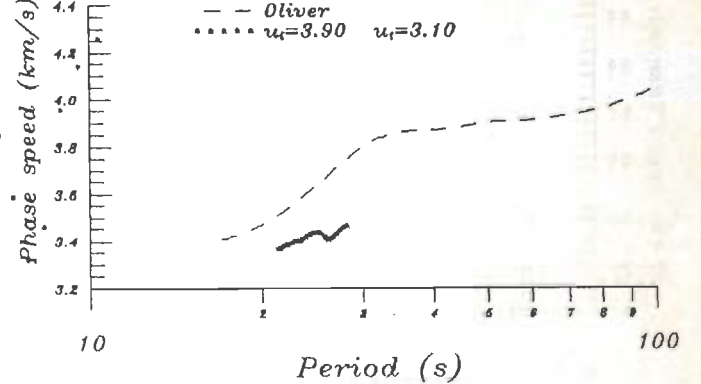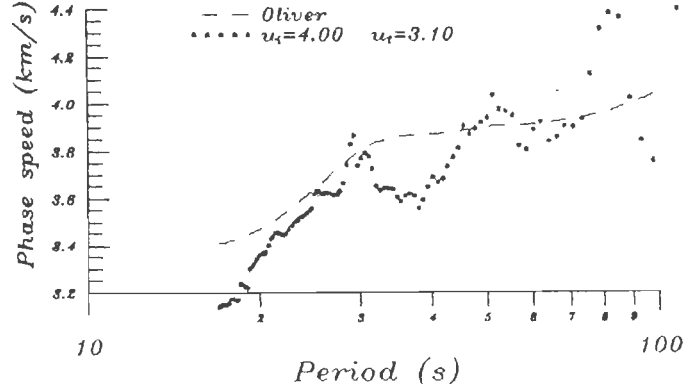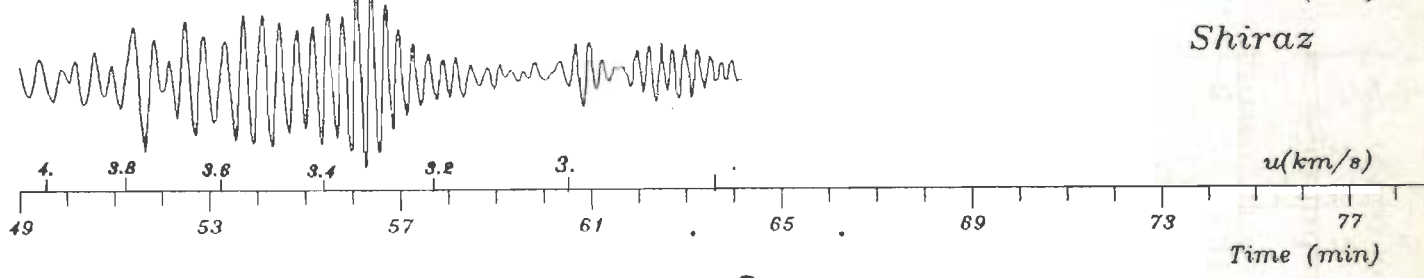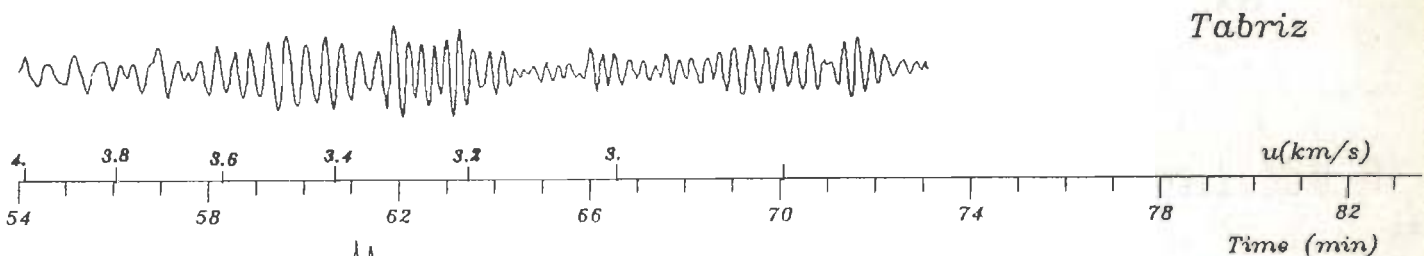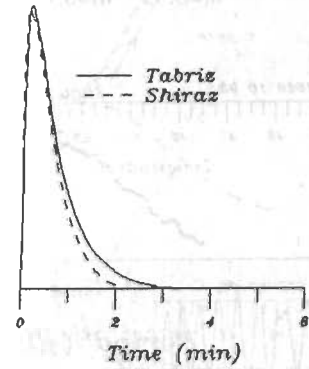
FIG. 5.7 A PHASE SPEED DETERMINATION FOR THE ZAGROS REGION. THIS
FIGURE IS SIMILAR TO FIG 5.1 IN THE METHOD OF PRESENTATION OF
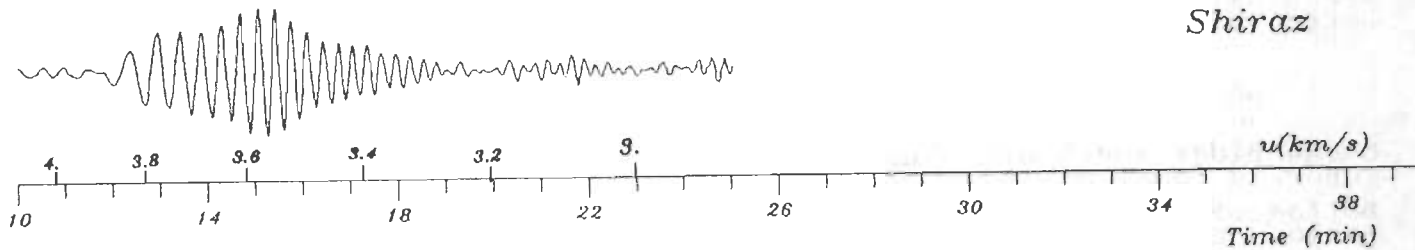DATA.

133

Hypocentral Data

Date	Orig. Time	Epicenter	Location	mb	Depth
1968 10 08	07 43 23.1	39.86S 87.72E	SE Mid Indian Ocean ridge	6	76

| Ep. distanc		Azimuth to:	
Tabriz	Shiraz	Tabriz	Shiraz
9637	8541	328.57°	329.03°

Tabriz
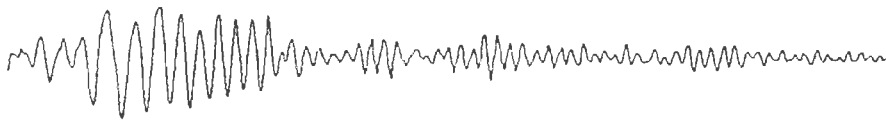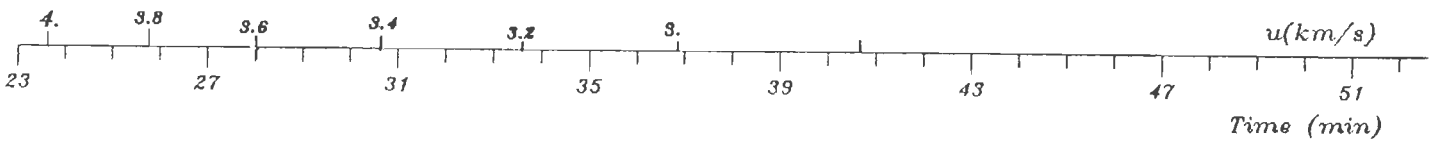
Shiraz
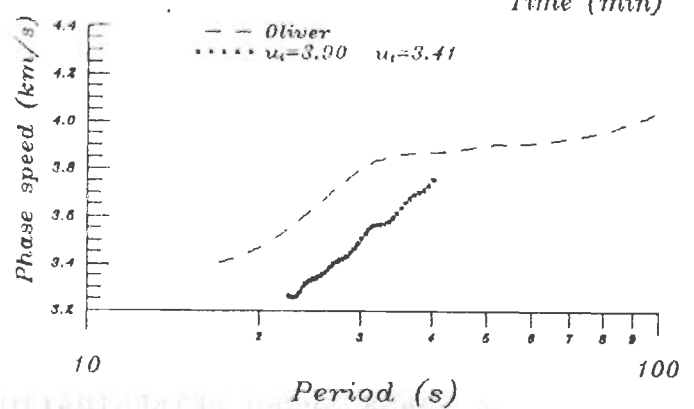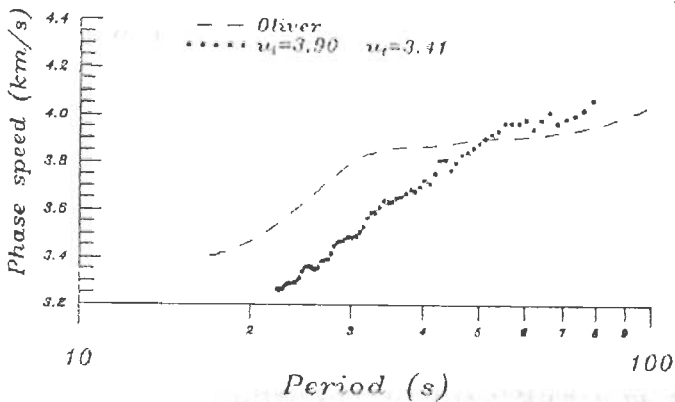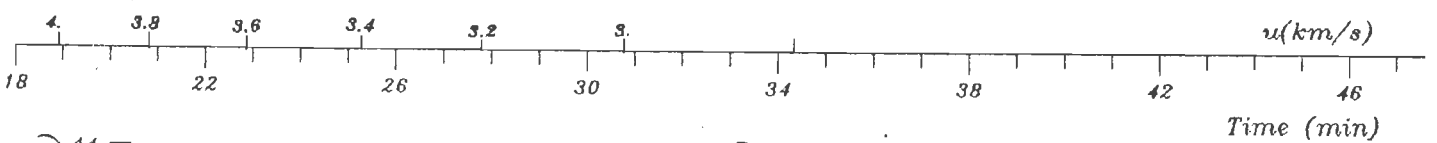
FIG. 5.8 A PHASE SPEED DETERMINATION FOR THE ZAGROS REGION. THIS FIGURE IS SIMILAR TO FIG 5.1 IN THE METHOD OF PRESENTATION OF DATA.

134

Date	Orig. Time	Epicenter	Location	mb	Depth
1971 08 11	14 23 31.6	62.75S 155.71E	SE Mid Indian Ocean ridge	5.4	33

Ep. distanc	
Tabriz	Shiraz
14667	13570

Azimuth to:	
Tabriz	Shiraz
273.85°	273.39°
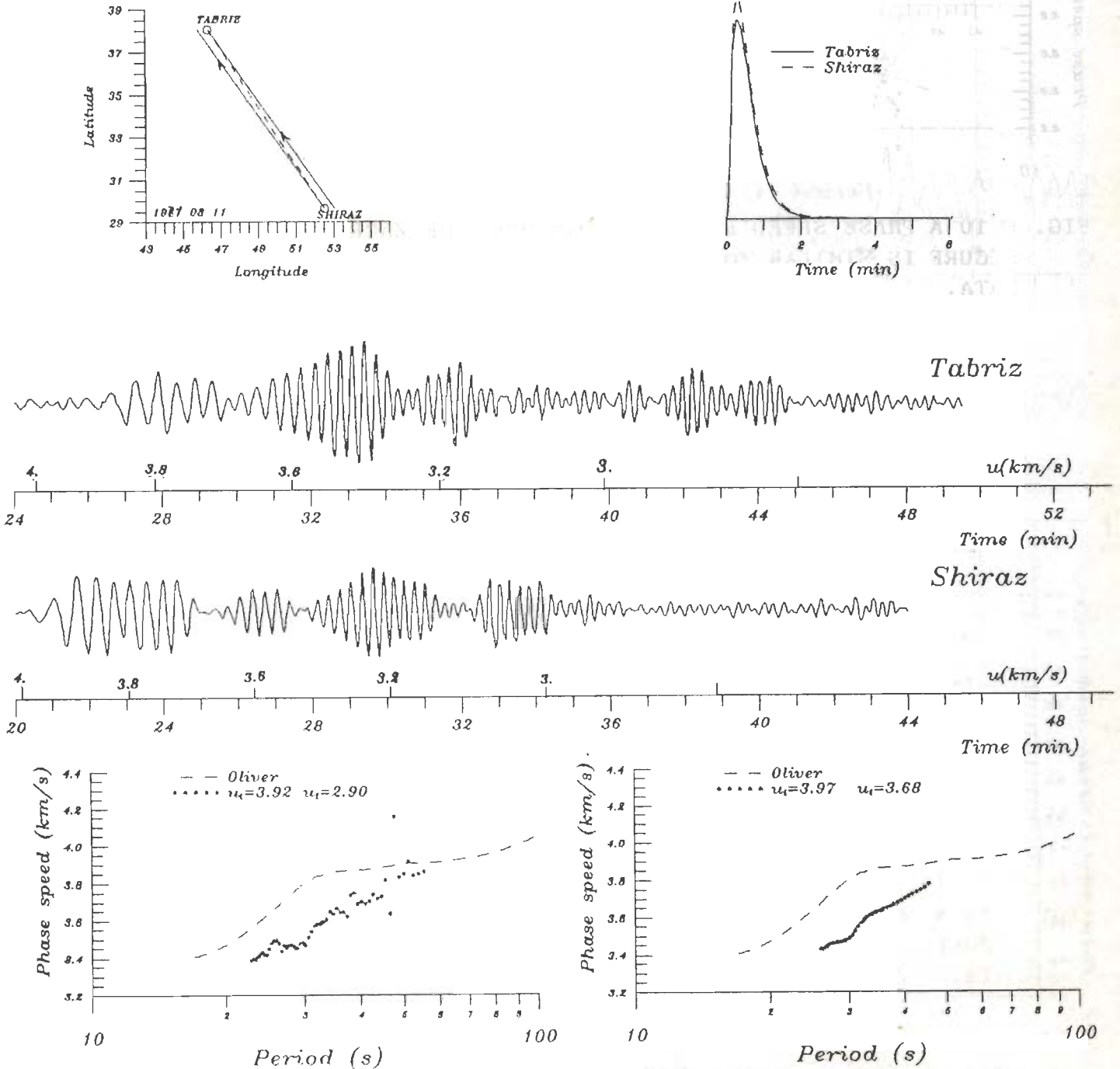
FIG. 5.9 A PHASE SPEED DETERMINATION FOR THE ZAGROS REGION. THIS FIGURE IS SIMILAR TO FIG 5.1 IN THE METHOD OF PRESENTATION OF DATA.

135

Hypocentral Data

Date	Orig. Time	Epicenter	Location	mb	Depth
1972 10 20	08 17 48.6	18.78N 106.73W	South Coast of Mexico	5.7	38

Ep. distanc	
Tabriz	Shiraz
13096	14190

Azimuth to:	
Tabriz	Shiraz
23.85°	22.88°

Tabriz

Shiraz
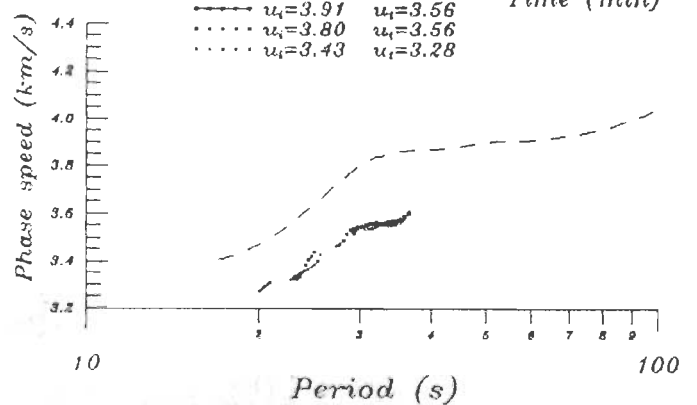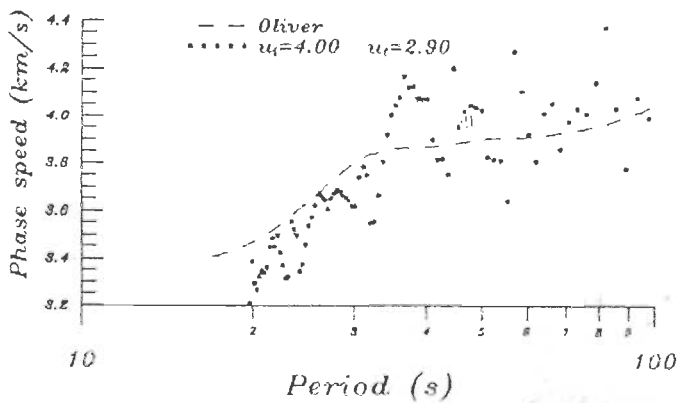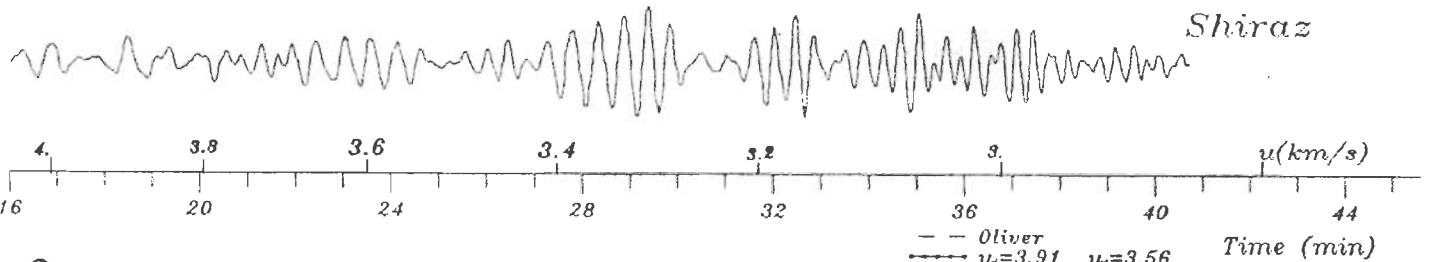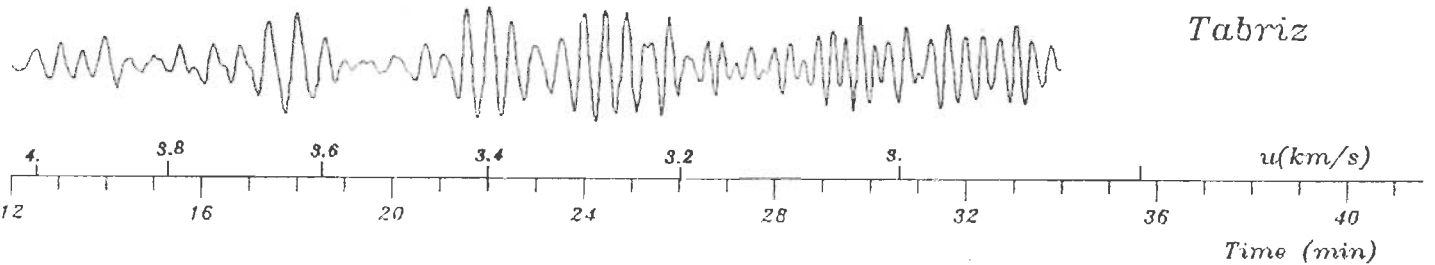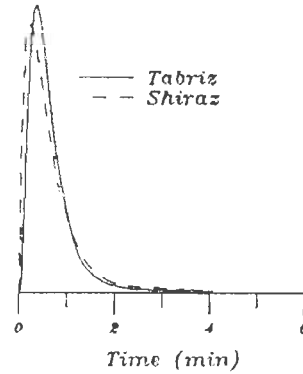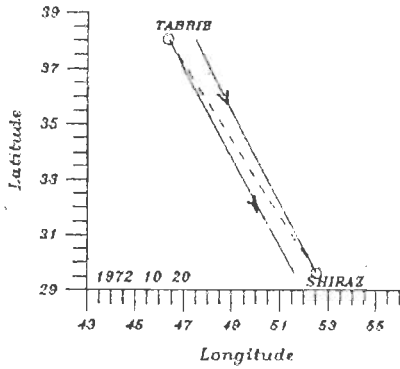
FIG. 5.10 A PHASE SPEED DETERMINATION FOR THE ZAGROS REGION. THIS FIGURE IS SIMILAR TO FIG 5.1 IN THE METHOD OF PRESENTATION OF DATA.

Date	Orig. Time	Epicenter	Location	mb	Depth
1973 08 09	13 06 36.6	56.27S 147.42E	SE Mid Indian Ocean ridge	5.6	33

Ep. distanc	
Tabriz	Shiraz
14083	13000

Azimuth to:	
Tabriz	Shiraz
285.65°	283.81°
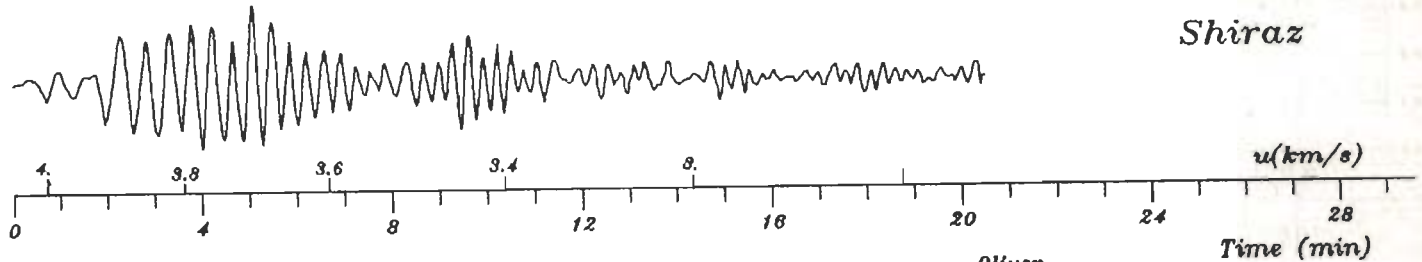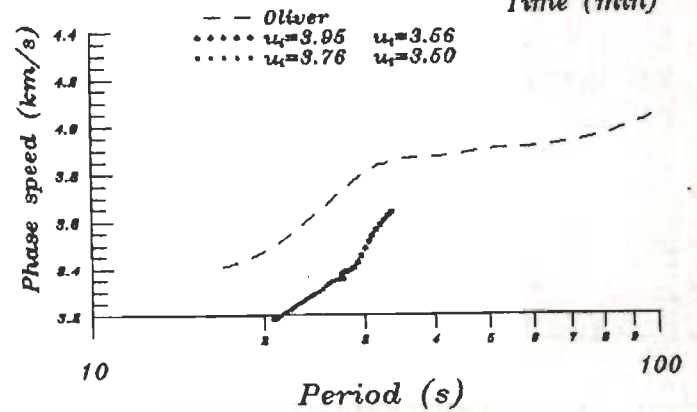
FIG. 5.11 A PHASE SPEED DETERMINATION FOR THE ZAGROS REGION. THIS FIGURE IS SIMILAR TO FIG 5.1 IN THE METHOD OF PRESENTATION OF DATA.

Date	Orig. Time	Epicenter	Location	mb	Depth
1973 08 28	09 50 40.	18.27N 96.60W	SE Mexico	6.8	84

Ep. distanc	
Tabriz	Shiraz
12652	13744

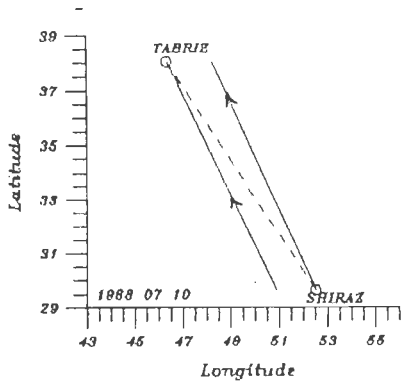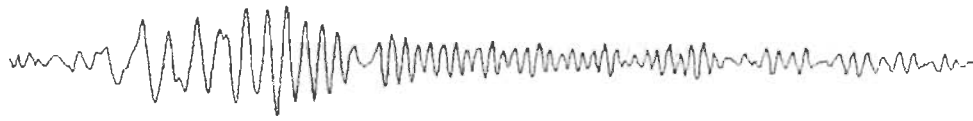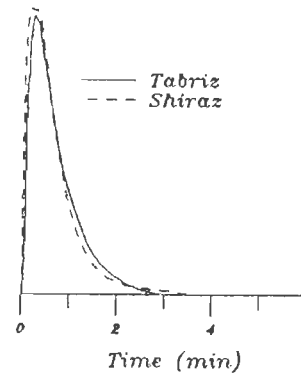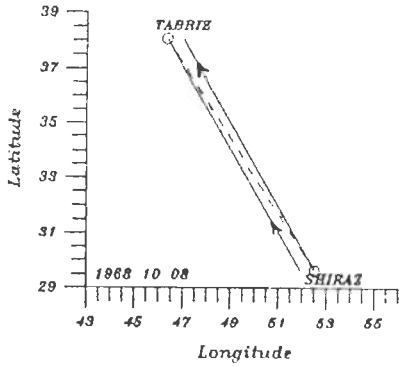| Azimuth to:	
Tabriz	Shiraz
31.24°	32.38°
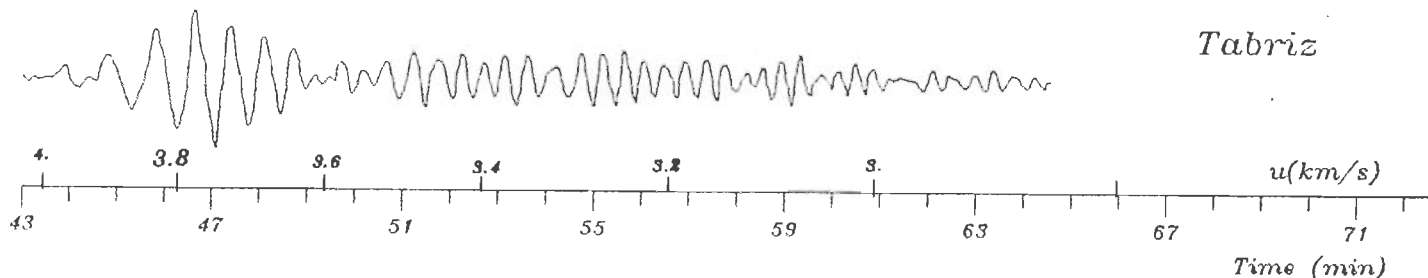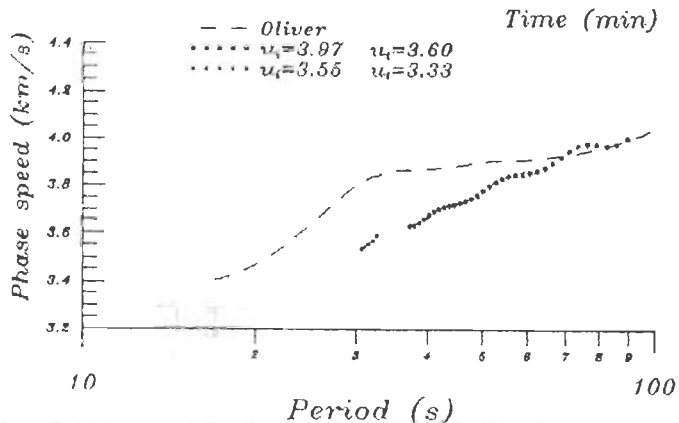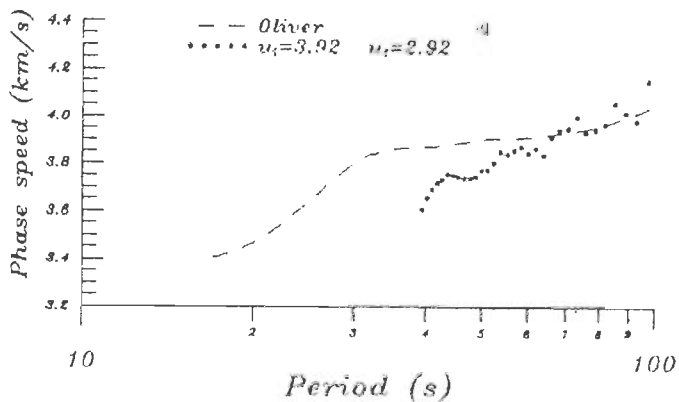
FIG. 5.12 A PHASE SPEED DETERMINATION FOR THE ZAGROS REGION. THIS FIGURE IS SIMILAR TO FIG 5.1 IN THE METHOD OF PRESENTATION OF DATA.

5.4 CUMULATIVE PHASE SPEED RESULTS FOR THE CENTRAL IRAN REGION

Data for 8 earthquakes could be utilized to measure phase speeds along this path. The cumulative results (from bottom part of Fig. 5.15 to 5.22) for all 8 earthquakes are shown in Fig. 5.13 and 5.14. The displays in these two parts are similar to those of Fig. 5.2 and Fig. 5.3 explained in section 5.3. The phase speed results for two earthquakes, one occurring in southern Chile and the other in Kuril Islands, are displayed in these figures. But the curves lie well below those for other earthquakes. They were not used in computing the average phase speeds for this region.

The average phase speed curves for this region are also lower than the average continental curve of Oliver (1962). However the differences between the average phase speeds for Central Iran paths and Oliver's values are less than in the case of the Zagros paths. In other words the crust and upper mantle structure should be closer to the average continental structure in the case of the Central Iranian region as compared to that in the Zagros region.

5.4.1 SELECTED REMARKS FOR INDIVIDUAL CASES OF CENTRAL IRAN REGION

The earthquake of Jun 12, 1967, occurred in Kuril Islands The results of analyzing the signals in the group speed range of $u_{L1}=u_{L2}=3.1$ km/s and $u_{L1}=u_{L2}=2.8$ km/s are shown at the bottom right of Fig. 5.15. This group speed range was selected because the seismogram of Mashhad has the most prominent Rayleigh wave signals in this range.

The earthquake of July 28, 1968, occurred in Komandorski Island region. The results are shown at the bottom of Fig. 5.16.
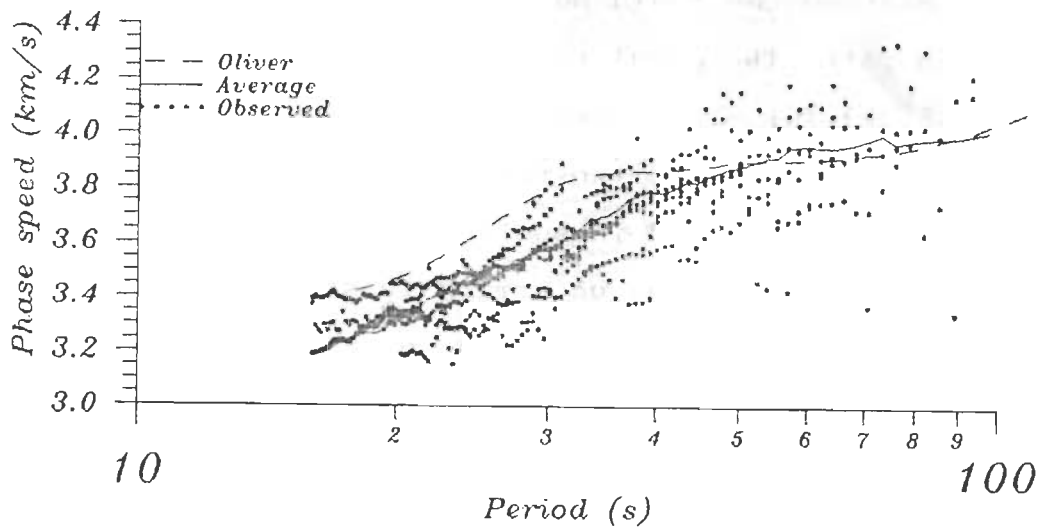
FIG. 5.13 A SUMMARY FIGURE IN WHICH PHASE SPEED DATA SHOWN AT BOTTOM RIGHT CORNER OF FIGS. 5.15 TO 5.22 IS COMPILED. SEE TEXT UNDER SECTION 5.3 FOR FURTHER DETAILS. AVERAGE CURVE HERE IS ACTUALLY THE AVERAGE CURVE OF FIG. 5.14.
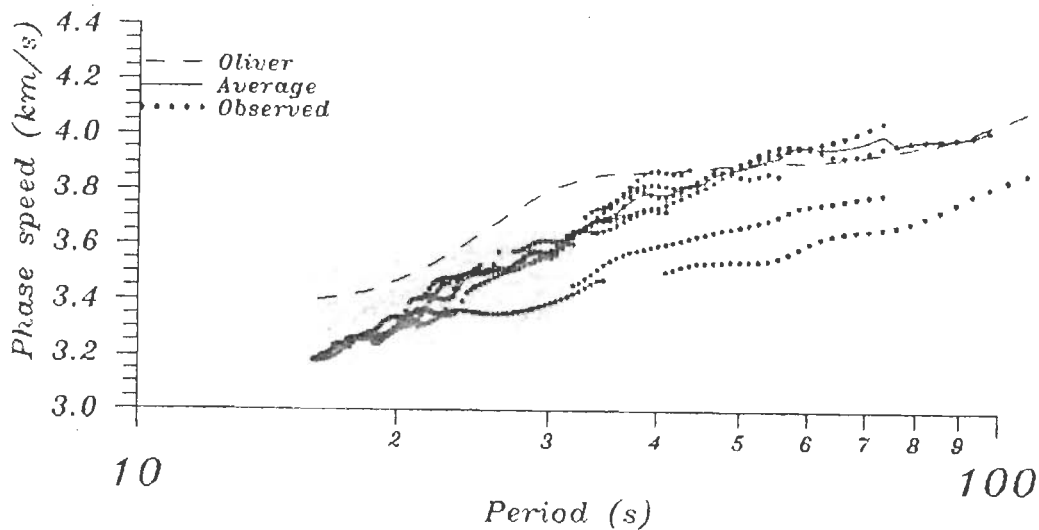
FIG. 5.14 A SUMMARY FIGURE IN WHICH PHASE SPEED DATA SHOWN AT BOTTOM RIGHT CORNER OF FIGS. 5.15 TO 5.22 IS COMPILED. SEE TEXT UNDER SECTION 5.3 FOR FURTHER DETAILS.

Hypocentral Data

Date	Orig. Time	Epicenter	Location	mb	Depth
1967 06 12	23 22 46.	47.47N 154.30E	Kuril Island	5.4	56

Ep. distanc	
Shiraz	Mashhad
8438	7448

Azimuth to:	
Shiraz	Mashhad
298.68°	299.24°
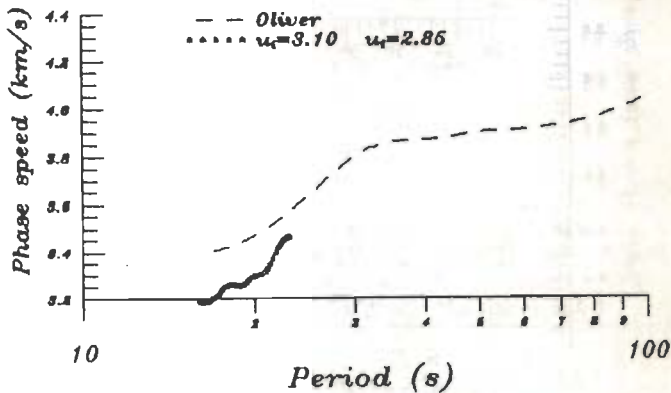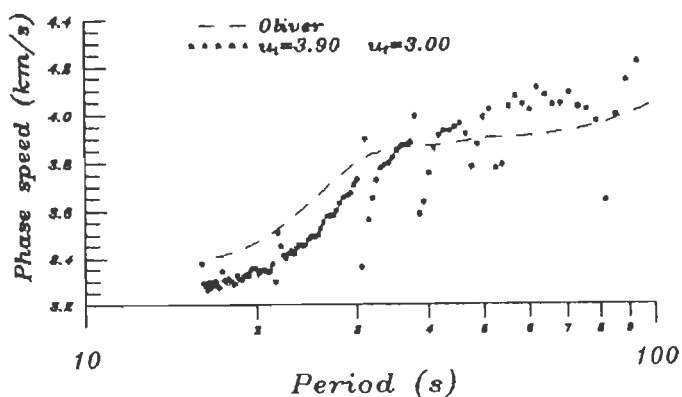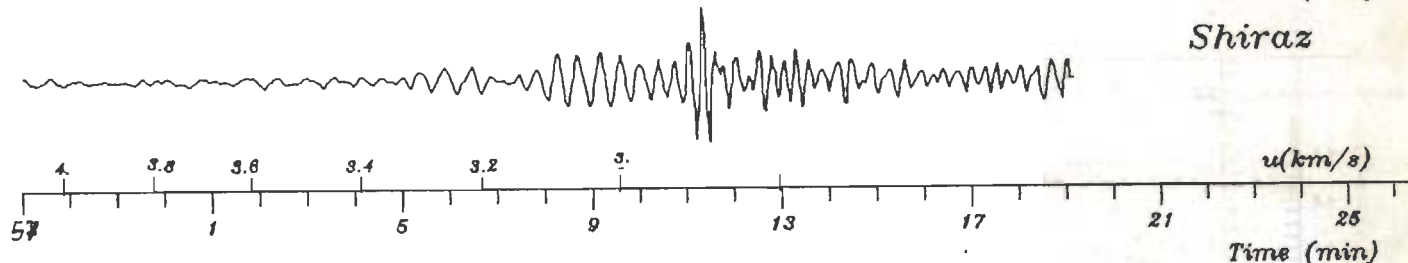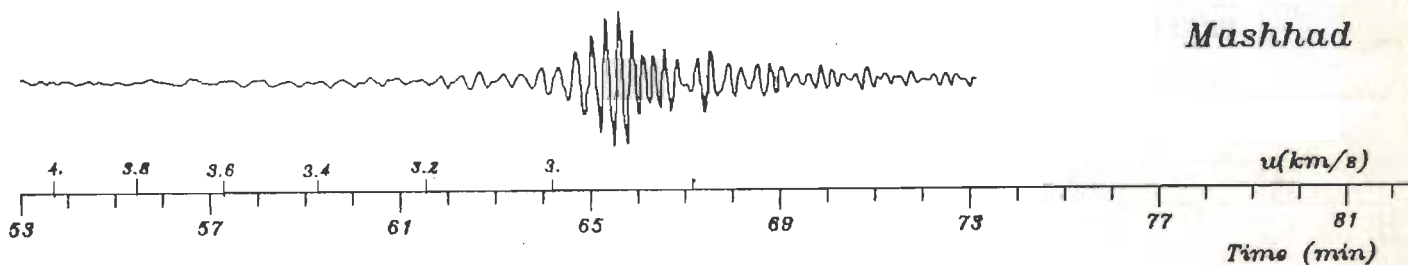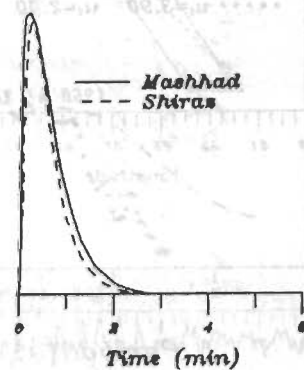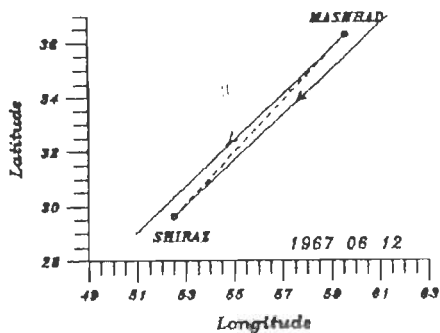
FIG. 5.15 A PHASE SPEED DETERMINATION FOR THE CENTRAL IRAN REGION. THIS FIGURE IS SIMILAR TO FIG 5.1 IN THE METHOD OF PRESENTATION OF DATA.

Hypocentral Data

Date	Orig. Time	Epicenter	Location	mb	Depth
1968 07 28	21 12 38.	55.43N 166.58E	Komandoriski Island region	5.4	27

Ep. distanc

Shiraz	Mashhad
8688	7705

Azimuth to:

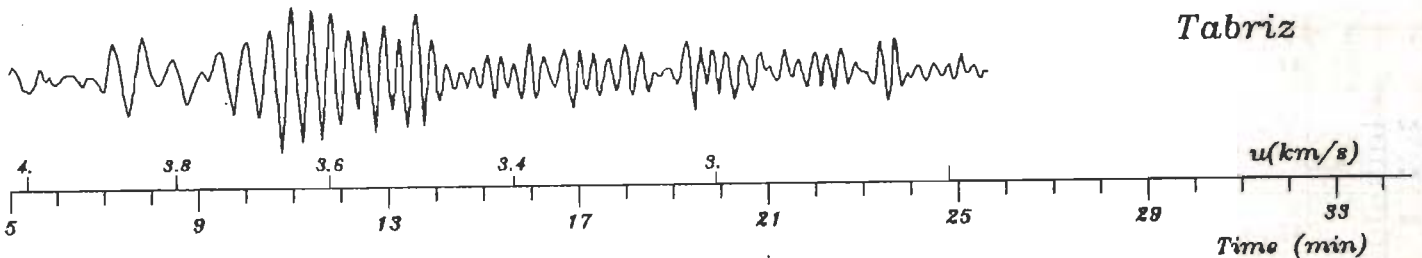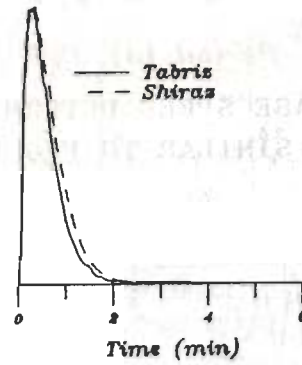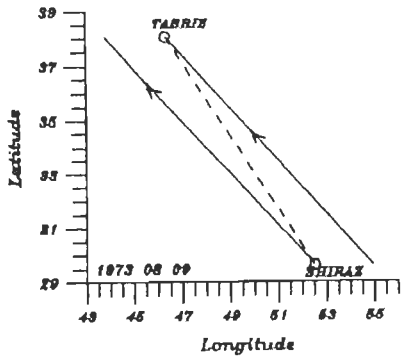| Shiraz	Mashhad
305.82°	304.54°
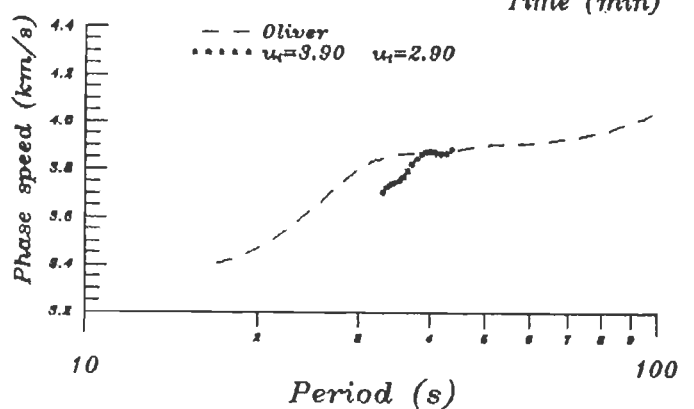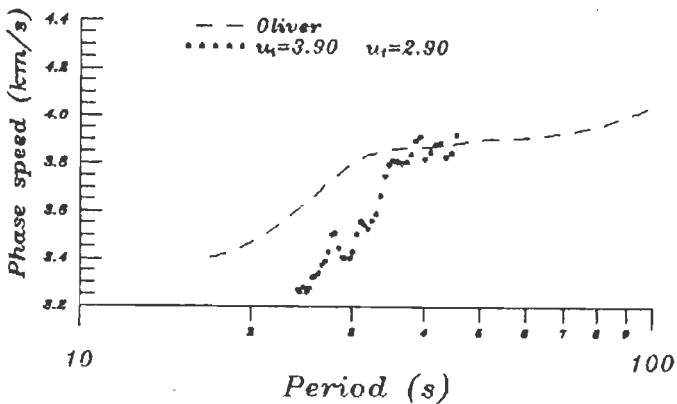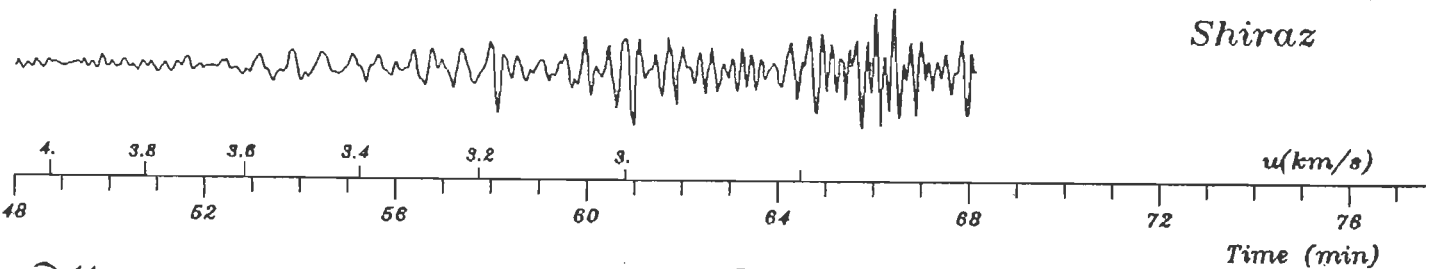
FIG. 5.16 A PHASE SPEED DETERMINATION FOR THE CENTRAL IRAN REGION. THIS FIGURE IS SIMILAR TO FIG 5.1 IN THE METHOD OF PRESENTATION OF DATA.

The earthquake August 22, 1968, occurred west of Bering Sea. The results are shown at the bottom of Fig. 5.17.

The earthquake Jun 14, 1970, occurred in southern Chile. The waves arrived in Iran from the SE. The results are displayed at the bottom of Fig. 5.18 and lie much below the curve of Oliver (1962).

The earthquake of July 18, 1970, occurred in the Rat Island region. The results are shown at the bottom of Fig. 5.19.

The earthquake of September 9, 1971, occurred in Kuril Islands. The estimated focal depth is 7 km. The phase speed curves for selected segments of Rayleigh waves are quite smooth (bottom of Fig. 5.20) even though they lie well below the curve of Oliver (1962).

The earthquake of December 2, 1971, occurred in Kuril Islands also. The surface waves are well recorded and the results are shown at the bottom of Fig. 5.21.

The earthquake of August 4, 1972, occurred in Onekotan Islands east of Kamchatka. The seismograms have a slightly noisy appearance. The results are shown at the bottom of Fig. 5.22.

On the whole the recorded Rayleigh wave trains for the Central Iran region are noisier than for the Zagros region. Hence in individual case, it was necessary to consider more than one small segment of Rayleigh wave trains more frequently for the Central Iran path than for the Zagros path.

Date	Orig. Time	Epicenter	Location	mb	Depth
1968 08 22	14 00 07	53.01N 171.30E	W Bering Sea	5.4	33

Ep. distanc	
Shiraz	Mashhad
9077	8094

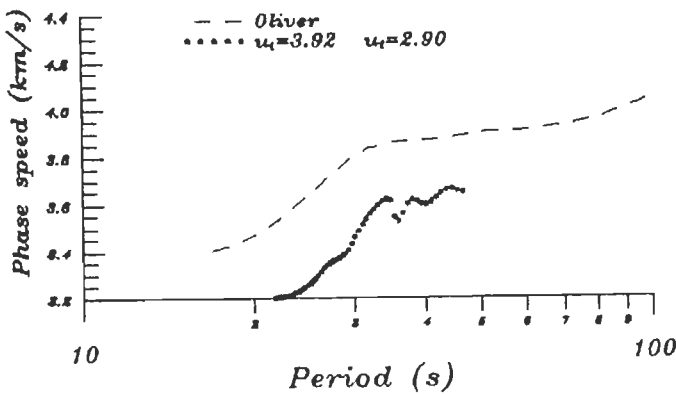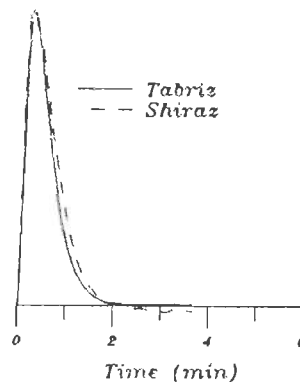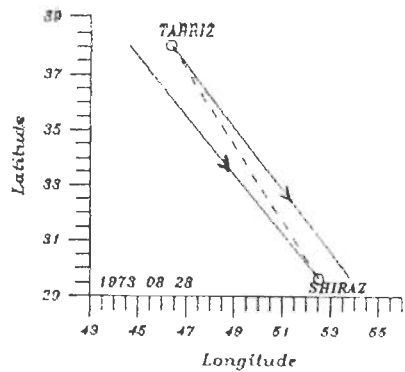| Azimuth to:	
Shiraz	Mashhad
309.45°	308.25°

Mashhad

Shiraz
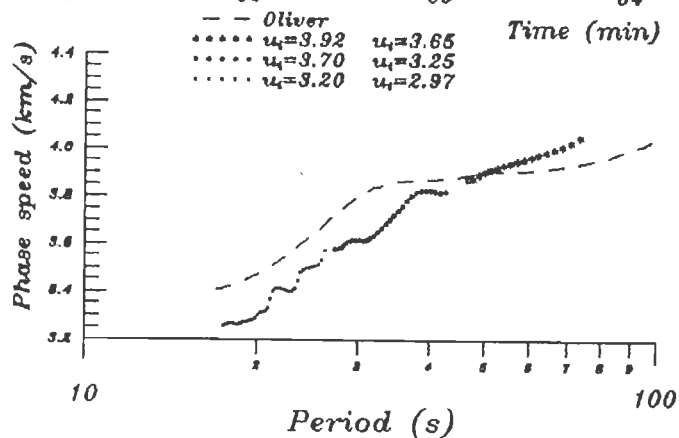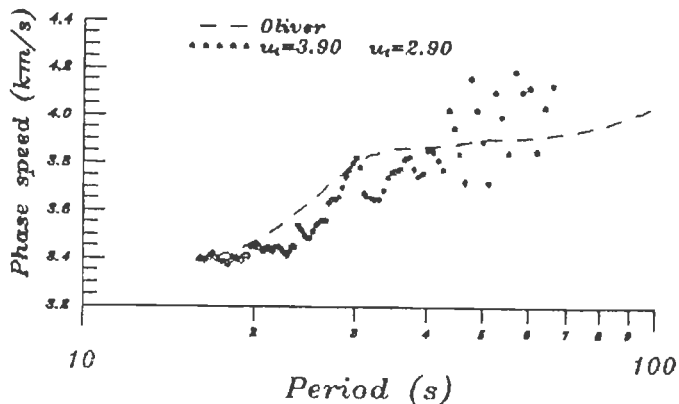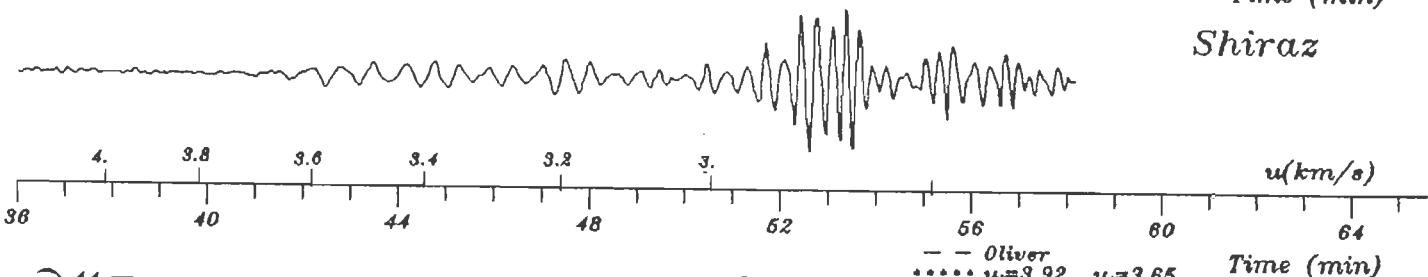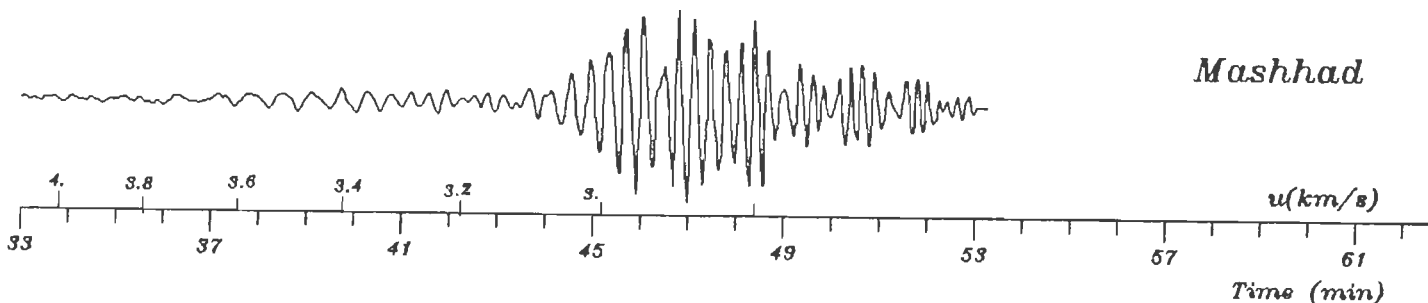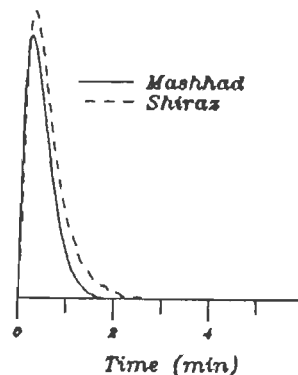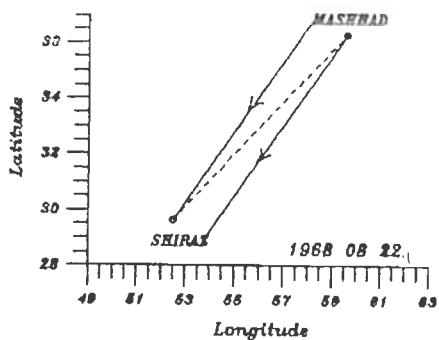
FIG. 5.17 A PHASE SPEED DETERMINATION FOR THE CENTRAL IRAN REGION. THIS FIGURE IS SIMILAR TO FIG 5.1 IN THE METHOD OF PRESENTATION OF DATA.

Hypocentral Data

Date	Orig. Time	Epicenter	Location	mb	Depth
1970 06 14	00 00 11.	51.95S 73.85W	S Chile	6	33

Ep. distanc	
Shiraz	Mashhad
15007	15995

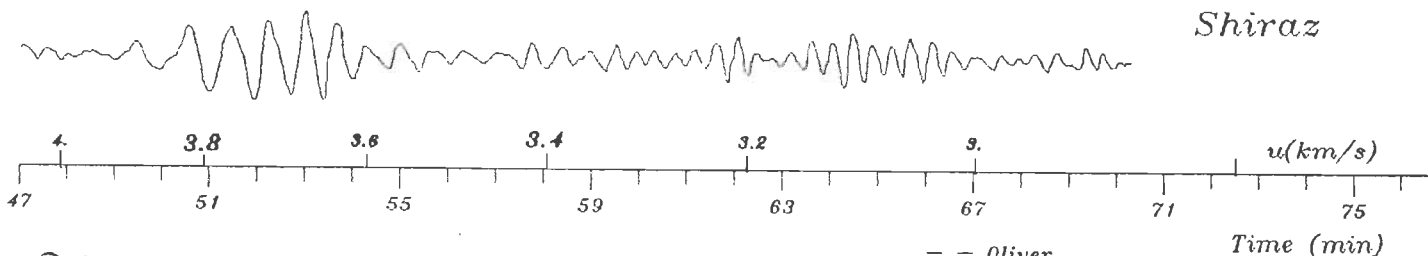| Azimuth to:	
Shiraz	Mashhad
98.22°	96.97°
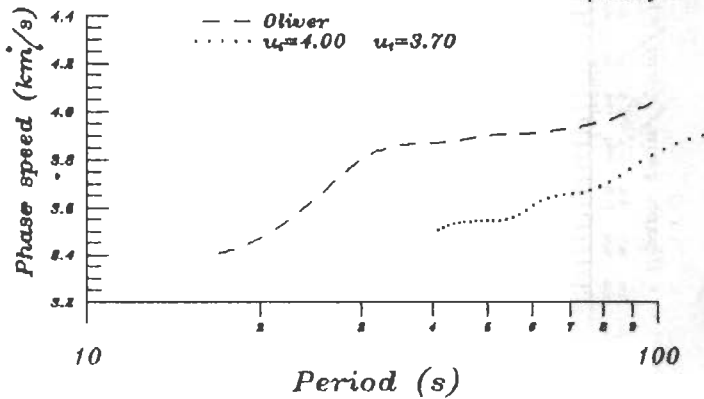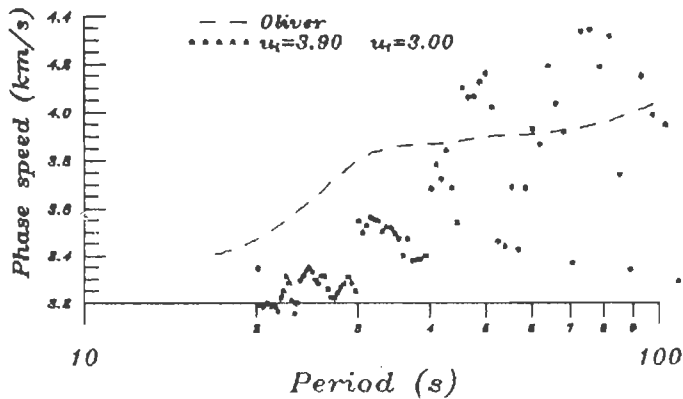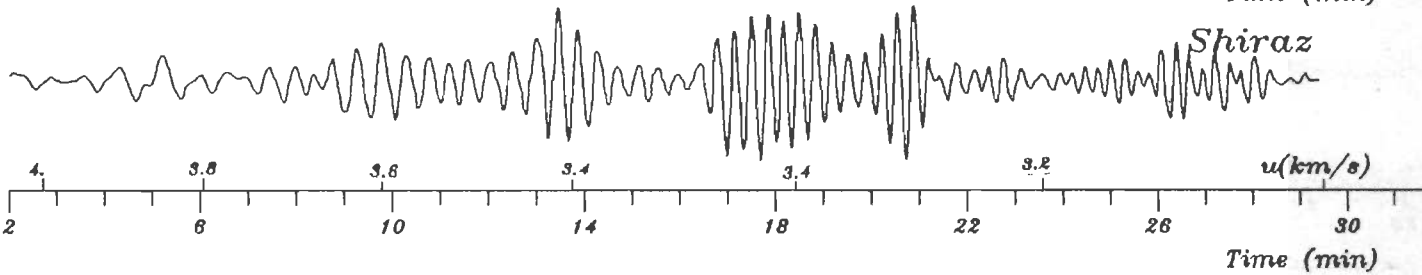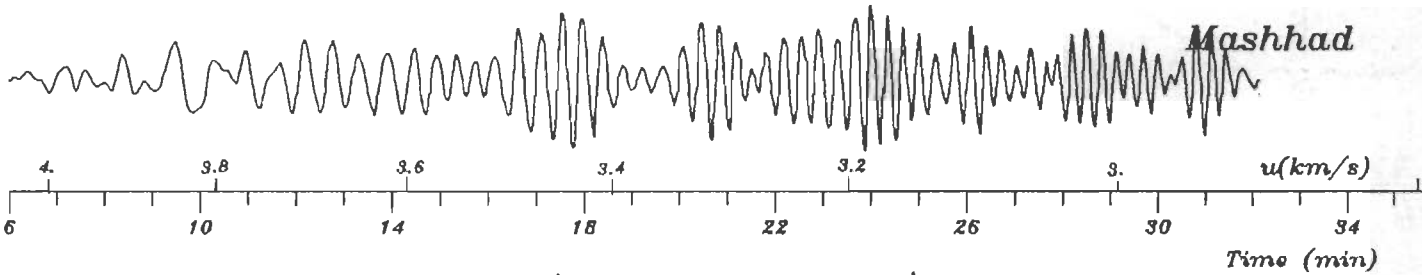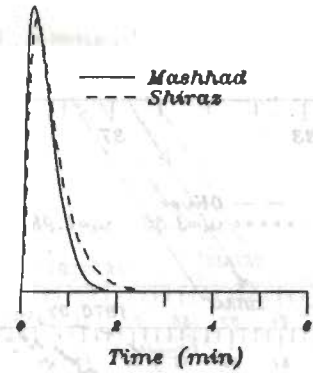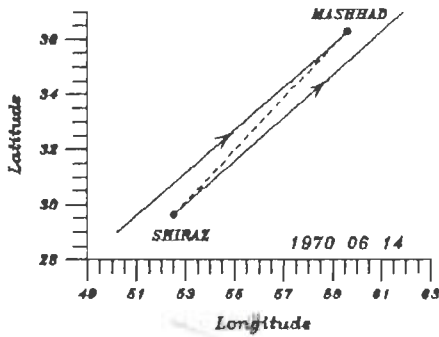
FIG. 5.18 A PHASE SPEED DETERMINATION FOR THE CENTRAL IRAN REGION. THIS FIGURE IS SIMILAR TO FIG 5.1 IN THE METHOD OF PRESENTATION OF DATA.

145

Date	Orig. Time	Epicenter	Location	mb	Depth
1970 07 18	01 48 39.	51.4 N 178.5 E	Rat Island	5.7	46

Ep. distanc	
Shiraz	Mashhad
9718	8744

Azimuth to:	
Shiraz	Mashhad
317.44°	315.76°
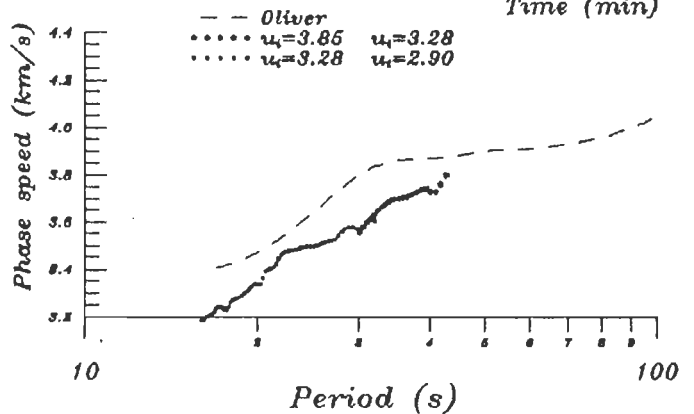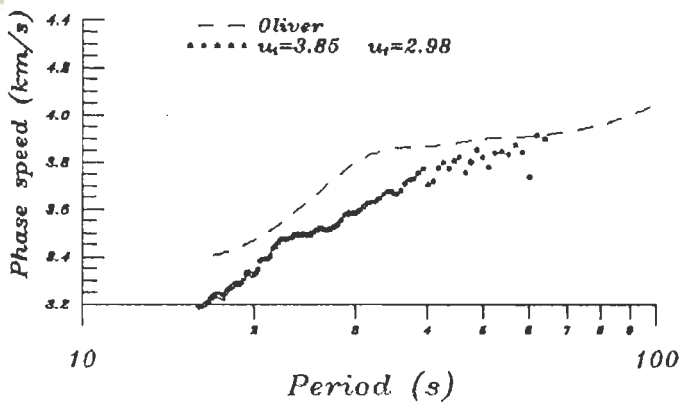
FIG. 5.19 A PHASE SPEED DETERMINATION FOR THE CENTRAL IRAN REGION. THIS FIGURE IS SIMILAR TO FIG 5.1 IN THE METHOD OF PRESENTATION OF DATA.

Date	Orig. Time	Epicenter	Location	mb	Depth
1971 09 09	23 01 07.	44.44N 150.89E	Kuril Island	6	7

Ep. distanc

Shiraz	Mashhad
8361	7378

Azimuth to:

Shiraz	Mashhad
297.20°	298.42°
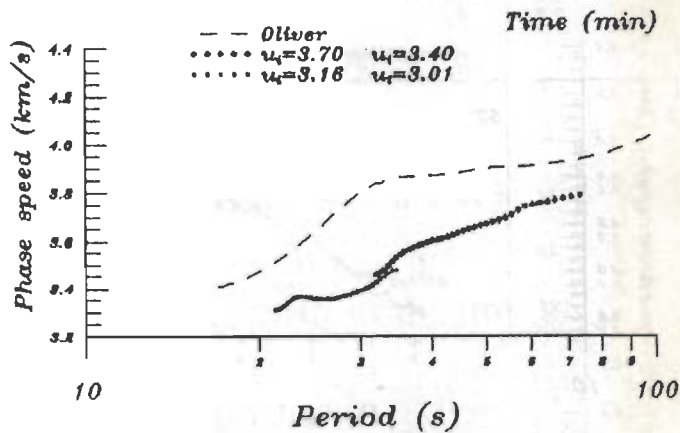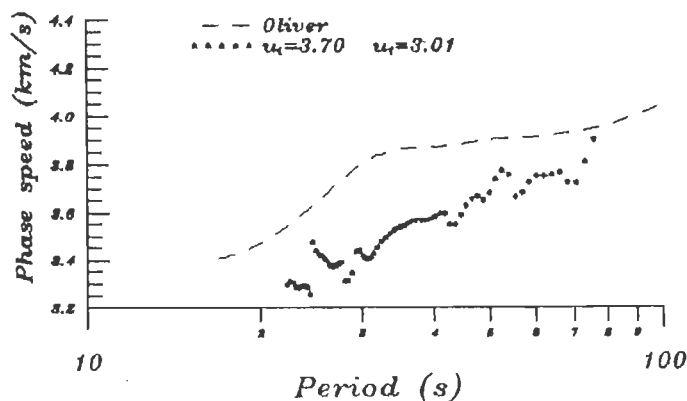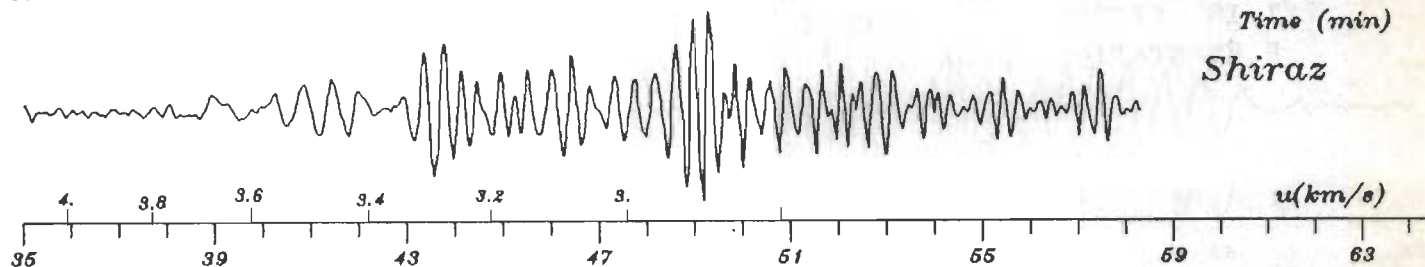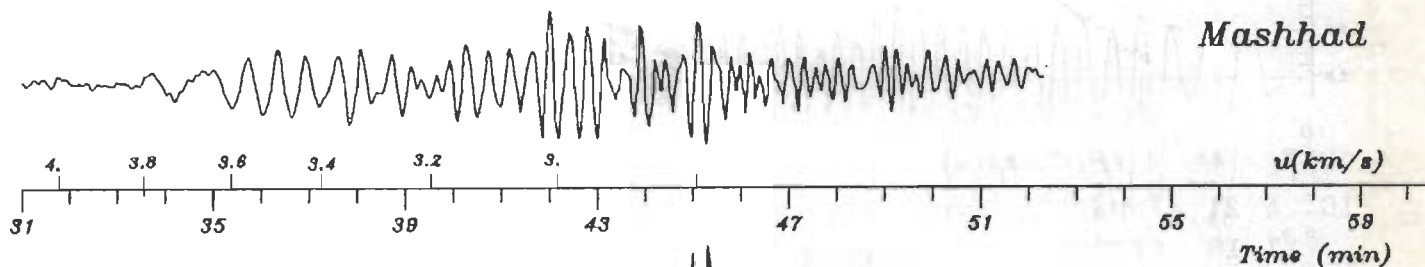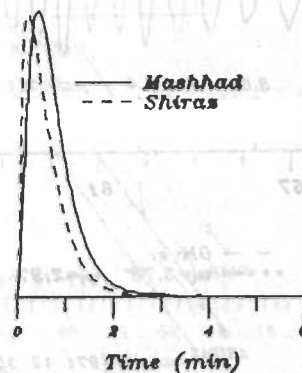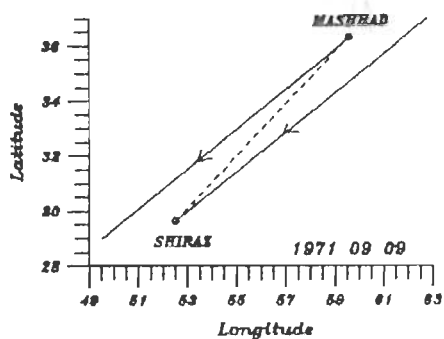
FIG. 5.20 A PHASE SPEED DETERMINATION FOR THE CENTRAL IRAN REGION. THIS FIGURE IS SIMILAR TO FIG 5.1 IN THE METHOD OF PRESENTATION OF DATA.

Hypocentral Data

Date	Orig. Time	Epicenter	Location	mb	Depth
1971 12 02	17 18 22.	44.83N 153.34E	Kuril Island	6.1	33

Ep. distanc	
Shiraz	Mashhad
8510	7524

Azimuth to:	
Shiraz	Mashhad
298.62°	299.62°
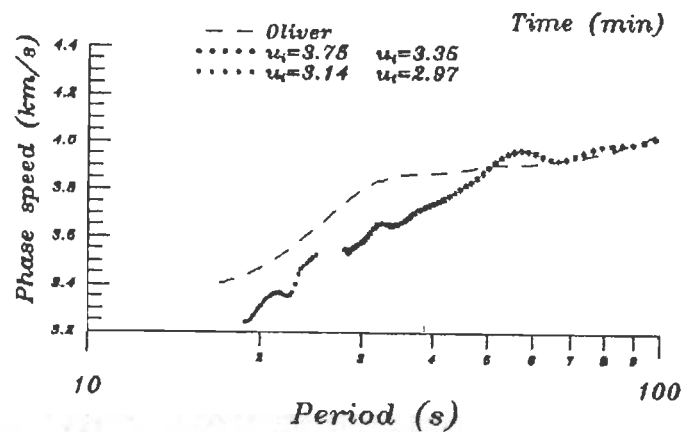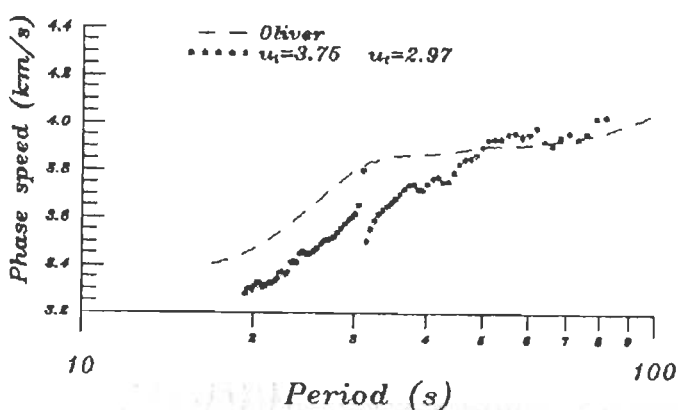
FIG. 5.21 A PHASE SPEED DETERMINATION FOR THE CENTRAL IRAN REGION. THIS FIGURE IS SIMILAR TO FIG 5.1 IN THE METHOD OF PRESENTATION OF DATA.

148

Hypocentral Data

Date	Orig. Time	Epicenter	Location	mb	Depth
1972 08 04	17 51 13.	49.16N 159.07E	Onekaton Island E Kamchatka	5.7	54

Ep. distanc	
Shiraz	Mashhad
8457	7465

Azimuth to:	
Shiraz	Mashhad
299.48°	299.67°
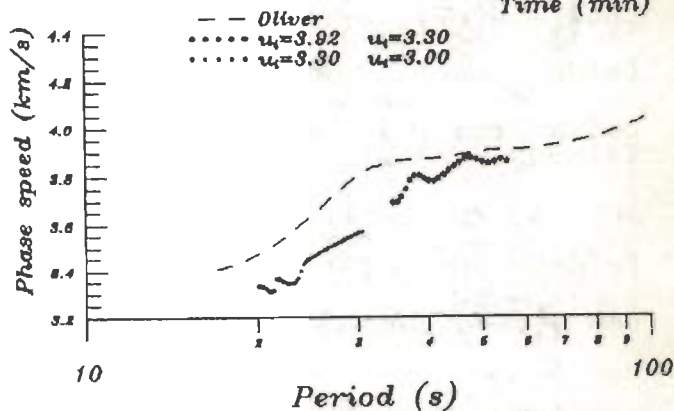
FIG. 5.22 A PHASE SPEED DETERMINATION FOR THE CENTRAL IRAN REGION. THIS FIGURE IS SIMILAR TO FIG 5.1 IN THE METHOD OF PRESENTATION OF DATA.

149

5.5 CUMULATIVE PHASE SPEED RESULTS FOR THE ALBORZ REGION

There were 11 pairs of seismograms for the Alborz region (Mashhad-Tabriz path). Fig. 5.23 and 5.24 display the results obtained for all 11 paths together. In the manning of Figs. 5.2 and 5.3 (Section 5.3) and Figs. 5.13 and 5.14 (Section 5.4) it can be said that, on the whole, the Alborz path represents an average continental crust and upper mantle.

A special feature of this set of observation is that mantle Rayleigh waves were seen on seismograms for three earthquakes. In one case these waves are seen for R1 type Rayleigh waves only and in the two other cases for both R1 and R2 type waves.

5.5.1 SELECTED REMARKS FOR INDIVIDUAL CASES OF ALBORZ REGION

The earthquake of January 8, 1970, whose results are shown in Fig. 5.25 and 5.26 are exceptional. It occurred north of New Zealand and its reported focal depth is 179 km. The recorded seismograms show inversely dispersed mantle Rayleigh waves both for the direct (R1) and the oppositely arriving (R2) Rayleigh waves. In the latter case only the inversely dispersed mantle Rayleigh waves are seen. The phase speeds results for the R1 waves are shown at the bottom of Fig. 5.25 and for the R2 waves at the bottom of Fig. 5.26.

The earthquake of August 28, 1970, occurred in Solomon Islands. The phase speed dispersion curves (bottom of Fig. 5.27) show a very erratic behavior. An examination of seismograms (middle part of Fig. 5.27) reveals that a prominent wave train in the period range of 32 to 20 s approximately is well recorded at

150
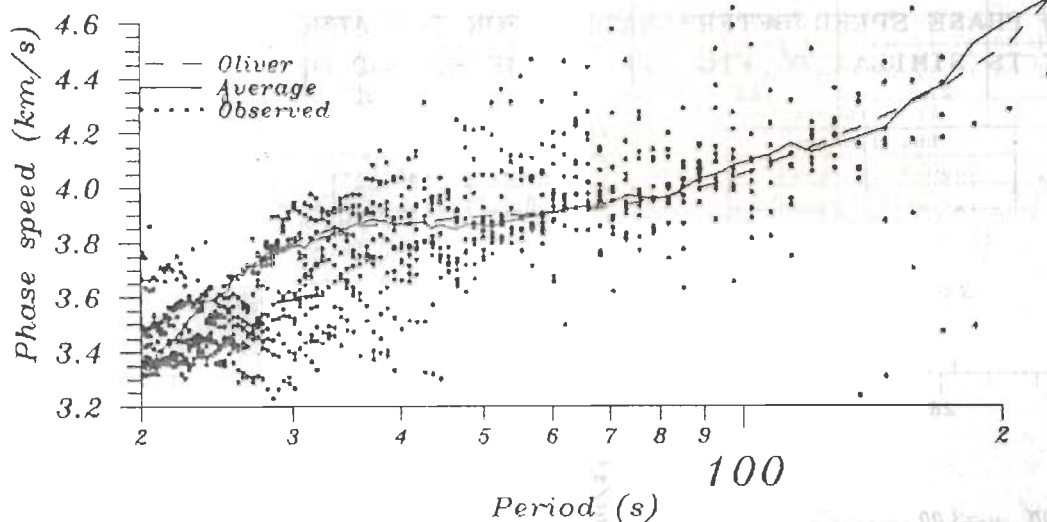
FIG. 5.23 A SUMMARY FIGURE IN WHICH PHASE SPEED DATA SHOWN AT BOTTOM RIGHT CORNER OF FIGS. 5.25 TO 5.37 IS COMPILED. SEE TEXT UNDER SECTION 5.3 FOR FURTHER DETAILS. AVERAGE CURVE HERE IS ACTUALLY THE AVERAGE CURVE OF FIG. 5.24.
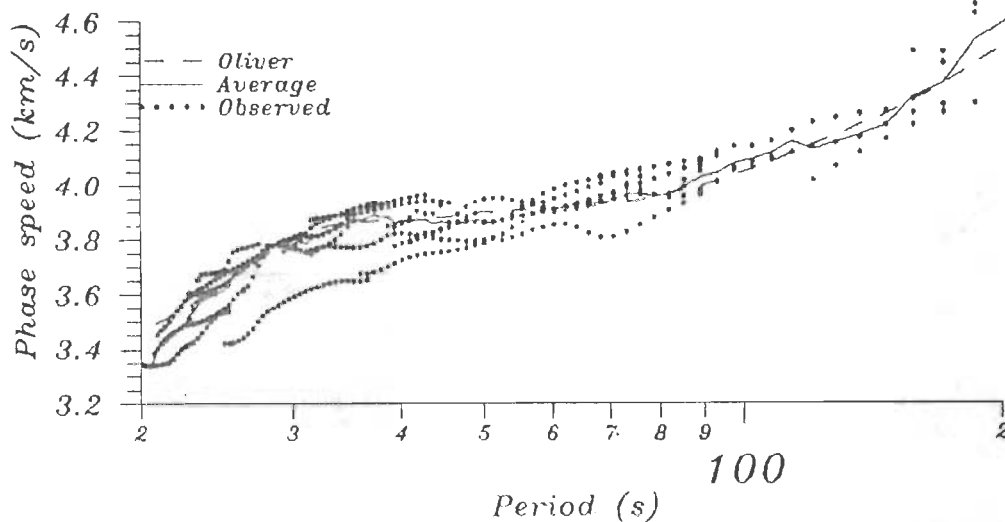
FIG. 5.24 A SUMMARY FIGURE IN WHICH PHASE SPEED DATA SHOWN AT BOTTOM RIGHT CORNER OF FIGS. 5.25 TO 5.37 IS COMPILED. SEE TEXT UNDER SECTION 5.3 FOR FURTHER DETAILS.

Date	Orig. Time	Epicenter	Location	mb	Depth
1970 01 08	17 12 39.	34.74S 178.57E	N New Guinea	6.1	179

Ep. distanc	
Mashhad	Tabriz
14586	15772

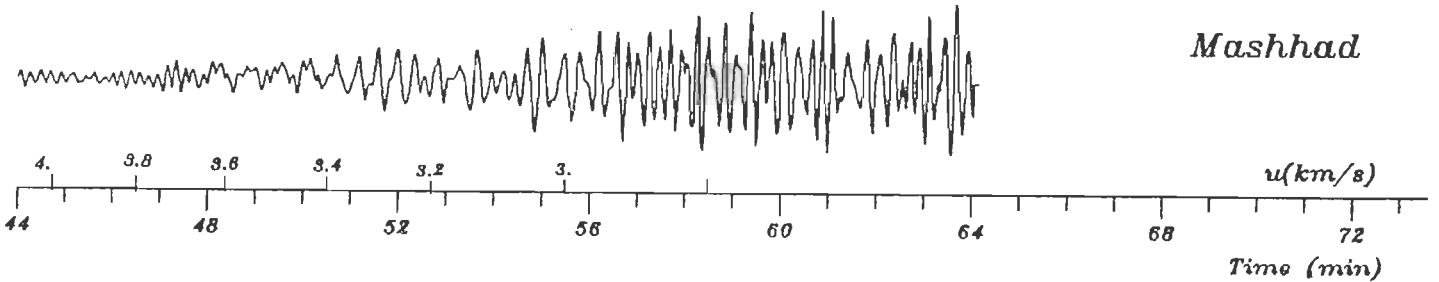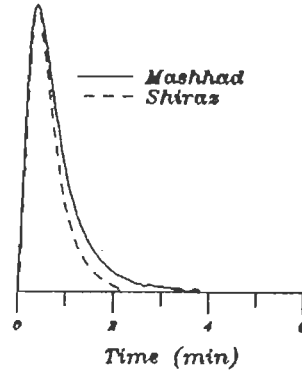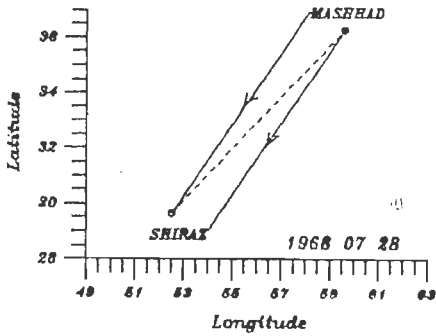| Azimuth to:	
Mashhad	Tabriz
290.54°	289.38°
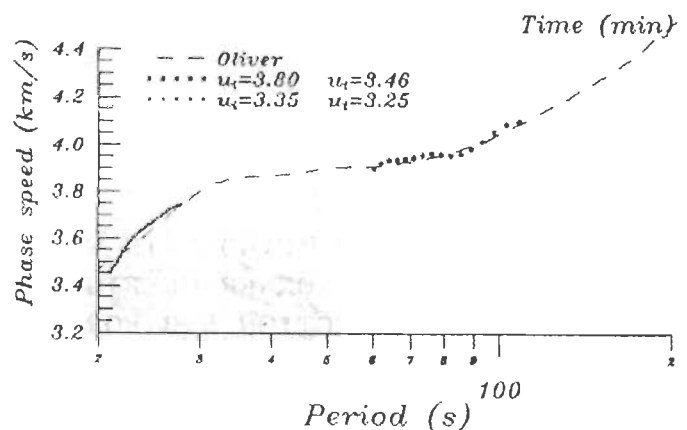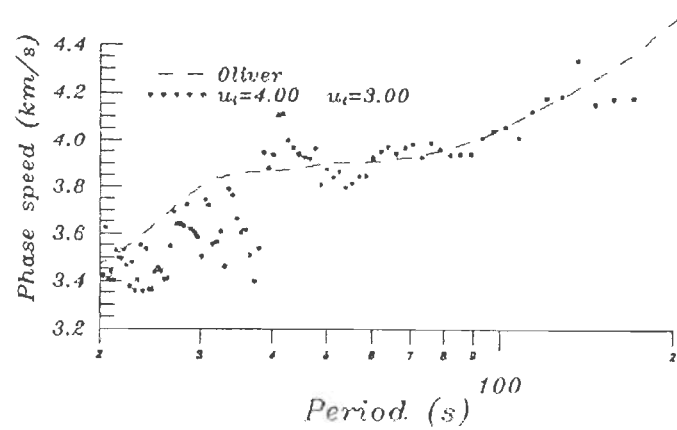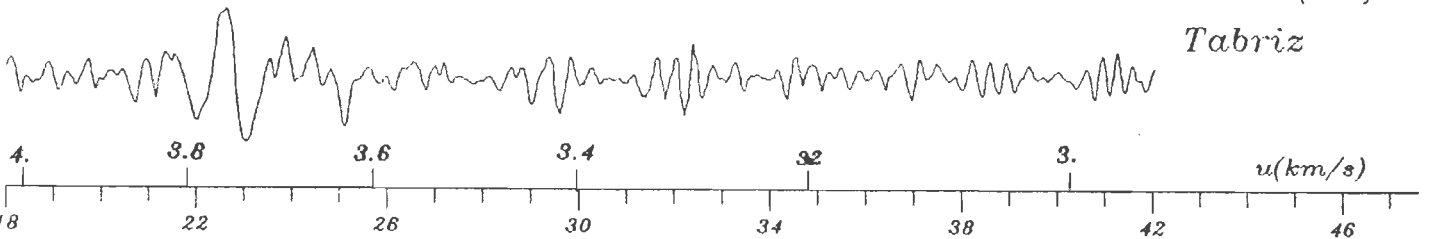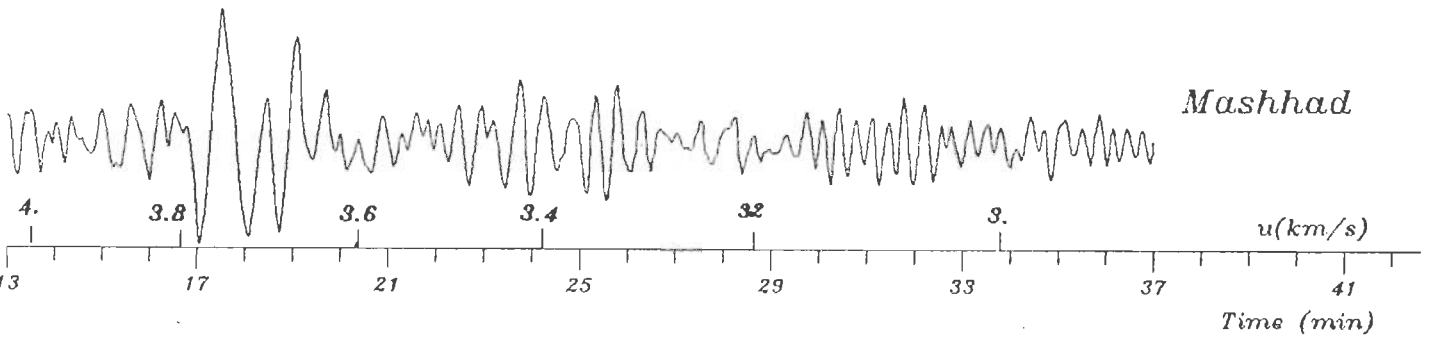
FIG. 5.25 A PHASE SPEED DETERMINATION FOR THE ALBORZ REGION. THIS FIGURE IS SIMILAR TO FIG 5.1 IN THE METHOD OF PRESENTATION OF DATA.

Hypocentral Data

Date	Orig. Time	Epicenter	Location	mb	Depth
1970 01 08	17 12 39.	34.74S 178.57E	N New Zealand	6.1	179

Ep. distanc	
Mashhad	Tabriz
25445	24259

Azimuth to:	
Mashhad	Tabriz
110.54°	109.38°

Mashhad

Tabriz
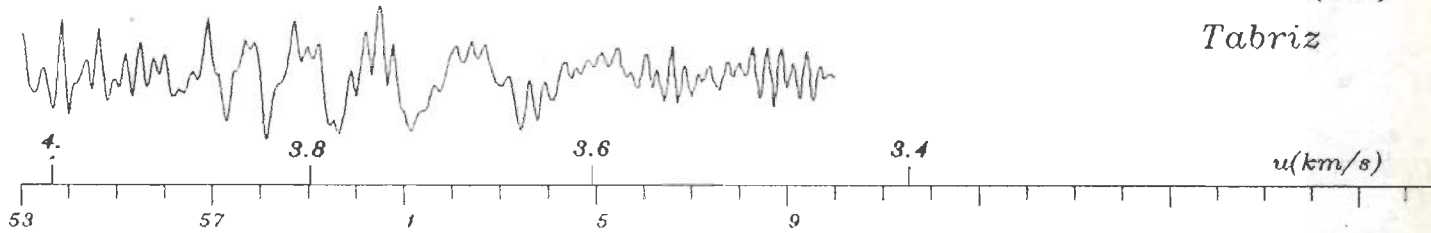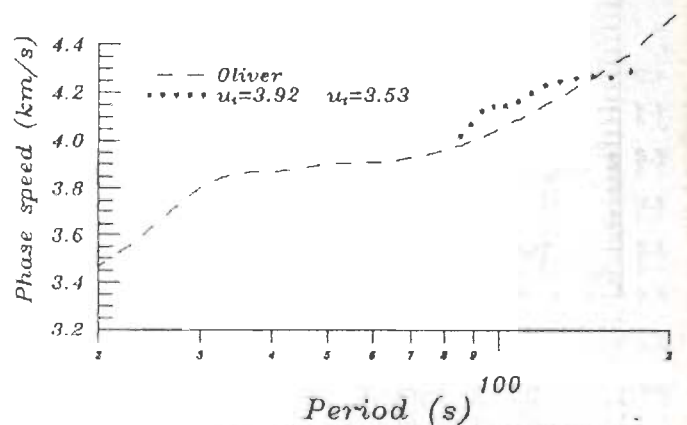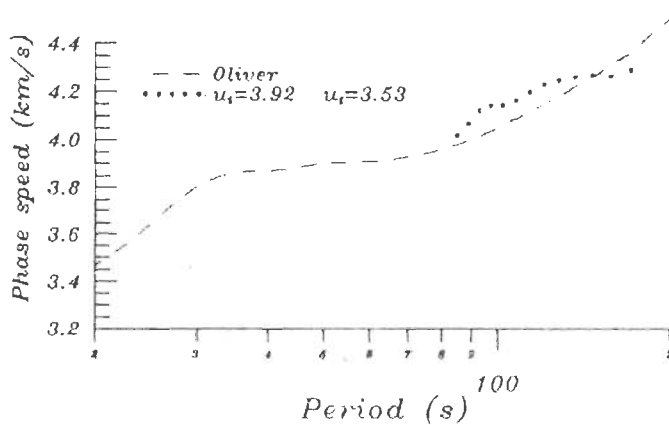
FIG. 5.26 A PHASE SPEED DETERMINATION FOR THE ALBORZ REGION. THIS
FIGURE IS SIMILAR TO FIG 5.1 IN THE METHOD OF PRESENTATION OF
DATA. IT IS TO BE NOTED THAT WE ARE CONSIDERING HERE R2 TYPE
RAYLEIGH WAVES.

Date	Orig. Time	Epicenter	Location	mb	Depth
1970 08 28	01 09 49.	4.57S 153.06E	Solomon Island	5.9	88

Ep. distanc

Mashhad	Tabriz
10619	11783

Azimuth to:

Mashhad	Tabriz
306.09°	308.35°
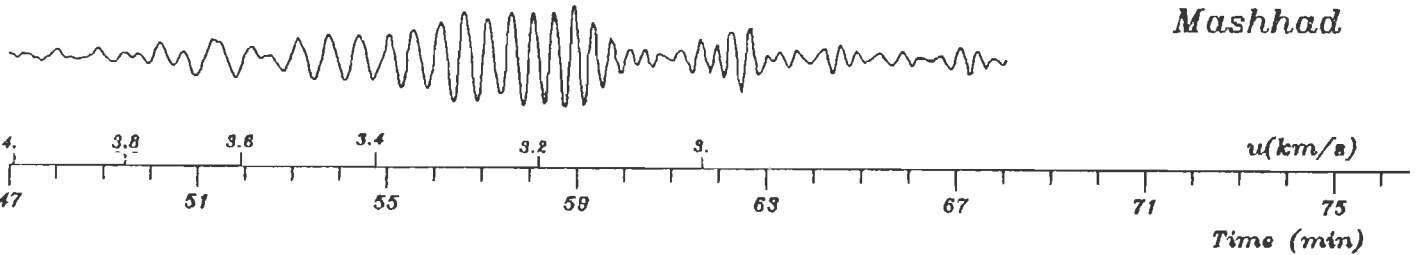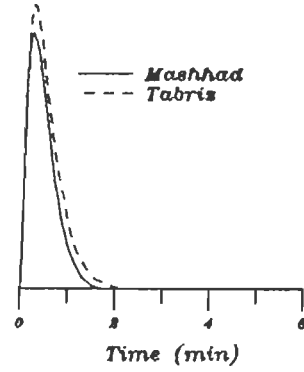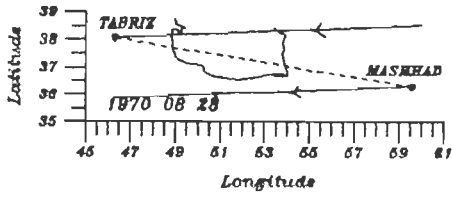
Mashhad
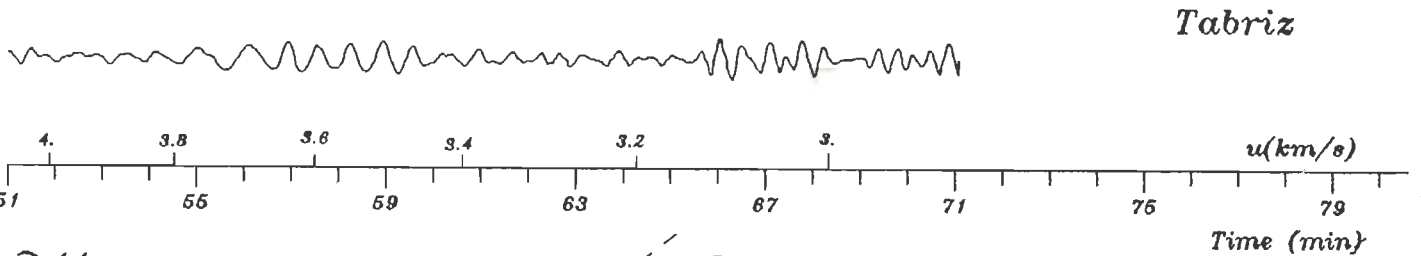
Tabriz
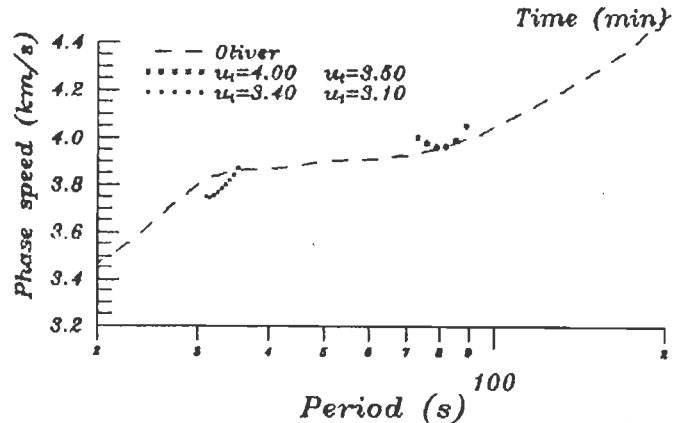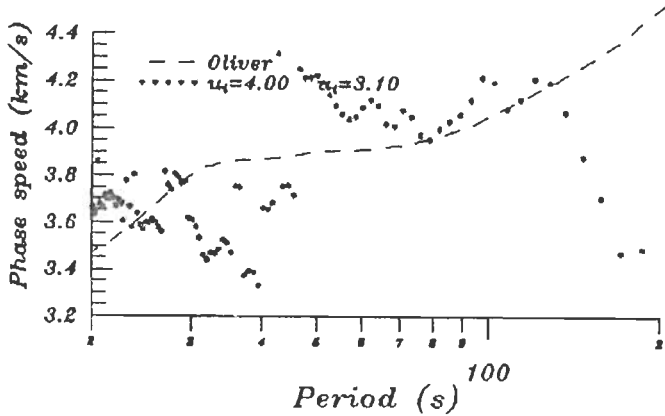
FIG. 5.27 A PHASE SPEED DETERMINATION FOR THE ALBORZ REGION. THIS FIGURE IS SIMILAR TO FIG 5.1 IN THE METHOD OF PRESENTATION OF DATA.

154

Mashhad and weakly recorded at Tabriz. The earthquake of May 28, 1972, (see below) occurred about 167 km SW of the earthquake under discussion. The Rayleigh wave trains at both Mashhad and Tabriz are well recorded over the full period range in that case. We conclude that the absence of shorter period Rayleigh waves on the Tabriz seismogram in the case of earthquake of August 28, 1970, is due to path effects somewhere midway between the epicenter and the Tabriz station . The phase speed results of this earthquake are not taken into account when estimating average phase speeds along the Alborz region.

The earthquake of October 31, 1970, occurred east of New Guinea and had a reported focal depth of 42. The results of the phase speed computations (Fig. 5.28) are surprisingly good for mantle Rayleigh waves, although such long period waves with inverse group speed dispersion are slightly difficult to observe on the seismograms for (R1) Rayleigh waves. In other words these long period waves are not as well seen on the seismograms as in the case of earthquake of Jan. 8, 1970 (Fig. 5.26). We note that a group of waves in the later part ($u_{t1}=u_{t2}=3.82$ km/s to $u_{t1}=u_{t2}=3.36$ km/s) of the Rayleigh wave train (see middle part of Fig. 5.28) gives good results (see bottom right of Fig. 5.28). A close scrutiny of seismograms for the earthquake of Oct. 31, 1970, shows that the oppositely arriving (R2) type Rayleigh waves are seen weakly. We have carried out the analysis and the results are shown in Fig. 2.29. the scatter in results is greater in this case than in the case of R2 waves shown in Fig. 5.26.

Hypocentral Data

Date	Orig. Time	Epicenter	Location	mb	Depth
1970 10 31	17 53 09.	4.93S 145.47E	E New Guinea	6	42

| Ep. distanc		Azimuth to:	
Mashhad	Tabriz	Mashhad	Tabriz
9965	11146	306.51°	307.83°
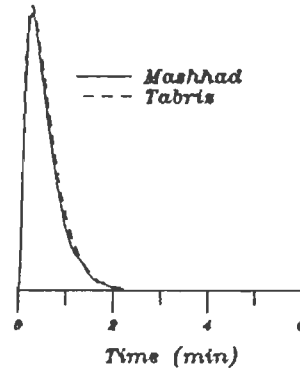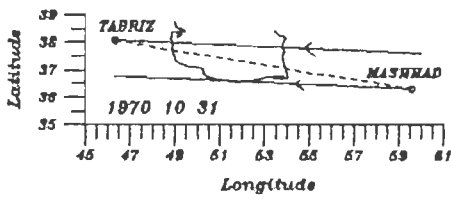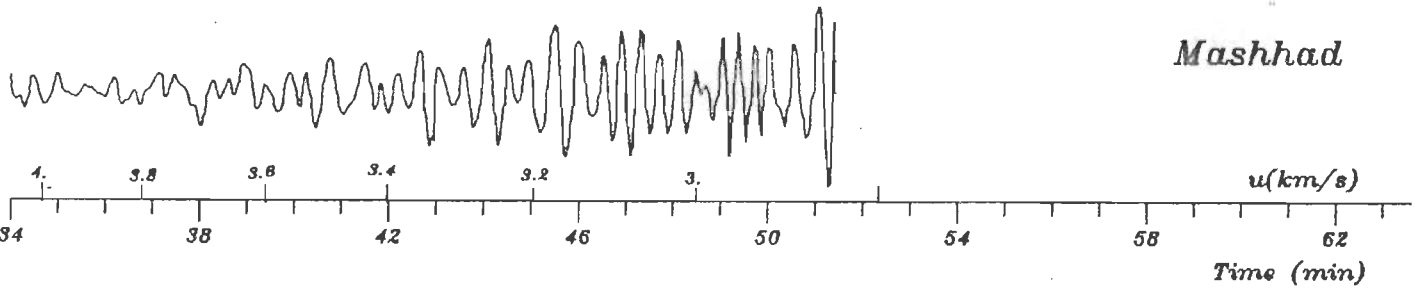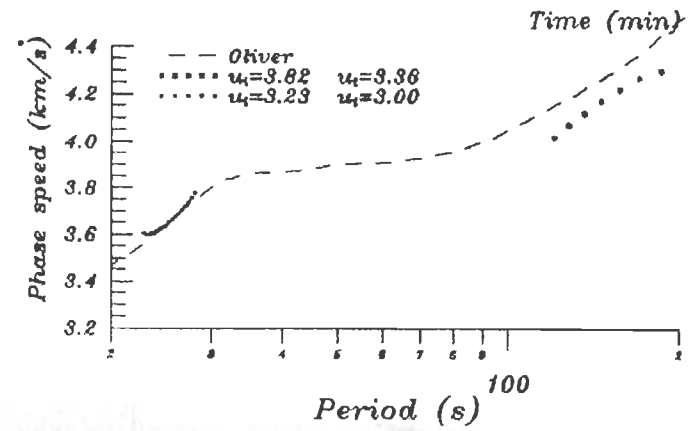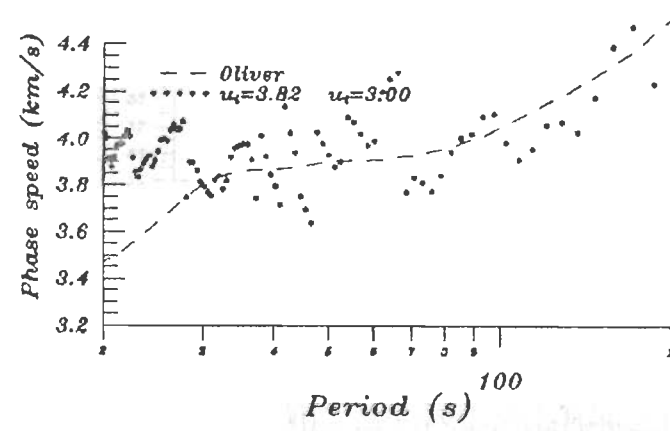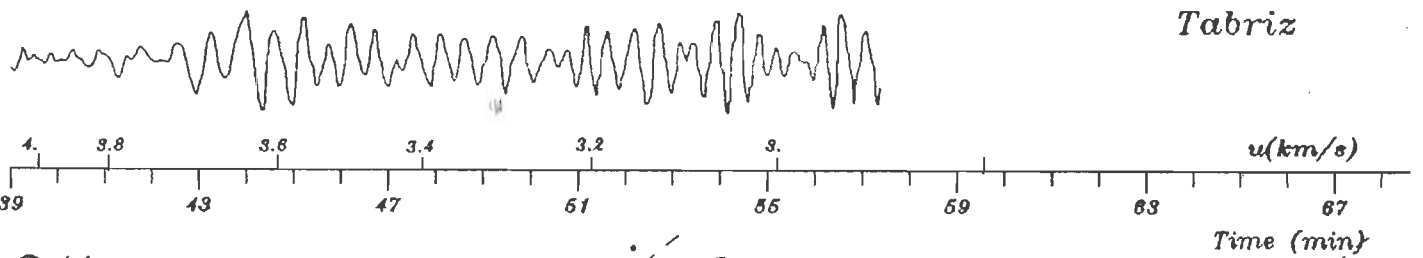
FIG. 5.28 A PHASE SPEED DETERMINATION FOR THE ALBORZ REGION. THIS
FIGURE IS SIMILAR TO FIG 5.1 IN THE METHOD OF PRESENTATION OF
DATA.

156

Hypocentral Data

Date	Orig. Time	Epicenter	Location	mb	Depth
1970 10 31	17 53 09.	4.93S 145.47E	E New Guinea	6	42

Ep. distanc

Mashhad	Tabriz
30066	28885

Azimuth to:

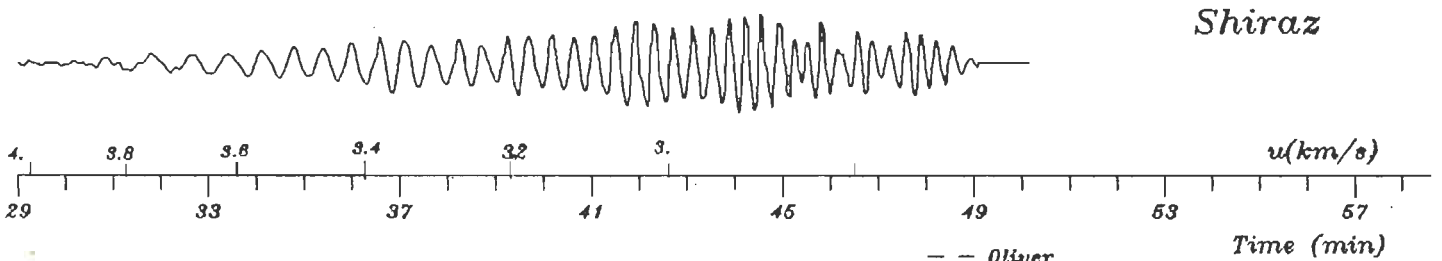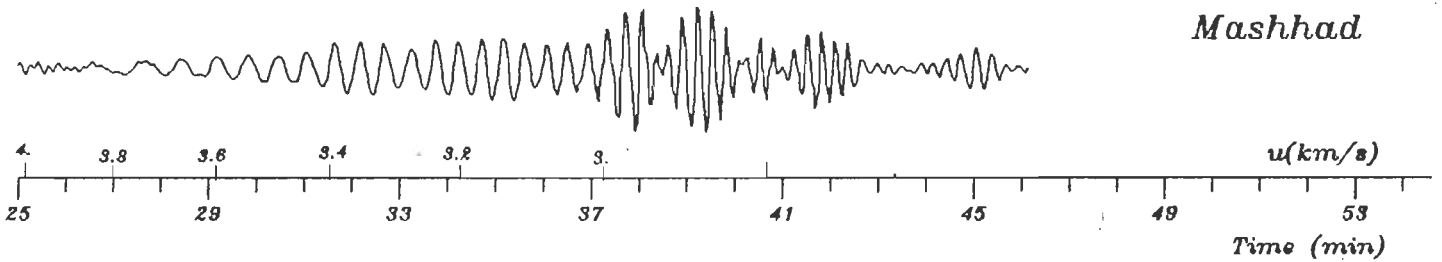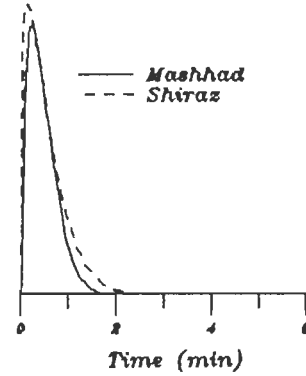| Mashhad	Tabriz
126.51°	127.83°
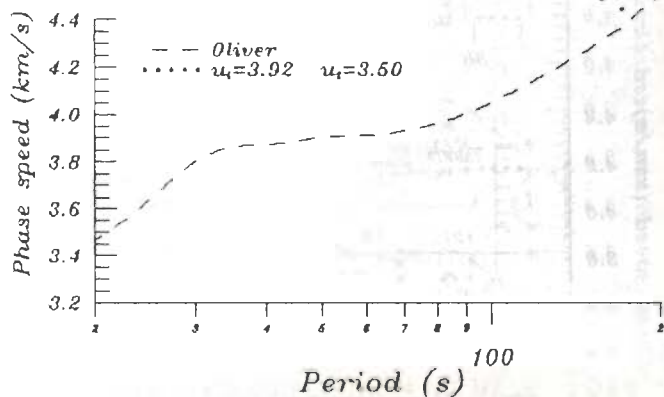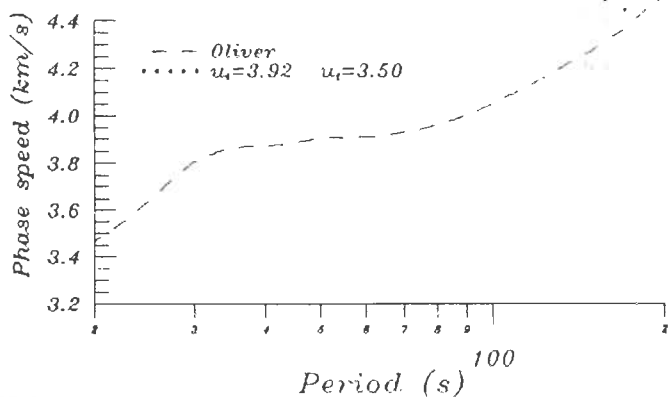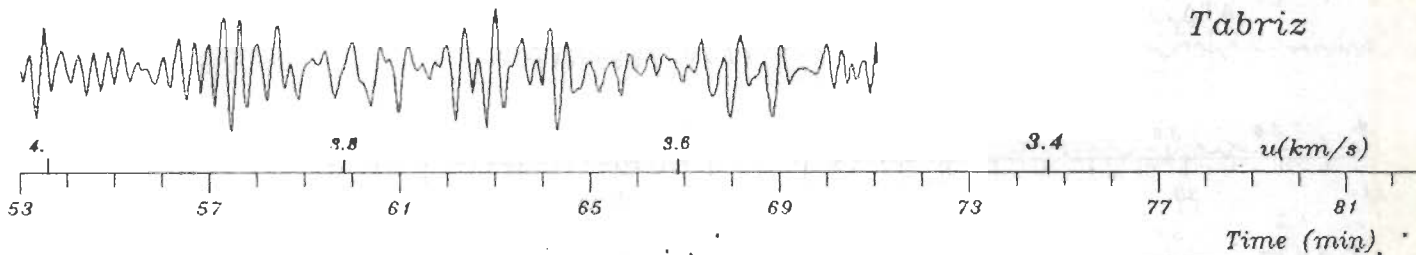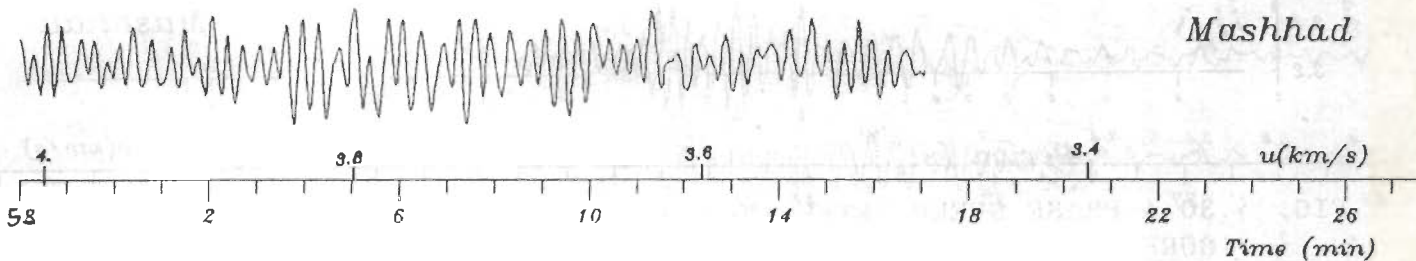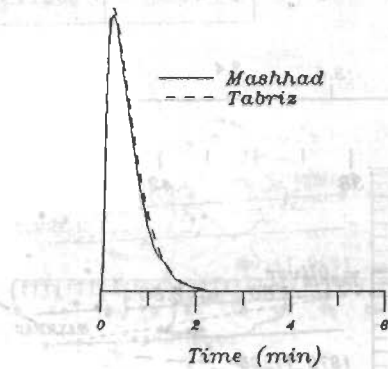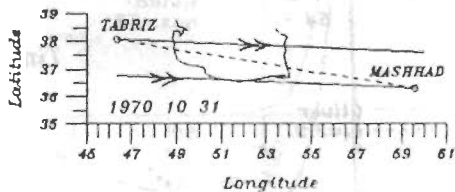
FIG. 5.29 A PHASE SPEED DETERMINATION FOR THE ALBORZ REGION. THIS FIGURE IS SIMILAR TO FIG 5.1 IN THE METHOD OF PRESENTATION OF DATA. IT IS TO BE NOTED THAT WE ARE CONSIDERING HERE R2 TYPE RAYLEIGH WAVES.

Date	Orig. Time	Epicenter	Location	mb	Depth
1970 11 08	14 58 54.	9.13N 126.33E	SSE Philippines	5.7	22

Ep. distanc

Mashhad	Tabriz
7329	8511

Azimuth to:

Mashhad	Tabriz
305.81°	307.13°

Mashhad

Tabriz
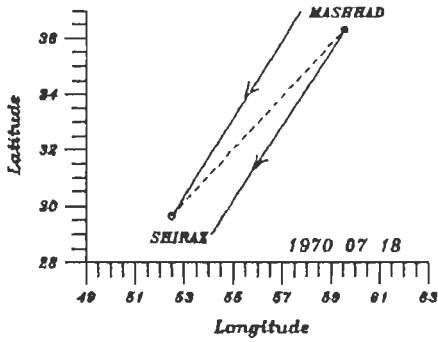
Mashhad

$u(km/s)$

Time (min)

Tabriz

$u(km/s)$

Time (min)
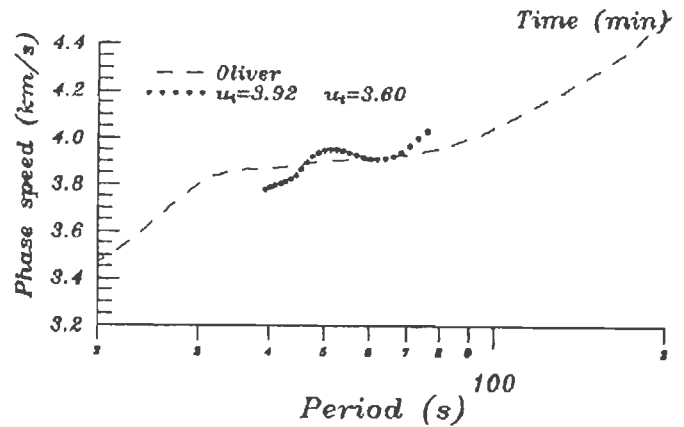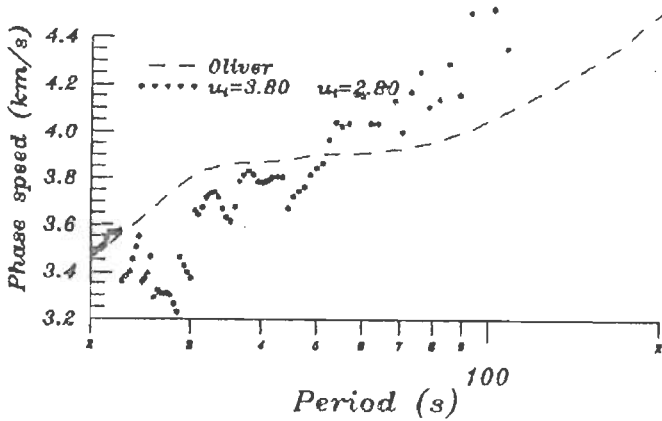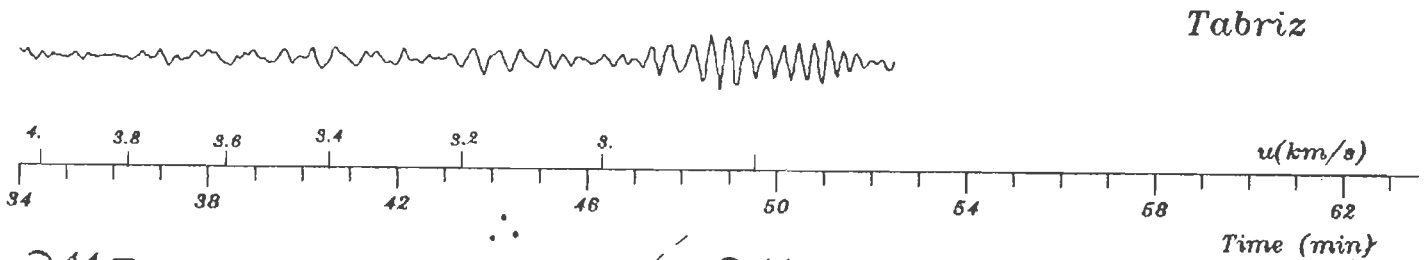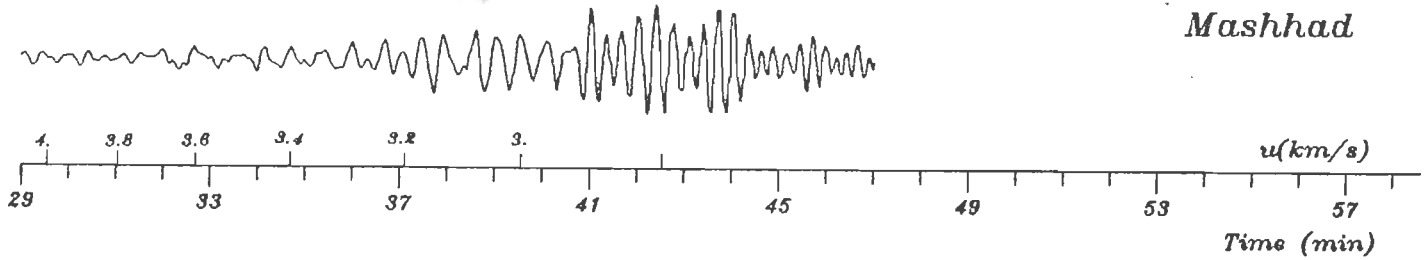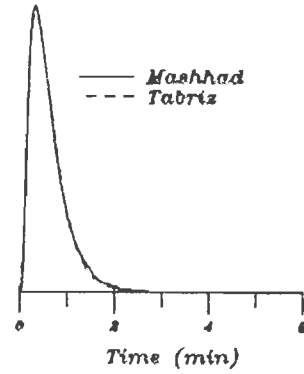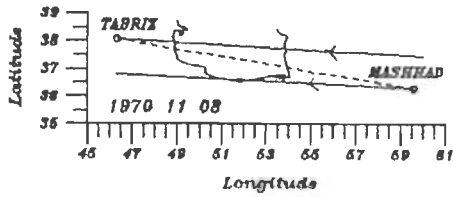
FIG. 5.30 A PHASE SPEED DETERMINATION FOR THE ALBORZ REGION. THIS FIGURE IS SIMILAR TO FIG 5.1 IN THE METHOD OF PRESENTATION OF DATA.

The earthquake of November 8, 1970, occurring southsoutheast of Philippines yields reasonable phase speed dispersion curve in the period range of 40 to 80 seconds (Fig. 5.30). A short segment of wave train in the group speed range of $u_{t1}=u_{t2}=3.3$ km/s to $u_{t1}=u_{t2}=3.15$ km/s gives reasonable results for phase speeds also (bottom right of Fig. 5.30).

The earthquake of November 8, 1970, occurred north of New Guinea. Rayleigh waves phase speeds obtained from analyzing restricted segment of the seismograms corresponding to group speeds between $u_{t1}=u_{t2}=3.45$ km/s and $u_{t1}=u_{t2}=3.15$ km/s give reliable results in the period range 40 to 100 s (bottom of Fig. 5.31).

The earthquake of May 5, 1972, occurring east of New Guinea yielded reasonable results by considering Rayleigh wave trains in the group speed ranges of $u_{t1}=u_{t2}=3.92$ km/s to $u_{t2}=u=3.65$ km/s and $u_{t1}=u_{t2}=3.27$ km/s to $u_{t1}=u_{t2}=3.0$ km/s (bottom of Fig. 5.32).

The earthquake of may 28, 1972, occurred east of New Guinea. As seen from the bottom of Fig. 5.33, good phase speed results are obtained over a wide period range.

The earthquake of May 31, 1973, occurred east of Bangladesh. The map at the top left of Fig. 5.34 shows that great circles from the epicenter to Mashhad and Tabriz are nearly coincident. The phase speed dispersion curves are obtained over a wide period range (bottom of Fig. 5.34).

159

Hypocentral Data

Date	Orig. Time	Epicenter	Location	mb	Depth
1970 11 08	22 35 47.	3.44S 135.63E	N New Guinea	6.2	33

Ep. distanc	
Mashhad	Tabriz
8994	10183

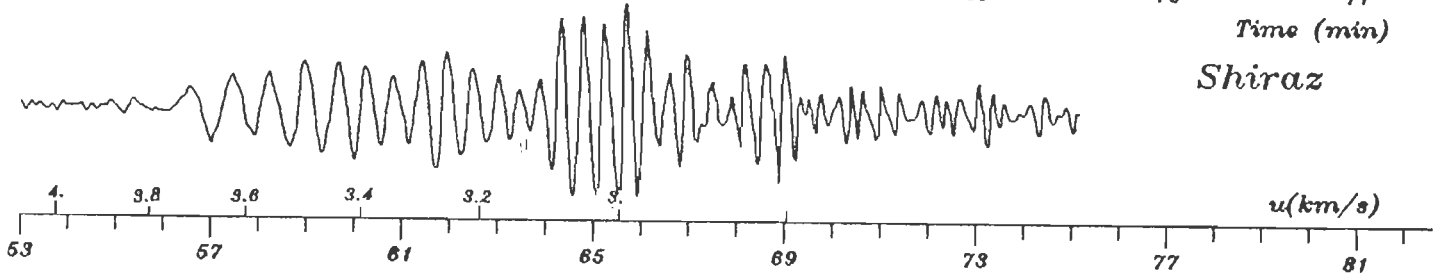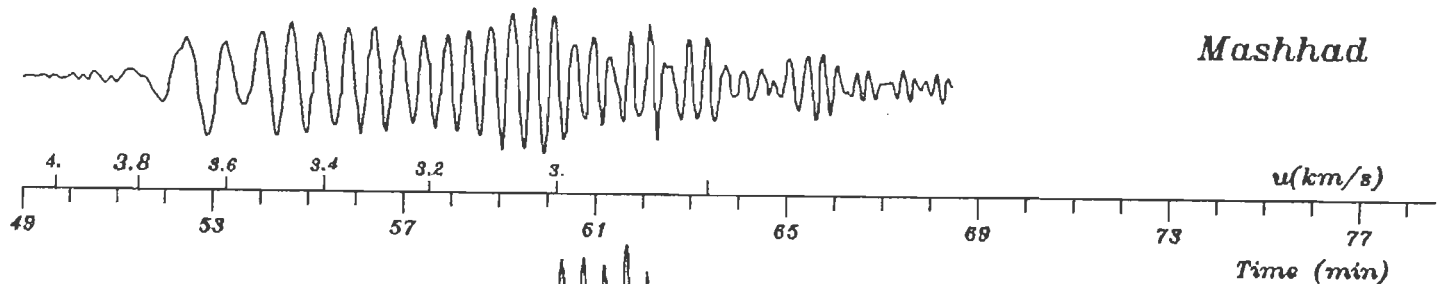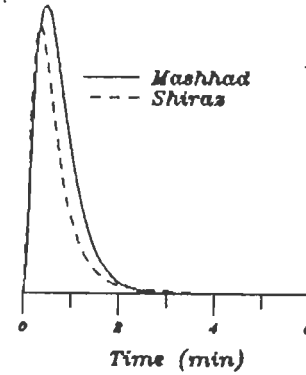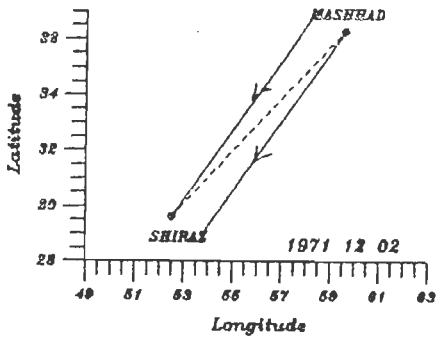| Azimuth to:	
Mashhad	Tabriz
307.62°	308.05°
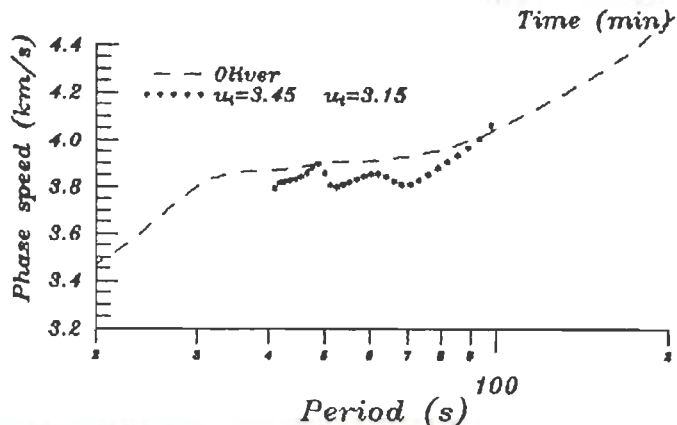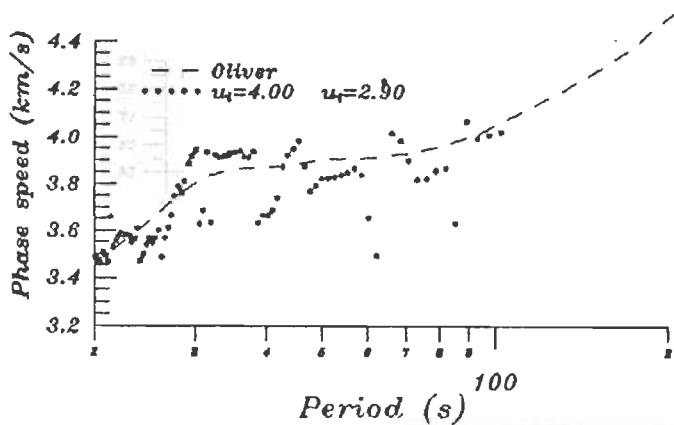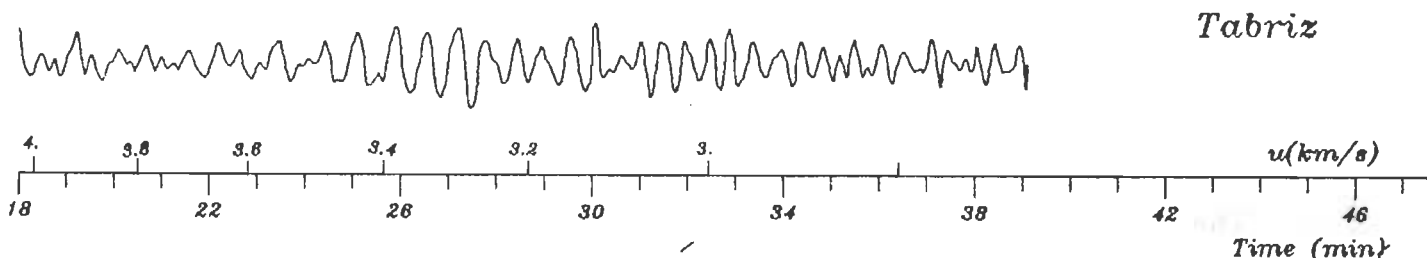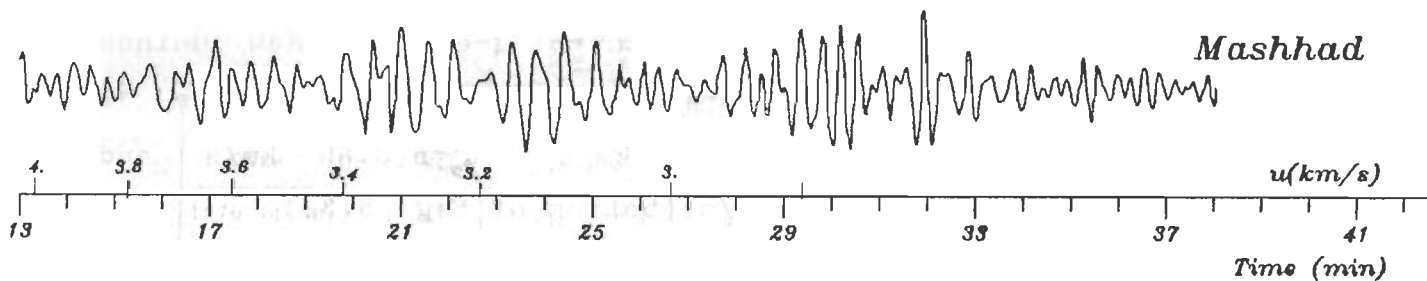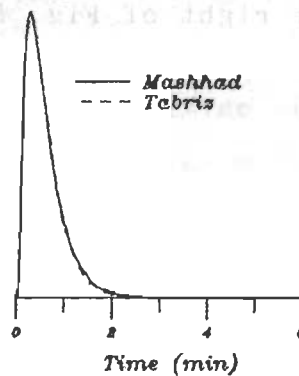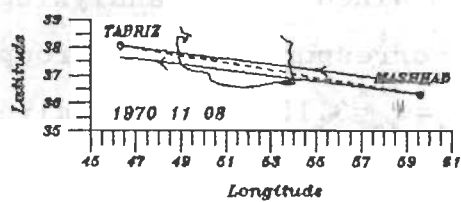
FIG. 5.31 A PHASE SPEED DETERMINATION FOR THE ALBORZ REGION. THIS FIGURE IS SIMILAR TO FIG 5.1 IN THE METHOD OF PRESENTATION OF DATA.

160

Date	Orig. Time	Epicenter	Location	mb	Depth
1972 05 05	23 16 28.	4.16S 152.68E	New Guinea	5.6	32

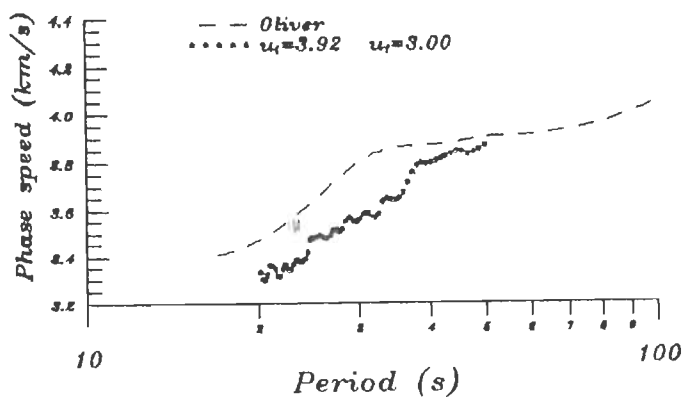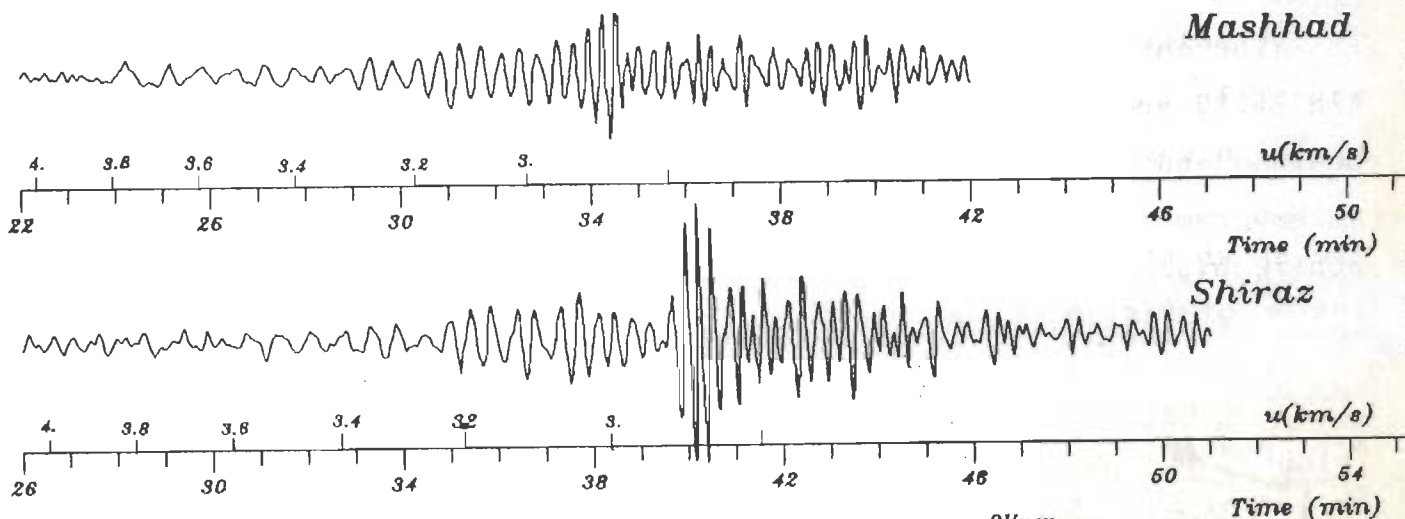| Ep. distanc		Azimuth to:	
Mashhad	Tabriz	Mashhad	Tabriz
10558	11722	306.13°	308.41°

FIG. 5.32 A PHASE SPEED DETERMINATION FOR THE ALBORZ REGION. THIS FIGURE IS SIMILAR TO FIG 5.1 IN THE METHOD OF PRESENTATION OF DATA.

161

Hypocentral Data

Date	Orig. Time	Epicenter	Location	mb	Depth
1972 05 28	01 40 42.	6.00S 151.12E	New Guinea	5.5	69

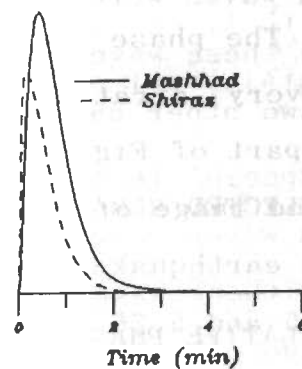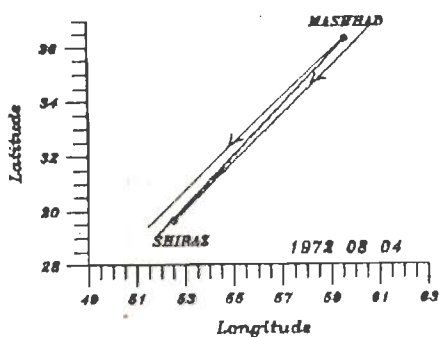| Ep. distanc		Azimuth to:	
Mashhad	Tabriz	Mashhad	Tabriz
10539	11712	306.07°	307.88°
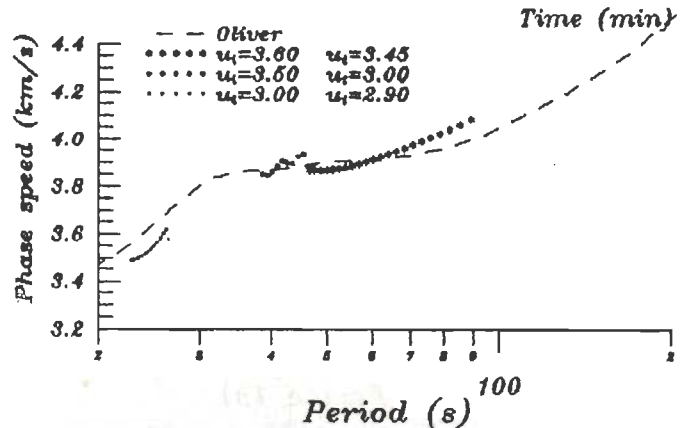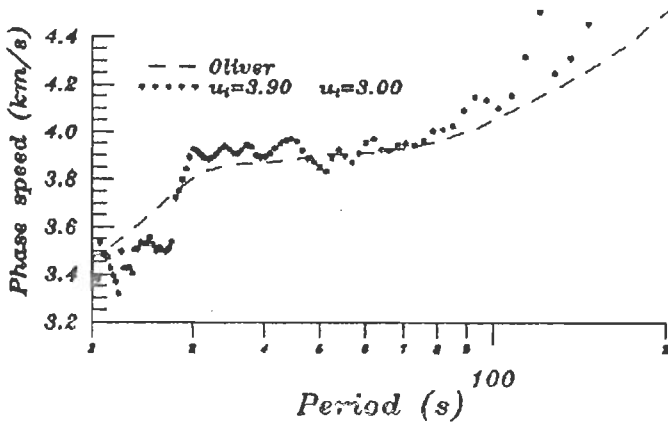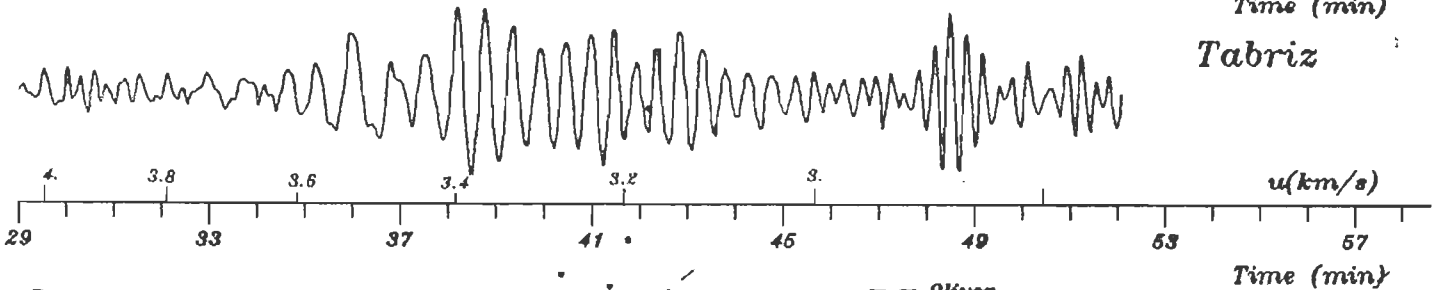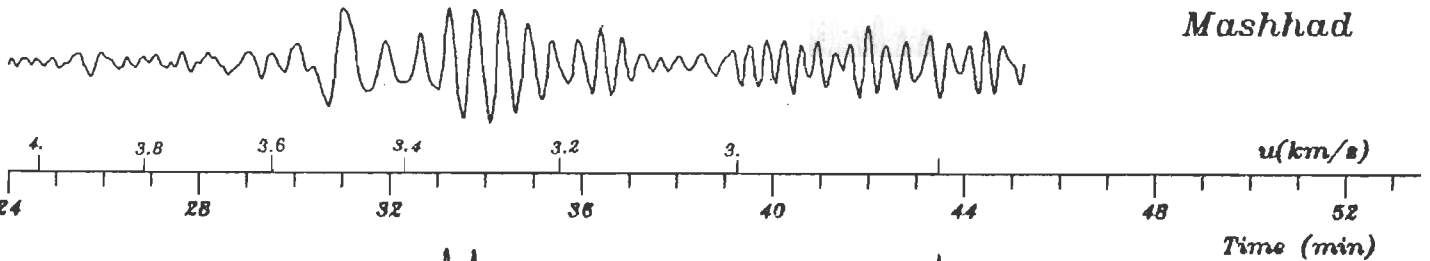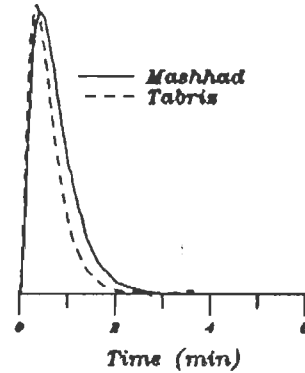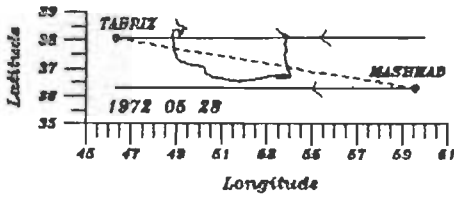
FIG. 5.23 A PHASE SPEED DETERMINATION FOR THE ALBORZ REGION. THIS FIGURE IS SIMILAR TO FIG 5.1 IN THE METHOD OF PRESENTATION OF DATA.

Hypocentral Data

Date	Orig. Time	Epicenter	Location	mb	Depth
1973 05 31	23 39 57.	24.48N 93.55E	Bangladesh	5.9	30

Ep. distanc	
Mashhad	Tabriz
3502	4691

Azimuth to:	
Mashhad	Tabriz
306.13°	308.41°

Mashhad

Tabriz
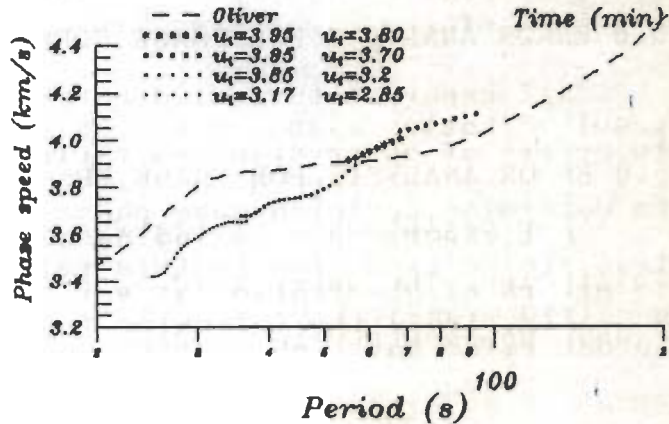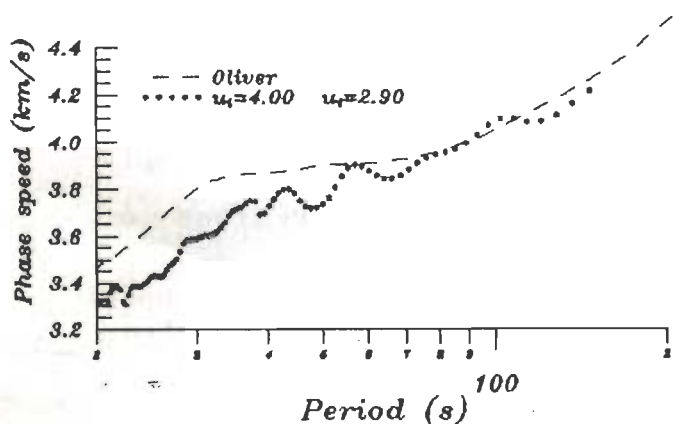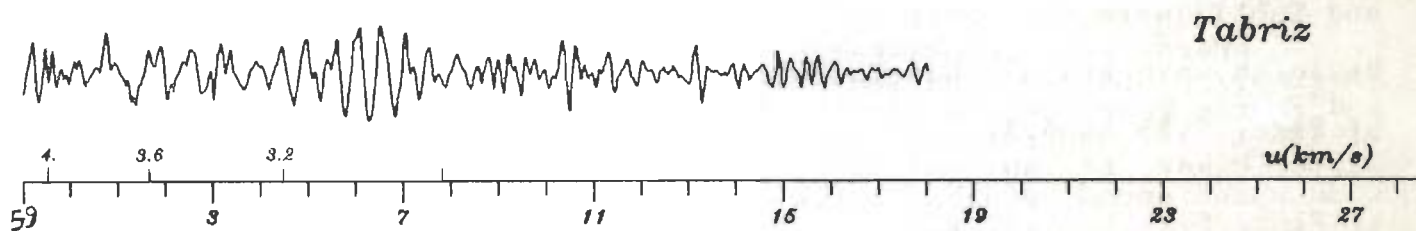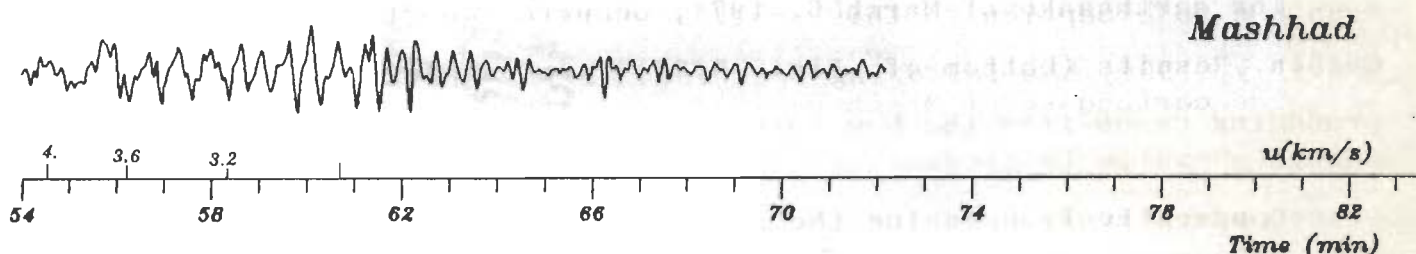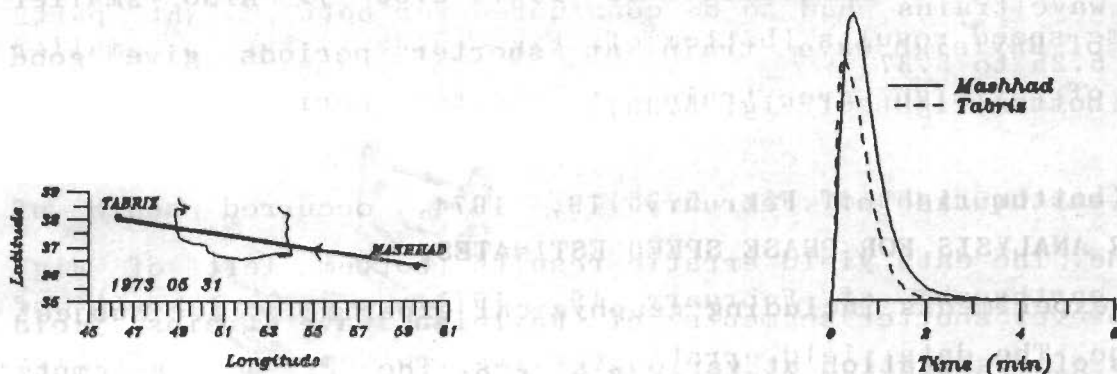
FIG. 5.34 A PHASE SPEED DETERMINATION FOR THE ALBORZ REGION. THIS FIGURE IS SIMILAR TO FIG 5.1 IN THE METHOD OF PRESENTATION OF DATA.

163

The earthquake of December 29, 1973, occurred south of Solomon Islands. Although the reported focal depth is only 47 km, inversely dispersed long period Rayleigh waves in the period range of 100 to 180 seconds are seen on the seismograms and they yield good phase speed results (bottom of Fig. 5.35). Also smaller segments of Rayleigh wave train at shorter periods give good results (bottom right of Fig. 5.35).

The earthquake of February 19, 1974, occurred south of Philippine. The data yield erratic results (bottom left of Fig. 5.36). However shorter segments of Rayleigh wave trains yield smoother results (bottom right of Fig. 5.36).

The earthquake of March 6, 1974, occurred northwest of New Guinea. Results (bottom of Fig. 5.37) are analogous to other preceding cases from the New Guinea region.

Comparatively speaking the seismograms recorded at Mashhad and Tabriz were the noisiest. Hence many smaller segments of Rayleigh wave trains had to be considered for bottom right parts of Figs. 5.25 to 5.37.

5.6 ERROR ANALYSIS FOR PHASE SPEED ESTIMATES

All experiments including geophysical experiments are subject to errors of observation at various stages. The present attempts to determine Rayleigh wave phase speed for the three regions of Iran are no exception to this roll. We obtain (as was also done by McEvilly, 1964) the following fractional error relationship from

Hypocentral Data

Date	Orig. Time	Epicenter	Location	mb	Depth
1973 12 29	00 19 31.	15.12S 166.90E	S Solomon Island	6.2	47

Ep. distanc	
Mashhad	Tabriz
12532	13698

Azimuth to:	
Mashhad	Tabriz
303.50°	305.91°
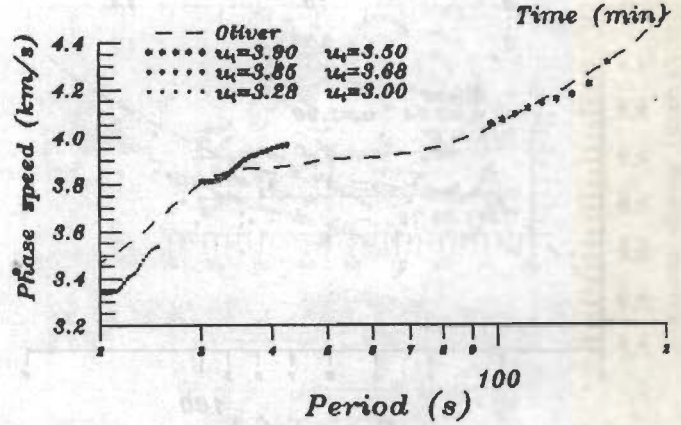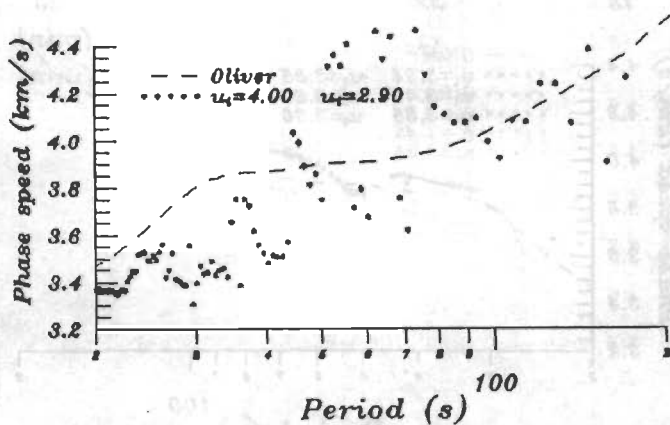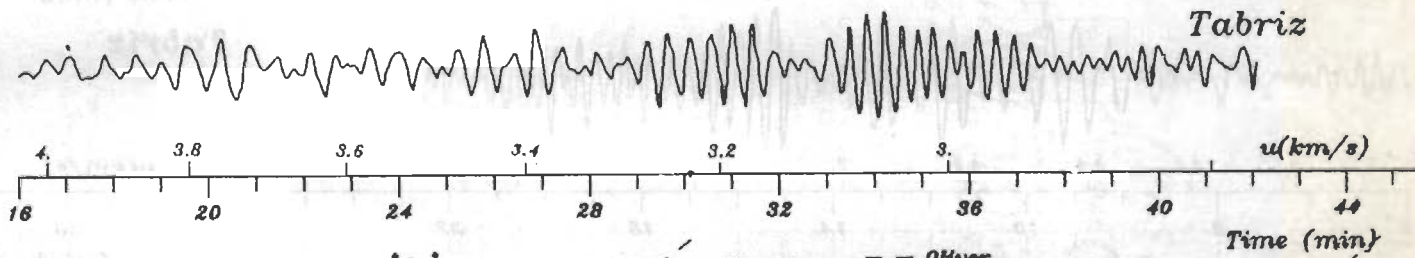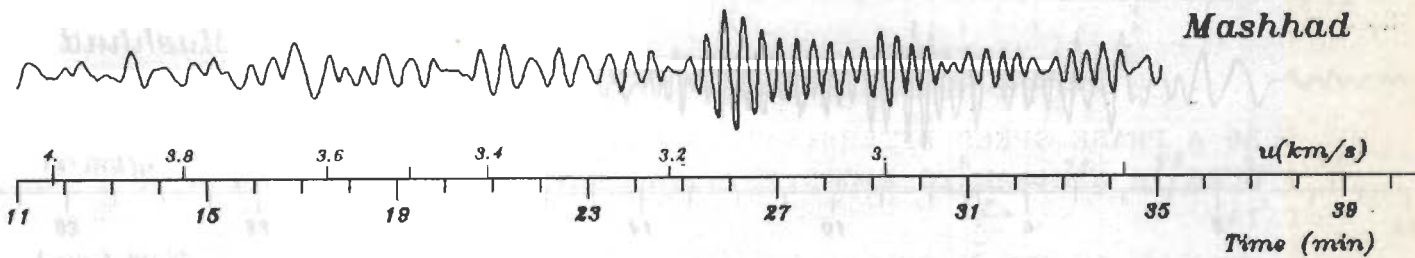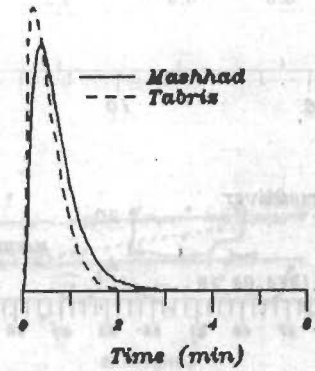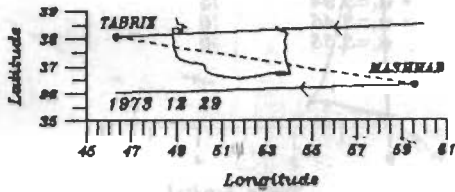
FIG. 5.35 A PHASE SPEED DETERMINATION FOR THE ALBORZ REGION. THIS
FIGURE IS SIMILAR TO FIG 5.1 IN THE METHOD OF PRESENTATION OF
DATA.

165

Date	Orig. Time	Epicenter	Location	mb	Depth
1974 02 19	03 30 22.	13.91N 122.12E	S Philippine	5.7	17

Ep. distance	
Mashhad	Tabriz
6649	7829

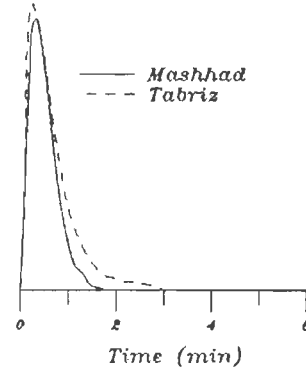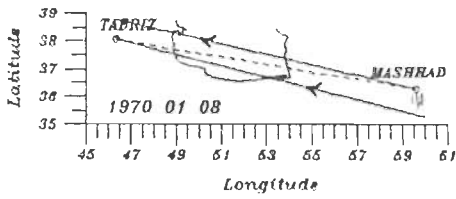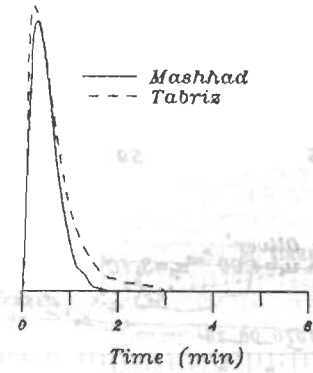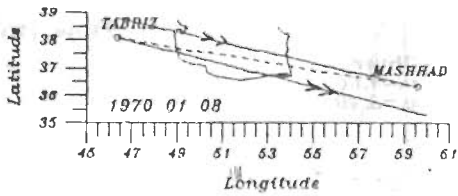| Azimuth to:	
Mashhad	Tabriz
304.18°	305.88°

Mashhad

Tabriz
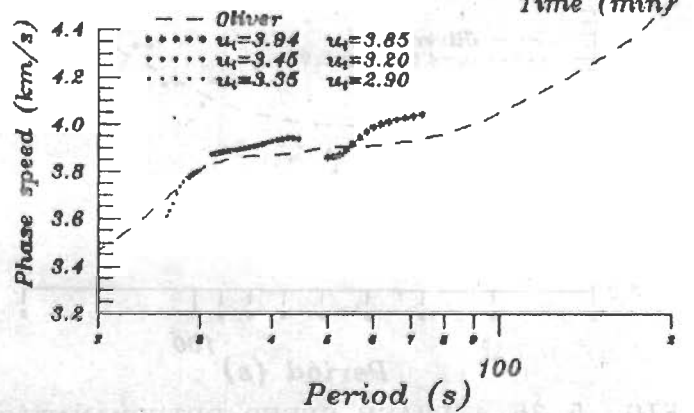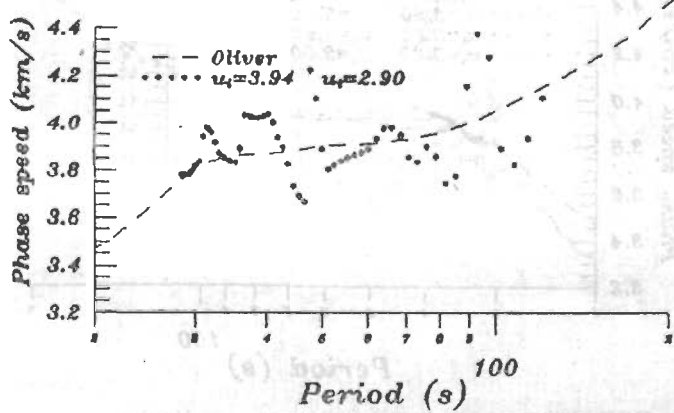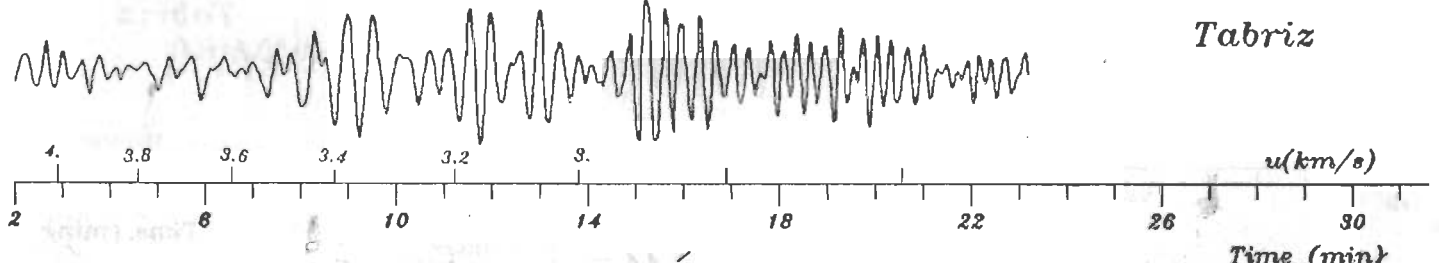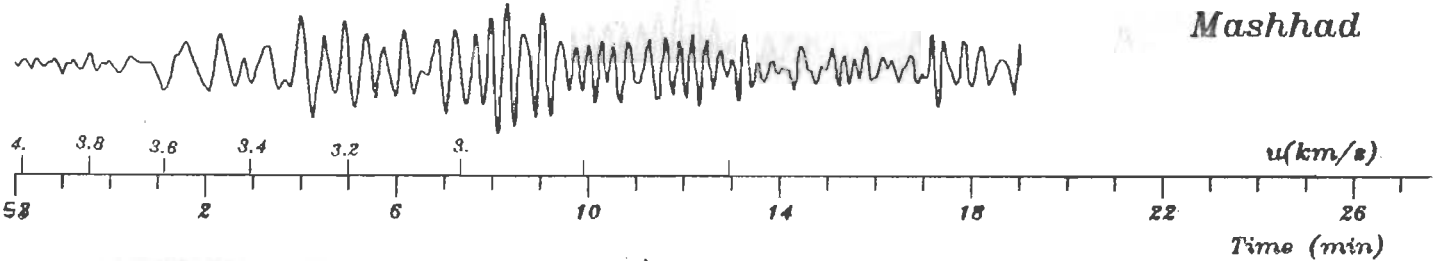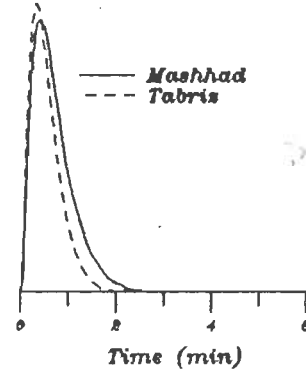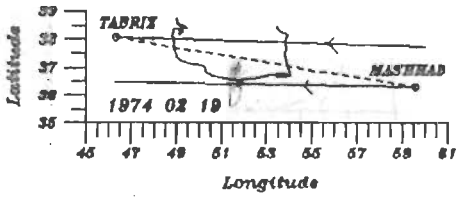
FIG. 5.36 A PHASE SPEED DETERMINATION FOR THE ALBORZ REGION. THIS
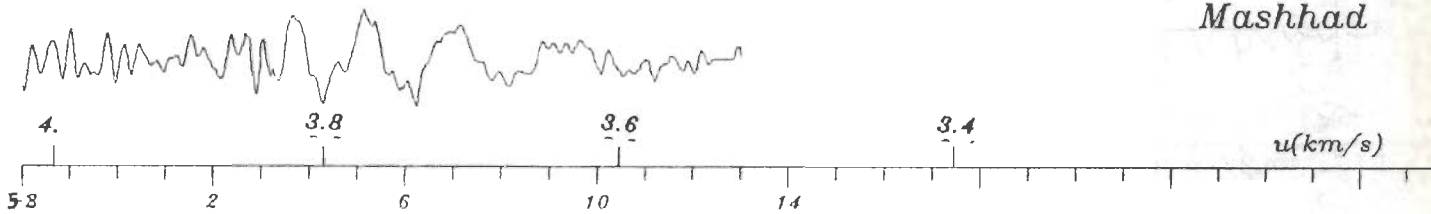FIGURE IS SIMILAR TO FIG 5.1 IN THE METHOD OF PRESENTATION OF
DATA.

Hypocentral Data

Date	Orig. Time	Epicenter	Location	mb	Depth
1974 03 06	19 29 08.	6.6 S 128.98E	New Guinea	5.7	26

Ep. distanc	
Mashhad	Tabriz
8636	9822

Azimuth to:	
Mashhad	Tabriz
309.46°	308.63°
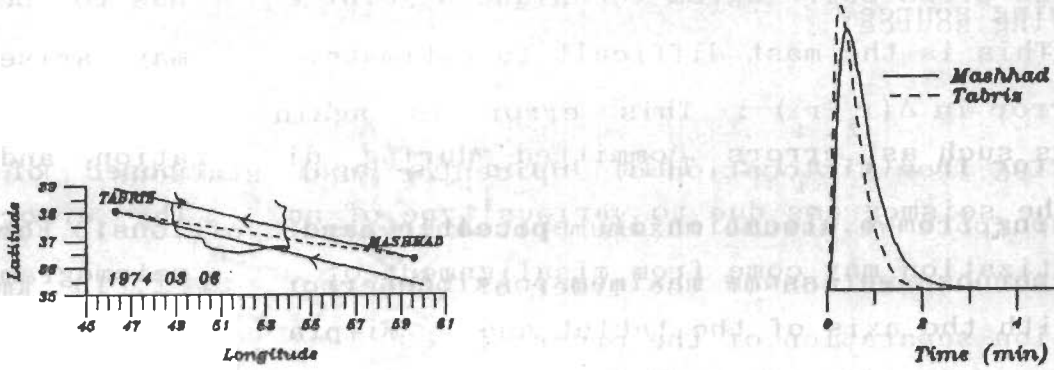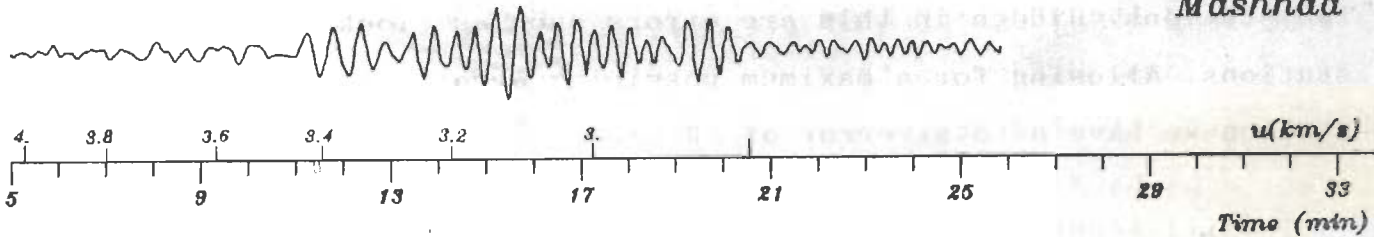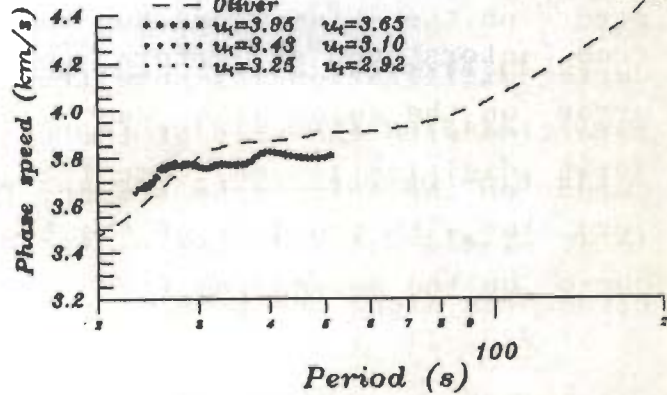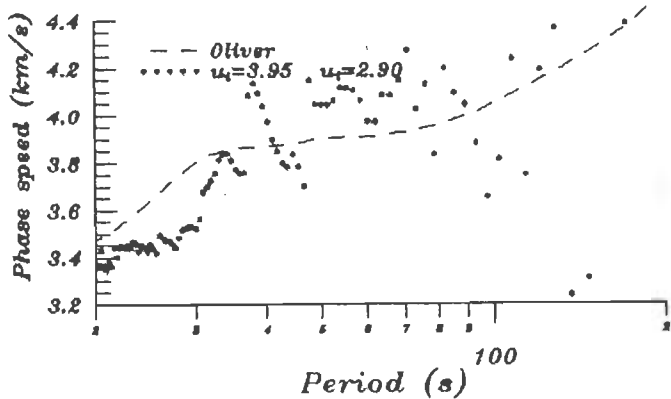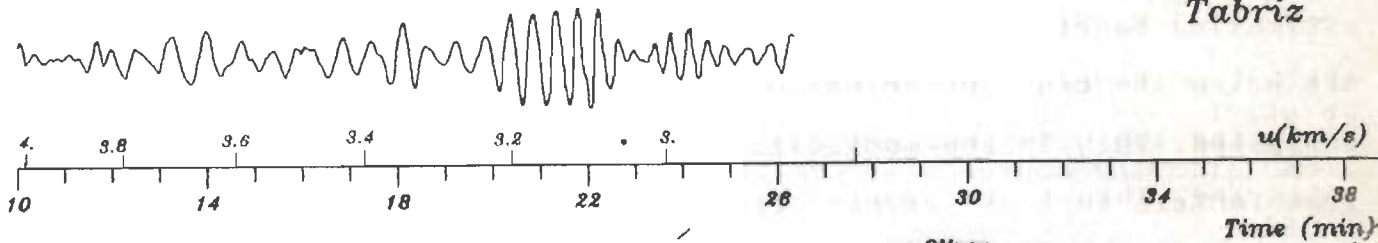
FIG. 5.37 A PHASE SPEED DETERMINATION FOR THE ALBORZ REGION. THIS
FIGURE IS SIMILAR TO FIG 5.1 IN THE METHOD OF PRESENTATION OF
DATA.

167

Eq. 2.12.

$$\frac{\Delta c}{c} = \frac{\Delta(r_2 - r_1)}{r_2 - r_1} + \frac{\Delta(t_2 - t_1)}{t_2 - t_1} + \frac{cT\Delta(\phi_2 - \phi_1)}{2\pi(r_2 - r_1)}$$

In other words the error in the estimated phase speed can come from following source.

(i) **Error in** $\Delta(r_2 - r_1)$: This error is again composed of errors arising from mislocation of epicenter and stations. For estimation purpose we assume maximum possible error of $\pm$ 10 km over a station separation of the order of 1000 km.

(ii) **Error in** $\Delta(t_2 - t_1)$: This errors refer to errors in estimating the starting time for digitization of seismograms at two stations. Hidden in this are errors such as clock error at the stations. Allowing for a maximum possible error ± 1 s for each station we have a total error of ± 2 seconds.

(iii) **Error in** $\Delta(\phi_2 - \phi_1)$: This error refers to errors in estimating Fourier phases at the two stations. However since we are using the cross correlogram technique a joint error has to be estimated. This is the most difficult to estimate. It may arise from factors such as errors committed during digitization and errors on the seismograms due to various type of noise. The error during digitization may come from misalignment of the seismogram zero line with the axis of the tablet and misplacement of the cursor on the seismogram tracer. The seismogram noise may include local random noise during recording and noise due to geological structures along the path of propagation which causes departures

of the actual wave paths from great circle paths assumed in the theory (see Discussion, Section 7.4). It is our estimate based on limited calculations specifically for the purpose that the period dependant phase error have should be less than 0.15 radians in all cases.

As a result the total error in phase speed, although period dependent, should be in the range of ±0.12 km/s or less. Fig. 5.38 displays phase speed curve of Fig 5.1 with error bars. Such bars are not shown in all the other case for the following reasons.

We have used the data plotted in Figs. 5.3, 5.14, and 5.24 for propose of inversion. The scatter in data for each period is greater than the estimated ±0.12 km/s error individual c(T) values. Finally for the accepted models the theoretical dispersion curve lies well within the scatter of these observations.
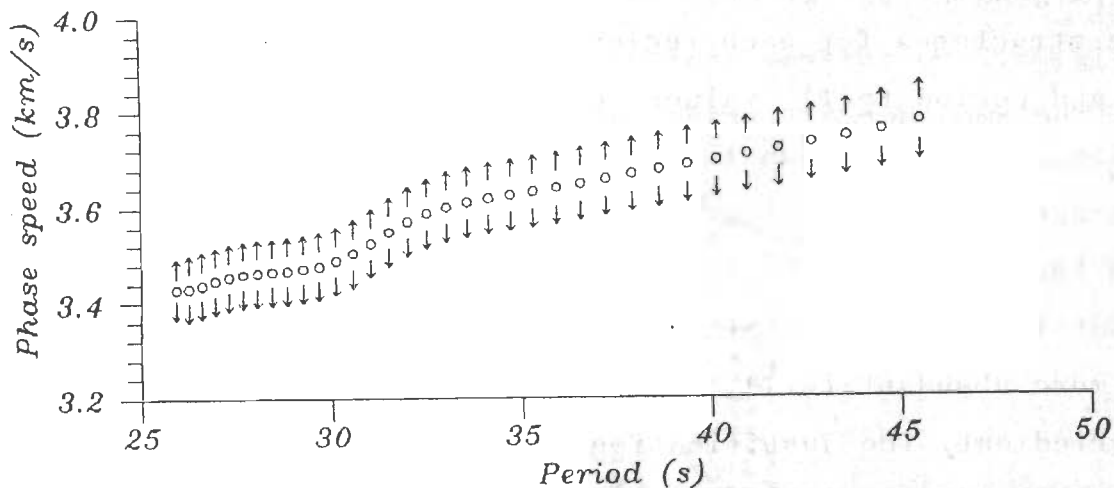
FIG. 5.38 PHASE SPEED RESULTS FOR THE ZAGROS PATH OBTAINED FROM ANALYSIS OF THE EARTHQUAKE OF AUG. 11, 1971, SHOWN WITH ERROR BARS.

5.7 SUMMARY

Fig. 5.39 is a display in which the average phase speed curves for the Zagros, Central Iran and Alborz regions are compared with the curve of Oliver (1962). The Iranian curves represent averages shown in Figs. 5.3, 5.14 and 5.24. For Rayleigh waves of periods less than about 50 to 60 seconds there is a definite gradation. The curve for the Alborz region is the closest to the average continental curve of Oliver (1962) while that for the Zagros region departs most from Oliver's the curve.

The three average curves for the different Iranian regions are significantly different from each other so that it is worthwhile to interpret them separately for the crust and upper mantle structures.

We like to point out also that the inversion for crust and upper mantle structures for each region is based on the actual phase speed and period (c,T) values obtained from analyses of recorded seismograms and shown in Fig. 5.3, 5.14, and 5.24 and not for the average curves (solid lines) in these figures. The inversion is the subject of the next chapter. It is important to note also that inversion of limited data shown in these figures and not the more abundant (c,T) data of Figs. 5.2, 5.13 and 5.23 is being carried out. The justification for this may be given by considering a specific region, say, the Zagros region and Figs. 5.2 and 5.3 related to it. Firstly the scatter in observations plotted in Fig. 5.2 comes from noise of various types on the seismograms. The smoother c-T graphs of Fig. 5.3 show that the

170
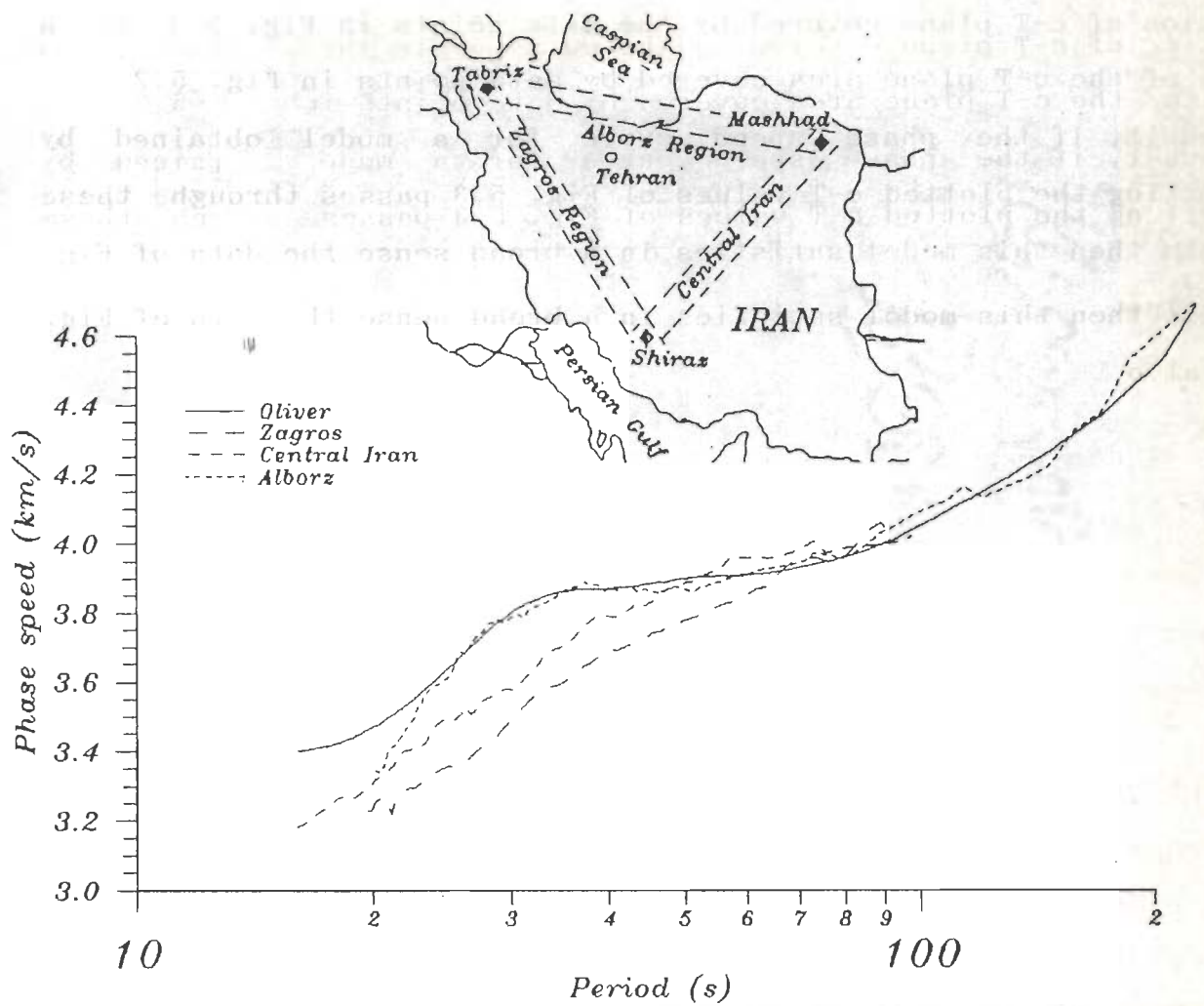
FIG. 5.39 INTERCOMPARISON OF AVERAGE PHASE SPEED CURVES FOR RAYLEIGH WAVES ALONG THE ZAGROS, CENTRAL IRAN, AND ALBORZ PATHS. A SMALL MAP IS INCLUDED FOR CONVENIENCE.

effect of noise is considerably controlled by using smaller
segments of Rayleigh wave trains. Secondly we find that the
portion of c-T plane covered by the data points in Fig. 5.3 is a
part of the c-T plane area covered by data points in Fig. 5.2. As
a result, if the phase speed curve for a model obtained by
inverting the plotted c-T values of Fig. 5.3 passes through these
points then this model satisfies in a broad sense the data of Fig.
5.2 also.

CHAPTER-6
INVERSION :
INTERPRETATION OF THE RAYLEIGH WAVE PHASE SPEED RESULTS
IN TERMS OF CRUST AND UPPER MANTLE STRUCTURES

6.1 INTRODUCTION

In this chapter we report on the results of our efforts to determine crust and upper mantle structures consistent with the observations of Rayleigh wave phase speed dispersion curves for the Zagros, Central Iran and Alborz regions.

It is well known (Ewing et al., 1957, McEvilly 1964, and our computations) that Rayleigh wave phase speeds are most sensitive to $\beta(z)$, the variation of shear wave speed with depth z in the earth along the path of their propagation. Therefore we also invert the observations of Rayleigh wave phase speeds for $\beta(z)$ primarily.

6.2 DATA INTERPRETED

During the process of inversion of observations for a given region, we used the totality of individual (c,T) points plotted in bottom right of figures for all eligible earthquakes of that region. In other words for example for the Zagros region we used all the data plotted in Figs. 5.3 which in turn is a collection

173

of data plotted at bottom right of Figs 5.4 to 5.12. Similarly for the central Iran and Alborz regions we used the data plotted in Figs. 5.14 and 5.24.

The period range of Rayleigh waves selected for inversion was from about 20 seconds up to 70 seconds as our data are most abundant in this range. A study of average dispersion curves of Oliver (1962) indicates that Rayleigh waves in this period range are sensitive to crustal structure. Therefore most of the following results refer to $\beta(z)$ in the crust, the half space of the layered models corresponding to the upper mantle.

However for the Alborz region we had inversely dispersed Rayleigh waves recorded for three earthquakes. The period range covered was from 70 to 210 seconds. We used these observations to investigate the upper mantle structure also in that region.

Number of models considered

For each of the three paths in Iran we considered 60 to 70 models at least. The number of crustal layers considered in these models varied between 1 and 18. The attempt in all cases was to construct models with similar number of layers for each of the three regions so that systematic differences between regions may be examined.

Non-Uniqueness of modelling

The general impression from the results of inversion for crustal structure along the three paths is that of pervasive non-ununiqueness. Models with reasonably different $\beta(z)$ can

explain the observations with similar root mean square (RMS) errors (Eq. 2.40).

$$\text{RMS error} = \left[\frac{1}{N} \sum_{i=1}^{N} (c_i^{obs} - c_i^{th})^2 \right]^{1/2} \qquad ...(2.40)$$

Still for the sake of an objective choice from amongst models, we use the following two criteria. Firstly the RMS error for the model should be minimum. Secondly we looked for a model which would give the smallest value of the maximum difference between any of the observations and the theoretical phase speed curve for that model.

6.3 INVERSION FOR ONE LAYERED CRUST ON UNIFORM MANTLE

In order to get the first feel of crust and upper mantle $\beta(z)$ profiles in the three regions of Iran under investigation we consider a simple one layer over a half space model. The layer represents the average crust and half space the average upper mantle. Thus, even though the inversion program has various options regarding parameters to be inverted for, we opted in this case to determine β's in crustal layer and upper mantle and thickness of the crustal layer.

The inversion program requires a starting model and the model shown in Table 6.1 was used. The results of inversion are displayed in Tables 6.2 to 6.4 for the Zagros, Central Iran and Alborz respectively. The inversion yielded average β's in the crusts for three regions in the narrow range of 3.42 to 3.47 km/s

175

and for the upper mantle in the narrow range of 4.36 to 4.51 km/s. The crustal thicknesses however varied significantly having values of 45.2, 39.5 and 35.1 km for the Zagros, Central Iran and Alborz respectively. The tables also give (i) RMS errors, and (ii) maximum difference (MD) between c^{obs}(T) observations and the corresponding theoretical dispersion curves at priod T and (iii) number of iterations necessary to obtain the inveryed model.

In a second series of experiments we changed the α in the mantle in steps of 0.1 km/s from 7.9 to 8.3. Tables 6.5 to 6.7 summarize the α's and β's in the crustal layer and half space. On the bases of the above two criteria it appears that α in the mantle (starred values in Tables 6.5 to 6.7) increases systematically with values of 8.1, 8.2 and 8.3 km/s for Zagros, Central Iran, and Alborz respectively. The corresponding shear wave speed models are displayed graphicaly in Fig. 6.1.
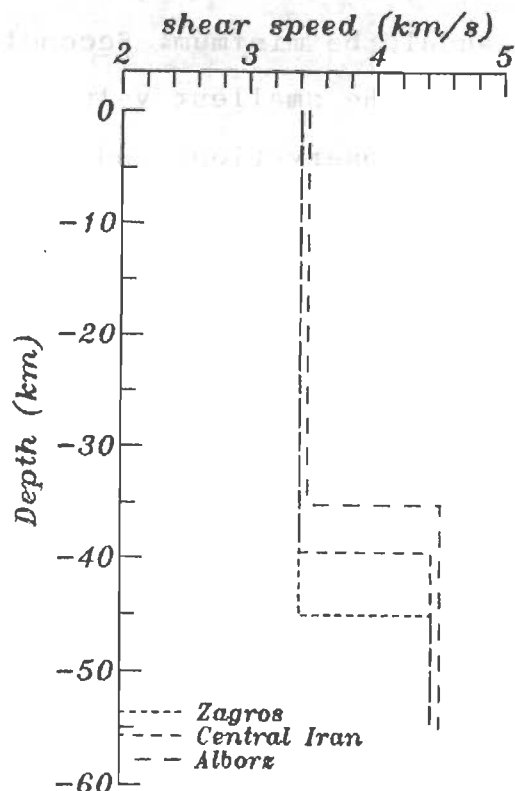
FIG. 6.1 SHEAR WAVE SPEEDS IN THE CRUSTAL LAYER AND HALF SPACE CORRESPONDING TO STARRED LINES IN TABLES 6.5 TO 6.7.

Fig. 6.2 is a composite display in which the observed data points for the Zagros, Central Iran, and Alborz regions and the

computed phase speed dispersion curves for the starred models
shown in Tables 6.5 to 6.7 are compared.

We turn to more detailed modelling in the following
paragraphs.

TABLE 6.1 STARTING MODEL FOR ONE LAYERED CRUST (see Section 6.3)

Layer No.	Thickness km	α (km/s)	β (km/s)	ρ (g/cm^3)
1	70.0	6.3	3.5	2.8
H.S.	—	8.3	3.3	3.3

TABLE 6.2 INVERTED MODEL FOR ONE LAYERED CRUST UNDER ZAGROS REGION

Layer No.	Thickness km	α (km/s)	β (km/s)	ρ (g/cm^3)
1	45.1	6.3	3.41	2.8
H.S.	—	8.3	4.44	3.3
RMS-error=0.0532 No. of itration= 5 MD=0.131				

TABLE 6.3 INVERTED MODEL FOR ONE LAYERED CRUST UNDER CENTRAL IRAN
REGION.

Layer No.	Thickness km	α (km/s)	β (km/s)	ρ (g/cm^3)
1	39.53	6.3	3.42	2.8
H.S.	—	8.3	4.44	3.3
RMS-error=0.0400 No. of itration= 7 MD=0.104				

177

TABLE 6.4 INVERTED MODEL FOR ONE LAYERED CRUST UNDER ALBORZ REGION

Layer No.	Thickness km	α (km/s)	β (km/s)	ρ (g/cm^3)
1	35.15	6.3	3.47	2.8
H.S.	—	8.3	4.51	3.3
RMS-error=0.0776 No. of itration=43 MD=0.211				

TABLE 6.5 SUMMERY TABLE SHOWING INVERTED β FOR SINGLE CRUSTAL LAYER AND HALF SPACE FOR DIFFERENT α's IN THE HALF SPACE FOR ZAGROS REGION

α_2	Crastal thickness	β_1	β_2	RMS-error	Max.# Diff.
8.3	45.05	3.41	4.44	0.053226	0.131
8.2	45.12	"	4.38	0.042474	0.093
8.1*	45.20	"	4.36	0.040779	0.096
8.0	45.25	"	"	0.040804	0.096
7.9	34.32	"	"	0.040831	0.096

*, # See text under Section 6.3

TABLE 6.6 SUMMERY TABLE SHOWING INVERTED β FOR SINGLE CRUSTAL LAYER AND HALF SPACE FOR DIFFERENT α's IN THE HALF SPACE FOR CENTRAL IRAN REGION.

α_2	Crastal thickness	β_1	β_2	RMS-error	MD
8.3	39.53	3.41	4.44	0.039987	0.104
8.2*	39.56	"	4.41	0.037817	0.093
8.1	39.84	3.42	4.42	0.038135	0.104
8.0	39.67	"	4.41	0.037906	0.094
7.9	39.72	"	4.42	0.037955	0.094
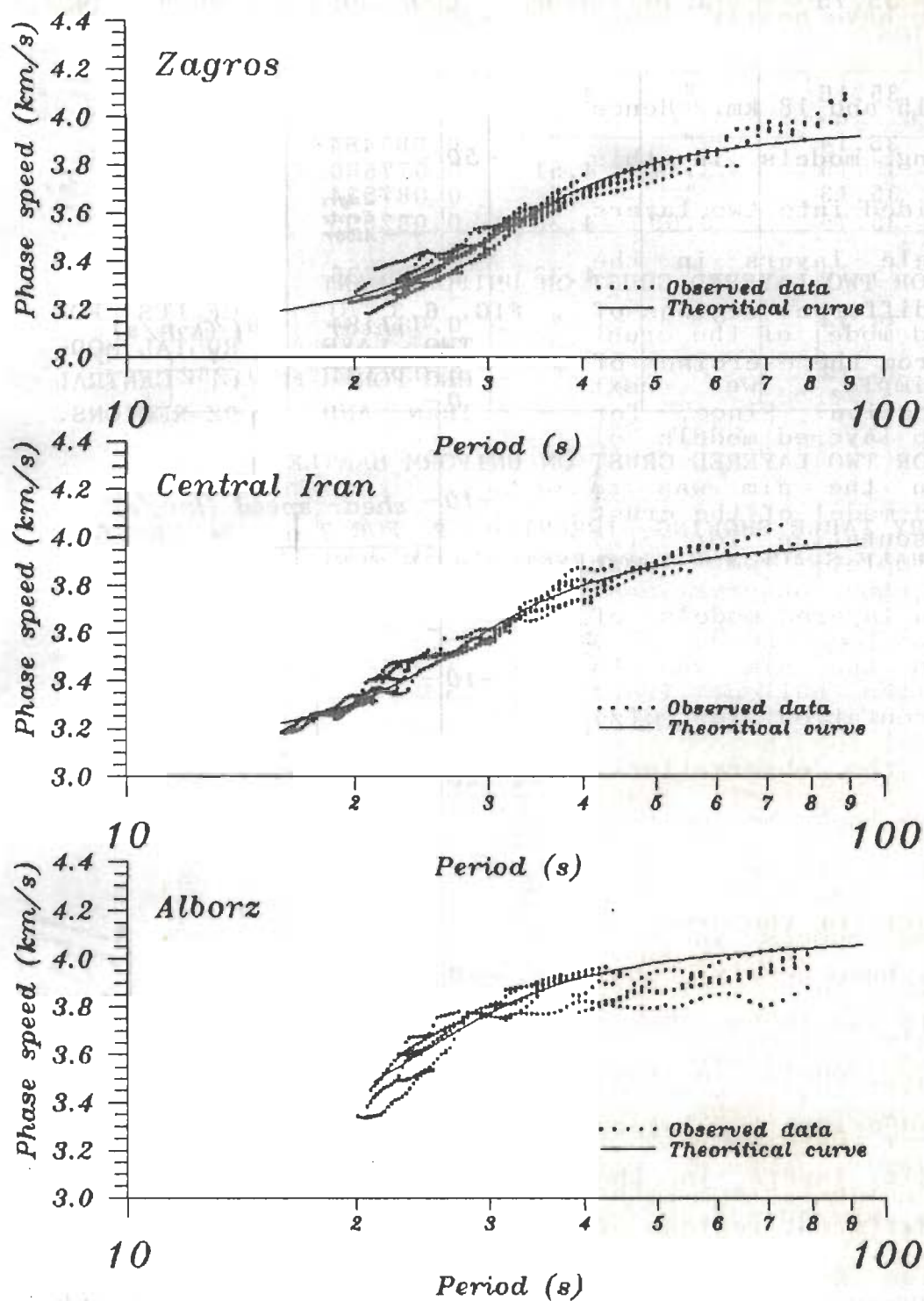
FIG. 6.2 COMPARISON OF OBSERVED   AND THE THEORETICAL PHASE SPEED
CURVES FOR THREE REGIONS OF IRAN FOR THE   STARRED   MODELS   OF
TABLES 6.5 TO 6.7

179

TABLE 6.7 SUMMERY TABLE SHOWING INVERTED β FOR SINGLE CRUSTAL LAYER AND HALF SPACE FOR DIFFERENT α's IN THE HALF SPACE FOR ALBORZ REGION.

α_2	Crastal thickness	β_1	β_2	RMS-error	MD
8.3[*]	35.15	3.47	4.51	0.077580	0.211
8.2	35.75	3.69	4.38	0.082695	0.257
8.1	35.16	"	4.33	0.086726	0.252
8.0	35.14	"	"	0.087484	0.251
7.9	35.13	"	"	0.087534	0.252

6.4 INVERSION FOR TWO LAYERED CRUST ON UNIFORM MANTLE

One layered model of the crust being too simple, we next investigated two layered models of the crust. Again the aim was to obtain a representation for $\beta(z)$ consistent with the observations. To start with we took the cue from the Jeffreys-Bullen (Bullen, 1963) two layered model for the crust in which the layers have nearly equal thicknesses of 15 and 18 km. Hence for the starting models in this exercise we divided into two layers each of the single layers in the models for the different regions of Iran obtained from the exercise of the preceding section. Since, for
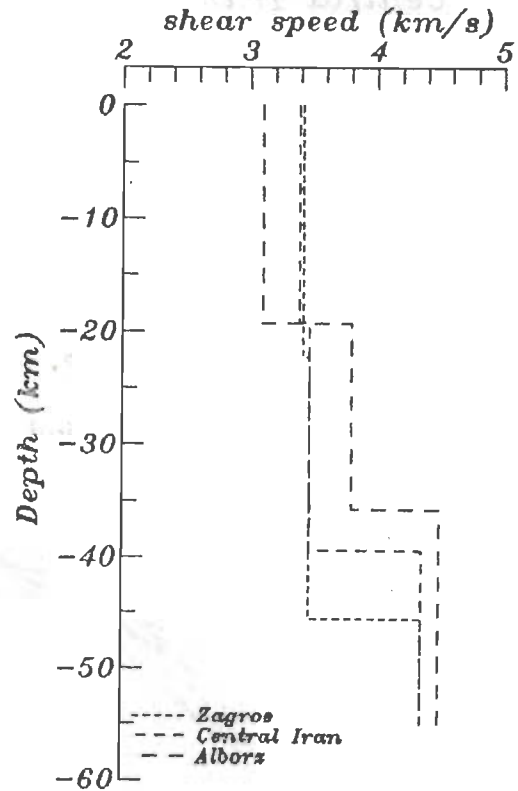
FIG. 6.3 $\beta(Z)$ PROFILES FOR TWO LAYERED CRUSTAL MODELS FOR ZAGROS, CENTRAL IRAN, AND ALBORZ REGIONS.

reasons discussed in Chap. 7 below, convergence was not obtained for every starting model using the inversion program and the available data, we had to adjust the starting models gradually. Fig. 6.3 is display of $\beta(z)$ profiles obtained for the three regions of Iran under investigation. Table 6.8 to 6.10 give the numerical values for the two crustal layers are threemodels.Theshearwavespeed seen to be nearly similar for the Zagros and Central Iran regions. The estimates of total crustal thicknesses differ negligibly by +0.3 km and -0.2 km respectively in comparison with those reported for the corresponding one layer models for Zagros and Central Iran regions. For the Alborz region although the crustal thickness for the two layered case is greater by .5 km than the single layer estimated, the shear wave speeds are significantly different. β_1 for Alborz region is lower by about 0.3 km/s than in the cases of Central Iran and Zagros. Similarly β_2 is higher by about 0.3 km/s. Finally estimated β for upper mantle is higher by about 0.1 km/s than the case of corresponding models for Central Iran and Zagros. Dispersion curves corresponding to these models are compared with the observations in Fig. 6.4.

TABLE 6.8 INVERTED TWO LAYERED CRUSTAL MODEL FOR ZAGROS REGION.

Layer No.	Thickness km	α (km/s)	β (km/s)	ρ (g/cm^3)
1	22.25	5.58	3.42	2.60
2	23.25	6.50	3.47	2.80
H.S.	——	8.10	4.35	3.30
RMS-error=0.0525 No. of itration=30 MD=0.113				

TABLE 6.9 INVERTED TWO LAYERED CRUSTAL MODEL FOR CENTRAL IRAN REGION.

Layer No.	Thickness km	α (km/s)	β (km/s)	ρ (g/cm^3)
1	19.16	5.58	3.39	2.60
2	20.17	6.50	3.47	2.80
H.S.	——	8.20	4.39	3.30
RMS-error=0.0436 No. of itration=30 MD=0.099				

TABLE 6.10 INVERTED TWO LAYERED CRUSTAL MODEL FOR ALBORZ REGION.

Layer No.	Thickness km	α (km/s)	β (km/s)	ρ (g/cm^3)
1	19.25	5.58	3.10	2.60
2	16.44	6.50	3.80	2.80
H.S.	——	8.30	4.49	3.30
RMS-error=0.0698 No. of itration=25 MD=0.193				
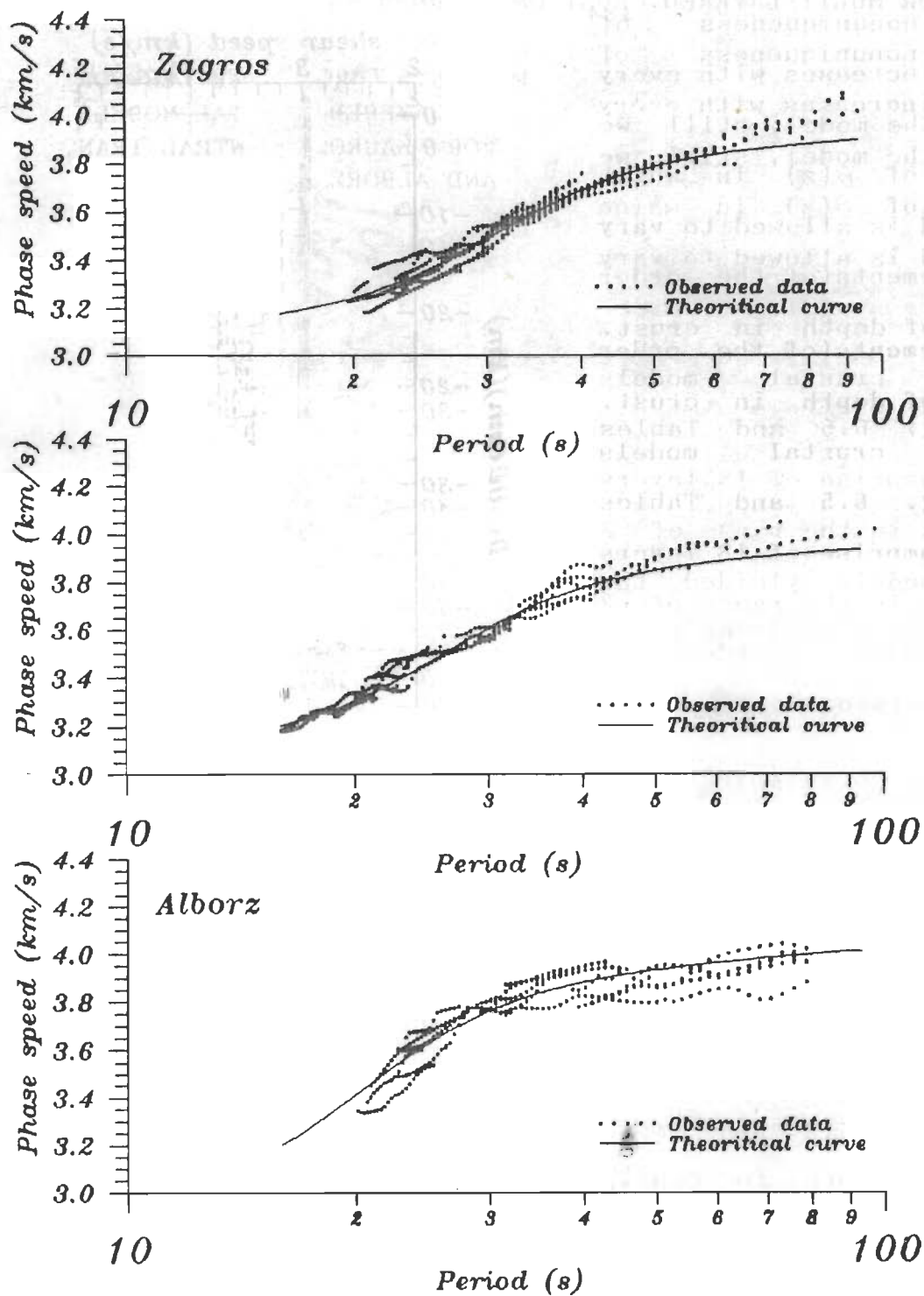
FIG. 6.4 COMPARISON OF OBSERVED AND THEORETICAL PHASE SPEED CURVES FOR THREE REGIONS OF IRAN FOR TWO LAYERED CRUSTAL MODELS OF TABLES 6.8 TO 6.10.

183

6.5 INVERSION FOR MULTI-LAYERED CRUST ON UNIFORM MANTLE

Although nonuniqueness of interpretation increases with every layer added to the model, still we sought images of $\hat{\beta}(z)$ in which shear wave speed is allowed to vary with small increments(of the order of 2 to 3 km) of depth in crust. Each of the crustal models displayed in Fig. 6.5 and Tables 6.11 to 6.13, comprise of 18 layers with thicknesses in the range of 2 to 3 km. These models yielded the phase speed dispersion curves shown in Fig. 6.6.
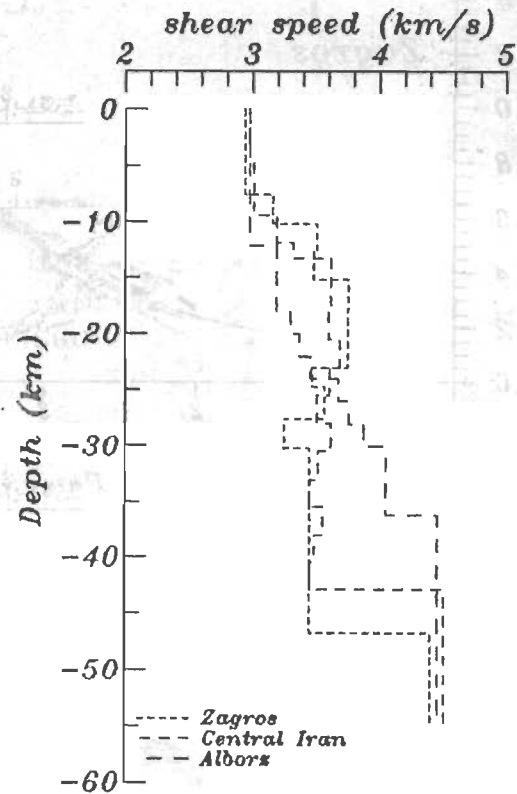
FIG. 6.5 $\hat{\beta}(Z)$ PROFILES FOR 18 LAYERED CRUSTAL MODELS FOR ZAGROS, CENTRAL IRAN, AND ALBORZ REGIONS.

TABLE 6.11 INVERTED DATA FOR A 18 LAYERED MODEL OF CRUST IN THE ZAGROS REGION.

Layer No.	α (km/s)	ρ (g/cm^3)	β (km/s)	Thickness (km)
1				
2			2.94	7.57
3	5.8			
4			3.16	2.54
5		2.7	3.51	2.55
6			3.48	2.56
7			3.76	2.67
8				
9	6.2		3.75	5.29
10			3.74	2.75
11			3.57	2.76
12			3.25	2.72
13				
14		2.8		
15				
16	6.7		3.45	16.46
17				
18				
H.S.	8.1	3.3	4.4	————

The inversion was for 18 layers. However in the display the layers with common value of parameter in a given column are grouped together for more vivid display of results.

The process of arriving at such detailed crustal models was a gradual and iterative one. We started, for each of these Iranian regions, with a three layered model. The option available in our inversion program whereby both β and h can be varied simultaneously was utilized. During these intermediate stages of inversion the program yielded some layers with thicknesses of less than 1 km. In subsequent iteration such layers were excluded from
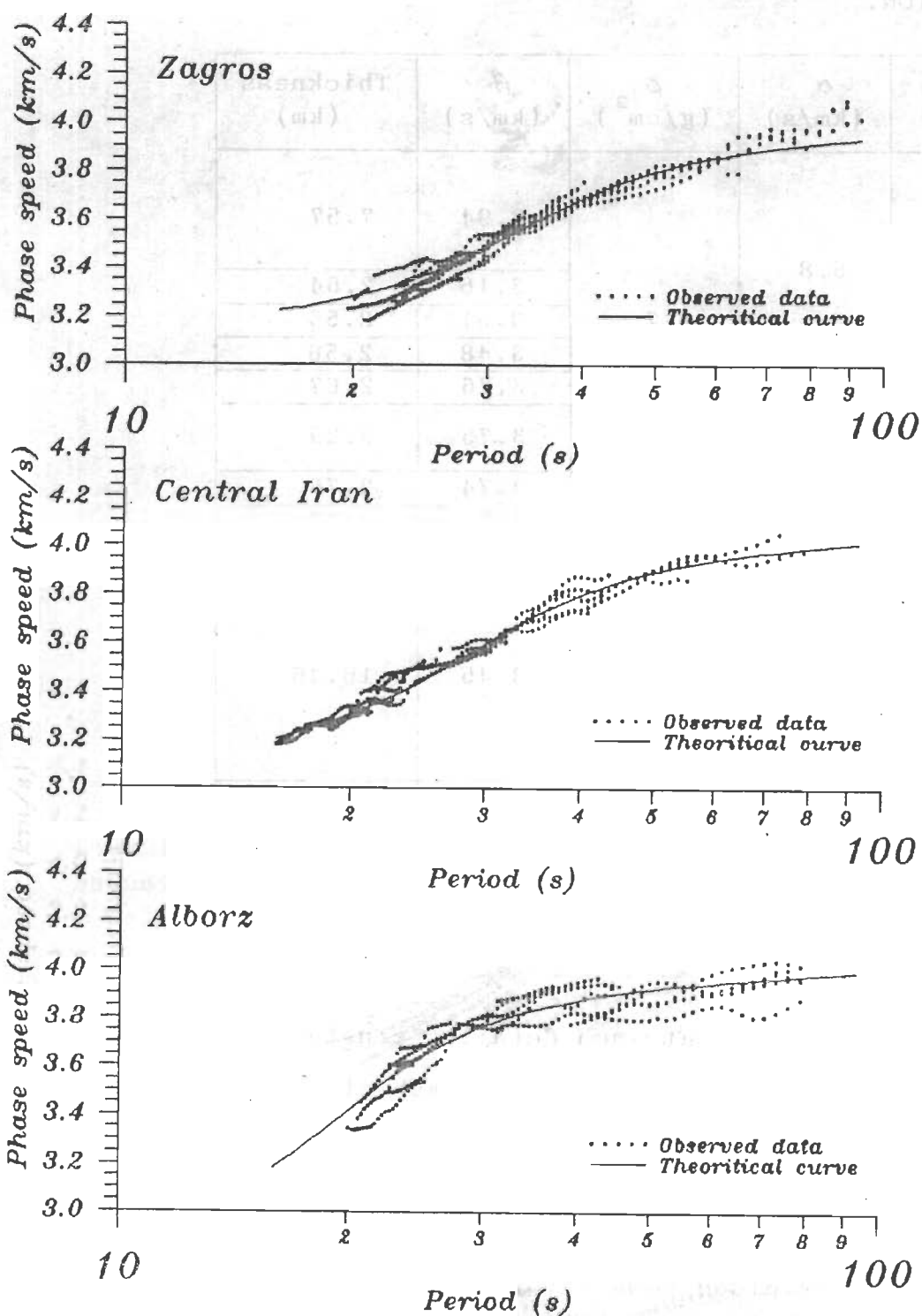
FIG. 6.6 COMPARISON OF OBSERVED AND THEORETICAL PHASE SPEED
CURVES FOR THREE REGION OF IRAN FOR 18 LAYERED CRUSTAL MODELS
OF TABLES 6.11 TO 6.13.

consideration. Also the thicknesses of some layers turned out to be relatively large. These layers were subdivided in thinner layers. An important feature of the results shown in Fig. 6.5 is that the total crustal thicknesses estimated for each of the three regions is still comparable to the estimates of thicknesses obtained with one and two layered crustal models Table 6.14. Even the broad trend in the variation of β with z in Zagros, Central Iran and Alborz regions is similar in one, two and multi-layered inversions (Figs. 6.1, 6.3 and 6.5).

The total number of converged model considered for each of the three regions were in the range of 50 to 70. 16, 16, and 23 of these models for Zagros, Central Iran, and Alborz regions respectively had total crustal thicknesses and shear wave speeds in the half space comparable to those for the one and two layered crustal models. We then used the two criteria listed under non-uniqueness of modelling in Section 6.2 to guide in to picking the three models shown in Tables 6.11 to 6.13.

TABLE 6.12 INVERTED DATA FOR A 18 LAYERED MODEL OF CRUST IN THE CENTRAL IRAN REGION.

Layer No.	α (km/s)	ρ (g/cm^3)	β (km/s)	Thickness (km)
1			2.98	4.71
2			2.98	4.71
3	5.8		3.01	4.72
4			3.01	4.72
5		2.7	3.19	2.37
6			3.32	2.38
7			3.62	4.87
8			3.62	4.87
9	6.2		3.60	2.44
10			3.69	2.49
11			3.61	2.49
12			3.51	2.49
13			3.62	2.50
14		2.9	3.52	2.50
15	6.7		3.45	2.50
16			3.56	2.49
17			3.49	2.49
18			3.45	2.49
H.S.	8.1	3.3	4.51	——

TABLE 6.13 INVERTED DATA FOR A 18 LAYERED MODEL OF CRUST IN THE ALBORZ REGION.

Layer No.	α (km/s)	ρ (g/cm^3)	β (km/s)	Thickness (km)
1				
2				
3	5.8		2.98	12.03
4				
5		2.7		
6				
7				
8			3.19	6.00
9	6.2			
10			3.30	1.99
11			3.37	1.99
12			3.46	1.99
13			3.68	2.01
14		2.9	3.76	2.01
15			3.88	2.01
16	6.7			
17			4.05	6.11
18				
H.S.	8.1	3.3	4.46	——

189

TABLE 6.14 COMPARISON OF TOTAL CRUSTAL THICKNESSES FOR 1, 2, AND 18 LAYERED MODELS FOR ZAGROS, CENTRAL IRAN, AND ALBORZ REGION.

Region	Thickness (km)		
	No. of layers		
	1	2	18
Zagros	45.2	45.5	47.5
Central Iran	39.6	39.3	43.9
Alborz	35.1	35.7	36.1

6.6 INVERSION FOR UPPER MANTLE STRUCTURE IN ALBORZ REGION

As mentioned earlier, Rayleigh waves of periods longer than 70 seconds were also clearly recorded at Mashhad and Tabriz for three earthquakes . In all three cases we could observe the longer period inversely dispersed waves under the shorter period normally dispersed waves coming directly from the epicenters (R1 type Rayleigh waves). In two cases we also observed the inversely dispersed longer period waves coming from the epicenters along the longer antipodal paths (R2 type Rayleigh waves).

The phase speed dispersion curves for these longer period waves were computed in the usual way. The analyses yielded phase speeds in the period range of 70 to 230 s.

Inversion of these long period phase speed data was carried out separately. The two crustal layers in these models were the same as obtained earlier using the shorter period Rayleigh waves.

The upper mantle was simulated with two additional layers between the crustal layers and the half space. After a number of trials it was found necessary to introduce a thin crustal layer of 2 km at the top. The inverted model (Table 6.15 and Fig. 6.7) for $\beta(z)$ indicated a low speed layer of 60 km with its top at a depth of 224 km. The theoretical phase speed dispersion curve is displayed in Fig. 6.8.

The important conclusion from this exercise is that the low speed layer for shear waves may exist at least in the Alborz region of northern Iran also. The lower value of α for this layer was introduced in the starting model and maintained runs of the inversion program for this exercise.
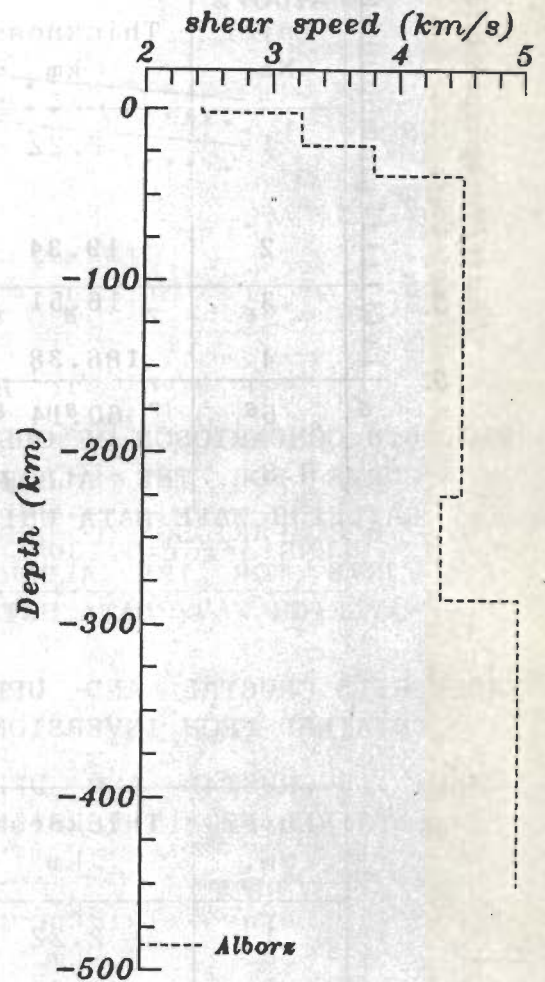
FIG. 6.7 GRAPHICAL DISPLAY OF $\beta(Z)$ FOR THE ALBORZ REGION BASED ON INVERSION OF MANTLE RAYLEIGH WAVE DATA.
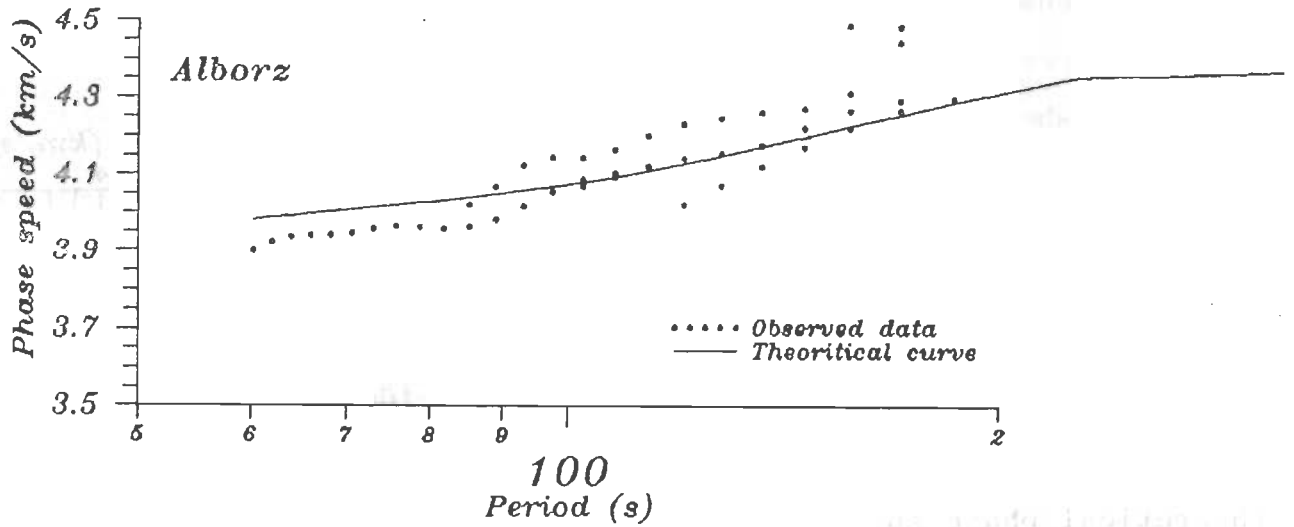
FIG. 6.8 COMPARIOSON OF OBSERVED AND THEORETICAL PHASE SPEED CURVE FOR THE ALBORZ REGION BASED ON INVERSION MANTLE RAYLEIGH WAVE DATA USING MODEL OF Table 6.15

TABLE 6.15 CRUSTAL AND UPPER MANTLE MODEL FOR ALBORZ REGION OBTAINED FROM INVERSION OF MANTLE RAYLEIGH WAVES.

Layer No.	Thickness km	α (km/s)	β (km/s)	ρ (g/cm^3)
1	2.22	4.50	2.447	2.30
2	19.34	5.80	3.229	2.60
3	16.51	6.50	3.802	2.80
4	186.38	8.30	4.514	3.34
5	60.14	8.00	4.351	3.35
H.S.	——	8.50	4.972	3.40

| RMS-error=0.1307 | No. of itration=29 | MD=0.374 |

6.7 JOINT INVERSION OF CRUSTAL AND MANTLE RAYLEIGH WAVE DATA FOR THE ALBORZ REGION.

In the last part of analysis for the Alborz region the mantle Rayleigh wave data (70 to 230 s) discussed in Section 6.6 was combined with the Rayleigh wave data in the period range of 20 to 70 s for this region used in the analyses of Section 6.2 to 6.5. The model shown in Table 6.16 and Fig. 6.9 was obtained. The thin low speed layer at the top of the crust, now has a thickness of 1.4 km instead of 2.2 km given in Table 6.15 for mantle Rayleigh wave data alone. The 60 km thick low speed layer survives in this model also. The phase speed dispersion curve for this model is displayed in Fig. 6.10.
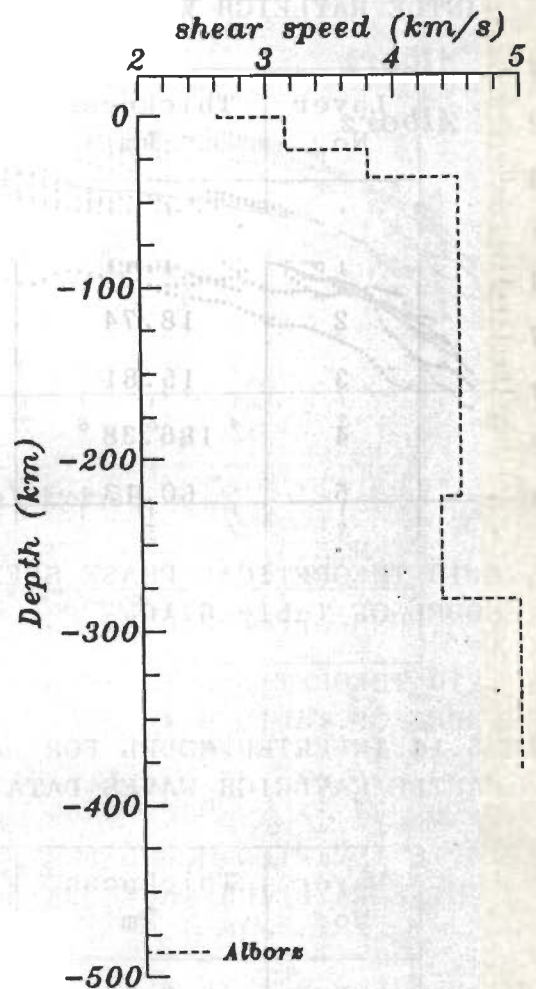
FIG. 6.9 GRAPHICAL DISPLAY OF $\beta(Z)$ FOR THE ALBORZ REGION BASED ON CRUSTAL AND MANTLE RAYLEIGH WAVE DATA

Phase speed (km/s) vs Period (s). Alborz.

Observed data ·····
Theoritical curve ——
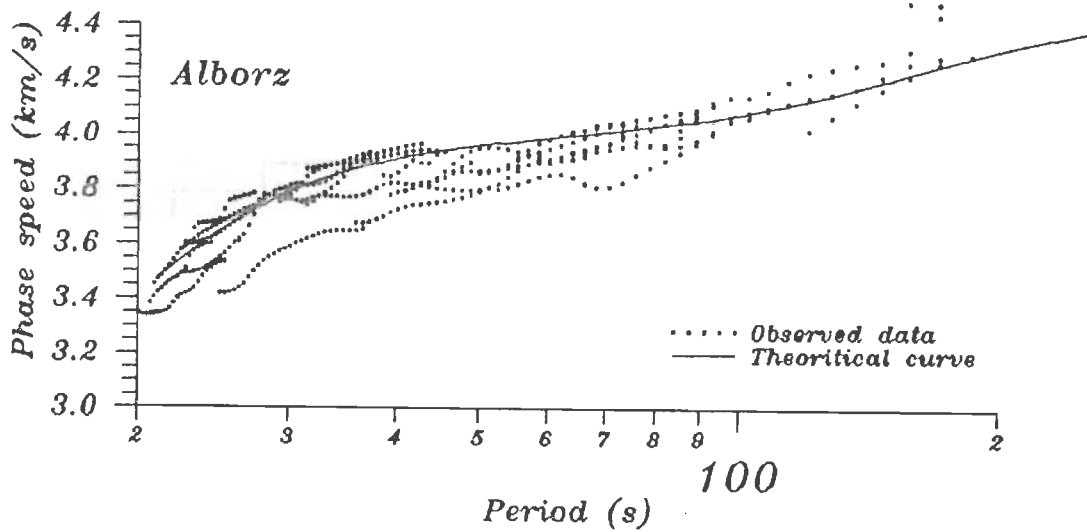
FIG. 6.10 THEORETICAL PHASE SPEEDDISPERSION CURVE CORRESPONDING TO
MODEL OF Table 6.16

TABLE 6.16 INVERTED MODEL FOR ALBORZ REGION USING CRUSTAL AND
MANTLE RAYLEIGH WAVES DATA.

Layer No.	Thickness km	α (km/s)	β (km/s)	ρ (g/cm^3)
1	1.41	4.50	2.63	2.30
2	18.74	5.80	3.15	2.60
3	15.81	6.50	3.80	2.80
4	186.38	8.30	4.51	3.34
5	60.13	8.00	4.35	3.35
H.S.	——	8.50	4.97	3.40

RMS-error=0.0797   No. of itration=14   MD=0.369

194

In a separate series of experiments using the mantle Rayleigh wave data of the preceding paragraph, we could obtain convergence in the inversion program with a model in which the top low speed and thin crustal layer was not required. However in these models the mantle low speed layer for shear waves is thicker and extends in the depth range of 165 to 290 km. The selected model is shown in Table 6.17 and Fig. 6.11. The non-uniqueness of inversion is emphasized again in this exercise.
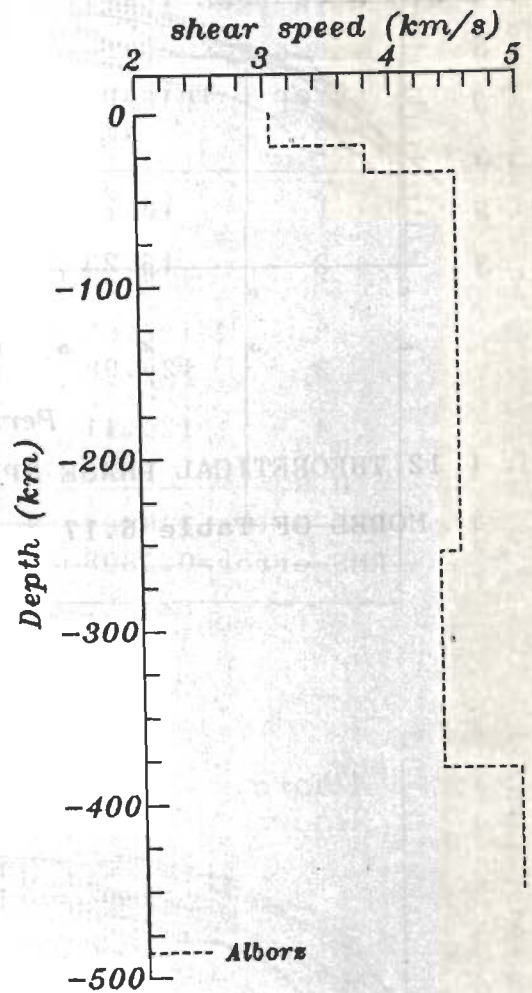
FIG. 6.11 DISPLAY OF $\beta(Z)$ FOR THE MODEL OF TABLE 6.17

TABLE 6.17 MODEL FOR ALBORZ REGION ALTERNATIVE TO THE MODEL OF Table 6.16 (SEE TEXT).

Layer No.	Thickness km	α (km/s)	β (km/s)	ρ (g/cm^3)
1	19.14	5.60	3.05	2.60
2	16.23	6.50	3.80	2.80
3	129.98	8.30	4.51	3.34
4	125.11	8.00	4.35	3.35
H.S.	——	8.50	4.97	3.40

RMS-error=0.0808   No. of itration=6   MD=0.401
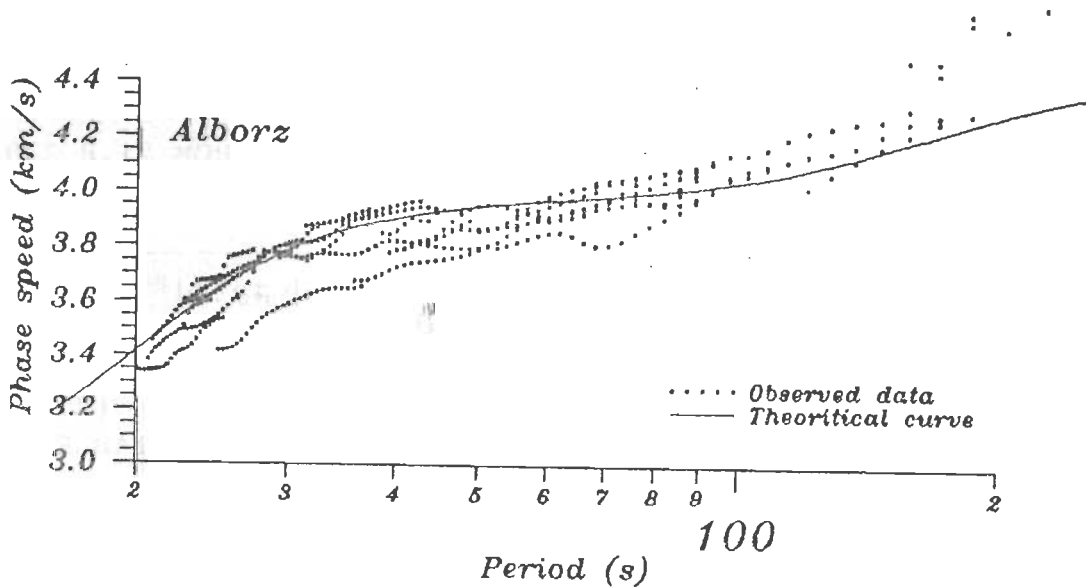
FIG. 6.12 THEORETICAL PHASE SPEED DISPERSION CURVE CORRESPONDING TO MODEL OF Table 6.17

6.8 COMPARISON OF OUR INVERTED $\beta(Z)$ PROFILES WITH THE RESULTS OF OTHER WORKERS.

6.8.1 COMPARISONS FOR THE ZAGROS REGION

Bird (1978) determined Rayleigh wave group speeds from local earthquake data. He presented a crust and upper mantle model based upon these observations. Fig. 6.13 is a comparison of the shear wave profile determined by him and the profiles determined by us for the Zagros region. It is very satisfying to note the close similarity in the $\beta(z)$ profiles, especially between our 18 layer model and the Bird model. In addition the estimate of crustal thickness given by Bird is 45.6 km and it compares very favorably with our estimate of 45.2, 45.5, and 47.5 km for 1, 2, and 18 layer crustal models.
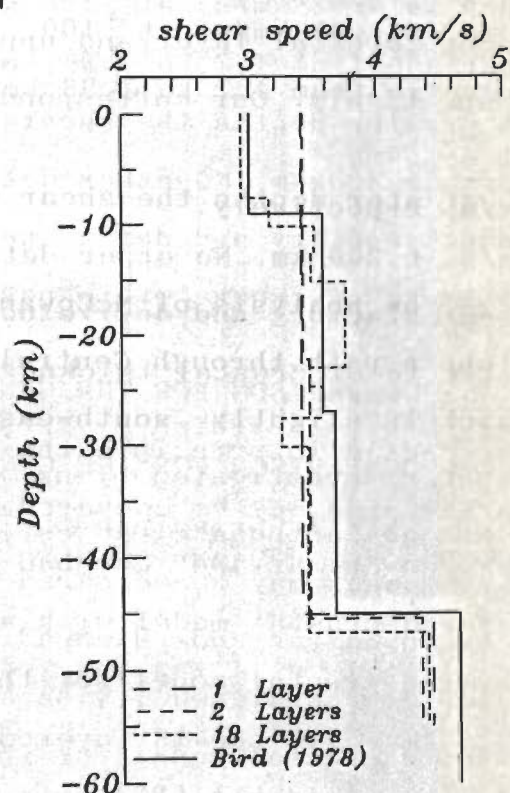
FIG. 6.13 COMPARISON OF $\beta(Z)$ PROFILES FOR THE ZAGROS CRUSTA ACCORDING TO BIRD (1978) AND OUR 1, 2, AND 18 LAYERS.

Asudeh (1982) reported a very intriguing crust and upper mantle model using limited phase speed data (Fig. 1.19). He suggested a single crustal layer in which shear speed increase

linearly from 2.66 km/s to 4.44 km/s. His model includes a small jump in shear speed at the Moho. However his Table 6 and Fig. 9 disagree regarding shear wave speed between depths of 46 and 100 km. Where as the table suggest a constant speed of 4.7 km/s with a jump to 4.98 km/s at 100 km, the figure indicates a linear increase from 4.7 to 4.98 km/s in the depth range of 46 to 100 km. At greater depths the shear wave speed decreases linearly to 4.74 km/s at 200 km. No other details are given. We regard this as unsatisfactory and derive no consolation from the fact that his estimate of crustal thickness agrees with our results closely.

6.8.2 COMPARISON FOR THE CENTRAL IRAN REGION

Again in principle the results of Asudeh (1982) for two earthquakes may be compared with our results because the path between Shiraz and Mashhad is identical. Asudeh gives a two layered crustal model with a total thickness of 43 km. Our two layered crustal model for this region gives a total thickness of 39.3 km while the 18 layered model gives a crustal thickness of 43.9 km. Asudeh (1982) estimated shear wave speed in first and second crustal layer and upper mantle as 3.31, 3.6, and 4.38 km/s respectively. Our corresponding values are 3.39, 3.47, and 4.39 km/s respectively.

The analysis of McCowan (1978) deals with Rayleigh waves along a path through Central Iran from southern Zagros to Mashhad which is slightly south-east of the path between Shiraz and Mashhad investigated by us. His analyses are based on data for just one earthquake. He estimated a thickness of 55 km for a crust

198

with two layers. This model is displayed in Fig. 1.18 and is included here for the sake of completeness.

6.8.3 COMPARISON FOR THE ALBORZ REGION

6.8.3.1 CRUSTAL STRUCTURE

Asudeh (1982) reports inversion results based on data for two earthquakes. The important point to note here is that the path investigated by him between Mashhad (SRO) and ILPA, located about 80 km south-west of Tehran, runs through the Alborz mountains more closely than the path between Mashhad and Tabriz investigated by us . Thus it is not surprising to us that Asudeh gives a thickness estimate of 45 km for a one layered crust while our estimate is 35.1 km only. Support for possible rapid decrease in crustal thickness from Alborz northward comes from crustal modelling by Dehghani and Makris (1983) based on gravity data (see our Fig. 1.7, lower part, northen end) Shear speeds in the crustal layer and upper mantle are 3.55 and 4.63 km/s according to Asudeh (1982) and 3.47 and 4.51 km/s according to our estimate.

6.8.3.2 MANTLE STRUCTURE

We have described above (Figs. 6.10 and 6.11) two models of upper mantle structure between Mashhad and Tabriz stations using inversely dispersed mantle Rayleigh wave up to a period of 230 seconds. In contrast Asudeh (1982) displays in his Fig. 5 phase speed curves for Rayleigh waves up to about 150 second for the Mashhad (SRO)-ILPA path. According to Asudeh's model the low speed layer starts at 71 km. The lowest shear wave speed is at 100 km

and there after the shear speed increases slowly.

It is interesting to note that Bird (1978), McCowan (1978) and Asudeh (1982) have constructed upper mantle models for different region of Iran. They all display a low speed layer in the upper mantle. But there is no agreement as to the depth of the top and bottom of this layer and the maximum drop in shear speed in this layer. It is our opinion that we must await accumulation of more long period shear wave data to investigate upper mantle structure in different parts of Iran.

CHAPTER-7
DISCUSSION

7.1 INTRODUCTION

The material presented in Chapter 1 to 6, although complete in itself, still needs comments for a more comprehensive synthesis. The following paragraphs are directed to this end.

7.2 ON THE ALGORITHMS SELECTED FOR DATA ANALYSIS AND INTERPRETATIONS

Apart from the new suggestion for taking care of the instrument responses in the two station method for phase speed determination (see sections 2.10 and 3.6) no new method for data processing and interpretation has been developed. However in selecting from the existing methods for the present work, an attempt was made to pick good and reliable ones. It is thus that we opted for (i) the FFT, (ii) the cross-correlogram (Dziewonski and Hales's 1972) variant of Aki's two station method for surface wave phase speed determination, (iii) singular value decomposition (SVD) variant of the method of generalized inverse for inversion of phase speed data (Yuan and Nazarian 1993)and (iv) Schwab and Knopoff's (1972) variant of the matrix method to evaluate Rayleigh wave phase speeds at differenct periods for a stack of elastic layers.

However the implementation of these methods and procedures through computer programs in FORTRAN was done by us independently and accepted after very thorough testing. Only Schwab and Knopoff's (1972) subroutine for evaluating layer matrices was adopted as such, but it also was tested.

In the same vein, considerable information exists among seismologists regarding the preparation of digitized data to be used as input for computation of surface wave phase speeds while making use of the FFT program. However, in a spirit of learning, we carried out 16 experiments on synthetic data to evolve a uniform and effective method for data preparation prior to phase speed computations (see section 3.3).

7.3 QUALITY CONTROL ON RAYLEIGH WAVE DATA BEFORE ANALYSIS

We have selected seismograms to be analyzed with particular care because this is the first detailed study of Rayleigh wave dispersion across Iran. We tried to ensure that the selected wave trains were well recorded and as noise free as possible at both stations. This selection of seismograms was completed before the data analysis was taken up. After this no further deletions of data were carried out. All phase speed results have been reported even if they differed significantly in a few cases from majority of the results for that region, and even if they were not used in computing the final estimates of average phase speeds for that region.

7.4 CAUSES OF NOISE ON SEISMOGRAMS USED FOR PHASE SPEED DETERMINATIONS

Even after taking the precautions outlined in the preceding section it could not be said that the Rayleigh waves analyzed by us were entirely noise free. The first and foremost possibility for noise on the surface wave portions of seismograms is that Rayleigh waves of many modes may be recorded, although one mode, say the fundamental, may be dominant. As a second possibility we note that invariably the great circle paths between the epicenters in different parts of the globe and the recording stations in Iran crossed various tectonically complex regions. This could have caused lateral refraction of Rayleigh waves and departures of actual paths taken by them from great circle paths. The possibility even exists that groups of Rayleigh waves within the same wave train may not have followed exactly identical paths. In our opinion, the noisy appearance of Rayleigh wave trains in many cases may arise from this cause. The possibility also exists in a few cases that, even though the angle made at the epicenter by the great circles to the two stations is small, the Rayleigh wave trains travelling along the great circle to one station may be perturbed to a much greater degree than the waves along the adjoining great circle to the other station.

Moreover, an examination of Jeffreys-Bullen (1967) travel time curves indicates that, in principle, many body waves reflected multiply through the core can arrive at the same time as the Rayleigh waves. This is especially true in the epicentral distance range of 50° to 120°. Ordinarily this has not been

considered as a major source of noise in surface wave studies. But if the earthquake has the hypocenter in the intermediate or deep range and the magnitude is large, then some noise could arise from this cause.

A further complication which may arise in many cases considered by us, is that, for reasons of local geology, the Rayleigh wave train at the second station may be contaminated by noise to a greater degree than at the first station. This seems to hold true for the Alborz and Central Iran regions particularly.

Our procedure to handle these problems has been to compute at least two phase speed dispersion curves in each case. In the first, we consider Rayleigh wave trains corresponding to a wide range of group speeds and, in the second, we consider one or more shorter segments of Rayleigh wave trains corresponding to narrower ranges of group speeds. In all cases, the phase speed curves from the second set of exercises are smoother than from the first.

7.5 ABOUT THE INVERSION ALGORITHM

7.5.1 FIRST LAYER SHEAR WAVE SPEED

Detailed tests of inversion program written and used by us have been given in Chapter 3. Using synthetic data as well as simulated error prone data it has been shown that the original known model could be recovered within limits through inversion. However in all cases, shear wave speed in the first layer indicated maximum departure from the known exact values. This was

ascribed to insensitivity of the inversion procedure for this parameter arising from the smallness of the derivative of phase speed with respect to first layer shear wave speed. A connected aspect appears to be that the lowest period of Rayleigh waves considered by us was between 16 and 20 seconds. If shorter period data were available then perhaps this parameter could have been resolved better.

7.5.2 INFLUENCE OF RANDOM NOISE

Since most of the other crustal and upper mantle values related to the $\beta(z)$ profile in the above synthetic exercise could be recovered from inversion even in the presence of 4% to 10% random noise on synthetic seismograms, we conclude that in our actual inversion of Iranian data this is not a limiting factor for investigation of crustal and upper mantle layers.

7.5.3 ROLE OF INITIAL MODEL

Since we have linearized the inversion problem, the importance of starting model for convergence to an improved model cannot be overemphasized. Innumerable number of times during inversion the program went into an iterative loop or stopped calculations altogether because of this reason. Certain amount of geophysical "intuition" about crustal structure is necessary to deal with this problem. See also the following subsection.

7.5.4 SOME DECLAMATORY REMARKS ABOUT INVERTED RESULTS

Although we have presented in Chapter 6 inverted results for 1, 2, and 18 layered crustal models, and they are all different from one another more or less, it is our sense that, for a given

205

region such as the Zagros, they still have intrinsic similarities. The possibility exists that a radically different set of models could also explain the data. May be those models represent the crustal structure in the Iranian region more closely. Perhaps we have sought biased crustal models which are similar to crustal models reported in the literature for other regions of the world. Inevitable constraints on time and resources prevent us from continuing the search.

7.6 COVERAGE OF IRANIAN REGION WITH AVAILABLE RAYLEIGH WAVE DATA

It is evident from the review of Section 1.2 and the geological map of Fig. 1.2 that the surface geology of Iran is quite complex. The triangle formed by the WWSSN stations of Tabriz, Shiraz and Mashhad is reasonably large with sides ranging in length from 992 to 1189 km. Still, information has been obtained through the present Rayleigh wave study only for three elongated swaths of country lying along the sides of Tabriz-Shiraz-Mashhad triangle in the northwest half of Iran.

The swaths arise because, inspite of our best efforts, we could not select sufficient number of earthquakes with epicenters lying exactly on the great circles through the station pairs of Tabriz-Shiraz, Shiraz-Mashhad and Mashhad-Tabriz.

Within the limitations of data available, the selected earthquakes that were recorded at Tabriz and Shiraz provide information about the geologically interesting Zagros mountain belt.

Similarly the data recorded at Mashhad and Tabriz provide information about the Alborz mountains. However we have to acknowledge that the waves approaching Tabriz from the ESE subparallel to the Mashhad-Tabriz great circle had crossed the Caspian Sea to a greater or lesser degree. The crust and upper mantle structure of the Alborz mountains was traversed mainly in the eastern and western parts of the interstation path (Fig. 1.2). The utility of the average results obtained from Rayleigh waves in this case is somewhat constrained in view of the suspected abnormal crustal structure under the Caspian Sea (e.g. Kadinsky-Cad et al. 1981).

Finally, the Rayleigh waves travelling subparallel to the Shiraz-Mashhad great circle traverse many different surface geologic provinces outlined by Stocklin (1968).

In the absence of information about how deep do the heterogeneities related to the surface geological structures penetrate the crust, and also because we ignore topographic variations along the paths of waves, we have to be satisfied with average information in the form of simplified flat layered earth models obtained from Rayleigh wave phase speed inversions.

We have used the data plotted in Fig. 5.3, 5.14, and 5.24 for puroposes of inversion. The scatter in data for each period is greater than the estimated ± 0.12 km/s error in individual $c(T)$ values. The theoretical dispersion curves for the accepted models for a region lie well with in the scatter of these observations.

7.7 ASSESSMENT OF PHASE SPEED DISPERSION CURVES FROM A VISUAL EXAMINATION

The geophysical investigations about Iran summarized in Chapter 1 give an indication that the crust and upper mantle structure may not be uniform in all parts of Iran. The gravity data interpreted by Dehghani and Makris (1983) and the various seismological studies based on local earthquake data further testify to this conjecture. Even the Fig. 5.39, comparing the average phase speed dispersion curves for the Zagros, Central Iran and Alborz regions, shows that some differences in the crust and upper mantle structures should exist in the three regions.

But having said this, we note from Fig. 5.39 that the differences in phase speed curves for the three regions are still within 0.3 km/s. The same holds for these curves individually when compare to the average curve of Oliver (1962). This suggest that Iranian crust is broadly similar to crust in other continental regions of the world.

7.8 ON THE POSSIBILITY THAT THE CRUSTAL LAYERS UNDER IRAN MAY HAVE UNIFORM SHEAR WAVE SPEEDS LATERALLY

An examination of $\beta(z)$ profiles obtained after inversion of observation for the three regions (Fig. 6.9) indicates that the maximum variation in shear wave speed at any depth is less than 0.6 km/s through actual differences at most depths are constentabily less. Therefore we may entertain that possibility that the shear wave speed in different crustal layers and upper mantle may be broadly uniform laterally. This is inspite of the

observation that the surficial geology shows considerable, even dramatic, variation from region to region.

7.9 VARIATION IN CRUSTAL THICKNESS

The relatively small differences in phase speed curves Fig. 6.9 have been interpretated in Chapter 6. The inversion program has consistently given the result that these differences can be explained by differences in crustal thicknesses in the three regions of Iran. As seen from Table 6.14 the maximum variation in crustal thicknesses is of the order of 10 km and this thickness decreases from 45 km in Zagros to 39 km in Central Iran and 35 km in Alborz region.

7.9.1 ZAGROS REGION

The estimated crustal thickness for the Zagros region is of the order of 45 km which is above average for a normal continental crust. As summarized in Chapter 1, estimates of crustal thickness in the Zagros mountains using local earthquakes data are in the rang of 42 to 59 km with majority of the estimates being close to 45 km. This is comparable to our estimates of 45.2 to 47.5 km (Table 6.14).

More interestingly, Snyder and Barazangi (1986) used gravity observations to make a plate tectonic based model of the Zagros mountains, and they also estimated a relatively thickened crust. Such thickening is understandable because of the implied convergence due to subduction of Arabian plate under the Zagros.

Because the period range of Rayleigh waves available in the observations is less than about 70 seconds, we are not in a position to test multi-layered models in which total thickness of layers above the half space runs into several hundreds km. Thus the influence of shear wave speed in subducting part of the Arabian plate at such depths on the Rayleigh wave phase speeds was not investigated by us for the Zagros region .

7.9.2 CENTRAL IRAN REGION

As noted in earlier chapters estimates of 43 km and 55 km (Asudeh 1982, McCowan 1978) had been reported for crustal thickness in Central Iran . These are comparable to our estimates of 39.6, 39.3 and 43.9 km for 1, 2, and 18 layered model.

The available geological observations suggest a complex tectonic history for this region. Volcanism has been important in the geological past. Some low level volcanic activity observed even today is probably related to subduction in the Makran region (Darvichzade 1992). Kadinsky-Cade et al. (1981) list three models for evolution of continental plateaus such as the Iranian plateau, namely, presence of a hot and low-density upper mantle, thickening of the crust by horizontal compression, and underthrusting of one crustal layer beneath another. The available geophysical data do not provide sufficient constraints to pick between these models (see e.g. Kadinsky-Cade 1981).

7.9.3 ALBORZ REGION

It has to be acknowledged that the swath of Iran traversed by Rayleigh waves between Mashhad and Tabriz has been called the

Alborz region. But strictly speaking this swath lies north of the Alborz mountains for the most part and passes through the Caspian Sea whose surface is few meters below sea level. Mountains occur in this swath at the northwest and southeast ends. Thus it is not too surprising that our inversion of phase speed data yields a 35 km thick crust comparable to normal shield type crust.

The Alborz mountains have a topographic relief of about 3 km and Asudeh's (1982) crustal models gives a crustal thickness of 45 km between Mashhad (SRO) and ILPA stations.

7.10 FINAL REMARKS

It is slightly disheartening that, after nearly four years of concerted effort which we have put in this work, the number of concrete statements that we can make about the Iranian region is almost negligible. The non-uniqueness of the geophysical inverse problem is fully evident here. Nature makes men work very hard to fathom it.

CHAPTER-8
CONCLUSIONS

The following conclusions appear to us reasonable. They are divided in to two groups, namely conclusions regarding the analytical procedure and conclusions regarding geophysical results about Iran.

8.1 CONCLUSIONS REGARDING ANALYTICAL PROCEDURES

1- We find that the use of carefully digitized Rayleigh wave signals, FFT, cross correlogram variant of Aki's two station method for surface wave phase speed determination, Schwab and Knopoff's (1972) matrix method for computation of theoretical phase speed curves, and the SVD variant of the generalized inverse constitute a reasonable package of algorithms and procedures for determination of crust and upper mantle structure from observed records of dispersed Rayleigh wave trains.

2- We reconfirm from a series of 16 numerical experiments (Section 3.2) that the following points should be kept in mind while preparing data for further analyses. Firstly, the rate of digitization should be the same for Rayleigh wave trains at both stations. Secondly, the start of digitization at both stations should correspond to identical initial group speeds. Similarly the

termination of digitization should correspond to identical terminating group speeds. Thirdly, the number of terms in both time series should be made equal to an integral power of 2, say 2^{10}, by adding suitable number of zeros at the end.

3- For taking into account instrumental effects in the two station method of phase speed determination, the proposed approach of convolving recorded Rayleigh waves at first station with the recorded calibration pulse of the second station and vice-versa before computing the cross-correlogram is workable (see section 3.6).

8.2 CONCLUSION BASED ON OBSERVED RAYLEIGH WAVE PHASE SPEED CURVES AND THEIR INVERSION

1- The average dispersion curves for the Zagros, Central Iran, and Alborz regions and the world average curve of Oliver (1962), are so nearly similar as to suggest that the Iranian crust is broadly similar to crust in other continental regions of the world.

2- The Rayleigh wave data analyzed are consistent with the possibility that the shear wave speed in the crustal layers and the upper mantle could be broadly uniform laterally under Iran.

3- The crustal thickness may vary from region to region in Iran. Among the three regions investigated by us, the crustal thickness is the greatest in the Zagros region and least in the Alborz region.

4- The relatively greater thickness of the crust in the Zagros region is consistent with the plate tectonics view that subduction of the Arabian plate is taking place in this region.

5- From the limited long period Rayleigh wave data for the Alborz region the possibility also arises that a low speed layer may exist in the upper mantle under Iran .

6- There is considerable similarity in the crustal models for Zagros region obtained by us using Rayleigh wave phase speeds and that obtained by Bird (1878) using Rayleigh wave group speeds from local earthquakes.

7- The non-uniqueness in inversion of Rayleigh wave phase speed curves is overwhelming. Nature guards its secrets zealously. But men must persevere.

SUGGESTIONS FOR FUTURE WORK

1- The number of seismograph stations in Iran should be increased. The southeastern in part of the country needs special attention in this matter.

2- Use of digitally recorded surface wave data would speed up the analyses for crust and upper mantle studies in Iran while increasing reliability and repeatability of the experiments.

3- Use of Love waves dispersion data should constrain the $\beta(z)$ profiles further.

4- Joint inversion of body wave arrival time data, surface wave dispersion data and gravity data should be attempted.

5- Analysis of group speeds obtained from surface waves recorded at one station may be considered also to enhance the database from existing resources.

6- Use of digitally recorded, controlled source, seismic studies of the crust in Iran could help in reducing the non-uniqueness of models based on surface wave interpretations.

REFERENCES

Ambraseys, N.N., and C.P. Melville

    1982   "A history of Persian earthquakes", Cambridge University Press

Anonymous

    1970   "Description of WWSSN stations in Iran", Institute of Geophysics Tehran University, Report No. 49 Supplement

Anzabi, A.

    1981   "The Pn velocity under crust and crustal thicknesses in Tabriz and Tehran", J. Earth & Space Phys. 10, 41-44 (in Persian)

Asudeh, I.

    1982   "Seismic structure of Iran from surface and body wave data", Geophys. J. R. astr. Soc., 71, 715-730

Backus, G.E., and F. Gilbert

    1967   "Numerical application of a formalism for geophysical inverse problems", Geophy. J. 13, 247-276

Baker, C., J. Jackson, and K. Priestley

    1993   "Earthquakes on the Kazerun line in the Zagros mountains of Iran : strike-slip faulting within a fold-and-thrust belt", Geophy. J. Int. 115, 41-61

Ben-Menahem, A.

    1964   "Mode-ray duality", Bull. Seismo. Soc. Am. 54, 1315-1321

Berberian, M.

    1976   "Tectonic and seismotectonic section contribution to the seismotectonics of Iran (part II)", Geological survey of Iran report No 39

Bird, P.
    1978   "Finite element modeling of lithosphere deformation: The
            Zagros collision orogeny", Tectonophysics 50, 307-336

Braile, L.W.
    1991   "Seismic   studies   of   the   earth's   crust", Review of
            Geophy. Supplement Am. Geophysical Union (1987-1990),
            680-687

Bullen, K.E.
    1963   "An introduction to the theory of seismology", Cambridge
            University press

Bullen, K.E., and B.A. Bolt
    1985   "An introduction to the theory of seismology", Cambridge
            University press

Chandra U., J.G. McWhorter, and A.A. Nowroozi
    1979   "Attenuation of intensities in Iran", Bull. Seismo. Soc.
            Am. 69, 237-250

Chen, C.Y., W.P. Chen, and P. Molnar
    1980   "The uppermost mantle P wave velocities beneath Turkey
            and Iran" Geophysical Res. Letters, 7, 77-80

Chen, W.P., and P. Molnar
    1975   "Short-period Rayleigh-wave   dispersion   across   the
            Tibetan plateau", Bull. Seismo. Soc. Am. 65, 1051-105

Cooley, J.M., and J.W. Tukey
    1965   "An algorithm for the machine computation of complex
            Fourier series", Math. Comput., 19, 297-301

Darvichzade, A.,
    1992   "Geology of Iran", Neda publication Tehran (in Persian)

Dehghani, G. A., and J. Makris
    1983   "The gravity field and crustal structure of Iran",
            (Geodynamic project (Geotraverse) in Iran, Geological
            Survey of Iran, Report No. 51, 51-68

Dewey, J.W., and A. Grantz
    1973   "The Qir (Ghir) earthquake of April 10, 1972 in Zagros mountains of southern Iran : seismotectonic aspects and some results of a field reconnaissance", Bull. Seismo. Soc. Am. 63, 2071-2090

Dorman J., M. Ewing, and J. Oliver
    1960   "Study of shear velocity distribution in the upper mantle by mantle Rayleigh waves", Bull. Seismo. Soc. Am. 50, 87-115

Dunkin, J.W. 1965
    1965   "computation of modal solution in layered, elastic media at high frequencies", Bull. Seismo. Soc. Am. 55, 335-358

Dziewonski, A.M., and A.L. Hales
    1972   "Numerical analysis of dispersed seismic waves", "Methods in computational physics Seismology: Surface waves and earth oscillations", Academic press, New York 11, 39-85

Ewing, M., W. Jardetzky, and F. Press
    1957   "Elastic waves in layered media", McGrawHill. New York

Golub, G.H., and C. Reinsch
    1970   "Singular value decomposition and least squares solution", Numerische mathematick, (Berlin) 14, 403-420 (in German)

Haskell, N.A.
    1953   "The dispersion of surface waves in multilayerd media", Bull. Seismo. Soc. Am. 43, 17-34

Hedayati, A., J.L. Brander, and M. Berberian
    1976   "Micro earthquake survey of Tehran region, Iran", Bull. Seismo. Soc. Am. 66, 1713-1725

Islami, A.A.
    1972   "A study of the depth of Mohorovicic discontinuity in western Iran and the velocity of Pn wave", J. Earth & Space Phys. 1, 1-11 (in Persian)

Islami, A.A.
   1974   "Detecting the thickness of the crust in Shiraz area
           using hypocenter situated below the crust", J. Earth &
           Space Phys. 3, 15-18

Jeffreys, H., and K.E. Bullen
   1967   "Seismological tables", Smith & Ritchie Ltd., Edinburgh

Kadinsky-Cade, K., M. Barazangi, and J. Oliver
   1981   "Lateral variations of high-frequency seismic wave
           propagation at regional distances across the Turkish and
           Iranian plateause", Jour. of Geophysical Res. 86,
           9377-9396

Kamalian, N., and S. Mehrabian
   1990   "Hypocenters of Iranian earthquakes", A project report
           Institute of Geophysics University of Tehran

Kamalian, N., and P. Mozaffari
   1990   "Study of Roudbar earthquake July, 20 1990 according to
           aftershocks ", Institute of Geophysics University of
           Tehran

Knopoff, L.
   1964   "A matrix method for elastic wave problems", Bull.
           Seismo. Soc. Am. 54, 431-438

Kohn, M. C.
   1987   "Practical numerical methods algorithms and programs",
           Macmillan Publishing Company New York

Lamb, H.
   1904   "On the propagation of tremors over surface of an
           elastic solid.", Philosophical transactions of the Royal
           Socity of London. A203:1-42

Love, A.E.H.
   1911   "Some problems of geodynamics.", Cambridge University
           Press

Maleki, E.
    1980   "Study on crust and seismocity of Iran according to recorded earthquakes in ILPA (Tehran)", ME. Thesis

McCowan D.W.
    1978   "High-resolution group velosity analysis", Geoexploration, 16, 97-109

McEvilly, T.V.
    1964   "Central U.S. crust-upper mantle structure from Love and Rayleigh wave phase velocity inversion", Bull. Seismo. Soc. Am. 54, 1997-2015

McKenzie, D.
    1972   "Active tectonics of the Mediterranean region", Geophy. J. Res. Astro., 30, 109-185

Mesko, A.
    1984   "Digital filtering applications in geophysical exploration for oil", Academia Kiado, Budapest

Mitchell, B.J., and M. Landisman
    1969   "Electromagnetic seismograph constants by least squares inversion", Bull. Seismo. Soc. Am. 59, 1335-1348

Moazami-Goudarzi, K.
    1972   "Seismology", Ofset Lim. Comp. Tehran (in Persian)

Moazami-Goudarzi, K. and N. Sadeghzadeh
    1972   "Un modele a deux couches pour la croute terrestre dans le sud de l'Iran", J. Earth & Space Phys. 1, 43-49. (in Franch)

Nowroozi, A.A.
    1971   "Seismo-tectonics of the Persian Plateau, Eastern Turkey, Caucasus and Hindo-Kush regions", Bull. Seismo. Soc. Am. 61, 317-341

Nowroozi, A.A.
    1976   "Seismotectonic provinces of Iran", Bull. Seismo. Soc. Am. 66, 1249-1276

Nuttli, O.W.
  1980   "The excitation and attenuation of seismic crustal
          phases in Iran", Bull. Seismo. Soc. Am. 70, 469-485

Oldham, R.D.
  1899   "Report on the great earthquake of June 12, 1897", Mem.
          Geol. Surv. India 29, 1-379

Oliver, J.
  1962   "A   summary   of   observed   seismic   surface   wawe
          dispersion", Bull. Seismo. Soc. Am. 52, 81-86

Pekeris, C.L.
  1948   "Theory of propagation of explosive sound in shallow
          water", Geological Socity of America Memories No.27

Pennington, R.H.
  1965   "Introductory computer method and analysis", McMillan
          New York

Pomeroy, P.W., G. Hade, J. Savino, and R. Chander
  1969   "Preliminary   Results   from   high-gain   wide-band
          long-period electromagnetic seismograph systems", Jour.
          Geophy. Res. 74, 3295-3298

Schwab, F.
  1970   "Surface-wave   dispersion   computations: Knopoff's
          method", Bull. Seismo. Soc. Am. 60, 1491-1520

Schwab, F.A., and L. Knopoff
  1972   "Fast surface wave and free mode computations", Methods
          in computational physics "Seismology: Surface waves and
          earth oscillations", Academic press, New York 11, 87-180

Sheriff, R.E.
  1984   "Encyclopedic dictionary of exploration geophysics",
          Tusla: Socity of Exploration Geophysics

Snyder, D.B., and M. Barazangi
  1986   "Deep crustal structure and flexure of the Arabian plate
          beneath the Zagros collisional mountain belt as inferred
          from gravity observations", Tectonics 5, 361-373

Stearns, S.D., and R.A. David
   1988   "Signal processing algorithms", Prentice-Hall Inc. New
           Jersey

Stocklin, J.
   1968   "Structural history and tectonic of Iran: A review",
           American Association of Petroleum Geologists Bulletin
           52, 1229-1258

Stoneley, R.
   1924   "Elastic waves at surface of separation of two solid",
           Proceeding of the Royal Socity of London A 106:A 16-428

Watson, T.H.
   1970   "A note on fast computation of Rayleigh waves dispersion
           in the multilayered elastic half-space", Bull. Seismo.
           Soc. Am. 60, 161-166

Yuan, D., and S. Nazarian
   1993   "Automated surface wave method: Inversion technique",
           Journal Geotechnical Engineering. 119, 7, 1112-1126

APPENDIX A
SUMMARY OF BACKGROUND THEORY FOR THE FFT PROGRAM

A.1 FOURIER SERIES

The basic idea of Fourier series is that a piecewise continuous periodic function g(t) of period T can be expressed as the following sum of sine and cosine terms.

$$g(t)=a_0+2.\sum_{k=1}^{\infty}a_k \cos \frac{2\pi}{T}kt +2\sum_{k=1}^{\infty} b_k \sin \frac{2\pi}{T}kt \quad . \qquad \ldots(A.1)$$

Here the coefficient $a_0, a_1, \ldots, b_0, b_2, \ldots$ are defined through the integrals

$$a_0 =\frac{1}{T}\int_{-T/2}^{T/2} g(t)dt,$$

$$a_k =\frac{2}{T}\int_{-T/2}^{T/2} g(t).\cos\frac{2\pi}{T}kt \, dt, \qquad k=1,2,\ldots; \qquad \ldots(A.2a)$$

$$b_k = \frac{2}{T}\int_{-T/2}^{T/2} g(t).\sin\frac{2\pi}{T}kt \, dt. \qquad k=1,2,\ldots; \qquad \ldots(A.2b)$$

This series may also be written in the following complex form.

$$g(t) = \sum_{k=-\infty}^{\infty} c_k e^{i\frac{2\pi}{T}kt} . \qquad \qquad \ldots(A.3)$$

Here $i = \sqrt{-1}$. The coefficients c_k are defined through the integrals

$$c_k = \frac{1}{T} \int_0^T g(t) . e^{-\frac{2i\pi}{T}kt} dt. \qquad k=-\infty,\ldots,0,\ldots\infty \qquad \ldots(A.4)$$

A.2 THE FOURIER TRANSFORM

The Fourier Transform $G(f)$ of the nonperiodic function $g(t)$ defined over the range $-\frac{T}{2} \leq t \leq \frac{T}{2}$ is defined as

$$G(f) = \int_{-\infty}^{\infty} g(t) e^{-2i\pi ft} dt. \qquad \qquad \ldots(A.5)$$

Here f is frequency. The inverse Fourier Transform is

$$g(t) = \frac{1}{2\pi} \int_{-\infty}^{\infty} G(f) e^{2i\pi ft} df. \qquad \qquad \ldots(A.6)$$

The amplitude spectrum $A(f)$ is defined by

$$A(f) = \left| G(f) \right| = \left\{ \Big(\mathrm{Re}[G(f)] \Big)^2 + \Big(\mathrm{Im}[G(f)] \Big)^2 \right\}^{1/2} . \qquad \ldots(A.7)$$

And the phase spectrum is defined by

$$\phi(f) = \tan^{-1} \frac{\mathrm{Im}[G(f)]}{\mathrm{Re}[G(f)]} + 2\pi N \qquad . \qquad \ldots(A.8)$$

Here N is an integer. In some applications, we need a continuous phase spectrum. Then we may choose those branches of the multivalued inverse tangent function which make $\phi(f)$ a continuous

function of f. This is achieved by assigning appropriate integral values to N in different frequency ranges. The procedure is called **unwrapping** the phase curve (Mesko 1984).

A.3 CONVOLUTION, CROSS CORRELATION, AND AUTO CORRELATION

The convolution of two signals $g(t)$ and $h(t)$ is defined as

$$y_{gh}(t) = \int_{-\infty}^{\infty} g(\tau).h(t-\tau)d\tau = g(t)*h(t) \qquad ...(A.9)$$

Cross correlation function of these signals is defined by:

$$c_{gh}(\tau) = \int_{-\infty}^{\infty} g(t).h(t+\tau).dt = g(\tau)*h(-\tau) \qquad ...(A.10)$$

When the $h(t)=g(t)$ the c_{gg} is called the auto correlation of $g(t)$. The Fourier transform $Y(f)$ of the convolution is

$$Y(f) = G(f).H(f) \qquad ...(A.11)$$

Thus,
$$\left|Y(f)\right| = \left|G(f)\right|\left|H(f)\right| \qquad ...(A.12)$$

and
$$\phi_y(f) = \phi_g(f) + \phi_h(f) \quad . \qquad ...(A.13)$$

The Fourier transform of cross correlation function c_{gh} (Eq. A.10) is

$$C(f) = \bar{G}(f).H(f) \quad . \qquad ...(A.14)$$

Thus $\quad \phi_c(f) = \phi_g(f) - \phi_h(f)$,

where $\bar{G}(f)$ is complex conjugate function of $G(f)$.

A.4 THE DISCRETE FOURIER TRANSFORM (DFT)

Consider a periodic sequence g_j (j=0,1,... N-1) such that $g_{j+N} = g_j$. The Discrete Fourier Transform (DFT) G_k of this sequence is

$$G_k = \sum_{j=0}^{N-1} g_j \cdot w^{jk} \qquad (k=0,1, \qquad N-1) \qquad \qquad \dots(A.15)$$

Here $w = e^{\frac{2i\pi}{N}}$. The Inverse Discrete Fourier Transform $(DFT)^{-1}$ is defined as

$$g_j = DFT^{-1}\{(G_k)\} = \frac{1}{N} \sum_{k=0}^{N-1} G_k \cdot w^{jk} \qquad . \qquad \qquad \dots(A.16)$$

A.5 FAST FOURIER TRANSFORM (FFT)

The calculation of Eq. A.15 requires a large amount of time if the sequence g_i is a long one, i.e., if N is a large number. But if N equals an integral power of 2 then, with the well known method of Cooley-Tukey (1965), the computing time is approximately reduced by a factor of $(1/2N) \cdot \log_2 N$ (Stearns and David, 1988). This is the Fast Fourier Transform (FFT) method. The result of FFT and DFT of same sequences are same. The saving in computation time is achieved because of the following observation.

We define two subsequences, the first comprising the odd numbered terms and the second even numbered terms of the original sequence. That is, let $g_k^* = g_{2k}$, and $g_k^{**} = g_{2k+1}$. Here k=0,1,.....n_1-1, and N=$2n_1$, in both cases. Then, using the concept of eq. (A.15),

228

$$G_j^* = \sum_{k=0}^{n_1-1} g_k^* \cdot w^{2jk} = \sum_{k=0}^{n_1-1} g_{2k} \cdot w^{2jk} , \qquad\qquad (A.17)$$

and
$$G_j^{**} = \sum_{k=0}^{n_1-1} g_k^{**} w^{2jk} = \sum_{k=0}^{n_1-1} g_{2k+1} w^{2jk} \qquad j=(0,1,\ldots,n_1-1)$$

Thus we see that

$$G_j^* + w^j \cdot G_j^{**} = \sum_{k=0}^{N-1} g_k \cdot w^{jk} = G_j , \qquad\qquad j=(0,1,\ldots,n_1-1) \qquad .(A.18)$$

In other words the jth DFT of the original complete sequence is the sum of the jth DFT of even number terms of the original sequence and the jth DFT of odd number terms of the original sequence with the latter multiplied by w^j .By this method the time of computation of DFT is reduced by a factor of 2. If $N=2^k$ then the above process can be repeated.k times and the total reduction in time is by a factor of $k/(2N)$.

A.6 TESTING OF THE COMPUTER PROGRAM FOR FFT

Although many computer programs for FFT have been actually reproduced in the literature, our experience has been that some little twist is given in each case because of which the results are not always up to expectation. In order to overcome this difficulty and also to learn thoroughly we wrote over own computer program for FFT. In this section we display the results of a stringent test of this program. Fig. A.1 is a display of 1024 samples obtained by adding the following 45 cosine terms
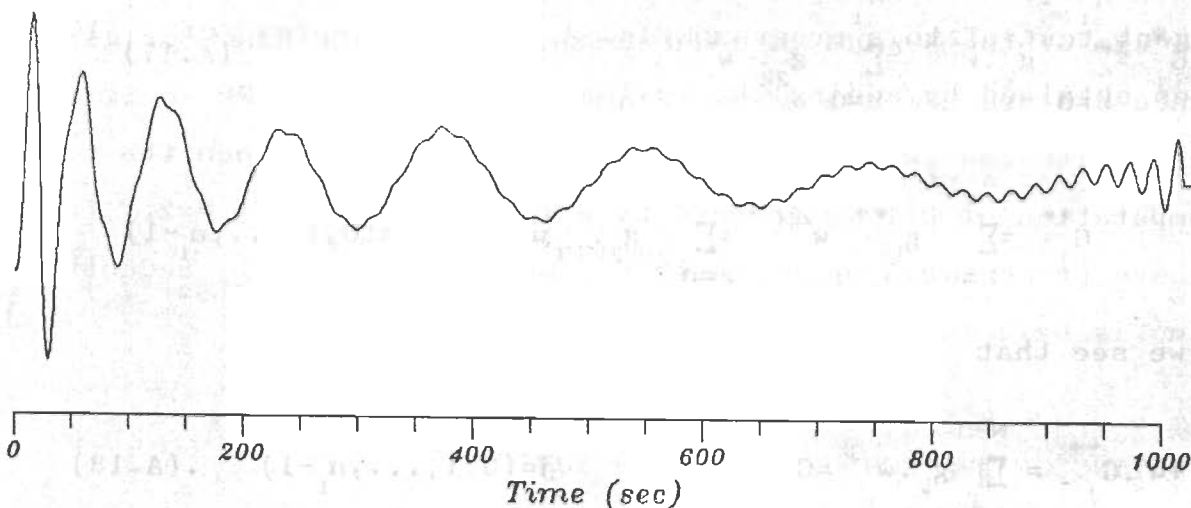
Time (sec)

FIG A.1 DISPLAY OF SYNTHETIC TIME SERIES CORRESPONDING TO Eq. A.19

$$y(t) = \sum_{i=1}^{45} A_i \cos\left(\frac{2\pi}{T_i} \cdot t + \phi_i\right) \qquad t=0,1,\ldots,1023. \qquad \ldots (A.19)$$

The amplitudes A_i were specified according to the rule $A_i = 0.05 T_i$ where $T_i = 1024/(i+5)$ and $171 > T > 20$. Similarly the initial phase ϕ_i is specified according to the rule $\phi_i = 0.1 T_i$.

The Fourier transform of the time series y(t) of Eq. (A.19) was computed using our program and the results for amplitudes and phases for different periods are displayed in Fig. A.2 and A.3. Table A.1 is a direct numerical comparison for selected periods.

This and many other such tests convinced us that the FFT program written by us is working to expectations and could be used for analysis of Iranian surface wave data.
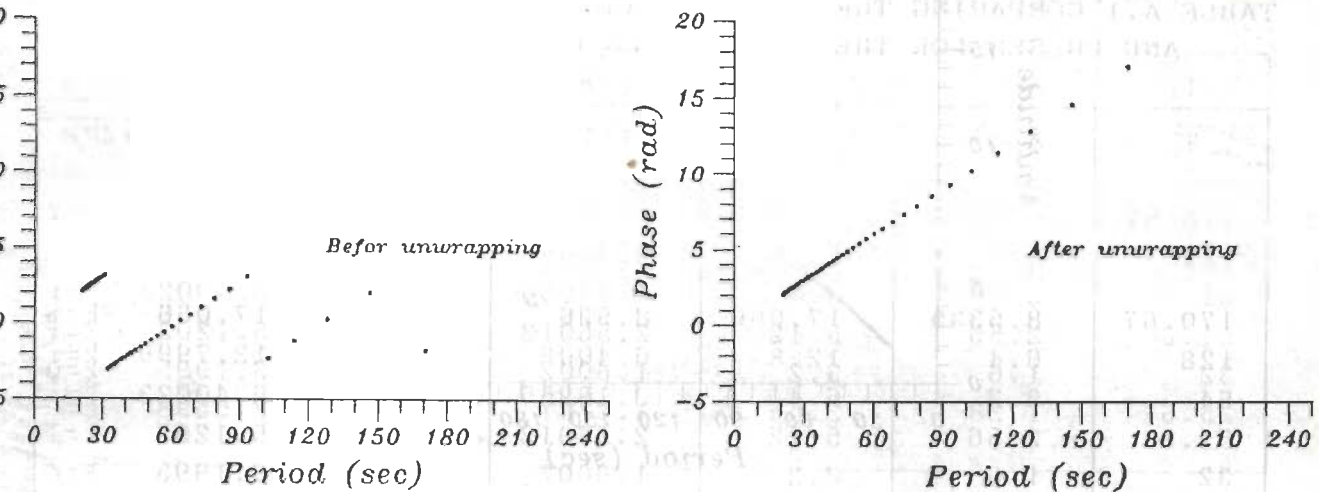
FIG. A.3 SIMILAR TO FIG. A.2 BUT DISPLAYING FOURIER PHASE AS FUNCTION OF PERIOD. PART (a) SHOWS THE PHASE WITHOUT UNWRAPPING AND PART (b) ILLUSTRATE THE EQUATION $\phi(T)=0.1T$. THUS THE CORRESPONDING OF OUR FFT PROGRAM IS TESTED.

TABLE A.1 COMPARING THE ORIGINAL AND FFT BASED AMPLITUDES AND PHASES FOR THE TIME SERIES OF Fig. A.1.

T	A_T (org)	ϕ_T (org)	A_T (FFT)	ϕ_T (FFT)	ϕ_T (FFT)$+2\pi k$	
170.67	8.5335	17.066	8.536	10.7836	17.066	k=1
128	6.4	12.8	6.4006	.23355	12.7999	k=1
64	3.2	6.4	3.19955	.11705	6.40023	k=1
51.2	2.56	5.12	2.56013	5.1203	5.1203	k=1
32	1.6	3.2	1.6002	3.1995	3.1995	k=0
25.6	1.28	2.56	1.2787	2.5598	2.5598	k=0
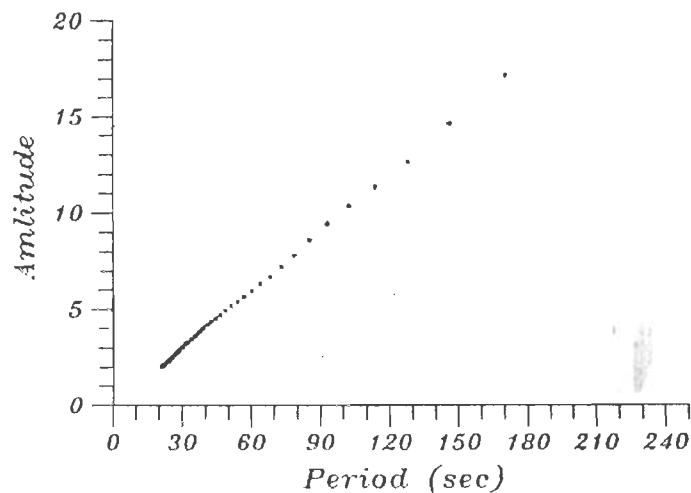
FIG. A.2 GRAPH DISPLAYING AMPLITUDE VALUES FOR DIFFERENT PERIOD BY COMPARING FOURIER TRANSFORM OF THE TIME SERIES IN FIG. A.1 USING THE FFT PROGRAM. THE POINTS ILLUSTRATE THE EQUATION $A=0.05T$ IN THE PERIOD RANGE OF 20 TO 170 S. THUS THE CORRESPONDING OF OUR FFT PROGRAM IS TESTED.

APPENDIX B
MAIN RESULTS OF HASKELL'S FORMULATION

Haskell in 1953 gave a very efficient method of computing Love and Rayleigh wave dispersion curves for a multi-layered half space. Fig. B.1 shows the necessary numbering of layers and interfaces and the coordinate system. Each of the n layers is homogeneous isotropic, and perfectly elastic with nth layer being a half space. A given layer, say the ith, is in welded contact with the layer i-1 at the top and i+1 at the bottom. As a result, at the ith interface (i≠0), there is continuity of normal and tangential displacements and normal and tangential stresses. The top surface of the model is stress free, that is the normal and tangential stresses are zero on this surface. Haskell considers such wave propagation in this multi-layered medium as would have zero displacements and stresses at z=∞ .
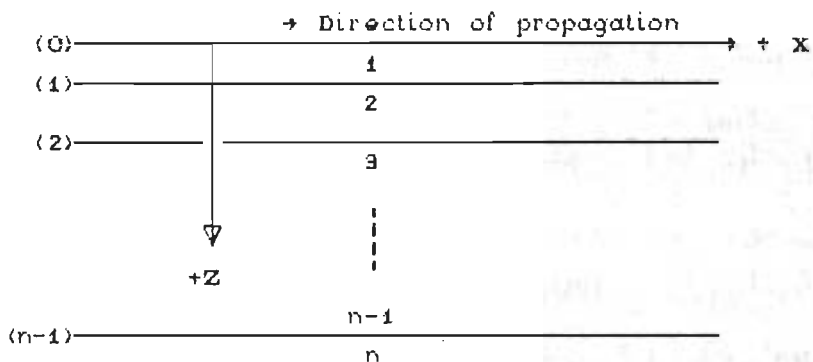
Fig B.1 DIRECTION OF AXES AND NUMBERING OF LAYERS AND INTERFACES.

(After Haskell 1953)

Using elasticity theory Haskell derives the following matrix relationship

$$(\Delta_n', \Delta_n', p_n', p_n')^T = J(u_o'/c, w_o'/c, 0, 0)^T . \qquad \qquad \ldots(B.1)$$

Here Δ_n', and p_n' are the amplitudes of dilatational and rotational waves respectively in the half space. Specifically the dilatation Δ_m in this layer is given by

$$\Delta_m = (\delta u/\delta x) + (\delta w/\delta z) = \exp[i(\omega t - kx)][\Delta_m' \exp(-ikr_{\alpha m} z)]; \quad .(B.2)$$

similarly p_m,

$$p_m = (1/2)(\delta u/\delta z) - (\delta w/\delta x) = \exp[i(\omega t - kx)][p_m' \exp(-ikr_{\beta m} z)] \quad \ldots(B.3)$$

u_o and w_o in Eq. B.1 are the x and z components of particle velocity at the free surface z=0. The matrix J is the 4×4 matrix given by $E^{-1} a_{n-1} a_{n-2} \ldots \ldots a_1$. The matrix E^{-1} is given by

$$E^{-1} = \begin{bmatrix} -2(\beta_m/\alpha_m)^2 & 0 & (\rho_m \alpha_m)^{-1} & 0 \\ 0 & c^2(\gamma_m-1)/\alpha_m^2 r_{\alpha m} & 0 & (\rho_m \alpha_m^2 r_{\alpha m})^{-1} \\ (\gamma_m-1)/\gamma_m r_{\beta m} & 0 & -(\rho_m c^2 \gamma_m r_{\beta m})^{-1} & 0 \\ 0 & 1 & 0 & (\rho_m c^2 \gamma_m)^{-1} \end{bmatrix} . \qquad \ldots(B.4)$$

The elements of the 4×4 matrix a_m (m=1,...,n-1) are given as follows.

$$(a_m)_{11} = \gamma_m \cos(P_m) - (\gamma_m-1)\cos Q_m \qquad \qquad ;$$
$$(a_m)_{12} = i[(\gamma_m-1)r_{\alpha m}^{-1} \sin P_m + \gamma_m r_{\beta m} \sin Q_m] \qquad ;$$
$$(a_m)_{13} = -(\rho_m c^2)^{-1}(\cos P_m - \cos Q_m) \qquad \qquad ;$$

$$(a_m)_{14} = i(\rho c_m^2)^{-1}(r_{\alpha m}^{-1}\sin P_m + r_{\beta m}\sin Q_m) \quad ;$$

$$(a_m)_{21} = -i[\gamma_m r_{\alpha m}\sin P_m + (\gamma_m-1)r_{\beta m}^{-1}\sin Q_m] \quad ;$$

$$(a_m)_{22} = -(\gamma_m-1)\cos P_m + \gamma_m \cos Q_m \quad ;$$

$$(a_m)_{23} = -(\rho c_m^2)^{-1}(r_{\alpha m}\sin P_m + r_{\beta m}^{-1}\sin Q_m) \quad ;$$

$$(a_m)_{24} = (a_m)_{12} \quad ;$$

$$(a_m)_{31} = \rho c_m^2 \gamma_m(\gamma_m-1)(\cos P_m - \cos Q_m) \quad ;$$

$$(a_m)_{32} = i\rho c_m^2[(\gamma_m-1)^2 r_{\alpha m}^{-1}\sin P_m + \gamma_m^2 r_{\beta m}\sin Q_m] \quad ;$$

$$(a_m)_{33} = (a_m)_{22} \quad ;$$

$$(a_m)_{34} = (a_m)_{12} \quad ;$$

$$(a_m)_{41} = i\rho c_m^2[\gamma_m^2 r_{\alpha m}\sin P_m + (\gamma_m-1)^2 r_{\beta m}^{-1}\sin Q_m] \quad ;$$

$$(a_m)_{42} = (a_m)_{31} \quad ;$$

$$(a_m)_{43} = (a_m)_{12} \quad ;$$

$$(a_m)_{44} = (a_m)_{11} \qquad \ldots\{B.5\}$$

Haskell has proved that the elements of a_m have the following property.

$$a_m = \begin{bmatrix} R & I & R & I \\ I & R & I & R \\ R & I & R & I \\ I & R & I & R \end{bmatrix} , \qquad m=1,\ldots,n-1$$

where an R indicates a real quantity (not, of course, the same quantity in all positions) and an I indicates an imaginary quantity. The product of any two matrices of this form is also a matrix of the same form.

The various symbols used in these matrices are

$$\rho_m = \text{density}$$

$$d_m = \text{thickness}$$

$$\lambda_m, \mu_m = \text{Lame's elastic constant}$$

$$\alpha_m = [(\lambda_m + 2\mu_m)/\rho_m]^{1/2} = \text{speed of propagation of dilatational waves}$$

$$\beta_m = [\mu_m/\rho_m]^{1/2} = \text{speed of propagation of rotational waves}$$

$$k = \omega/c = 2\pi/\text{wave length (horizontal)}$$

$$\gamma_m = 2(\beta_m/c)^2$$

$$r_{\alpha m} = \begin{cases} +[(c/\alpha_m)^2 - 1]^{1/2} & c > \alpha_m \\ -i[1-(c/\alpha_m)^2]^{1/2} & c < \alpha_m \end{cases}$$

$$r_{\beta m} = \begin{cases} +[(c/\beta_m)^2 - 1]^{1/2} & c > \beta_m \\ -i[1-(c/\beta_m)^2]^{1/2} & c < \beta_m \end{cases}$$

$u, w = $ displacement components in x and z direction

$\sigma = Z_x = $ normal stress

$\tau = X_z = $ tangential stress

When the four simultaneous equations of matrix Eq. B.1 are written explicitly, we have

$$\Delta'_n = J_{11}\dot{u}_0/c + J_{12}\dot{w}_0/c$$

$$\Delta'_n = J_{21}\dot{u}_0/c + J_{22}\dot{w}_0/c$$

$$p'_n = J_{31}\dot{u}_0/c + J_{32}\dot{w}_0/c$$

$$p'_n = J_{41}\dot{u}_0/c + J_{42}\dot{w}_0/c$$

By eliminating Δ'_m and p'_n we have,

$$\frac{\dot{u}_0}{\dot{w}_0} = \frac{J_{22} - J_{12}}{J_{11} - J_{21}} = \frac{J_{42} - J_{32}}{J_{31} - J_{41}} \tag{B.6}$$

236

Since the elements of the matrix J are functions of the parameters c and k, the right hand equality in Eq. B.6 provides an implicit relationship between c and ω,

$$F_R(\omega,c)=(J_{22}-J_{12})(J_{31}-J_{41})-(J_{11}-J_{21})(J_{42}-J_{32})=0 \qquad \ldots(B.7)$$

This is the desired phase speed dispersion function for Rayleigh waves. We have used the Newton–Raphson and interval halving techniques (Pennington 1965) to find the roots of this equation.

APPENDIX-C
THE OVERFLOW PROBLEM IN EVALUATION OF LAYER MATRICES

The computation of Rayleigh wave phase speeds for a layered earth model has been problematic always. Before the advent of computers the evaluation was hindered by the very long calculations required to be carried out manually. Haskell (1953) suggested the layer matrix approach to systematice the calculations. The arrival of computers permitted efficient programs to be written for matrices. It was soon realized that when the layer thickness H was large and/or the wave length λ was small the computations experienced overflow problem because H/λ appears as the positive argument of exponentials frequently.

Schwab and Knopoff (1972) offer the following condition so that overflow does not occur for Rayleigh wave type layer matrices.

$$\frac{\ln(\frac{Max}{7.16})}{4.\pi} > \frac{H}{\lambda} \qquad \qquad \text{...(C.1)}$$

Here Max refers to maximum floating point number accommodated in computer. Many clever schemes (e.g. Dunkin 1965, Watson 1970, and Schwab and Knopoff 1972) have been suggested to over come this problem. However with the progress in the computer hardware the

239

problem is becoming less acute. The computer used by us uses 1.78×10^{308} as the largest floating point number. For our calculations, the minimum value of λ is 45 km and maximum layer thickness could be 300 km. Thus the worst case $\frac{H}{\lambda}$ value would be 6.6. This is less than the permissible of 56.5 for the left hand side ratio in Eq. C.1 for our computer.

APPENDIX D
DISTANCES AND AZIMUTHS ON A SPHERICAL EARTH

Let us consider a spherical coordinate system with coordinates (r, θ, λ), where r is the radial distance, θ is colatitude and λ is longitude. Let us have a sphere of unit radius in this coordinate system. Let $A(1, \theta_1, \lambda_1)$ and $B(1, \theta_2, \lambda_2)$ be two points on this unit sphere. The North pole P will have coordinate $(1, 0, 0)$ in this system.

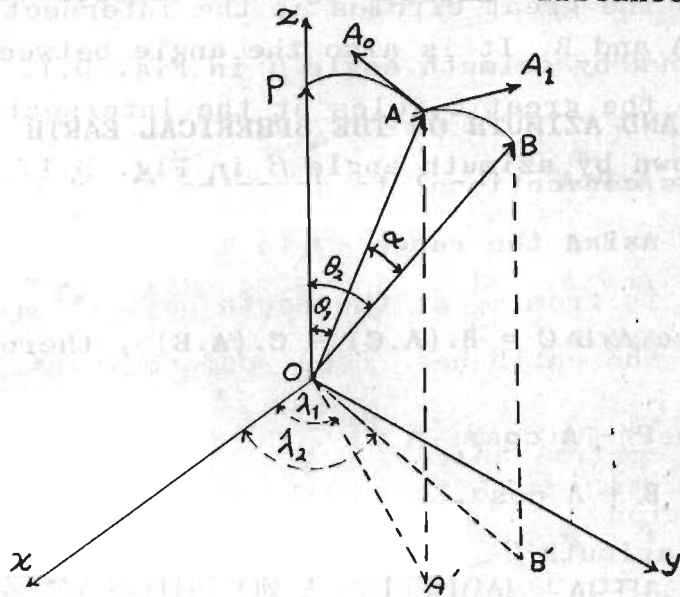FIG. D.1 A FIGURE TO EXPLAINE THE NOTATION AND THE COORDINATE SYSTEMS.

The position vectors A, B, and P of the spherical system will have following from in the Cartesian (x,y,z) coordinate system of Fig. D.1,

$$A = i\, \sin\theta_1 \cos\lambda_1 + j\, \sin\theta_1 \sin\lambda_1 + k \cos\theta_1$$
$$B = i\, \sin\theta_2 \cos\lambda_2 + j\, \sin\theta_2 \sin\lambda_2 + k \cos\theta_2$$
$$P = k \quad .$$

241

The central angle α between vectors A and B is obtained from the equation

$$\cos\alpha = A.B = \cos\theta_1\cos\theta_2 + \sin\theta_1\sin\theta_2\cos(\lambda_2-\lambda_1) . \qquad ...(D.1)$$

The azimuth to B at point A is the angle measured in the spherical surface from North towards East. It is the angle in the spherical surface between great circles through P and A and through A and B. It is also the angle between tangent vector A_o and A_1 to the great circles at the intersection point A in the sense shown by azimuth angle β in Fig. D.1. From vector algebra we have

$$A_o = A\times P\times A$$
$$A_1 = A\times B\times A$$

Since $A\times B\times C = B.(A.C) - C.(A.B)$, therefore

$$A_o = P - A\cos\theta_1$$
$$A_1 = B - A\cos\alpha.$$

Thus the azimuth β

$$\beta = \cos^{-1}\left(\frac{A_o.A_1}{|A_o|.|A_1|}\right) = \frac{\cos\theta_2 - \cos\theta_1\cos\alpha}{\sin\theta_1\sin\alpha} \qquad ...(D.2)$$

DISTANCE AND AZIMUTH ON THE SPHERICAL EARTH

It is conventional to describe the longitude λ of a point on the earth using the range $-\pi$ to π. The latitude θ is $(\frac{\pi}{2} -\theta)$ and its range is from $-\frac{\pi}{2}$ at the South pole to $\frac{\pi}{2}$ at the North pool. The radius of the earth has been defined in following ways among others.

242

R_v =6371.221 km if the volume of spherical earth is equal the volume of ellipsoidal earth.

R_a =6371.228 km if the area of the spherical earth is equal to the area of the ellipsoidal earth.

R_m =6371.229 km if R = (2a+c)/3 where R is the radial distance of a point on the ellipsoidal earth and a and c are the equatorial and polar radii of the ellipsoidal earth.

We see that there is only 8 m difference between the largest and smallest values. So the best value for this study is the average of these values and it is R_a =6371.226 km. Therefore one degree of arc on the earth will be L_0 =111.199 km and we can write (D.1) and (D.2) as:

$$D_{AB} = L_0 \cdot \alpha = L_0 \cdot \cos^{-1}(\sin N_A \sin N_B + \cos N_A \cos N_B \cos(E_B - E_A)) \quad (km)$$

$$\beta = \cos^{-1}\left(\frac{\sin N_B - \sin N_A \cos\alpha}{\sin\alpha \cdot \cos N_A}\right) \qquad \beta = \begin{cases} \beta & \sin(E_B - E_A) \geq 0 \\ 360 - \beta & \sin(E_B - E_A) < 0 \end{cases}$$

Where N_G and E_G are the latitude and longitude of a point G on the earth respectively. North latitude and east longitude are a positive and south latitude and west longitude are negative in these formulas.

In this study A is always the epicenter of earthquake and B is the seismograph station. Back azimuth is the azimuth of seismograph station at the earthquake epicenter.

243